

DEVELOPMENT OF SYNCHROTRON-BASED IMAGING TOOLS FOR  
BENIGN PROSTATIC HYPERPLASIA USING AN INDUCED CANINE  
MODEL

A Thesis Submitted to the College of  
Graduate and Postdoctoral Research  
In Partial Fulfillment of the Requirements  
For the Degree of Master of Science  
In the Department of Small Animal Clinical Sciences  
University of Saskatchewan  
Saskatoon, Saskatchewan, Canada

By

Natalia Cavalca Cardoso, DVM

©Copyright Natalia Cavalca Cardoso, September 2019. All rights reserved.

## PERMISSION TO USE

In presenting this thesis in partial fulfillment of the requirements for a Postgraduate degree from the University of Saskatchewan, I agree that the Libraries of this University may make it freely available for inspection. I further agree that permission for copying of this thesis in any manner, in whole or in part, for scholarly purposes may be granted by the professor who supervised my thesis work, and the College of Graduate and Postdoctoral Studies or, in their absence, by the Head of the Department or the Dean of the College in which my thesis work was done. It is understood that any copying or publication or use of this thesis or parts thereof for financial gain shall not be allowed without my written permission. It is also understood that due recognition shall be given to me and to the University of Saskatchewan in any scholarly use which may be made of any material in my thesis.

Requests for permission to copy or to make other use of material in this thesis in whole or part should be addressed to:

Dean of the College of Graduate and Postdoctoral Studies  
University of Saskatchewan  
116 Thorvaldson Building, 110 Science Place  
Saskatoon, Saskatchewan, S7N 5C9, Canada

Or

Head of the Department of Small Animal Clinical Sciences  
Western College of Veterinary Medicine  
52 Campus Drive  
University of Saskatchewan  
Saskatoon, SK S7N 5B4 Canada

## ABSTRACT

Benign prostatic hyperplasia (BPH) is a disease that develops spontaneously in men and dogs, and the dog is an accepted model to study BPH in men. As the gland can also be the site of a malignant cancer, definitive diagnosis relies on histological evaluation of prostate tissue following an invasive biopsy. The use of a new imaging technique, synchrotron-based phase contrast computed tomography (PC-CT) for excised prostates shows great detail of the internal structure of the gland, comparable to that of low power histology. Considering this fact, our main objective was to induce BPH in dogs using a combination of hormones dihydrotestosterone (DHT) and estradiol and verify if PC-CT imaging of *in situ* prostate glands of live dogs allowed for improved non-invasive imaging details compared to conventional medical imaging modalities and early diagnosis of BPH. Two studies were conducted to achieve the objectives.

The first study involved the induction of BPH using intact male dogs with DHT and estradiol. The control group (n=3) received triolein carrier and the BPH induction group (n=3) received the hormone combination of DHT and estradiol (dissolved in triolein) injections three times/week for 35 weeks. Parameters that were assessed to diagnosis BPH were *in vivo* prostate volumes calculated using computed tomography (CT) images, volume of excised prostates determined using water displacement, 3D measurements of the excised gland, semen analysis, digital rectal exam (DRE), hormone analysis (estradiol, testosterone, DHT and canine prostate specific esterase CPSE), morphometric analysis and histological assessment of the tissue slides. The results showed that the gland volumes calculated both *in vivo* and *ex vivo* and the 3D measurements from BPH induction group were numerically higher than the control group. Sperm count

decreased for all dogs but was reduced to zero or almost zero in the BPH induction group. The CPSE hormone analysis indicated that 1 dog from the treatment and 1 dog from the control group had BPH according to the manufacture's defined threshold value. DHT hormone levels were higher for the induction group than controls throughout the entire study. This consequently affected the endogenous testosterone and estradiol, which were both decreased due to the negative feedback in the hypothalamic-pituitary-gonadal (HPG) axis. For DRE, prostates from all dogs were found to be enlarged in size by the end of the study and the histological diagnosis revealed that all dogs have a certain degree of BPH.

The second study involved the imaging of all six dogs with conventional non-invasive modalities (magnetic resonance imaging, MRI; CT; positron emission tomography, PET-CT; ultrasound, US; radiographs) plus the innovative PC-CT technique at the Canadian Light Source (CLS). None of these techniques resulted in images with the same level of fine detail as that obtained with previous PC-CT imaging of excised canine prostates. Comparisons among images from the various modalities determined that the best modality for the visualization of the internal structures of the prostate gland such as capsule, parenchyma, septa, lobe, urethra and cysts was MRI (T2), followed by US and CT. PC-CT images were comparable with PET-CT, allowing the visualization of the lobes and urethra filled with tracer.

In conclusion, all dogs developed BPH, either spontaneously (control group) or following induction (treatment group). Also, images of the *in situ* prostate gland of dogs were acquired for the first time at the CLS with the PC-CT technique. Although the quality and resolution was not as expected in comparison with PC-CT images of excised

canine prostates, this technique shows promise and with additional study and development has the potential to become a useful diagnostic methodology.

Keywords: BPH, PC-CT, DHT, estradiol, prostate gland, dog, CLS, synchrotron, *in vivo* imaging

## ACKNOWLEDGEMENTS

“Alone we can do so little, together we can do so much”  
Helen Keller

This thesis can be translated in the achievement of my MSc degree, the pursuit of science through research, the involvement of a lot of hand and minds in which each of them were important for the conclusion of this work. I dedicate it for everyone that was part of it and for all the animals that donate their lives to research.

First, thank you God for my life and for everything I am.

For those who guided me throughout this process, my supervisors Dr. Liz Snead and Dr. Murray Pettitt, my gratitude, admiration and respect. Thank you for believing in me, for pushing me towards my self-improvement and for the insights and lessons taught. I am also thankful to my co-supervisor Dr. Jaswant Singh for his inspiration and help during my MSc.

I am thankful for the WCVU Graduate Education Enhancement Fund for the financial support, which was essential for the completion of my studies.

A huge thanks for the Prostate Research Team, Dr. Rajni Chibbar, Dr. Ali El-Gayed, Dr. Kishore Visvanathan, Dr. Ahmad Al-Dissi, Dr. Mary Buhr, Dr. James Montgomery, Dr. Michal Wesolowski, Jay Keith, Amitoj Singh and Alexa Woodward. Each of you was essential for the conclusion of this project.

Thank you for the brilliant minds at BMIT-Beam team Dr. George Belev, Dr. Denise Miller, Dr. Ning Zhu, Dr. Adam Webb and Dr. Dean Chapman and Dr. Tomasz Wysokinski, who made this experiment possible.

I couldn't forget to thank the Animal Care Unit, Monique Burmester and all the techs Brandee, Natalie, Bev, Heather as well as the anesthesia team Dr. Ambros, Dr. Duke, Dr. Carrozzo, Dr. Jones, and the techs Sharron, and Terri, the radiology team Dr. Sukut, Dr. Paisley and the imaging techs Nadine, Michelle, Cindy and Lianne. Also, I would like to thank the PET CT team at RUH Scott Mildenberger and all the techs, the MRI team at RUH Shawn Kisch and the techs. Thank you for all the assistance: Susan Cook, Kim Tran, Danielle Carriere, Dr. Sarah Parker, Dr. Tasha Epp, Dr. Peqiang Yu, Bethany Baker. The participation of each of you in this project was extremely valuable.

Thanks for the support and friendship: Ana Rita, Celina, Emy, Priscila, Zoe, Miyuki.

All my love and gratitude to my family: Marcos, Luci, Lais and Luigi for being by my side and giving me strength and support, in every moment of my life and Kush for his inspiration, care, love and patience with me.

Last, but not least, thank you for your precious lives and souls: Bolt, Waldo, Patty, Marley, Shy and Choco. You guys will be forever in my memory.

## TABLE OF CONTENTS

PERMISSION TO USE .....	i
ABSTRACT .....	ii
ACKNOWLEDGEMENTS .....	v
TABLE OF CONTENTS .....	vii
LIST OF TABLES .....	x
LIST OF FIGURES.....	xii
COMMONLY USED ABBREVIATIONS .....	xvii
CHAPTER 1: INTRODUCTION .....	1
CHAPTER 2: LITERATURE REVIEW .....	4
2.1. Anatomy of the Prostate.....	4
2.1.1 Man .....	4
2.1.2 Dog .....	7
2.2 Biomarkers of the Prostate Gland .....	8
2.2.1 Men .....	8
2.2.2 Dog .....	9
2.3 Histology of the Normal Prostate and BPH.....	10
2.3.1 Man .....	10
2.3.2 Dog .....	14
2.4 Pathophysiology of BPH.....	17
2.4.1 Man .....	19
2.4.2 Dog .....	23
2.5 Diagnosis of BPH.....	28
2.5.1 Men .....	28
2.5.2 Dog .....	29
2.6 Biopsy of Prostate Gland.....	31
2.6.1 Man .....	31
2.6.2 Dog .....	33
2.8 Treatment of BPH .....	34
2.8.1 Man .....	34
2.8.2 Dog .....	36
2.9 Imaging the prostate .....	39
2.9.1 Radiographs.....	39



2.9.2 Ultrasound.....	42
2.9.3 Computed Tomography (CT).....	47
2.9.4 Magnetic Resonance Imaging - MRI .....	53
2.9.5 Positron Emission Tomography .....	58
2.9.6 PC-CT Phase Contrast Computed Tomography Synchrotron.....	64
CHAPTER 3: OBJECTIVES .....	69
CHAPTER 4: INDUCTION OF BENIGN PROSTATIC HYPERPLASIA IN INTACT DOGS WITH 17 $\beta$ -ESTRADIOL AND 5 $\alpha$ -DIHYDROTESTOSTERONE HORMONES .....	70
4.1 Abstract .....	70
4.2 Introduction.....	71
4.3 Materials and Methods .....	73
4.3.1 Animals.....	73
4.3.2 Physical Exams and Samples Collected.....	74
4.3.3 Preparation of the Injection Solutions .....	75
4.3.4 Hormone Injections .....	76
4.3.5 Hormone Analysis.....	77
4.3.6 <i>In vivo</i> Imaging.....	79
4.3.7 Prostate Volume Measurements .....	80
4.3.8 Histological Preparation .....	80
4.3.9 Morphometric Analysis.....	82
4.3.10 Histological Scoring .....	83
4.3.11 Statistical Analysis.....	84
4.4 Results.....	86
4.4.1 Physical examination .....	86
4.4.2 Creatine kinase (CK) analysis .....	87
4.4.3 Routine diagnostic laboratory data: CBC, serum biochemistry analysis, urinalysis (UA) and semen analysis .....	87
4.4.4 CPSE, DHT, testosterone and estradiol .....	90
4.4.5 Physical Measurements and Volume of the Prostate Glands .....	94
4.4.6 Morphometric analysis .....	96
4.4.7 Histological analysis of the prostate slices .....	97
4.5 Discussion.....	97
CHAPTER 5: LIVE IMAGING OF IN SITU DOGS' PROSTATES WITH PC-CT TECHNIQUE AT THE CANADIAN LIGHT SOURCE SYNCHROTRON AND ITS COMPARISON WITH CONVENTIONAL IMAGING MODALITIES.....	106

5.1 Abstract .....	106
5.2 Introduction.....	107
5.3 Material and Methods .....	109
5.3.1 Animals and Experimental Model.....	110
5.3.2 Imaging.....	110
5.3.2.1 Sedation and General Anesthesia .....	111
5.3.2.2 Radiographs .....	112
5.3.2.3 Ultrasonography .....	113
5.3.2.4 CT .....	113
5.3.2.5 MRI .....	114
5.3.2.6 PET-CT .....	114
5.3.2.7 PC-CT .....	115
5.4 Results.....	121
5.5 Discussion and Conclusion.....	130
CHAPTER 6: GENERAL DISCUSSION AND FUTURE PERSPECTIVE .....	138
APPENDIX.....	141
REFERENCES.....	173

## LIST OF TABLES

2.1	A study of the administration of different steroid hormones to dogs and the changes on their prostate weight. Five different groups were created (group I to V) and the prostate was then collected after 12 months of hormone induction, weighed and compared with its initial weight (Walsh & Wilson, 1976).	25
2.2	A study of steroid hormones given to dogs and the effects on the prostate weight and its histological features. Dogs were assigned into two main groups – castrated and intact dogs – and within these groups eight subgroups received different hormonal treatments. After four months of hormone protocol induction, the glands were removed and evaluated (DeKlerk et al., 1979).	26
2.3	Classification of LUTS in men into three categories according to the patient’s symptoms (Vuichoud & Loughlin, 2015).	29
2.4	Comparison of three biopsy techniques used for the detection of prostate cancer (Shah & Ming, 2012).	33
4.1	Random Assignment of dogs to a control or BPH induction group.	73
4.2	DRE score for baseline (week -4) and for last evaluation (week 35). Control dogs: 1, 2 and 5 and treatment dogs: 3, 4, and 6.	87
4.3	Semen analysis of all six dogs displaying volume, motility, progressive motility and concentration of sperm. Baseline data for all dogs are from week -4, except dogs #5 and #6, collected at week 0 and week 4 respectively. End of collection date for all dogs was week 32. $P>0.05$ for all parameters: control baseline vs end, treat baseline vs end and control end vs treat end, except volume treatment baseline vs end was $P<0.05$	88
4.4	Statistical analysis of the semen. P value, mean and SEM for control and BPH induction (treatment) groups are shown below for both baseline and end time points. (treatment= treat)..	88
4.5	CPSE mean concentration (ng/mL) detected by ELISA in two groups of dogs (control and treatment) over time. SEM= standard error of mean. $P =0.6615$ for treatment, $P=0.0029$ for week. Within row, means without a common superscript are significantly different.	90
4.6	DHT mean concentration (ng/mL) detected by ELISA in two groups of dogs (control and treatment) over time. SEM= standard error of mean. $P =0.0058$ for treatment, $P=0.0273$ for week. Within row and column, means without a common superscript are significantly different.	91
4.7	Estradiol mean concentration (pg/mL) detected by RIA in two groups (control and treatment) over time. SEM= standard error of mean. $P=0.1227$ for treatment,	92

P=0.0020 for week. Within row, means without a common superscript are significantly different.

4.8	Testosterone mean concentration (ng/mL) detected by RIA in two groups (control and treatment) over time. SEM= standard error of mean. P=0.1173 for treatment, P<0.0001 for week. Within row and column, means without a common superscript are significantly different	93
4.9	Mean and SEM values for morphometric analyses of each virtual slide of the prostate and also p values are shown below. OlyVIA software was used to assess the parameters. Area of acini was calculated using 15 random acinis/ slide and the same acinis had their intrapappillary projections counted. Surface area of prostate was drawn and calculated for each slide. Thickness of interlobular septa was calculated at three random locations.	96
4.10	Histopathological diagnosis scoring system (0-3) used for all six dogs (control 1, 2 and 5, and treatment 3, 4 and 6) based on three categories: cystic formation, glandular hyperplasia, and connective tissue hyperplasia. The average score of the two slides are displayed below.	97
5.1	Side by side PC-CT images of the prostate gland of the treatment dogs imaged pre (A3, A4 and A6) and post (B3, B4 and B6) euthanasia	130
A.1	Complete Blood Count and Serum Biochemistry profile data for all six dogs (control #1, #2 and #5, and treatment #3, #4, and #6) at week -4	141
A.2	Urinalysis findings of all six dogs (control #1, #2 and #5, and treatment #3, #4, and #6) in week -4.	141
A.3	Semen analysis (volume, motility, progressive motility and sperm concentration) for all dogs during the study.	142
A.4	Testis and epididymis weight (g) for both control and BPH induction groups	143
A.5	DRE score (0-3) for all the six dogs during the study.	143

## LIST OF FIGURES

2.1	Coronal section displaying anatomy of the human prostate gland.	5
2.2	Schematic sagittal section of the man's body showing the digital rectal examination of the prostate gland and its position related to the urinary bladder and rectum.	5
2.3	Sagittal section of the human prostate gland showing its zonal anatomy: central zone (CZ), transitional zone (TZ), peripheral zone (PZ) and anterior fibromuscular stroma (AFS); rectum is located in posterior direction and bladder in anterior direction (a). Coronal section of the human prostate gland showing its anatomy: only the CZ and PZ are visible in this view (b).	6
2.4	<i>In situ</i> anatomy of the canine prostate showing its oval shape and surrounding structures. Sagittal view on top and coronal view on the bottom.	8
2.5	Normal prostatic tissue of a man and its tubuloalveolar glands forming lobules and being enclosed by fibromuscular stroma (X4).	12
2.6	Glandular epithelium, connective tissue and smooth muscle are represented. Tissue section of a human prostate gland (X10).	12
2.7	Micrograph showing corpora amylacea inside tubuloalveolar glands of a human prostate gland (x10).	13
2.8	Micrograph of a stromal hyperplasia showing a fibrotic nodule in a man with BPH.	13
2.9	Micrograph of glandular hyperplastic nodule in a man.	14
2.10	Tissue section of the canine prostate gland. The glandular epithelium is pseudostratified and contains secretion inside some acini (x10).	15
2.11	Tissue section of the canine prostate gland showing the capsule encircling the gland and the trabecula or septa originated from the capsule, dividing the gland into lobules (x4).	15
2.12	Comparison between tissue section of the normal dog's prostate gland processed by histology (left) and an image a dog's <i>ex vivo</i> prostate (right) collected at CLS facility with the PC-CT technique.	16
2.13	Tissue section of a canine prostate gland with BPH.	17
2.14	Conversion of plasma testosterone into two different hormones: 17 $\beta$ estradiol and 5 $\alpha$ dihydrotestosterone.	18
2.15	Illustrative comparison between three biopsy techniques for prostate cancer in men: sextant, extended and saturation biopsy	32
2.16	Lateral radiograph of a dog showing the distance from the sacral promontory to the pubis (DSPP) (black line). The cranio-caudal distance of the prostate is measured parallel to the DSPP.	42
2.17	Schematic illustration of an ultrasound probe placed in contact with a tissue showing the electric pulses being converted into sound waves.	43
2.18	Normal prostate gland of a dog: longitudinal ultrasonography (A); transversal ultrasonography (B).	46
2.19	Ultrasound of a canine prostate gland with BPH. Longitudinal ultrasound showing a cyst and heterogeneity of the parenchyma.	46
2.20	The tube emits X-rays that reaches the detector on the opposite.	47

2.21	Cross sectional representation of CT slices of the body.	48
2.22	Cross section of a CT slice showing the 2D pixels represented by the squares and a 3D voxel represented by a cube.	49
2.23	CT Reconstruction using backprojection. (b) The reconstructed image is generated from four views; (c) The reconstructed image is generated using numerous views and display blurriness.	50
2.24	CT Reconstruction using filtered backprojection. (a) Filter is applied before generating the images; (b) The reconstructed image is generated using numerous views; (d) The final image has a better quality.	51
2.25	CT images of a dog's prostate gland with BPH characteristics: a) irregular prostatomegaly, b) pre-contrast image showing cysts, c) post contrast image showing cysts.	53
2.26	Illustration of the random pattern of protons spinning inside a human body. After an external magnetic field is applied, most of the protons align in the same direction as the main magnetic field ( $B_0$ ).	54
2.27	A RF pulse is applied making the protons flip to the transverse plane.	55
2.28	T1 Relaxation time	55
2.29	T2 Relaxation time	56
2.30	MRI T2 weighted imaged of a human patiente. (a) Normal prostate gland with hyper-intense peripheral zone; (b) BPH gland with an enlarged and heterogeneous central zone compressing the peripheral zone.	58
2.31	Beta plus decay. Parent element (carbon-10) originates a daughter element (boron-10), a positron and a neutrino.	60
2.32	Annihilation process showing a positron reacting with an electron and originating two photons in opposite directions ( $180^\circ$ ).	61
2.33	(A) Transaxial PET, (B) CT, (C) PET-CT fusion of the prostate of a man with prostate cancer using F18-FDG.	63
2.34	Transaxial (A) CT, (B) PET, (C) PET-CT fusion of the prostate of a man with prostate cancer using C11-choline.	64
2.35	An illustration of a synchrotron facility and its components: electron gun (source of electrons), linear accelerator (linac, that accelerates the electrons), an evacuated booster ring (more acceleration for the electrons. The electrons are injected into the storage ring, kept in a path passing through bending magnets and insertion device, generating radiation. The beamlines are tangentially and use the light from insertion devices (wigglers or undulators) and from the bending magnets. The radio frequency (RF) supply recharge the energy lost by the electrons.	65
2.36	The scanning setup for a PC-CT imaging, showing Fresnel fringes forming as the beam propagates towards the detector	67
2.37	Illustration of PC-CT. X-rays penetrating an object are attenuated and deflected due to refraction at boundaries where there is a change in tissue densities.	67
4.1	Flow diagram outlining the study design (wk=week)	75
4.2	Dorsal view of a dog showing a site for injections in the epaxial muscle of the lumbar region	77

4.3	Preparation steps for excised prostates. 1) Excised prostate is embedded in gelatin initially in a cylinder container (removed here) and 2) the prostate encased in gelatin is placed inside the custom-made slicer with additional gelatin added. 3) Slicing of the prostate gland was done where the yellow dividers were placed (3mm of distance between each divider). 4) The individual slices were removed and inked on the cranial (orange ink) and right side (blue ink but not shown) for orientation purposes, and 5) then the separated slices of the prostate encased in gelatin are placed on a sheet of paper with numbers assigned to each slice (arranged in a cranial to caudal direction) with the caudal surface visible. Extra gelatin was carefully removed and the cranial and right sides of each slice were then re-inked and then each individual single slice was placed inside a named and numbered cassette with the caudal surface facing up for histological processing (4).	82
4.4	Scanned slides for morphometric analysis. Low power magnification (4x) was used for the calculation of the surface area of the gland, which was drawn around each slide, and the measurement of thickness of the interlobular septa (left). The surface area of acini along with the count of the intrapapillary projections were measured using high power magnification 20x(right).	83
4.5	A histological slide displaying the acini (A) and the supporting stroma (S) of the prostate gland.	84
4.6	Sperm concentration over time for control dogs 1, 2 and 5 (blue) and treatment (BPH induction) dogs 3, 4 and 6 (red).	89
4.7	Treatment*week interaction for mean CPSE concentrations for the control and treatment groups and SEM (black bars) over time (P=0.1785).	90
4.8	Treatment*week interaction for mean DHT concentrations for the control and treatment groups and SEM (black bars) over time (P=0.0388). Means without a common superscript are significantly different	91
4.9	Treatment*week interaction for mean estradiol concentrations for the control and treatment groups and SEM (black bars) over time (P=0.1423).	92
4.10	Treatment*week interaction for mean testosterone concentrations for the control and treatment groups and SEM (black bars) over time (P=0.0013). Means without a common superscript are significantly different.	93
4.11	Prostatic volume calculated based on <i>in vivo</i> CT images for the control and treatment groups at week -4 (baseline) and week 17 (mean $\pm$ SEM and volume for each dog). Volume is not statistically different between the dogs in the control (week -4 vs week 17, control (P=0.6250) and treatment groups (week -4 and week 17, P=0.2170) or between the control and treatment groups during week -4 (P=0.4139) or week 17 (P=0.4164).	95
4.12	Mean $\pm$ SEM prostatic volume of <i>ex vivo</i> control and treatment groups at week 35 and individual volumes for each dog. Volume is not statistically different between the control and treatment groups (P=0.0538).	95
4.13	Mean $\pm$ SEM prostate gland measurements ( <i>ex vivo</i> ) for the control and treatment groups at week 35. The mean $\pm$ SEM height, length and width (cm) are plotted; there were no significant statistical differences between any of the measurements between the 2 groups observed (height P=0.1649, length P=0.1185 and width P>0.9999)	96

5.1	Illustration of the lateral view of the caudal abdomen of a dog (1a) with the position of a hyperplastic prostate shown in relation to other surrounding structures (P is prostate and B is bladder); in comparison 1b shows a lateral radiographic projection of the caudal abdomen of a dog (1b) where the red arrow shows the distance between the sacral promontory and the pubis (DSPP) which is used to evaluate for prostatic enlargement	112
5.2	A schematic set up for live dog PC-CT imaging at the BMIT-ID at the CLS. The Sample here represents the dog held in a vertical position using the Conine holding device	115
5.3	A live dog being imaged at the CLS BMIT ID Beam Line inside the Conine holder (white) located on top of the rotating stage (metallic) and the ventilator that was used can be seen within the hutch (a). The small oxygen cylinder, the remote anesthesia monitor and the dog inside the conine are also displayed (b).	117
5.4	Schematic representation of one raw tomographic projection (on the left), and the ROI is grey in color located in the center of it. By trimming and removing the extra top and bottom black strip, we obtain the final grey strip that contains the data (on the right).	119
5.5	A raw tomographic projection showing the vertical center line (on the left) and the selection of the two adjacent pixels with the center line to calculate the median (on the right).	120
5.6	X-Ray attenuation and absorption calculator. The target material in this case is PMMA and the calculation is based on tomographic and flats values for transmission. The X-ray energy level (in this case 120 keV) and the target length (variable, according to the information provided by the scientists from the CLS) are entered for flats and tomographs one at a time. The website then calculates the transmission value obtained for the tomograph transmission/flat transmission ratio.	120
5.7	Side by side lateral radiographic projections from control dogs #1(A and B), #2 (C and D), #5 (E and F), obtained at week – 4 (left) and week 17 (right). L6 is the sixth lumbar vertebrae, C is for colon, P is the prostate.	122
5.8	Side by side lateral radiographic projections from treatment dogs #3(G and H), #4(I and J), #6 (K and L), obtained at week – 4 (left) and week 17 (right). L6 is the sixth lumbar vertebrae, C is for colon, P is the prostate.	123
5.9	<i>In situ axial</i> images of the prostate of control (top row) and treatment dogs (bottom row) taken with the imaging modalities: CT, PET-CT and MRI-T1 all collected at week 17.	125
5.10	<i>In situ axial</i> images of the prostate of control (top row) and treatment dogs (bottom row) taken with the imaging modalities: MRI-T2 (collected at week 17), US and PC-CT (collected at week 35).	126
5.11	Side by side PC-CT images of the prostate gland of the control dogs imaged pre (A1, A2, A5) and post (B1, B2 and B5) euthanasia.	127
5.12	Side by side PC-CT images of the prostate gland of the treatment dogs imaged pre (A3, A4 and A6) and post (B3, B4 and B6) euthanasia	128
A.1	Cylinder container	144
A.2	Prostate inside gelatin.	144



A.3	Yellow dividers and parafilm placed in the slicer.	145
A.4	Prostate in the slicer filled with gelatin	145
A.5	Microtome blade attached to the holder device.	146
A.6	Slicing prostate in the specified spacing (yellow dividers).	146
A.7	Series of three images showing (a) the prostate, gelatin and parafilm removed as a block from the slicer, (b) inking the right part with red ink, (c) ink applied for orientation purposes: red on right and blue on dorsal.	147
A.8	Slices of prostate and gelatin inked and numbered.	147
A.9	Applying notch on the right side of the prostate	148
A.10	a) Pat drying gently with paper towel; b) re-inking the prostate tissue; c) trimming excess of gelatine	148
A.11	Measuring thickness of prostate slice (dorsal, left, ventral and right side resulting in a mean value) with electronic digital caliper	148
A.12	Cassette labeled with dog name and number of slice	149
A.13	Excised prostate glands attached to urinary bladder in control dogs (#1, 2 and 5). Ventral (a) and dorsal (b) views.	149
A.14	Excised prostate glands attached to urinary bladder in BPH induction dogs (#3, 4 and 6). Ventral (a) and dorsal (b) views.	150
A.15	<i>In situ</i> axial images of the prostate of control dogs #1, 2 and 5 taken with different imaging modalities: A) CT, B) US, C) PET-CT, D) MRI-T1, E) MRI-T2, F) PC-CT.	151
A.16	<i>In situ</i> axial images of the prostate of treatment dogs #3, 4 and 6 taken with different imaging modalities: A) CT, B) US, C) PET-CT, D) MRI-T1, E) MRI-T2, F) PC-CT.	152

## COMMONLY USED ABBREVIATIONS

<sup>11</sup>C – Carbon 11 Choline  
<sup>18</sup>F-FDG – Fluorine 18 Fluorodeoxyglucose  
2D – Two Dimensional  
3D – Three Dimensional  
AFS – Anterior Fibromuscular Stroma  
B-Mode – Brightness mode  
BMIT – Biomedical Imaging and Therapy  
BPH – Benign Prostatic Hyperplasia  
CBC – Complete Blood Count  
CLS – Canadian Light Source  
CPSE – Canine Prostate Specific Esterase  
CT- Computed Tomography  
CZ – Central Zone  
DHT – Dihydrotestosterone  
DRE – Digital Rectal Examination  
DSPP – Distance Sacral Promontory to the Pubis  
FSH – Follicle Stimulating Hormone  
Gy – Gray  
HPG axis – Hypothalamic Pituitary Gonadal Axis  
Hz – Hertz  
LH – Luteinizing Hormone  
LUTS – Lower Urinary Tract Symptom  
MHz – Mega Hertz  
MRI – Magnetic Resonance Imaging  
PBI – Propagation Based Imaging  
PC-CT – Phase Contrast Computed Tomography  
PCa – Prostate Cancer  
PET-CT – Positron Emission Tomography- Computed Tomography  
PSA – Prostate Specific Antigen

PZ – Peripheral Zone

Sv – Sievert

T ½ life – Physical Half Life

T1W MR– T1 weighting magnetic resonance

T2W MR – T2 weighting magnetic resonance

TE – Time of Echo

TGF-β – Transforming Growth Factor Beta

TR – Time of Repetition

TRUS – Transrectal Ultrasound

TZ – Transitional Zone

US – Ultrasound (Percutaneous)

## CHAPTER 1: INTRODUCTION

Benign prostatic hyperplasia (BPH) refers to the intrinsic and natural hormone-induced enlargement of the prostate that occurs in men with advanced age. According to the Canadian Cancer Society, almost all men that are 70 years of age or older will have some degree of prostate enlargement. The costs associated with BPH treatment are high. In Canada, in 2006 the direct expenses associated with the medical care of men with BPH was estimated to be \$1.1 billion (Nickel, 2006). Hidden costs include lost productivity associated with treatment and the emotional effects.

Thanks to the publicity and advertising regarding men's health, including more knowledge related to prostate cancer, and new medical treatments, more men are requesting medical assistance for prostate related disorders, including for BPH, than did so formerly. Lower urinary tract symptoms (LUTS) including problems associated with voiding (urine retention and dysuria), storage (pollakiuria) and post-micturition (urethral discharge) are the most common reasons why men with BPH present themselves to their physicians. One of the most common symptoms related to the enlargement of the prostate is the variable degrees of urethral obstruction resulting in urine retention and other urinary tract problems. This is a direct consequence of the urethra passing through the middle of the prostate and the resultant compression of the urethral lumen secondary to prostatic enlargement from BPH.

In addition to men, dogs also commonly experience the naturally occurring pathological condition of BPH. Indeed at the present time, the dog is the only widely available model for studying BPH in humans. However, despite this there are some important pathophysiologic differences with respect to BPH in dogs versus man. In men, BPH is mostly seen as a nodular enlargement localized in the inner zone of gland, whereas in the dog enlargement commonly is diffuse and cystic changes are common. The pathogenesis of BPH is not completely understood, however, the hormone dihydrotestosterone (DHT) is known to play a key role.

The early differentiation between BPH and prostate cancer (PCa) in men can be crucial when determining the most appropriate medical therapy for an individual patient. Digital rectal exam (DRE) is performed by a physician as part of a medical check-up is used to detect for any sign of alteration in prostate anatomy; however, findings are very subjective and not considered highly sensitive or specific for BPH. Also, higher blood levels of prostate specific antigen (PSA) are used as a biomarker to detect prostatic cancer, this test is not very specific and hence it is not possible to determine with certainty if enlargement of the prostate is the result of prostate cancer, benign prostatic hyperplasia, or prostatitis. Lack of specificity for differentiating PCa from other more benign conditions makes this test problematic.

Different medical imaging modalities have been used to provide adjunct information for the diagnosis of the different diseases affecting the prostate gland. Ultrasound (US) is the most widely available and used imaging modality for evaluating the prostate gland, however, differentiation of the different prostatic disorders is not always possible using this technique. Advanced imaging techniques such as computed tomography (CT), magnetic resonance imaging (MRI) and positron emission computed tomography (PET-CT) have also been used to evaluate the prostate gland. MRI and PET-CT have provided some reliable results for distinguishing PCa from BPH. However, in some studies it is controversial if these modalities are accurate and precise enough to reliably differentiate these two conditions.

Biopsy of the prostate, guided by ultrasound, is an invasive method, but is the commonly relied on to provide samples for histological analysis required to establish a specific diagnosis that can confirm what pathological condition is affecting the prostate. Recently, Phase Contrast Computer Tomography (PC-CT), a novel imaging modality has been investigated. Based on preliminary results from the Prostate Research Group at the University of Saskatchewan, this technique has demonstrated improved results in imaging the excised prostate, with a thousand times more resolution than a conventional CT (Wolkowski et al., 2015).

This literature review describes the anatomy and histology of the normal prostate in men and dogs as well as the expected changes that occur with BPH. In addition, the pathophysiology, diagnosis and treatment of BPH in men and dogs are reviewed. Finally, a discussion of the various imaging modalities that are used to diagnose and differentiate prostatic diseases, specifically to differentiate BPH from PCa in cases where this has not been possible by more routine methods is also presented.

## CHAPTER 2: LITERATURE REVIEW

### 2.1. Anatomy of the Prostate

#### 2.1.1 Man

The prostate is considered to be the major male accessory sex gland in the human species (C. H. Lee, Akin-Olugbade & Kirschenbaum, 2011; Risbridger & Taylor, 2006). As shown in Figure 2.1, it is a “walnut shaped” gland (C. H. Lee et al., 2011) and conventionally divided into two portions mistakenly called “lobes” (Epstein, Cubilla & Humphrey, 2011; Setchell & Breed, 2006). The prostate gland is encircled by a pseudocapsule (C. H. Lee et al., 2011) and has a superficial dorsal median septum (Risbridger & Taylor, 2006; Setchell & Breed, 2006) that can be felt during a digital rectal examination (DRE) (C. H. Lee et al., 2011). A DRE is a useful subjective tool for providing valuable information to the physician on the prostate gland’s size, shape and symmetry as well as to assess for any pain associated with palpation (Tanguay et al., 2009). Anatomically, the prostate is located inferior to the urinary bladder and anterior to the rectum, thus allowing DRE (Figure 2.2) (C. H. Lee et al., 2011). Also, the urethra transverses through the middle of the prostate gland with ducts from each lobe of the prostate draining into the urethral lumen (Risbridger & Taylor, 2006).

As it is illustrated in figure 2.2 and 2.3, the base of the human prostate gland is adjacent to the neck of the bladder (Risbridger & Taylor, 2006). The prostatic urethra enters from the bladder at the base and courses through the gland and then exits on the other side of the prostate (Epstein et al., 2011). As the urethra traverses through the prostate gland, it angles forward at 35 degrees and the angle divides the urethra into proximal and distal parts (Epstein et al., 2011; Wadhera, 2013). The tissue immediately surrounding the proximal urethra at the base of the gland contains smooth muscle fibres that help prevent retrograde movement of ejaculate (Risbridger & Taylor, 2006).

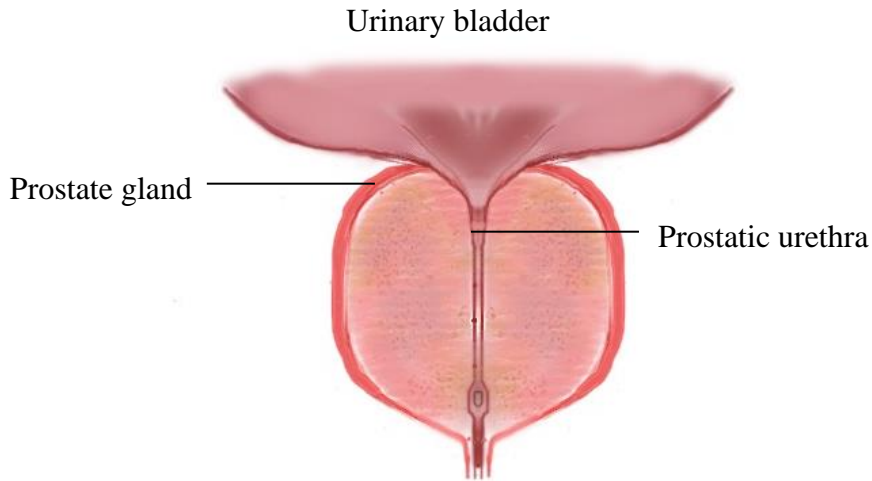


Figure 2.1. Coronal section displaying anatomy of the human prostate gland (Cavalca Cardoso, 2019)

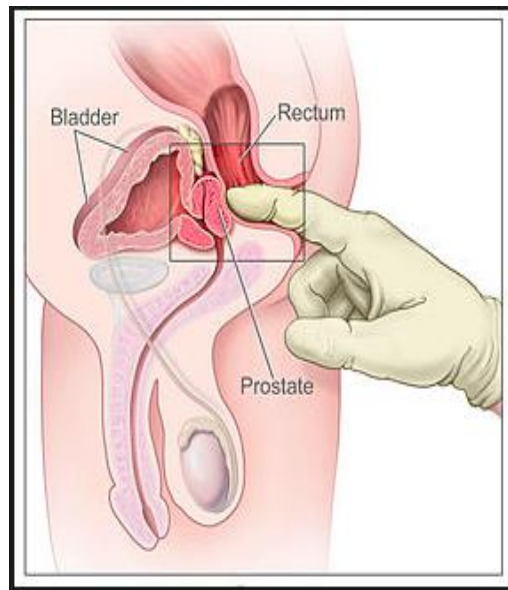


Figure 2.2. Schematic sagittal section of human male body showing the digital rectal examination of the prostate gland and the prostate's position relative to the urinary bladder and rectum. "Exam, Digital Rectal", August 2008. Retrieved from National Cancer Institute, on September 2017, <https://visualsonline.cancer.gov/details.cfm?imageid=7136> Reprinted with permission.



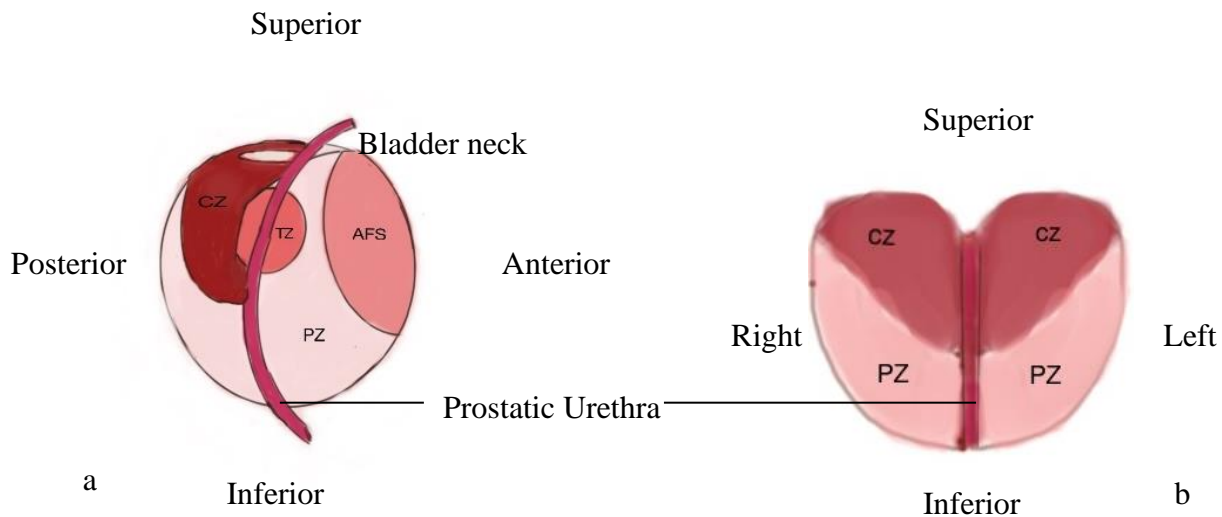


Figure 2.3. Sagittal section of the human prostate gland showing its zonal anatomy: central zone (CZ), transitional zone (TZ), peripheral zone (PZ) and anterior fibromuscular stroma (AFS); rectum is located in posterior direction and bladder in anterior direction (a). Coronal section of the human prostate gland showing its anatomy: only the CZ and PZ are visible in this view (b). (Cavalca Cardoso, 2019).

According to McNeal (considered one of the pioneers studying prostatic anatomy and structure), the human male prostate gland can be divided into three parts – a peripheral zone (PZ), a central zone (CZ) and a transition zone (TZ). In addition there is a patch of nonglandular tissue referred to as the anterior fibromuscular stroma (AFS) located at the peripheral caudal aspect of the gland (figure 2.3) (Wadhwa, 2013). Each zone can be differentiated based on its embryological origin, histology, and anatomic and functional features (Epstein et al., 2011). In addition these zones are distinguished based on the different disorders that arise from them (Epstein et al., 2011). The (CZ) is derived embryologically from the Wolffian duct, contains the submucosal glands (Mescher, 2016) and demonstrates low occurrence of PCa (C. H. Lee et al., 2011). By comparison, the (PZ) is derived from the urogenital sinus, contains the main tubuloacinar glands (Mescher, 2016) and is the most frequent site of origin of PCa (70%) (C. H. Lee et al., 2011). The (TZ) also originates from the urogenital sinus (C. H. Lee et al., 2011) and contains mucosal glands (Mescher, 2016). The TZ has a lower occurrence rate for PCa (25%), but it is the most commonly affected zone with BPH (C. H. Lee et al., 2011).

### 2.1.2 Dog

Identified as the only main accessory sex gland in the male dog (Leroy et al., 2013), the prostate gland can vary with respect to its position depending on the age of the dog and their sexual status (Williams, 2013). In young and older dogs that are neutered the gland is typically located completely within the pelvic cavity, while in older, intact dogs due to increased size and weight of the gland from hormonally induced hyperplasia, it is often located within the abdominal cavity (Geddes, 2011).

The canine prostate gland has an oval shape and surrounds the proximal urethra (figure 2.4) (Johnston, S. D., Kamolpatana, Root-Kustritz, & Johnston, G. R., 2000; J. Smith, 2008) and is entirely derived from the urogenital sinus (Bacha & Bacha, 2012). While in men the prostatic urethra curves within the gland, the same is not observed in dogs where the course of the urethra is straight (Cooney et al., 1992). The canine prostate is enclosed by a fibromuscular capsule and contains both a dorsal and ventral midline groove that divides the prostate into two lobes (J. Smith, 2008; Williams, 2013). During a DRE both lobes and the dorsal sulcus can be appreciated (Johnston et al., 2000) as well as anatomic features such the size, overall shape and symmetry and the consistency of the gland (J. Smith 2008). In the dog's body, the prostate is located caudal to the urinary bladder and ventral to the rectum as demonstrated in figure 2.4 (J. Smith, 2008).

Unlike the human prostate that can be divided into zones according to their histological differences as described by McNeal (central, peripheral, and transitional zone along with the anterior fibromuscular stroma) this is not observed in the dog's prostate (Cooney et al., 1992). In the dog, the epithelium of the prostate gland is similar to the epithelium of the peripheral zone in men (Cooney et al., 1992).

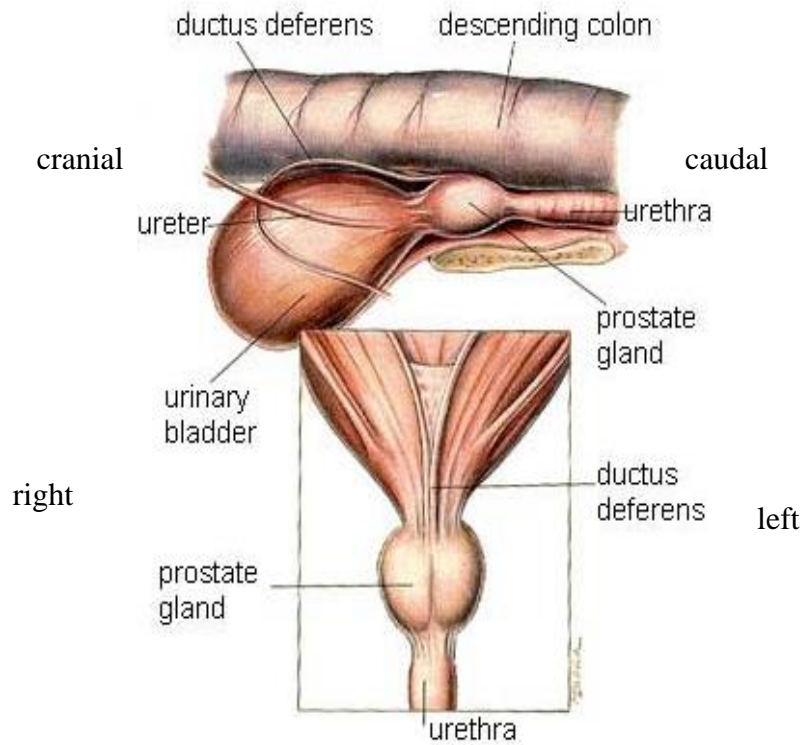


Figure 2.4. *In situ* anatomy of the canine prostate showing its oval shape and surrounding structures. Sagittal view on top and coronal view on the bottom. (Genital Organs Male - Prostate) Retrieved from Washington State University (WSU) website on April 2017, <https://www.vetmed.wsu.edu/outreach/Pet-Health-Topics/categories/cat-and-dog-anatomy/urogenital-system-of-the-dog>). Reprinted with permission from both WSU and Hill's Pet Nutrition - Atlas of Veterinary Clinical Anatomy.

## 2.2 Biomarkers of the Prostate Gland

### 2.2.1 Men

The prostate gland produces prostatic fluid, which is a milky solution (Cormack, 2001) that contributes 30-50% by volume to the seminal fluid volume (Young, B., Woodford, P., & O'Dowd, G. 2014). The rest of the seminal fluid consists of sperm produced by the testes and secretions from the other two accessory sex glands, the seminal vesicle and bulbourethral gland (Informed Health Online, 2016; Young et al., 2014). The entire secretion of these glands and the testes make up the ejaculate (Informed Health Online, 2016). The prostatic fluid portion is slightly acidic and contains citrate and zinc (Cormack, 2001; Costello and Franklin, 2009). It is known to be important for male fertility as it helps to maintain sperm cell viability (Informed Health Online, 2016).

One of the main elements investigated in the prostatic fluid is prostate specific antigen (PSA), which is a glycoprotein produced by the epithelial glands of the prostate and it can be measured in serum ([Informed Health Online, 2016](#); [Kashefi, Partin & Parson, 2010](#)). Although the name indicates that is “specific” to the prostate, it is possible to identify small quantities of PSA in other tissues and organs of the body such as the liver, pancreas, salivary gland and breast (of both males and females) ([Harvard Health Publishing, 2009](#)). However, the detection of an increased level of PSA in the blood in men can be seen with different disorders including PCa, BPH, prostatitis, urinary tract infections as well as following procedures such as prostatic massage, ejaculation and transrectal ultrasound (TRUS) ([Brett, 2011](#); [Harvard Health Publishing, 2009](#); [Kashefi, Partin & Parson, 2010](#)).

Physicians use PSA to screen for PCa in patients with symptoms that may indicate potential prostatic disease or in cases where there is a family history of PCa ([Kashefi et al., 2010](#)). However, PSA test is not considered *per se* a definitive diagnostic test for prostate cancer ([Brett, 2011](#)). The usefulness of screening for PCa using PSA is controversial, and the Canadian Task Force on Preventive Health Care and the Canadian Urological Association have both suggested that healthy men should not be screened for PCa using this test ([Harvard Health Publishing, 2009](#)). However, if testing for PSA is done, it is recommended to use age-specific adjusted PSA reference ranges as this may increase the chances of diagnosing PCa that could have been missed in young men and at the same time, avoiding repeated and excessive biopsies in senior men ([Singh, Moore & Emberton, 2013](#)).

### 2.2.2 Dog

In the dog, the prostate gland is also responsible for production of the prostatic fluid, which constitutes the bulk of the total volume of the ejaculate – more than 90 % ([Geddes, C. 2011](#)) – and it is part of the first and third fractions of the ejaculate ([Johnston et al., 2000](#); [Kustritz, 2006](#); [Solano-Gallego, 2010](#); [J. Smith, 2008](#)). Canine prostatic fluid contains citrate,

lactate, cholesterol and enzymes but unlike other species, it does not seem to contain reducing sugars (J. Smith, 2008). The prostatic fluid is believed to provide two main functions: it helps promote sperm viability and motility, while also supporting and transporting the sperm by decreasing the viscosity of the overall ejaculate (Geddes, 2011; J. Smith, 2008). It is also assumed that the acidic nature of prostatic fluid has bactericidal properties (Nizański, Levy, Ochota, & Pasikowska, 2014) so is part of the male urinary systems host defence mechanisms against urinary tract infections (Geddes, 2011).

Similarly to the PSA in men, a novel ELISA test developed by Odelis® can be performed to detect canine prostate specific esterase (CPSE) in dog's serum (Geddes, 2011; Lévy, Nizański, von Heimendahl, & Mimouni, 2014). CPSE is a protein that is naturally produced by the epithelial cells of the prostate glands under the influence of testosterone, and to date, this has been found in canine seminal fluid in two situations: in healthy dogs and in dogs affected by BPH (Johnston et al., 2000). When the CPSE concentration is increased it can be a biomarker of prostate enlargement in the dog (Geddes, 2011; Levy et al., 2014).

## 2.3 Histology of the Normal Prostate and BPH

### 2.3.1 Man

As described previously, the main function of the prostate gland is the production of a mucous prostatic fluid – rich in enzymes and glycoproteins – that is mixed during ejaculation with the seminal fluid. The tubuloalveolar glands, whose duct system ultimately drains into the prostatic urethra, are responsible for the production and secretion of the prostatic fluid (Mescher, 2016). These tubuloalveolar glands are composed of multiple secretory acini each consisting of secretory epithelium surrounding a central lumen and enclosed and supported by fibromuscular stromal tissue (figure 2.5) (Mescher, 2016). The fibromuscular stromal tissue (figure 2.6) consists of fibroblasts, connective tissue, smooth muscle cells, endothelial cells,

nerves and other infiltrating cells such as lymphocytes (Junqueira & Carneiro, 2005). The stromal tissue helps to move the fluid collected in lumen of the glands into the ducts and ultimately into the urethra (Mescher, 2016). A fibroelastic pseudocapsule (Epstein et al., 2011) containing smooth muscle surrounds the entire prostate and infiltrates into it through branching septa (Junqueira & Carneiro, 2005). These septa divide the gland in lobes, which are not always distinct in adults (Junqueira & Carneiro, 2005).

The secretory epithelium of the glands consists of a pseudostratified columnar epithelium with basal and glandular epithelial cell layers (Young et al., 2014). The basal cell layer, which has a stem cell function, gives rise to the glandular epithelium and it also secretes the basement membrane supporting the acini on which the epithelium lies (Young et al., 2014). The glandular epithelial layer, which rests on the basal cell layer and extends to the lumen, consists of the secretory cells responsible for production of the prostatic fluid (Young et al., 2014). It is the glandular epithelial cells that have the androgen receptors and that synthesize and secrete into the acinar lumen distinct prostate differentiation markers (e.g. PSA) (Kashefi et al., 2010). The appearance of the glandular epithelium can change based on its activity in response to varying levels of testosterone (Cormack, 2001). When testosterone levels are normal or high it appears as a pseudostratified columnar epithelium but when levels of testosterone are low it can have a simple cuboidal appearance (Cormack, 2001).

*Corpora amylacea* or prostatic concretions are structures that can range from 0.2 to 2mm in diameter and are usually seen in the lumen of the prostatic glands (Junqueira & Carneiro, 2005). These structures consist of a mixture of glycoproteins and sulfated glycosaminoglycans and can be calcified or not (figure 2.7) (Junqueira & Carneiro, 2005).

Histological alterations in men with BPH are mostly seen as a nodular proliferation of glandular and stromal elements (Epstein et al., 2011). This is referred to as stromal (figure 2.8), and glandular hyperplasia (figure 2.9) respectively (Epstein et al., 2011). Epithelial hyperplasia can predominant or a combination of epithelial and stromal hyperplasia may be seen within



these nodules (Epstein et al., 2011). The nature of the epithelium changes within BPH nodules becoming more high columnar but in some cases, it can be low columnar to cuboidal (less common) when glands are cystically dilated (Epstein et al., 2011). Also, at low power, it is possible to spot variable size and shape of glands, as well as papillary projections and newly formed duct-acinar structures (Epstein et al., 2011).

Other alterations noticed and that are common within BPH nodules are cystic changes, inflammation that can lead to duct or acinar rupture, and squamous cell metaplasia in inflamed or infarcted regions (Epstein et al., 2011).

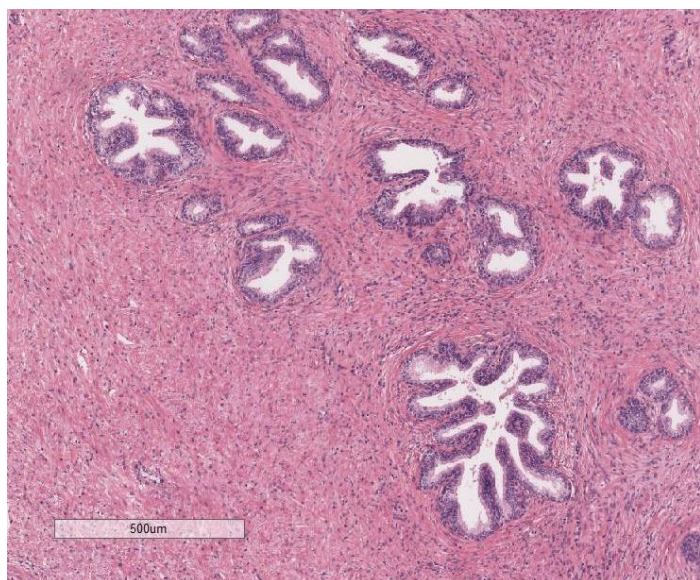


Figure 2.5. Normal prostatic tissue of a man and its tubuloalveolar glands forming lobules and being enclosed by fibromuscular stroma (X4). (Cavalca Cardoso, 2019)

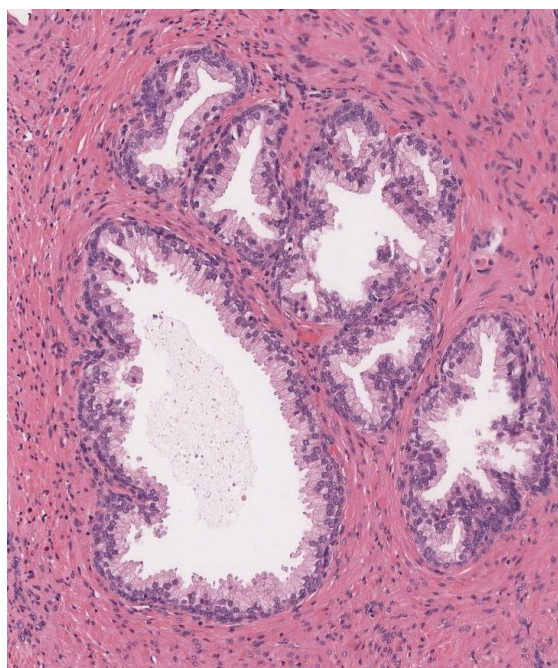


Figure 2.6. Glandular epithelium, connective tissue and smooth muscle are represented. Tissue section of a human prostate gland (X10). (Cavalca Cardoso, 2019)

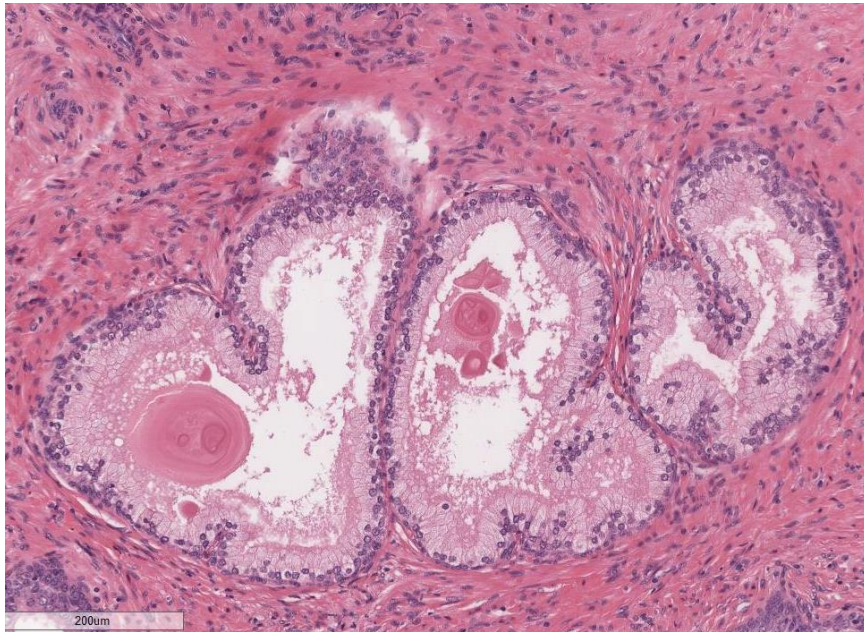


Figure 2.7. Micrograph showing corpora amylacea inside tubuloalveolar glands of a human prostate gland (x10). (Cavalca Cardoso, 2019).

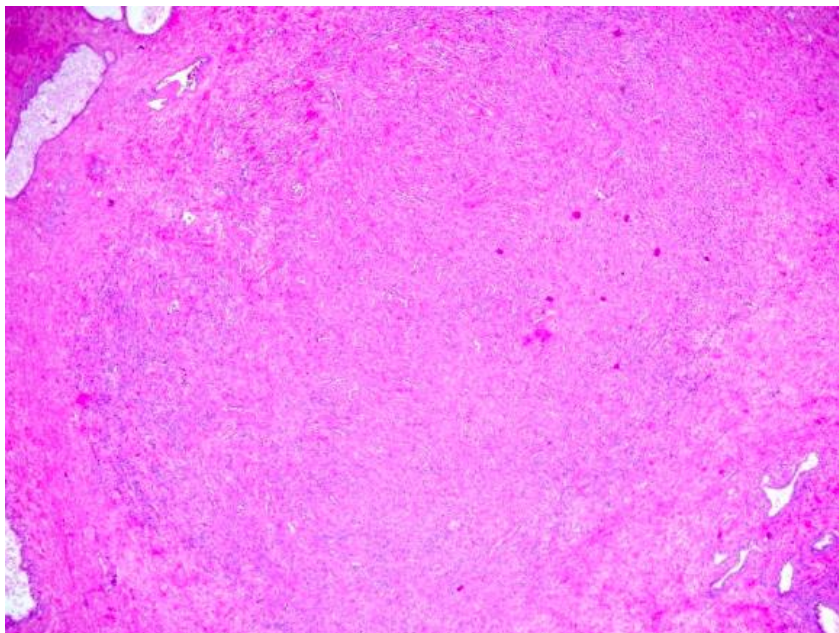


Figure 2.8. Micrograph of a stromal hyperplasia showing a fibrotic nodule in a man with BPH. Stromal nodule, a normal component of BPH, Contributed by Kenneth Iczkowski, M.D. Retrieved from PathologyOutlines.com – Prostate, benign lesions/conditions: nodular hyperplasia on September, 2018. <http://www.pathologyoutlines.com/topic/prostatenodhyper.html> Reprinted with permission.



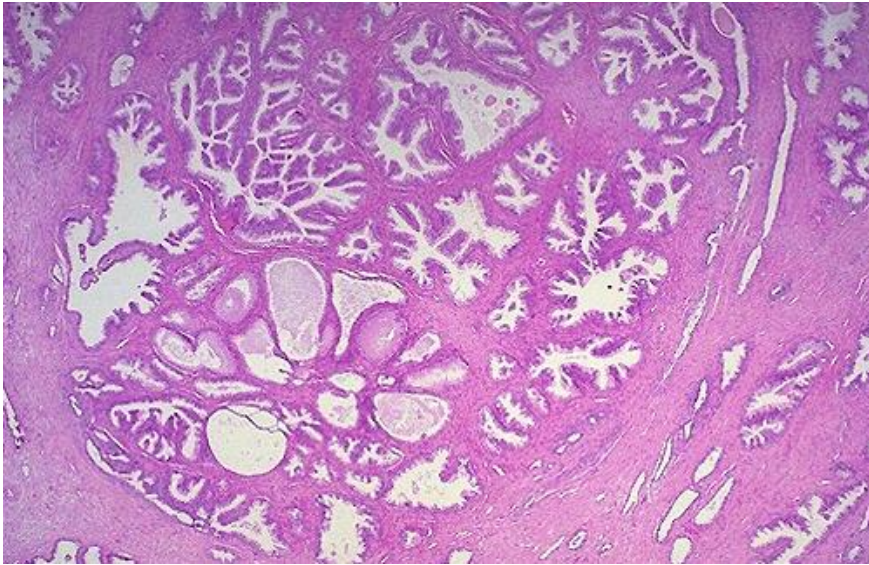


Figure 2.9. Micrograph of glandular hyperplastic nodule in a man. A large hyperplastic nodule of prostate glands. Retrieved from The WebPath® The Internet Pathology Laboratory for Medical Education, Hosted by The University of Utah Eccles Health Sciences Library - Male Genital Pathology Index, on September 2018. <https://library.med.utah.edu/WebPath/MALEHTML/MALE072.html> Reprinted with permission.

### 2.3.2 Dog

Histologically, the canine prostate gland has some similarities and differences when compared to the human prostate gland. Similar to men, the prostate of the dog contains tubuloalveolar glands composed of basal and secretory epithelial cells (Bacha & Bacha, 2012). The epithelium can be classified as a mixture of pseudostratified columnar or cuboidal cells (figure 2.10) (Bacha & Bacha, 2012; Solano-Gallego, 2010). The acini are drained by a system of branching ducts surrounded by a fibromuscular stroma that ultimately drain into the urethra (Solano-Gallego, 2010).

The prostate is surrounded by a *true* capsule of connective tissue and smooth muscle that branches into the stroma through septa that help define distinct lobules within the gland as seen in figure 2.11 (Bacha & Bacha, 2012). This is in contrast to the human prostate, which

only has a pseudocapsule. Different from other animal species, the prostatic secretion in dogs is also characterized as serous not mucous (Bacha & Bacha, 2012).

*Corpora amylacea* or concretions with the lumen of acini and ducts are uncommon in dogs, but when these structures occur they range from 1-5mm in diameter, consisting of phosphates, carbonates of calcium, urates and oxalates, and they are often moulded around organic material such as desquamated and mineralized epithelial cells (Foster, 2015).

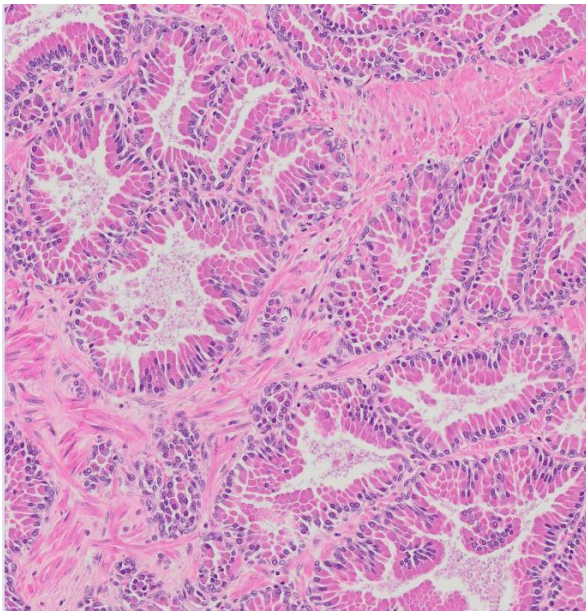


Figure 2.10. Tissue section of the canine prostate gland. The glandular epithelium is pseudostratified and contains secretion inside some acini (x10). (Cavalca Cardoso, 2019).

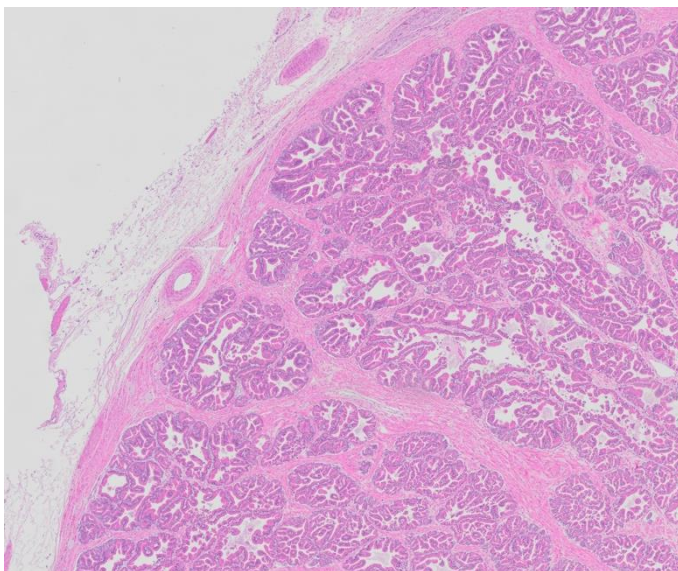


Figure 2.11. Tissue section of the canine prostate gland showing the capsule encircling the gland and the trabecula or septa originated from the capsule, dividing the gland into lobules (x4). (Cavalca Cardoso, 2019).

A comparison between a photomicrograph of the normal canine prostate gland with an *ex vivo* canine prostate obtained with PC-CT at the CLS facility at the University of Saskatchewan by our prostate research group in a previous study is shown in figure 2.12. It is possible to observe the same structures and details obtained with the photomicrograph in the PC-CT image, including the septa, urethra, stroma and glandular elements. This comparison demonstrates the high potential of this imaging modality for visualizing the internal structure of the prostate gland. Indeed, PC-CT produces images that are similar to a low power magnification of a histological slide under a microscope.

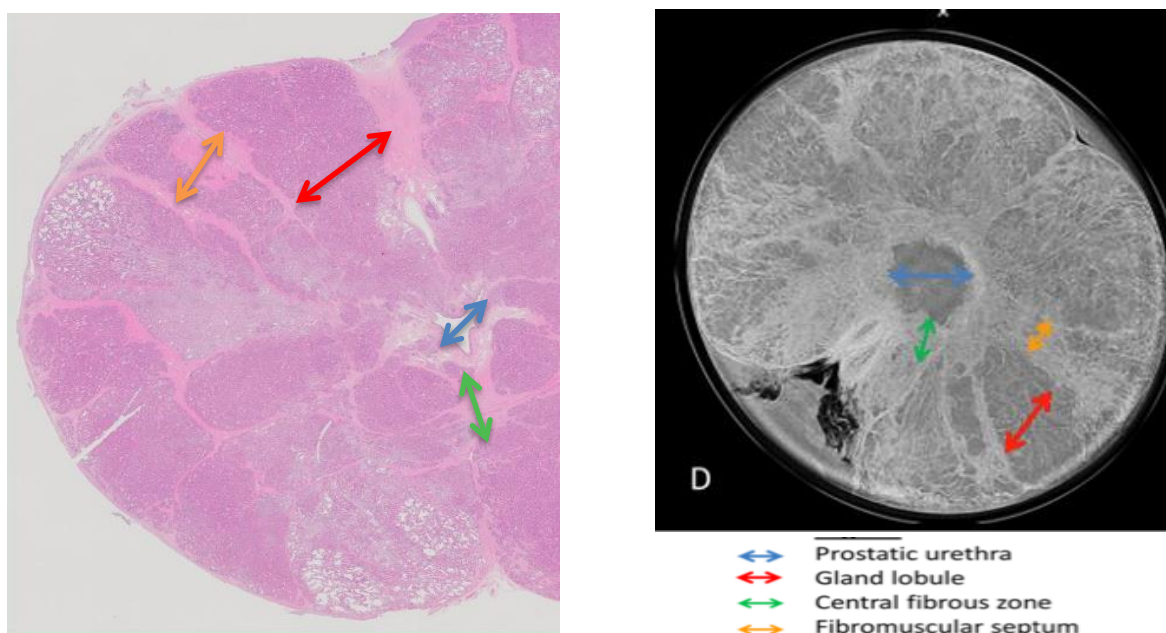


Figure 2.12. Comparison between tissue section of the normal dog's prostate gland processed by histology (left) and an image of a dog's *ex vivo* prostate (right) collected at the CLS facility with the PC-CT technique. Left image: Cavalca Cardoso, 2019. Right image retrieved from Montgomery JE, Barboza T, Pettitt M, Singh J, Snead E, Babyn P, Belev G, Wei Z, Chibbar R, Visvanathan K, Boire S, Chapman D, El-Gayed A, Buhr M, Adams G. (2013). Reprinted with permission

When BPH occurs in dogs, stromal hyperplasia, cystic dilation of the glands and squamous epithelial metaplasia can be seen (Sollano-Gallego, 2010). Squamous metaplasia of the prostatic epithelium is believed to occur in response to increased estrogen stimulation, which is believed in playing a role in the pathophysiology of BPH (Solano-Gallego, 2010).



With cystic dilation of the glands, collagen and bone in the walls can sometimes be seen to grow into and to compress the lumen of glands, and the lumen may contain fibrin debris, which is generally sterile but it can in some cases contain bacteria and lead to the formation of an abscess (Foster, 2015). In dogs with BPH, the epithelial cells of the gland also generally undergo both hyperplasia and hypertrophy leading to the formation of papillae and irregular cystic acini (figure 2.13) (Foster, 2015). An increase in the interlobular connective tissue that might even extend into the intralobular stroma can also be observed (Foster, 2015). Although these microscopic alterations can all be observed with advanced BPH, it is important to highlight that it can be challenging to differentiate a normal prostate from the dog with milder or early forms of BPH (Foster, 2015).

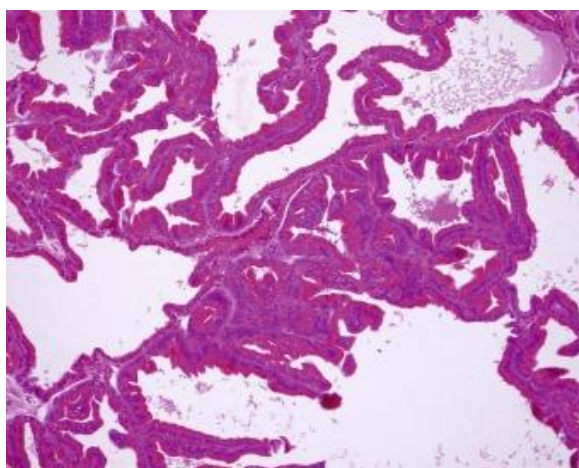


Figure 2.13. Tissue section of a canine prostate gland with BPH. Microscopic appearance of prostatic hyperplasia. Retrieved from Foster, 2015 Chapter 5 Male Genital System. In M. G. Maxie. *Jubb, Kennedy & Palmer's Pathology of Domestic Animals*. (6<sup>th</sup> ed, Vol 3) on December 2017. <https://ars-els-cdn-com.cyber.usask.ca/content/image/3-s2.0-B9780702053191000165-f005v003-055-9780702053191.jpg> Reprinted with permission.

#### 2.4 Pathophysiology of BPH

Since the early 70's, it has been known that BPH is a pathological condition seen in both man and intact dogs with advanced age (Walsh & Wilson 1976). Although some differences between the two species existed, including the distribution of the histological lesions and the symptom manifested, the dog is considered a model to investigate BPH in men

(DeKlerk et al., 1979). This stems from the fact that the disease occurs in both species with advanced age and development relies on having preserved testicles or normal and long-term exposure to sex hormones (Walsh & Wilson 1976). These shared features led to a series of experiments using dogs being performed to unravel the pathophysiology behind the development of BPH.

However, despite this and ongoing work, the pathophysiology of BPH remains not completely understood in both species (Brooks, Busch, Patanelli & Steelman, 1973). Much of the work to date has focused on understanding the role sex hormones play in the development of BPH (Brooks, Busch, Patanelli & Steelman, 1973). Specifically, the two main hormones are 5 $\alpha$ -dihydrotestosterone, which originates from irreversible intracellular conversion of testosterone within prostatic epithelial cells (McConnell, 1991) and 17 $\beta$ -estradiol, which originates from circulating testosterone that can be converted locally within the prostate stroma or in peripheral tissues, such as adipose tissue (figure 2.14) (Ajayi & Abraham, 2018; Wilson, 2011).

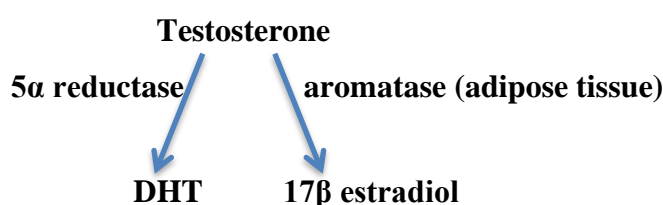


Figure 2.14. Conversion of plasma testosterone into two different hormones: 17 $\beta$  estradiol and 5 $\alpha$  dihydrotestosterone.

In men, BPH starts to develop in the region neighbouring the urethra (also called periurethral area or transition zone), and when severe resulting in a “multi-nodular process” (Brooks et al., 1973; DeKlerk et al., 1979). In contrast, BPH in dogs tends to involve the entire prostate, but consisting mainly of glandular growth (DeKlerk et al., 1979).

What follows is a brief summary of what is known about the pathophysiology of BPH in men and dogs.

#### 2.4.1 Man

As previously described, BPH refers to the proliferative process of the prostate leading to enlargement of the gland that results from an increase in the cell number and size as well as from inhibition of apoptosis (McConnell, 1991). This can lead to voiding dysfunction from urethral compression (McConnell, 1991). From a histological perspective, the proliferative process affects both the stromal and epithelial elements of the prostate but to highly varying degrees depending on the individual patient (McConnell, 1991). Pathological BPH develops in the transition zone of the prostate when there is hyperplasia in epithelial and stromal growth that coalesces into microscopic and macroscopic nodules in the prostate gland (McConnell, 1991). With enlargement, there is increased pressure from tissue expansion confined by the capsule, which may lead to compression of the prostatic urethra or bladder neck and result in LUTS (McConnell, 1991). These anatomical and functional changes may, in turn, induce significant alterations in the morphology and physiology of the urothelium and detrusor muscle, which may also contribute to the bothersome LUTS (Madersbacher, Sampson & Culig, 2019; McConnell, 1991).

Prostate tissue remodelling in the transition zone with BPH is observed by seven modification factors (Madersbacher et al., 2019) They include (1) hypertrophy of basal cells, (2) inflammation due to the altered secretions of epithelial cells and consequent calcification and clogged ducts, which leads to a (3) lymphocytic infiltration and release of cytokines (Madersbacher et al., 2019). Moreover, (4) its is observed damage of stromal and epithelial cells due to the production of oxygen free radical species; and (5) increased production of fibroblast and transforming growth factor B (TGF- $\beta$ ) leading to stromal proliferation, cellular reprogramming and extracellular matrix production (Madersbacher et al., 2019). Lastly, (6) stromal smooth muscle relaxation is decreased and adrenergic tone is increased; and (7) alteration of neuroendocrine cell function and neuroendocrine peptides occurs (Madersbacher et al., 2019).

The precise molecular etiology of BPH is complicated, poorly understood and likely multifactorial (Briganti et al., 2009; McConnell, 1991). The most important factors involved in the pathogenesis are ageing and hormonal dysregulation (Ajayi & Abraham, 2018; Madersbacher et al., 2019; McConnell, 1991). However, as mentioned previously, several additional risk factors for the development of BPH have been identified (Briganti et al., 2009). These include genetics, growth factors, inflammation, and lifestyle (Briganti et al., 2009; Lee & Kuo, 2017; Madersbacher et al., 2019). It has also been suggested that BPH comprises characteristics of a mesenchymal disease due to the presence of periurethral nodules, leading to speculation that there may be a “reawakening” of embryonic mesenchyme with BPH (Lee and Peehl 2004).

Age is recognized as a major risk factor for development of BPH and LUTS in men (Ajayi & Abraham, 2018; Lee & Kuo, 2017). With ageing changes in cellular mitogenesis and hormonal homeostasis occurs that within the prostate gland may lead to chromosomal aberration and alter normal apoptosis (Lee & Kuo, 2017; McConnell, 1991). The effect of ageing is illustrated by the increase in prostatic volume in patients (median of 58 y.o) without prostate cancer reported in men with the use of MRI; this shows a median growth rate for the prostate of 2.5% per year (Loeb et al., 2009). Ageing is also associated with inflammation and microvascular disease, which may lead to ischemia and oxidative stress, providing a favourable environment for BPH (Kyprianou, Tu, & Jacobs, 1996; Lee & Kuo, 2017). A genetic link for the development of BPH has been studied and men with early onset BPH (when it affects men < 60 yrs of age); in this subgroup the disease is thought to be a heritable possibly with an autosomal dominant inheritance pattern (Lee & Kuo, 2017; Madersbacher et al., 2019).

Sex steroid hormones, both androgens and estrogens, have been intimately linked with the development and progression of BPH (Ajayi & Abraham, 2018; McConnell, 1991). The role of androgen hormones has been the most extensively studied (Ajayi & Abraham, 2018; Lee & Kuo, 2017; McConnell, 1991). Androgens are known to have a permissive effect as they

stimulate the growth, maintenance and secretory functions of the prostate gland and their role is highlighted by the effects of removal of androgen hormones by castration or medical therapies that block the effects of androgens and lead to shrinkage of the prostate gland and resolution of signs associated with BPH (Ajayi & Abraham, 2018; McConnell, 1991).

Testosterone is the most important hormone involved in stimulating prostate growth and production of testosterone is under the control of the hypothalamic (LHRH)-pituitary (LH/FSH)-testicular (testosterone) hormone axis (Madersbacher et al., 2019). Although testosterone is the primary androgen hormone, it appears to function as a prohormone in that the most active form of the androgen in the prostate itself is dihydrotestosterone (DHT) (Madersbacher et al., 2019; McConnell, 1991). Irreversible intracellular conversion of testosterone by the enzyme 5 $\alpha$ -reductase leads to the formation of DHT (Madersbacher et al., 2019; McConnell, 1991). Increased intracellular DHT influences cell proliferation, differentiation, morphogenesis, and functional maintenance (Lee & Kuo, 2017). With ageing, the amount of testosterone in the blood will increase after puberty but then tends to remain fairly constant between the age of 25-60 (Madersbacher et al., 2019). After the age of 60, there is a steady decline in plasma testosterone concentrations seen in most men, but it is this population of men that develop signs of BPH so this cannot be the only hormone or factor involved in the pathogenesis (Madersbacher et al., 2019; McConnell, 1991).

Estrogen hormone and receptors are also known to play a role in BPH development with increased expression of estrogen receptors on epithelial and stromal cells occurring and possibly increased intracellular conversion of testosterone to estrogen within these same cells (Ajayi & Abraham, 2018; Madersbacher et al., 2019). Circulating testosterone hormone can also be converted to estrogen intracellularly through an irreversible process controlled by aromatase enzymes within adipose tissue and within the prostate (Ajayi & Abraham, 2018). With ageing in men, there is a documented change of the ratio of androgen: estrogen hormones leading to a relative increase in the concentration of estrogens (Ajayi & Abraham, 2018).



Indeed some believe that the estrogen-dominant status in men after middle age may be the most significant factor in the induction and progression of BPH (Ajayi & Abraham, 2018; McConnell, 1991). This increase in estrogen may, in turn, lead to an enhanced expression of androgen receptors by prostatic epithelial elements leading to more intracellular production of DHT (Ajayi & Abraham, 2018). Epigenetic alterations may be involved in triggering changes in estrogen receptor expression (Madersbacher et al., 2019; Ajayi & Abraham, 2018). To date, there is no clear and consistent link between other sex steroid hormones and BPH (Ajayi & Abraham, 2018).

There is evidence to suggest that inflammation is linked to the development of BPH and its associated LUTS (Madersbacher et al., 2019). This is supported by the observation of chronic inflammation coexisting with BPH histologic changes in pathologic specimens (Madersbacher et al., 2019). The degree of inflammation has also been shown to be positively correlated with both prostate volume and weight with BPH (Madersbacher et al., 2019).

Local inflammation possibly triggered by local infections, could lead to the secretion of cytokines, chemokines and growth factors associated with activation of inflammatory cells (Lee & Kuo, 2017; Madersbacher et al., 2019). As a consequence, “secondary deleterious effects” could have been noticed with the abnormal proliferation of prostatic cells (Madersbacher et al., 2019). There is also a hypothesis that prostatic self-antigens may keep inflammation and tissue damage, triggering an auto-immune response (Madersbacher et al., 2019). Important factors in this process are the prostatic stromal cells, which activate CD4+ lymphocytes and proinflammatory cytokines and chemokines, such as stromal-derived interleukin-8 (Madersbacher et al., 2019).

Several growth factors and their corresponding receptors have been identified in prostatic epithelium and stroma, which can stimulate or inhibit cell division and differentiation processes (Lee & Kuo, 2017). These include epidermal growth factor, fibroblast growth factor, and TGF- $\beta$  to name a few (Lee & Kuo, 2017). Activation of these growth factors alone or in

combination can induce stromal cell growth, followed by significant tissue remodelling, leading to prostate enlargement (Lee & Kuo, 2017).

Results from multiple pre-clinical and clinical studies indicate that several age-related metabolic aberrations (metabolic syndrome, obesity, dyslipidemia, hypertension and diabetes) influence both the development and the progression of BPH in men (Briganti et al., 2009; Lee & Kuo, 2017; Madersbacher et al., 2019). Metabolic syndrome and its related comorbidities, including sex steroid alterations and low-grade inflammation, have been related to BPH development and progression (Lee & Kuo, 2017; Madersbacher et al., 2019). In one study obese (BMI > 35 kg/m<sup>2</sup>) men had a 3.5-fold increased risk of prostate enlargement compared to non-obese (BMI < 25 kg/m<sup>2</sup>) men (Madersbacher et al., 2019). Most established aspects of the metabolic syndrome have also been linked to BPH development (Madersbacher et al., 2019). The underlying pathophysiologic mechanisms involved in the association of metabolic factors with BPH are not completely understood, but systemic inflammation, pelvic ischemia and increased sympathetic activity may play a role (Madersbacher et al., 2019). Heavy smoking, low physical activity, and high protein intake can also substantially alter the risks of symptomatic BPH and LUTS (Lee & Kuo, 2017; Madersbacher et al., 2019).

#### 2.4.2 Dog

Most of the studies in dogs with BPH have been done to understand the disease in men. This has been based on the assumption that the pathogenesis is similar in both species (Wilson, 1980). Before designing their experiment in 1976, Wash and Wilson had tried to induce BPH in dogs with just the administration of testosterone or DHT with no success, and then went on to further investigate the synergistic role of estradiol and androstenediol and were successful in inducing BPH (Wash & Wilson, 1976). Walsh and Wilson, 1976 developed different protocols for induction of BPH using five experimental groups (shown in table 2.1). Before the beginning of the study, the dogs all had a DRE performed and had 3D measurements of their prostate

glands taken following laparotomy to allow calculation of the individual dog's prostate gland volume. Using a derived nomogram, this also allowed an estimate of the prostate gland weight to be determined. Following this, all animals were neutered. Five experimental groups were formed with dogs assigned to groups according to their prostate size (group I n=3, group II n=5, group III n=5, group IV, n=5, group V n=3). Four groups had a normal prostate size and one group (group V) had evidence of prostatic enlargement consistent with early BPH at the outset of the study. Following this, each dog received 1mL of an intramuscular injection of a specific hormone cocktail three times per week for 12 months. The specific hormone cocktails that the different groups received were as follows: control group I received triolein (an oily solution without any anti-androgenic or androgenic effect in the prostate), group II received androstenediol alone, group III DHT plus estradiol and group IV and V with normal and evidence of early BPH at the time of castration received androstenediol plus estradiol. Measurements of the prostates were assessed twice during the study at 6 months intervals via laparotomy (same 3D measurements used to determine volume and estimate weight). At the end of the study when the animals were euthanized the prostate glands were then harvested, weighed and submitted for histological analysis.

As shown in table 2.1, [Walsh and Wilson, 1976](#) concluded that androstenediol alone or in combination with estradiol produced superior results with respect to inducing BPH leading to an increase in the weight of the prostate gland; DHT in combination with estradiol in the castrated dog did not produce any substantial change.

Table 2.1. A study of the administration of different steroid hormones to dogs and the changes on their prostate weight. Five different groups were created (group I to V) and the prostate was then collected after 12 months of hormone induction, weighed and compared with its initial weight (Walsh & Wilson, 1976).

Group	Initial condition	Treatment	Average weight (g) change
I - control (castrate)	Normal	Triolein	6.9
II - castrate	Normal	Androstanediol	10.1
III - castrate	Normal	Dihydrotestosterone plus estradiol	-0.9
IV - castrate	Normal	Androstanediol plus estradiol	31.2
V- castrate	Early prostatic hypertrophy	Androstanediol plus estradiol	38.9

In another study, DeKlerk et al., 1979 used beagles and administered different hormone combinations in order to induce BPH in dogs. Similar to what Walsh and Wilson, 1976 did, the prostate measurements were assessed via laparotomy, the volume calculated and a nomogram used to estimate the weight. As shown in Table 2.2 two main experimental groups were created – castrated dogs and intact dogs – along with subgroups within these based on which hormone protocol was administered. One month after castration was performed, treatment with the different hormone protocols started for each group with 1 mL of each hormone preparation being administered intramuscularly three times per week for four months (DeKlerk et al., 1979). According to the authors (table 2.2), BPH induction was successfully induced and confirmed not just by an increase in the prostatic weight, but also by the high incidence of histological identification of glandular hyperplasia at the end of the study in groups of intact and castrated dogs that received either androstanediol or DHT alone or in combination with estradiol. The findings by DeKlerk et al, that dogs developed BPH with the administration of DHT and estradiol or just DHT alone are in opposition to the work of Walsh and Wilson 1976. The disparities between those two studies might be related to differences such as age and

breed of dogs used, hormone preparation or castration style (Walsh and Wilson (1976) did not remove the epididymis of the dogs while DeKlerk et al. (1979), did) (DeKlerk et al., 1979).

Table 2.2. A study of steroid hormones given to dogs and the effects on the prostate weight and its histological features. Dogs were assigned into two main groups – castrated and intact dogs – and within these groups eight subgroups received different hormonal treatments. After four months of hormone protocol induction, the glands were removed and evaluated (DeKlerk et al., 1979).

Group	Hormone treatment	Change in weight %	Number of dogs with hyperplasia/ total dogs in the group
Castrate	Control (triolein)	-70	0/6
Castrate	Testosterone	120	0/5
Castrate	Dihydrotestosterone	181	Glandular 1/5
Castrate	Androstanediol	171	Glandular 1/5
Castrate	Estradiol	-13	0/5
Castrate	Estradiol plus Testosterone	138	Glandular 1/5
Castrate	Estradiol plus Dihydrotestosterone	508	Glandular 4/5
Castrate	Estradiol plus Androstanediol	451	Glandular 6/6
Intact	Control (triolein)	41	Glandular 1/6
Intact	Testosterone	199	Glandular 2/5
Intact	Dihydrotestosterone	291	Glandular 4/5
Intact	Androstanediol	258	Glandular 4/5
Intact	Estradiol	18	0/5
Intact	Estradiol plus Testosterone	120	0/5
Intact	Estradiol plus Dihydrotestosterone	377	Glandular 4/5
Intact	Estradiol plus Androstanediol	501	Glandular 5/5

In conclusion, dogs are in fact the only species apart from men known to naturally develop BPH. As seen above, researches were conducted in order to explore this common

characteristic shared by both species. BPH is a disease that spontaneously affects intact male dogs, although the majority of affected dogs do not develop clinical signs (J. Smith, 2008). The disease can be manifested in different ages, but has been reported in dogs as early as 2 to 3 years of age (DeKlerk et al., 1979). However, this would be unusual and it is more common that BPH develops in older intact old dogs; some reports put the incidence at more than 80% in dogs over 5 years of age (Johnston et al., 2000) and more than 95% for dogs older than 9 years of age (J. Smith, 2008). The disease in dogs is characterized by hyperplasia (cell number augmentation) and hypertrophy (cell size augmentation) (J. Smith, 2008), which affects both stromal and glandular components (Johnston et al., 2000) with less stromal involvement potentially than in men with BPH and the disease occurs as a uniform or diffuse manor rather than more commonly in the glandular region around the urethra unlike in men (DeKlerk et al., 1979; Nizanski et al, 2014).

Although the experiments using dogs and steroid hormones in the 80's were extremely important to investigate the induction of prostatic hyperplasia in the dog prostate, the pathogenesis of the BPH is still unknown. There is indeed a change of the ratio of androgen: estrogen hormones that occurs with aging and an increase in the concentration of estrogen enhances the expression of androgen receptors leading to more intracellular production of DHT (J. Smith, 2008). These studies have concluded and accepted that BPH is at least in part the result of an increase in the hormone DHT in the gland (Johnston et al., 2000; Wilson, 1980). In fact, BPH is a common disease of our era in ageing men and a conclusive and early diagnosis is important for the correct treatment, which will lead to a better quality of life for the patient. This will be possible with the advancement of research and new discoveries regarding hormones and receptors' participation in our body.

## 2.5 Diagnosis of BPH

### 2.5.1 Men

The diagnosis of BPH is typically established when men present for lower urinary tract symptoms (LUTS) and following a medical work-up to eliminate other potential differential etiologies (Pearson & Williams, 2014). Diagnosis relies on documentation of compatible clinical symptoms along with supportive findings of an enlarged prostate on a DRE and then either a positive response to therapy or evidence from further diagnostic testing, including potentially biopsy of the prostate or medical imaging, to rule out other potential causes and confirm BPH (Pearson & Williams, 2014). During the physical examination, the Canadian Urological Association recommends DRE as an important tool for assessing the prostate gland size, shape and symmetry, although it must be stressed that the DRE only provides a subjective evaluation of the gland (Vuichoud & Loughlin 2015). It is important to mention that BPH is often diagnosed based on clinical signs and that in the majority of cases a histological diagnosis is not obtained prior to attempting treatment. This would be the case in the majority of patients unless there is a family history of PCa or other reasons to be suspicious of PCa based on the initial findings (Epstein et al., 2011).

The history for patients with BPH typically reveals signs of lower urinary tract symptoms (hematuria, dysuria, stranguria, pollakiuria) and possibly sexual or erectile dysfunction (Vuichoud & Loughlin, 2015). The onset, duration of symptoms must be considered as well as the use of any medications that could cause LUTS (Vuichoud & Loughlin, 2015). Other diseases affecting the bladder, prostate, and urethra may also need to be ruled out (Vuichoud & Loughlin, 2015).

The tests that are recommended for a patient that presents with symptoms suggestive of BPH include determination of a blood PSA, a urinalysis, performed to investigate hematuria, proteinuria or leukocyturia and a urine culture to rule out prostatitis or cystitis as a cause of LUTS (Nickel, Méndez-Probst, Whelan, Paterson, & Razvi, 2010). In cases where the diagnosis

is unclear and a DRE indicates abnormalities of the prostate or drug treatment has failed, then further investigation including use of medical imaging and biopsy of the prostate is indicated (Nickel et al., 2010).

Table 2.3. Classification of LUTS in men into three categories according to the patient's symptoms (Vuichoud & Loughlin, 2015).

VOIDING SYMPTOMS	STORAGE SYMPTOMS	POST MICTURIATION SYMPTOMS
Urinary reluctance, delay in initiating micturition, intermittency, weak urinary stream and dysuria	Correspond to urinary frequency, nocturia, urgency with or without incontinence	Sensation of incomplete voiding, and/or postmicturition dribbling

Some examples of differential diagnosis for LUTS in men are BPH, bladder calculi, diabetes mellitus, use of medications such as anticholinergics or diuretics, prostate cancer, prostatitis, and urinary tract infection (Pearson and Williams, 2014).

### 2.5.2 Dog

The diagnosis of BPH is typically based on compatible findings and also detection of an enlarged prostate on DRE performed as part of the physical examination (Williams, 2013). Although the disease can be clinically silent, a common sign of BPH in dogs typically result from the enlargement of the prostate gland causing compression of the colon leading to faecal tenesmus; hematuria and urinary infections are may be also observed (Williams, 2013). Dogs with BPH are rarely systemically sick, but can be if they develop secondary prostatitis or prostatic abscesses or PCa. In such cases, it will be observed bloody discharge from the prepuce and/or hematospermia (genitourinary tract), stiffness and/or lameness (locomotor) and systemic



compromise such as pain and anorexia (Lévy et al., 2014; Nizański et al., 2014; Williams, 2013). Dysuria is uncommon in dogs, contrarily to humans with BPH (Nizański et al., 2014).

The physical examination is important to differentiate BPH from other prostatic diseases (J. Smith, 2008). DRE is an easy and quick exam that assesses the position, size and symmetry of the gland as well as allowing evaluation for any evidence of pain associated with palpation (Lévy et al., 2014). As in people, the DRE is subjective and not highly sensitive for detecting early prostatic disease or specific for differentiating enlargement caused by BPH versus other disorders (e.g., prostatitis or PCa) (Lévy et al., 2014). A normal prostate on DRE should be smooth, nonpainful, symmetrical and the dorsal median groove should be easily appreciated (J. Smith, 2008). With BPH, the enlarged prostate may not be palpable per rectum if it is large enough that it has moved from the pelvic canal into the abdominal cavity (Lévy et al., 2014). It is also important to appreciate that a DRE is an insensitive technique in extremely large breeds where it may not be possible to palpate the prostate *per rectum* (Lévy et al., 2014).

Depending on preliminary findings, further investigation of the prostate may be required (J. Smith, 2008). This could include routine medical imaging of the prostate by radiography and ultrasonography, along with cytology and microbiology of the prostatic fluid if indicated (J. Smith, 2008).

Concurrent nonseptic or septic prostatitis, associated with either gram positive or negative bacteria, can be diagnosed in cases of BPH due to disruption of normal host defence mechanisms from the damage to the normal function and alteration of the glandular structure that occurs (Nizański et al., 2014). Concurrent prostatitis can be classified as chronic or acute inflammation (Lévy et al., 2014). With development of BPH, intraprostatic cysts may form (Lévy et al., 2014). These are generally characterized as small and multiple or large and singular; uncommonly they may show bacterial contamination (Lévy et al., 2014).

Investigation of serum CPSE (canine secretory prostatic esterase) can be performed with an ELISA kit (Odelis®) (Williams, 2013). Increased level of CPSE is a biomarker for BPH

(>61ng/mL) and this test has a high sensitivity and specificity for the diagnosis of BPH (Lévy et al., 2014). Unfortunately, this test is not commercially available. Currently it is manufactured in France and needs to be imported by other countries (Johnston et al., 2000) resulting in untimely delays.

## 2.6 Biopsy of Prostate Gland

### 2.6.1 Man

When a patient has an enlarged prostate on DRE with abnormal features, a high PSA (adjusted to the age of the patient) and the cause of the prostatic enlargement remains unclear, more invasive techniques, such as biopsy, are needed to definitively differentiate BPH from PCa (Singh et al., 2013). In men there are three prostatic biopsy techniques that can be performed with transrectal guided ultrasound (TRUS) to rule in or rule out PCa; these include the sextant, the extended and the saturation biopsy techniques (figure 2.15) (Shah & Ming, 2012). These different techniques vary based on the number of cores collected (six, twelve and average of twenty-four respectively), the approach (paramedian and or lateral via transrectal versus transperineal route) and the need for anesthesia (see table 2.4) (Shah & Ming, 2012). The disadvantages often associated with a biopsy of the prostate are more highly correlated with either the sextant technique, which can present a high false negative rate or the saturation technique, which requires general anesthesia (Shah & Ming, 2012).

In order to avoid repeated biopsies to determine the progression and growth of a low risk and low-grade PCa, active surveillance involving close monitoring with imaging or PSA instead of repeated biopsies and/or attempting only focal therapy have been proposed as potential alternatives (Ukimura, Hung, & Gill, 2011). Most of the times in questionable cases repeated biopsies are performed to determine the progression and growth of PCa, but there can be an inconsistency between initial and follow-up biopsies (Ukimura et al., 2011). Generally,

the patient is not anesthetized to undergo the biopsy, and the preparation/recommendations can be variable amongst different urologists, including whether or not to provide post-biopsy analgesia, differences in whether an antibiotic is prescribed post-procedure and indeed differences in the number of biopsy cores performed (Davis, Sofer, Kim, & Soloway, 2002). Besides the pain and discomfort that deter some patients from undergoing repeat biopsy procedures (Acher, P., & Dooldeniya, M. 2013), there is also a risk of other possible complications from the biopsy including septicemia, hematuria and urinary retention (Singh et al., 2013). There is a need to improve the accuracy of current biopsy techniques (Ukimura et al., 2011). This could include the use of real time 3D imaging to allow precise targeting of lesions or areas of the prostate translating to increased accuracy and sensitivity and quality of life to the patient (Ukimura et al., 2011).

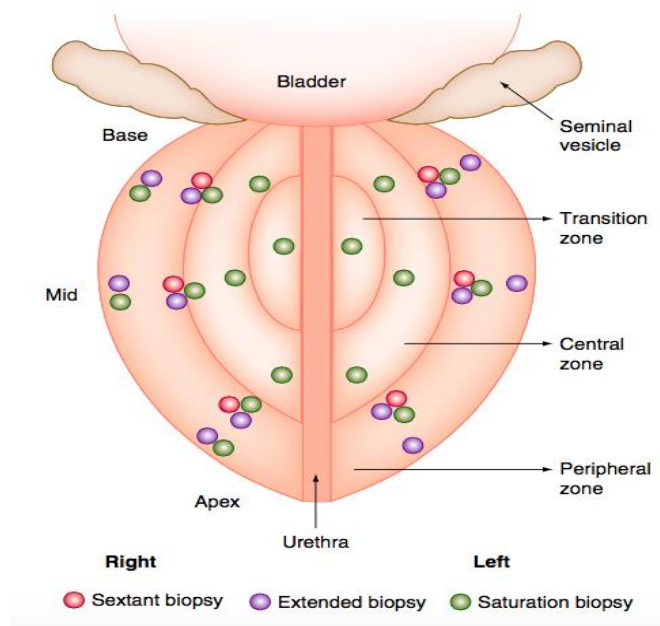


Figure 2.15. Illustrative comparison between three biopsy techniques for prostate cancer in men: sextant, extended and saturation biopsy. Retrieved from Shah and Ming, 2012, Prostate needle biopsy sampling techniques: Impact on pathological diagnosis. *Prostate biopsy interpretation: An illustrated guide*, on August, 2017. [https://link-springer-com.cyber.usask.ca/chapter/10.1007/978-3-642-21369-4\\_2](https://link-springer-com.cyber.usask.ca/chapter/10.1007/978-3-642-21369-4_2) Reprinted with permission.

Table 2.4. Comparison between three biopsy techniques for detection of prostate cancer (Shah & Ming, 2012).

Technique	Definition	Approach	Disadvantages
Sextant biopsy	Six cores from base, mid, apical paramedian parasagittal/ regions bilaterally of the prostate	Paramedian, via transrectally	False negative rate
Extended biopsy	Twelve core biopsy (sextant plus six lateral cores of the prostate on both sides)	Paramedian and lateral, transrectally	None
Saturation biopsy	More than fourteen cores (average 24) beginning laterally towards the median part of the gland bilaterally	Paramedian and lateral, via transrectal or transperineal method	General anesthesia, long time procedure (more than 1h).

## 2.6.2 Dog

The histological examination of a prostatic biopsy remains the gold standard test to determine what disease processes is causing enlargement of the prostate in dogs as for men (J. Smith 2008; Williams, 2013). In dogs, biopsy is generally performed when less invasive testing, such as fine-needle aspirate for prostatic cytology does not yield a diagnosis or when initial therapy for presumed BPH to reduce the size of the prostate does not resolve the clinical signs (J. Smith 2008; Kustritz, 2006). Biopsy samples can be obtained percutaneously (via a perirectal or transabdominal approach) or at surgery (J. Smith 2008). Although more invasive, culture of a biopsy sample rather than an aspirate from the prostate is a more accurate technique for definitively diagnosing or ruling out prostatitis (Kustritz, 2006).

A minimum sedation and local anesthesia are required to permit prostatic biopsy (J. Smith 2008). Simultaneous digital rectal palpation is used to guide perirectal biopsy whereas ultrasonography is used to guide biopsy done by a transabdominal approach (J. Smith 2008). A

surgical biopsy is commonly performed during an exploratory laparotomy or by laparoscopy using either a Tru-Cut needle or by performing a wedge resection from one of the prostatic lobes (J. Smith 2008).

Complications such as hematuria secondary to urethral damage (typically lasts for less than 4 days duration post biopsy), hemorrhage or infection can occur (Kustritz, 2006; J. Smith, 2008). Hemospermia may also be seen post procedure (Kustritz, 2006). A biopsy is contraindicated if the animal has a suspected prostatic abscess or if they have acute prostatitis due to the risk of seeding the infection along the needle tract or into the abdomen (Lévy et al., 2014; J. Smith, 2008). Prostatic biopsy samples should be submitted to a veterinary pathologist for interpretation (Kustritz, 2006; J. Smith, 2008).

## 2.8 Treatment of BPH

### 2.8.1 Man

Based on the severity of the symptoms and the degree of discomfort shown by a patient with BPH, the therapeutic decision is made based on the patient/physician preference following a discussion of the different treatment options (Nickel et al., 2010). To help objectively assess the extent of the patient's symptoms, the use of a "formal symptom inventory" clinical scoring system is recommended. The two most commonly used by physicians include the International Prostate Symptom Score (IPSS) or the American Urological Association (AUA) Symptom Index (Pearson & Williams, 2014). This is done at the time of initial presentation and at follow-up to allow a more objective assessment of the patient's response to treatment (Pearson & Williams, 2014).

Medical intervention is not required when patients have mild symptoms (IPSS <7 or AUA <7) where there is little or no impact in the patient's quality of life (McVary et al., 2011; Nickel et al., 2010; Pearson & Williams, 2014). Lifestyle changes such as weight loss,

decreasing in fluid intake during the evening, avoidance of alcohol, caffeine and restriction of medications that can cause LUTS may be effective for managing symptoms in mild cases (Nickel et al., 2010). Further intervention including medications and surgery are recommended when there is a moderate (IPSS 8-18 or AUA 8-19) to severe (IPSS 19-35 or AUA 20-35) state of BPH with bothersome symptoms (Pearson & Williams, 2014).

The most commonly used medications for treating BPH include 5-alpha reductase inhibitors, alpha-blockers, and anticholinergic agents (McVary et al., 2011; Nickel et al., 2010; Pearson & Williams, 2014). Examples of 5-alpha reductase inhibitors used for the treatment of BPH include dutasteride and finasteride (Nickel, 2006). These drugs block the enzyme 5-alpha reductase, impeding the conversion of testosterone to DHT, resulting in lower serum PSA levels, a reduction of the prostate size thus reducing the risk for progression of BPH and possibly eliminating the need for surgical intervention (Pearson & Williams, 2014). Adverse effects related to the use of 5-alpha reductase inhibitors include ejaculation disorder, erectile dysfunction and diminished libido (Nickel, 2006).

Alpha-blockers are used to provide relief from LUTS symptoms in patients with BPH (Nickel et al., 2010). They act by blocking alpha-1 receptors in the urethra and bladder leading to smooth muscle relaxation (Tanguay et al., 2009). They do not prevent progression of BPH as they do not influence hyperplasia but do reduce the severity of the LUTS (Nickel et al., 2010). Of the different alpha-blockers available the most recommended include alfuzosin (selective), tamsulosin (selective), doxazosin (non-selective) and terazosin (non-selective) (Tanguay et al., 2009). Side effects of alpha blockers include orthostatic hypotension and dizziness (McVary et al., 2011; Nickel, 2006).

In some patients with severe LUTS and significant prostatic enlargement combination therapy with an alpha-blocker and 5-alpha reductase inhibitor is recommended (McVary et al., 2011; Nickel, 2006; Tanguay et al., 2009). This is because when compared to either single

monotherapies, dual therapy has been shown to lead to a greater improvement in symptom score and urinary flow (McVary et al., 2011; Nickel, 2006; Tanguay et al., 2009).

Anticholinergics can be used in association with alpha-blockers in cases where patients with BPH develop bladder outlet obstruction (blockage at the base of the urinary bladder) and associated bladder detrusor muscle hyperactivity (Nickel et al., 2010). Anticholinergic agents (e.g., Tolterodine, Solifenacin) block the effects of acetylcholine on muscarinic receptors in the bladder wall, leading to decreased bladder contractions (Pearson & Williams, 2014). These drugs also help to alleviate irritative LUTS symptoms, resulting in a reduction in the symptom score (Pearson & Williams, 2014).

Surgical options for the treatment of BPH include transurethral resection of the prostate (TURP) as well as minimally invasive therapies (Nickel et al., 2010). TURP is the standard therapy for patients who either fail medical therapy or who develop “BPH-related complications” such as recurrent cystitis or prostatitis, hematuria, urinary retention and bladder calculi (Nickel et al., 2010; Pearson & Williams 2014). Among the minimally invasive surgical therapies (MIST), transurethral microwave therapy (TUMT) and transurethral needle ablation (TUNA) are options but are currently not available in all facilities (McVary et al., 2011). TUNA is a therapeutic option that reduces the chances of retrograde ejaculation and is considered for patients that desire maintenance of sexual function (Nickel et al., 2010). TUMT is recommended only for patients with moderate symptoms where the prostate gland is only moderately enlarged, and for those desiring a less invasive therapy compared to TURP (Nickel et al., 2010). The downside of TUNA compared to TURP is that it is a less effective treatment (Nickel et al., 2010).

### 2.8.2 Dog

The goal of any treatment for BPH is to reduce the size of the prostate to ameliorate the symptoms correlated with the disease (Johnston et al., 2000). The easiest and most effective

treatment is surgical castration; this is indicated when the affected dog is not intended for breeding (Johnston et al., 2000). If the male dog is intended for use in a breeding program, pharmacological treatment is typically chosen (Nizański et al., 2014). The treatment in this case is focused on either preventing androgen production or blocking its action to achieve a decrease in prostatic size (Nizański et al., 2014). However, pharmacological therapies should be avoided in cases of suspected concurrent prostatic and/or testicular neoplasia (Nizański et al., 2014). Progestagens, inhibitors of 5 $\alpha$ -reductase, inhibitors of steroid receptors, estrogens and antiestrogens are examples of medications that can also be used in the treatment of BPH in dogs (Nizański et al., 2014).

Progestagens reduce the testosterone concentration due to its anti-androgenic action through negative feedback at the level of the hypothalamus (Nizański et al., 2014). This class of drug may be selected when short duration and low cost therapy is required (Nizański et al., 2014). Medroxyprogesterone acetate and megestrol acetate are examples of progestogens used to treat BPH that do not adversely affect semen quality or libido (Nizański et al., 2014). They can, however, both affect spermatogenesis when administered at high doses (Nizański et al., 2014). Synthetic progestins may cause other adverse sequelae such as development of diabetes mellitus, inducing mammary hyperplasia, and development of iatrogenic hyperadrenocorticism (Johnston et al., 2000; J. Smith 2008; Nizański et al., 2014). Because of these potential side-effects and the availability of safer option, progestogens are rarely used today for the treatment of BPH in dogs (Johnston et al., 2000; J. Smith 2008).

As in humans, inhibitors of the 5 $\alpha$ -reductase enzyme, such as Finasteride, which block the pathway that converts testosterone to DHT are also used for treating BPH and today would be the most commonly used medical therapy (J. Smith, 2008). This drug leads to a decrease in semen volume, but it does not affect serum concentrations of testosterone or have any adverse effects on the testis histology or semen quality in dogs (Johnston et al., 2000).



Competitive inhibitors of the testosterone receptor such as osaterone acetate (OA) indirectly inhibit the action of 5 $\alpha$ -reductase by reducing its substrate (Nizański et al., 2014). This class of drug does not affect the testes and does not demonstrate side effects when used at an appropriate dose (Nizański et al., 2014). These drugs will lead to a reduction in testosterone levels in the serum (Nizański et al., 2014). Flutamide is an example of a drug used for treating BPH in this class; although flutamide has been used without negative effects on semen quality or libido, it is not approved for veterinary use in some countries (Nizański et al., 2014). Still in this category, GnRH agonists, such as deslorelin and nafarelin, have also been used to treat BPH by stimulating the production and release of gonadotrophins from the pituitary (Nizański et al., 2014). When given in high doses, after an initial stimulating period, they inhibit the pituitary-gonadal axis and result in a decrease in secretion of the hormones luteinizing hormone (LH) and follicle stimulating hormone (FSH), and ultimately lead to a reduction in testosterone and effectively induce pharmacological castration (Nizański et al., 2014).

Estrogen therapy (e.g. diethylstilbesterol) suppress the hypothalamic-pituitary-gonadal axis resulting in a reduction in the size of the prostate gland by decreasing the concentration of testosterone in the blood (J. Smith, 2008). However, the use of estrogens for the treatment of BPH is no longer recommended because of the potential serious and life-threatening adverse side effects (J. Smith 2008; Nizański et al., 2014). These include bone marrow suppression leading to thrombocytopenia, leukopenia and aplastic anaemia, and promotion of squamous metaplasia of the prostatic epithelium resulting in cyst formation that can predispose to prostatitis (Johnston et al., 2000; Nizański, et al., 2014).

Anti estrogen drugs have also recently been used to treat BPH in dogs (Nizański et al., 2014; Corrada et al., 2004). Tamoxifen is an example, which is classified as type I anti estrogenic compound, demonstrating both agonist and antagonist effects (Nizański et al., 2014; J. Smith, 2008). In a small trial, the oral use of tamoxifen in seven intact beagles with BPH for

28 days lead to a significant decrease in serum testosterone concentrations, ejaculate volume and volume of the prostate (Corrada et al., 2004). In a second study with normal dogs and dogs with BPH where tamoxifen was administered for a longer period of time (60 days), administration resulted in close to a 30% reduction in the size of the prostate gland in the dogs with BPH (Gonzalez et al., 2009). Side effects such as decreased in the testicle size and the semen quantity and quality have been noted, but are considered minimal and further studies are indicated (J. Smith, 2008; Nizański, et al., 2014).

## 2.9 Imaging the prostate

Some of the medical imaging modalities that are used in both human and veterinary medicine to investigate prostatic disorders include radiography, ultrasonography and computed tomography. MRI and PET-CT are not common in routine use in veterinary medicine for investigation of prostatic disease due to cost and availability. In human medicine, the use of such advanced imaging is more commonly employed and is the subject of considerable research. Lastly, PC-CT, a new medical imaging modality, is not in routine use in either veterinary or human medicine but offers some exciting possibilities for the future. In the following sections, the discussion of the various imaging modalities focus on their use in dogs, but where there is minimal clinical experience, this is based on their application for investigating prostatic disease in men.

### 2.9.1 Radiographs

The discovery of X-rays by Wilhelm C. Roentgen in 1895 was an innovative and historical landmark in medicine and led to the first Nobel Prize in Physics' being bestowed in

1901 (Panchbhai, 2015). Since their discovery, X-rays have been largely used in medicine as an important diagnostic tool (Brown, 2013).

X-rays are a combination of electric and magnetic fields, thus characterized as electromagnetic radiation, with wavelengths ranging from 0.01 to 10 nanometers and energy ranging from 100eV to 100keV (Thrall & Widmer, 2018). X-rays are classified as soft X-rays and hard X-rays depending on the energy and wavelength range being used (Attwood, 1999). Hard X-rays have high energy (above 10keV) and low wavelength (below 0.1nm) and are largely used in medical imaging (Attwood, 1999). On the other hand, soft X-rays have low energy (below 5keV) and high wavelength (above 0.2nm) and are not used in medical imaging (Attwood, 1999).

The production of X-rays inside of an evacuated X-ray tube occurs due to electron interactions (Bushberg et al., 2002). In the tube, there is a source of electrons (cathode) and the target of electrons (anode); between these a voltage or electric potential difference is applied, leading to the movement of electrons from cathode (negatively charged) to the anode (positively charged) (Bushberg et al., 2002). In this way, the kinetic energy of the electrons is converted into electromagnetic radiation (Bushberg et al., 2002).

When X-rays interact with matter, the following events happen depending on the nature of the object being imaged: some X-rays are absorbed, some X-rays are deflected or scattered and some pass through the object (Hoffmann, 2010). When an X-ray beam passes through a body, different types of tissue will absorb or allow them to penetrate them to a variable degree, and X-rays can be reflected or refracted at the interface between different mediums (air to body) or at the interface between different types of tissues (Thrall & Widmer, 2018). For diagnostic radiology, image formation is dependent on the differential absorption and scattering of X-rays by different types of tissues within the body (Aichinger, Dierker, Joite-Barfuß & Säbel, 2012). Attenuation is a measure of the differential absorption and scattering of X-rays by different tissues (Aichinger et al., 2012).

In the clinic, radiography involves generation of 2D images – radiographs – are collected with the use of photographic film or a digital detector when X-rays that exit the tube and hit the patient (Thrall & Widmer, 2018). X-rays interact differently with the internal structures of the body due to the different densities of the organs (Thrall & Widmer, 2018). Dense tissues such as bone block radiation and appear white, whereas less dense tissue such as fat or air allows more radiation to pass through and hit the film and appear as grey or black (Kealy, McAllister & Graham, 2011). Radiographs consist of an image of the internal parts of a patient in shades of black and white (Thrall & Widmer, 2018). It is the inherent and variable property of different tissues that results in differing attenuation characteristics (Aichinger et al., 2012).

Because there are risks associated with the exposure to X-rays, it is necessary to measure the degree of radiation exposure; this is done by quantifying both the absorbed dose and the effective dose (Zaer, Amini & Elsayes, 2014). Gray (Gy) is the unit that defines absorbed dose or, in other words, the amount of radiation that is absorbed by the total volume of a certain tissue (J/kg) mass (Zaer et al., 2014). Sievert (Sv) is the unit used to measure the effective dose, and it is a measurement that provides information related to biological effects that follow radiation exposure (Zaer et al., 2014). It is calculated based on a weighting factor for each tissue that is multiplied by the absorbed dose, reflecting the chances of developing stochastic damage to cells of a certain tissue type (Thrall & Widmer, 2018). So even if the absorbed dose for two different tissues is the same, they can have different effective doses (Zaer et al., 2014).

Although radiographs for dogs have limited use for diagnostic purposes for prostatic disease, they do allow the visualization of the size, shape, location and contour of the prostate gland (J. Smith, 2008). Due to the poor contrast in the caudal abdomen, supplementary use of retrograde contrast to obtaining an urethrocytogram can be performed to allow visualization of the prostatic urethra and urinary bladder and make it possible to more accurately identify the

contours of the prostate gland (J. Smith, 2008). When the prostate is hyperplastic, it is typically visible on a plain lateral radiographic view, and it may displace the urinary bladder cranially (Johnston et al., 2000). The prostate can be considered enlarged if the “prostatic diameter is greater than 70% of the distance sacral promontory to the pubis (DSPP)”, as shown in figure 2.16 (Johnston et al., 2000). Because radiography can overestimate the size of the prostate gland and other causes of prostatic disease lead to prostatic enlargement, it is not considered a reliable technique for diagnosis BPH in dogs (Lévy et al., 2014). In cases of prostatic neoplasia, survey radiographs of the spine, pelvis and lungs should also be taken to assess for metastasis (J. Smith, 2008).



Figure 2.16. Lateral radiograph of a dog showing the distance from the sacral promontory to the pubis (DSPP) (black line). The cranio-caudal distance of the prostate is measured parallel to the DSPP. (Cavalca Cardoso, 2019).

### 2.9.2 Ultrasound

Diagnostic ultrasound started to be used in veterinary medicine in 1980 in the field of reproduction (Ginther, 1995). Ultrasound uses sound waves frequencies in the range of 2 to 15MHz that are outside of the range audible by the human ear, which is only capable of perceiving frequencies in the 2 Hz to 20000Hz (or 0.02MHz) range (Bushberg et al., 2002).

The ultrasound machine consists of a transducer or probe, and a processor (Fulton, 2013). The transducer converts mechanical energy to sound waves, which are transmitted when the transducer is placed in contact to the skin or tissue and a gel is spread in between the transducer and the tissue (Ginther, 1995). There is a crystal on the transducer and when an electric current is applied to it, the crystal vibrates and generates ultrasound waves, a phenomenon known as the piezoelectric effect (figure 2.17) (Coltrera, 2010). With ultrasonography, the ultrasound waves sent by the transducer to the body are reflected back at the interface between different tissues to generate a signal known as an echo (Fulton, 2013). This echo is captured by the same transducer and the processor creates an image of the internal organs for display on a monitor (Fulton, 2013).

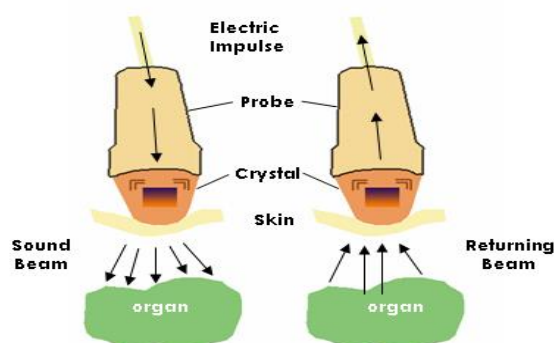


Figure 2.17. Schematic illustration of an ultrasound probe placed in contact with a tissue showing the electric pulses being converted into sound waves. “Generation of an ultrasound image” Retrieved from *Ultrasound for Regional Anesthesia*, on October 2017 <http://www.usra.ca/regional-anesthesia/introduction/basic.php#ultrasoundimage> Reprinted with permission

The images are dynamically generated and seen in different shades of gray and are a 2D display of dots representative of a B-mode US (brightness modality) (Fulton, 2013). The time it takes for the sound waves to be emitted and return as an echo is related to the distance travelled (Kealey et al., 2011). Also, the intensity of the signal shown on the screen is related to the strength of the returning echo, which is affected by the inherent properties of the tissue (Kealey et al., 2011). Tissues or structures imaged can be termed hyperechoic, anechoic or hypoechoic based on the degree of echogenicity (Ginther, 1995). Hyperechoic tissues or structures appear

as bright or white in comparison to surrounding tissues because they are dense and reflect back most of the sound waves. Anechoic structures are black since the entire echo waves pass through the structure with no reflection. Hypoechoic structures are darker or gray compared to surrounding tissues because only a portion of the wave returns reflective of an intermediate density (Ginther 1995).

The frequency used by the ultrasound transducer varies between low frequency (2 to 3.5 MHz) and high frequency (7.5 to 15 MHz) (Kealey et al., 2011). Lower frequencies can penetrate deeper into the body, but this can affect the quality of the image (Kealey et al., 2011). Higher frequencies are better suited for imaging structures or tissue that are closer to the transducer (not as deep), and provide a better image quality (Kealey et al., 2011).

When ultrasound waves are transmitted through the tissues within the body reflection, refraction, scattering, absorption, attenuation, reverberation and acoustic impedance can occur (Fulton, 2013). Most of the wave is absorbed but a part is reflected and it is the combination of these two events that allows the generation of the signal (Fulton, 2013). This results from differences in attenuation and the acoustic impedance of tissues (Drost, 2018). Analogous to the situation with X-rays as they travel through different tissues, with ultrasound *attenuation* refers to the loss of energy of the sound waves as they pass through different tissues with different densities, from reflection, scattering and absorbance (Drost, 2018). *Acoustic impedance* defines the reflection and transmission properties for sound waves of a tissue, which relies on the density of the tissue and the velocity of the waves as they travel through the tissue (Drost, 2018).

For the investigation of prostatic disease in dogs, ultrasonography is often the first imaging technique utilized, allowing for the visualization of the size, margins, homogeneity of the parenchyma of the gland and for detecting the presence of possible intraparenchymal cysts (Yayla, Öztürk, Aksoy, Kiliç, & Yildiz, 2012) as seen in figures 2.18 and 2.19. Ultrasound can sometimes underestimate the size of the prostate gland missing early stages of BPH (Lévy et

al., 2014). This is because the diagnosis of this disease should not only focus on finding enlargement of the prostate gland (Lévy et al., 2014) but should also look for altered homogeneity of the parenchyma (Yayla et al., 2012). If BPH is suspected but not supported by the ultrasound findings, a biopsy should be performed to help confirm the diagnosis (Lattimer & Essman, 2018). It is also important to realize that visualization of structures such as a cyst or secondary abscessation can be seen with both BPH or sometimes with PCa so their presence cannot be assumed to be confirmatory of BPH (Troisi et al., 2015). This may require further analysis of prostatic fluid and/or biopsy of the gland to differentiate the two disorders (Troisi et al., 2015).

Johnston et al., 2000 describe a formula  $([L \times W \times D]/2.6 + 1.8)$  that can be used to calculate the volume of the prostate in cubic centimeters in the dog, where “L is the greatest craniocaudal diameter, W is the transverse diameter and D is the dorsoventral diameter of the prostate seen with ultrasound. It is essential to emphasize that as ultrasonography is a highly user dependent diagnostic imaging modality, measurements can depend on the operators’ and also on the observers’ experience (Leroy et al., 2013). Also, due to the presence of the penis, it is challenging to position the probe in a transverse plane and precisely identify the margins of the prostate, especially at the caudal aspect (Leroy et al., 2013).

As an alternative to transabdominal ultrasonography, transrectal ultrasound of the prostate can be performed (Juniewicz, Lemp, Batzold, & Reel, 1989). Juniewicz et al., 1989 proved that this is an accurate method of estimating canine prostatic size evaluating both transaxial and sagittal images with specifically designed probes. This is not commonly done in veterinary medicine because probes designated for rectal exam needs to be small enough to be used in different breeds without causing discomfort to the animal and they are not readily available (Juniewicz et al., 1989). In addition, deep sedation or anesthesia would be required which are not essential for percutaneous ultrasound imaging of the prostate (Juniewicz et al., 1989).



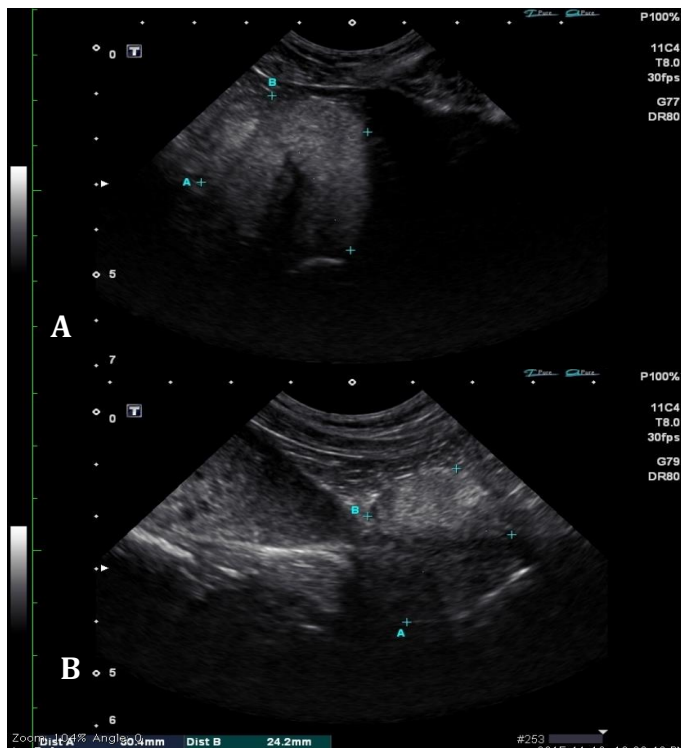


Figure 2.18. Normal prostate gland of a dog: longitudinal ultrasonography (A); transversal ultrasonography (B). (Cavalca Cardoso, 2019).

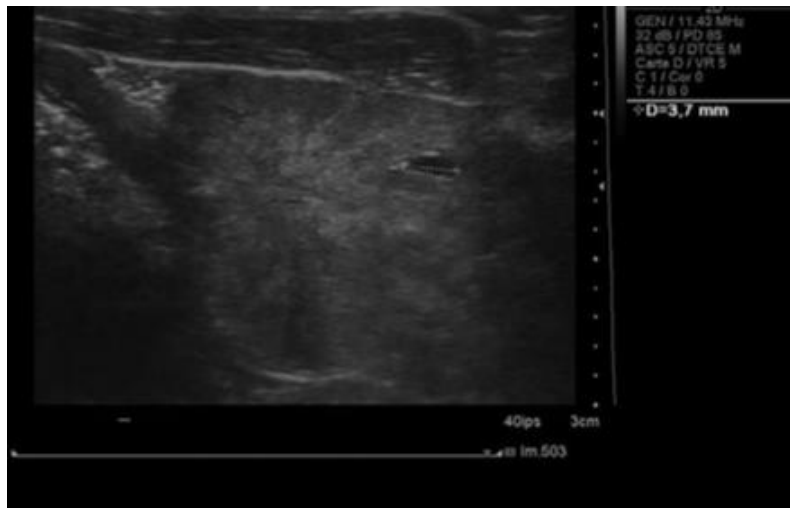


Figure 2.19. Ultrasound of a canine prostate gland with BPH. Longitudinal ultrasound showing a cyst and heterogeneity of the parenchyma. Retrieved from Lévy et al., 2014. Reprinted with permission.

### 2.9.3 Computed Tomography (CT)

The equipment necessary for a CT exam consists mainly of a circular gantry (the scanning unit), sliding table, hardware gear, and an operator console equipped with a computer, which adjusts acquisition and image reconstruction (Saunders & Ohlerth, 2011). The patient lies down on the table that slides through the hole in the gantry (Saunders & Ohlerth, 2011). During this, the X-ray tube, which generates x-rays, moves in a rotation around the patient in the axial or transverse plane. The X-rays generated will hit the detector on the opposite side of the gantry (Saunders & Ohlerth, 2011). The detector is made of a scintillation crystal that produces light that is converted into digital pulses after x-rays transverse through the tissue to strike it (figure 2.20) (Saunders & Ohlerth, 2011).

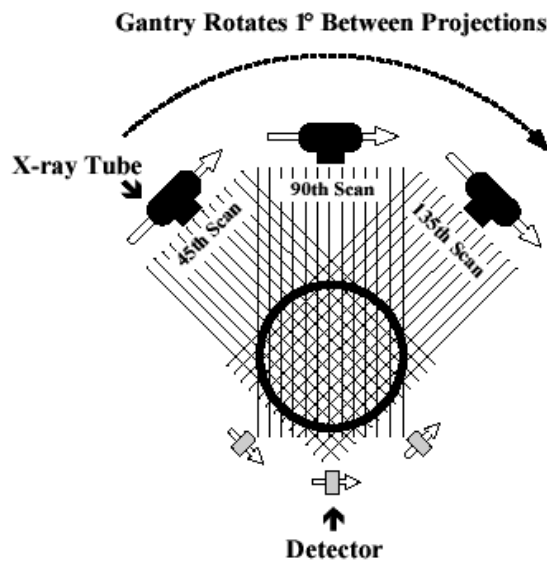


Figure 2.20. The tube emits X-rays that reaches the detector on the opposite. KieraMahen. First generation CT scanner design. Adapted with permission from Applied Imaging Technology by Heggie, Liddell & Maher (2001). Marz 03:23, 3 October 2006 (UTC) en;/Images. Retrieved from Wikimedia Commons, on September 14<sup>th</sup> 2017. Reprinted under public domain (file: NM19\_60)

CT is an imaging technique based on the Radon's principle, whose basic idea is to acquire an infinite number of 2D projections of an object to produce a three dimensional cross

sectional image of the internal structure of the object (Bushberg et al., 2002). In other words, cross sectional radiographic views are obtained with a small angular interval between them around the patient until a circumference (360°) is completed (Bushberg et al., 2002). The resulting images are slices of the body (figure 2.21), tomographs, that put together represent a 3D projection of each particular segment of the patient's body, allowing better visualization of the organs and individual structures (D'Anjou, 2018).

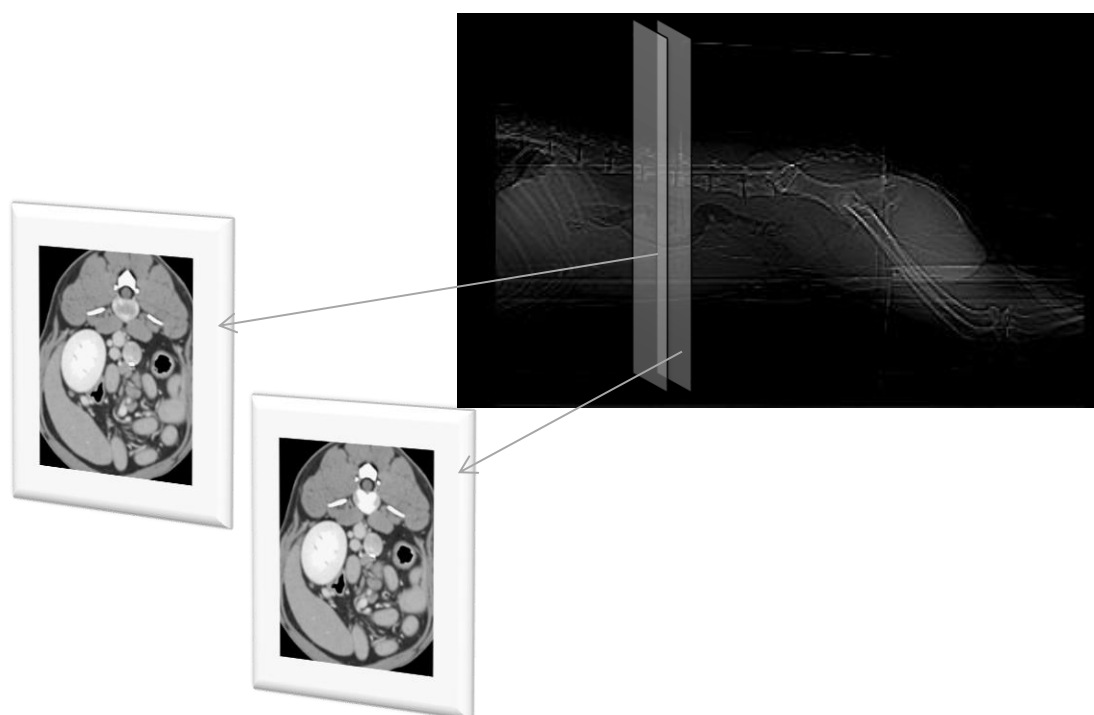


Figure 2.21. Cross sectional representation of CT slices of the body. (Cavalca Cardoso, 2019).

The reconstructed output from a CT scanner is a stack of images. Each slice or image generated by a CT exam is formed by *pixels* (picture element) and *voxels* (volume element) (D'Anjou, 2018). Pixels are the tiny small 2D squares that together, generally a combination of 512x512 pixels, form the image slice and they represent the average X-ray attenuation of the tissue (Bushberg et al., 2002). The voxel is the third dimension or the volumetric form of the pixel, and it represents the slice thickness of the CT image as seen in figure 2.22 (Bushberg et al., 2002). The intensity of each pixel displayed in the monitor is, as described previously, a

uniform average of the X-ray attenuation of the structure imaged and, therefore, reflects a shade of grayscale – brighter if more attenuation and darker if less attenuation – perceived accordingly to the characteristic of that area (D’Anjou, 2018).

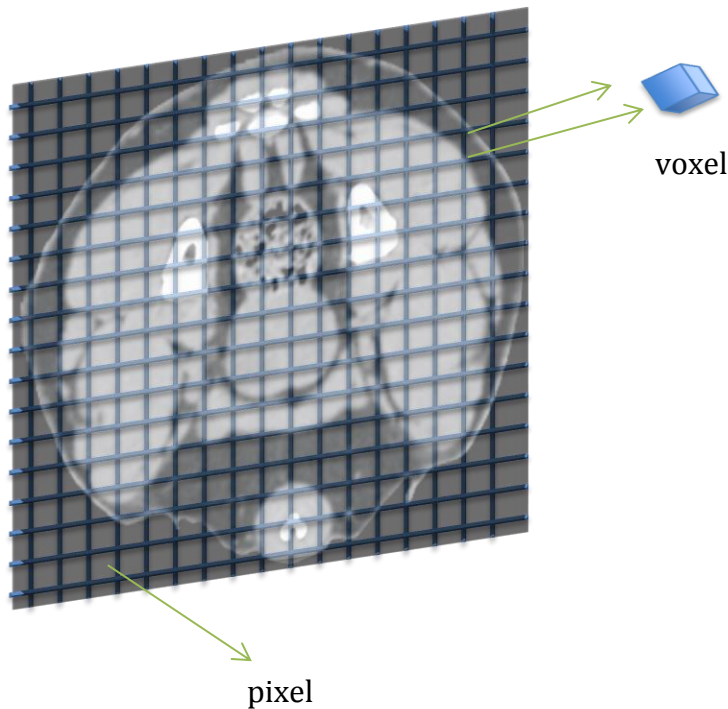


Figure 2.22. Cross section of a CT slice showing the 2D pixels represented by the squares and a 3D voxel represented by a cube. (Cavalca Cardoso, 2019).

Contrast resolution and spatial resolution are two important characteristics that determine the quality of the final image. Contrast resolution is improved in CT compared to conventional radiography, and it is related to the differentiation among tissues with similar shades of gray (D’Anjou, 2018). On the other hand, spatial resolution is not improved in CT compared to conventional projection radiography (D’Anjou, 2018). Spatial resolution is linked to the detector size, the slice thickness – the thinner, the better – and number of pixels – with more being better – determining the quality and details of the structures (D’Anjou, 2018).

With CT, acquisition of the images is done initially in the transaxial plane (Haaga & Jordan, 2016). Computer algorithms can then later be used to reconstruct and generate sagittal or coronal images that display slices of the tissue (Haaga & Jordan, 2016). Among the many different reconstruction algorithms that can be applied to the collected scans, filtered back

projection has been widely used in the clinic (Haaga & Jordan, 2016). The backprojection reconstruction is based on the process of acquiring repeated views that are “smeared” along the path they were obtained and summing all these backprojected views, resulting in an image, which has an intrinsic characteristic of being a blurred final image (figure 2.23) (Smith, 1998). In order to remove this undesired effect and enhance the edges, a filter is applied to the data before it is backprojected (Smith, 1998), and this process is illustrated in figure 2.24.

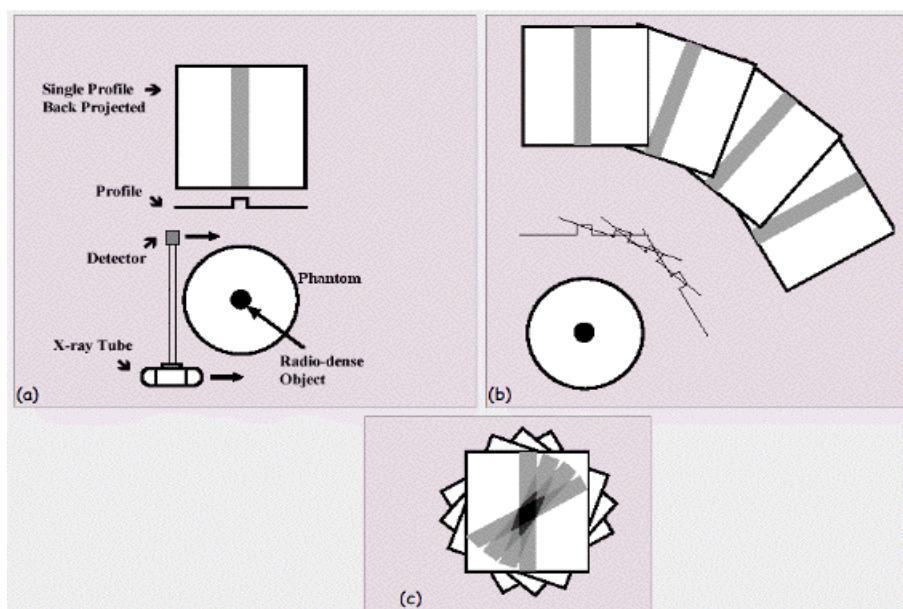


Figure 2.23. CT Reconstruction using backprojection. (b) The reconstructed image is generated from four views; (c) The reconstructed image is generated using numerous views and display blurriness. KieraMahen. Demonstration of back projection, adapted with permission from Heggie, Liddell & Maher (2001), <http://homepage.mac.com/kieranmaher/ait/> Applied Imaging Technology by Kieran Maher using Graphic Converter. Marz 12:45, September 2006. Retrieved from Wikimedia Commons, on September 12<sup>th</sup>, 2017. Reprinted under public domain (file:NM19.3). [https://commons.wikimedia.org/wiki/File:NM19\\_3.gif](https://commons.wikimedia.org/wiki/File:NM19_3.gif)

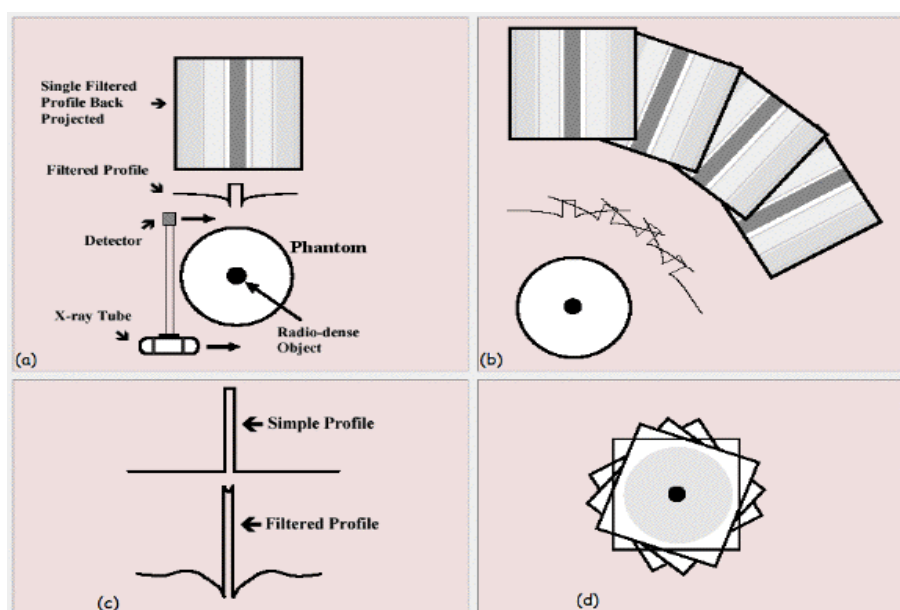


Figure 2.24. CT Reconstruction using filtered backprojection. (a) Filter is applied before generating the images; (b) The reconstructed image is generated using numerous views; (d) The final image has a better quality. KieraMahen. Demonstration of filtered back projection, adapted with permission from Heggie, Liddell & Maher (2001), <http://homepage.mac.com/kieranmaher/ait/> Applied Imaging Technology by Kieran Maher using Graphic Converter. Marz 13:30, September 2006. Retrieved from Wikimedia Commons, on September 12<sup>th</sup>, 2017. Reprinted under public domain (file:NM19.5). [https://commons.wikimedia.org/wiki/File:NM19\\_5.gif](https://commons.wikimedia.org/wiki/File:NM19_5.gif)

The image obtained can be evaluated based on quantitative numbers known as Hounsfield Units (HU) that reflect the linear transformation of the measured attenuation coefficients from the conversion of pixels and voxels signal intensity values for each tissue (Haidekker, 2013). By convention, pure water has HU equal to zero and structures causing more X-ray attenuation than water have an HU value higher than zero and tissues with a lower attenuation will generate HU values below zero (Kalender, 2011). This property allows the differentiation of soft tissue and liquid media using their HU values, which provides better contrast resolution with CT compared to radiographs (Kalender, 2011).

A second scan is often performed after iodinated contrast medium, which is a very strong attenuating substance, is administered intravenously (D'Anjou, 2018). This technique can be used to increase the HU value of a tissue and consequently, enhance the structures



visualized and improve the contrast resolution of the CT images and may aid in making a definitive diagnosis (D'Anjou, 2018).

Although CT is clearly a more advanced technique than conventional projection radiography, there have been limited studies describing the CT features of the prostate gland of dogs (Kuhnt, Harder, Nolte, & Wefstaedt, 2017). One of the first research papers to describe CT findings in dogs with BPH was conducted in 2015 (Pasikowska, Hebel, & Nowak, 2015). In this study, there were 40 dogs (with different breed, age and weight) distributed in two groups, a control group and dogs clinically presenting with signs of BPH (Pasikowska et al., 2015). The parameters assessed were the size of the prostate gland and other features of BPH seen with CT were described (Pasikowska et al., 2015). These features included symmetrical prostatomegaly, an intact prostate capsule, heterogeneity of the parenchyma (both pre- and post-contrast injection with Iopromide) and cysts of different number and size (figure 2.25) (Pasikowska et al., 2015). A positive correlation between the age of the dog and prostatic dimensions was also found due to the natural enlargement of the gland seen in older dogs and presence of cysts (Pasikowska et al., 2015). CT has the advantage that in addition to providing information on the position and morphological features of the prostate gland it can be used to investigate whether there is evidence of concurrent disease, local lymphadenopathy or possible evidence of metastasis if PCa is present (Pasikowska et al., 2015).

CT is a superior modality to detect minor changes in size and shape of the prostate gland when compared to ultrasound or radiograph (Lee K.J. et al., 2011). However, it is a modality that requires more time to be performed, necessitates sedation of the canine patient and it is more expensive (Lee K.J. et al., 2011). According to Kuhnt et al., 2017, early stages of prostatic changes can be identified with the use of contrast agents when compared to ultrasound imaging of the gland.

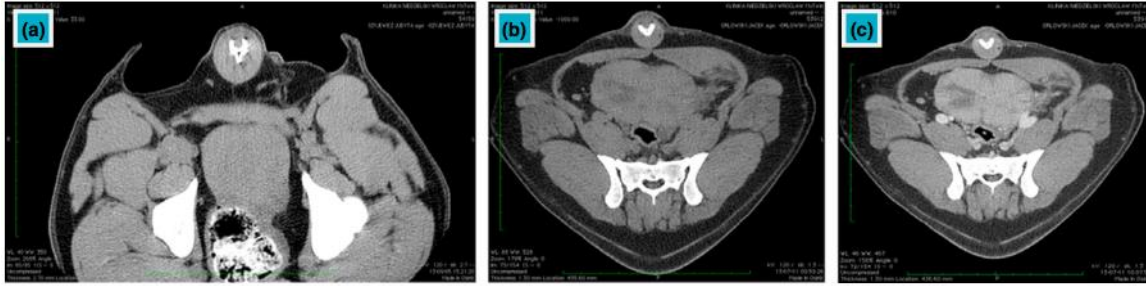


Figure 2.25. CT images of a dog’s prostate gland with BPH characteristics: a) irregular prostatomegaly, b) pre-contrast image showing cysts, c) post contrast image showing cysts. Retrieved from Pasikowska et al., 2015. Reprinted with permission.

#### 2.9.4 Magnetic Resonance Imaging - MRI

Similarly to CT equipment, an MRI system contains a table for the patient to lie down on that slides into and out the center of a gantry (Currie, Hoggard, Craven, Hadjivassiliou, & Wilkinson, 2013). However, this gantry is surrounded by the magnet and the coil, and a computer sends RF pulse to the gantry and receives the signals, converting analog into digital pulses that are transformed and displayed as images (Currie et al., 2013).

Magnetic Resonance Imaging (MRI) is an imaging modality that is different from radiography and computed tomography, in that it does not make use of ionizing radiation (Bushberg et al., 2002). Only the basic concepts of how MRI works is summarized here; a more detailed analysis of the physics involved is beyond the scope of this review.

The “*magnetic*” in MRI refers to the magnetic field that is generated (Bushberg et al., 2002). *Resonance* is the phenomenon where protons in different tissues absorb and release a characteristic energy when positioned in a strong external magnetic field (Bushberg et al., 2002). When positioned in a magnetic field, protons in the body’s tissues absorb energy and “flip their spins” (Bushberg et al., 2002). When the magnetic field is turned off the protons return to their normal spin generating a signal that can be measured by a scanner to generate an image (Bushberg et al., 2002).



All mammals including dogs and humans are composed of water (approximately 60%), which serves as a main source of hydrogen ( $H^+$ ) (Lakrimi et al., 2001). It is the properties of the nucleus of  $H^+$  atoms, formed by a single proton, that are exploited in the MRI exam (Lakrimi et al., 2001). These nuclear protons naturally and randomly spin about their axis in different directions (figure 30) (Lakrimi et al., 2001). When a strong external, and powerful magnetic field  $B_0$  (1.5 T or 3 T) is applied to the patient, most of these  $H^+$  ions align in the same direction (parallel) to the magnetic field (figure 2.26), a process called precession (Currie et al., 2013). These protons precess at a frequency called the Larmor frequency that is proportional to the main magnetic field strength (Currie et al., 2013).

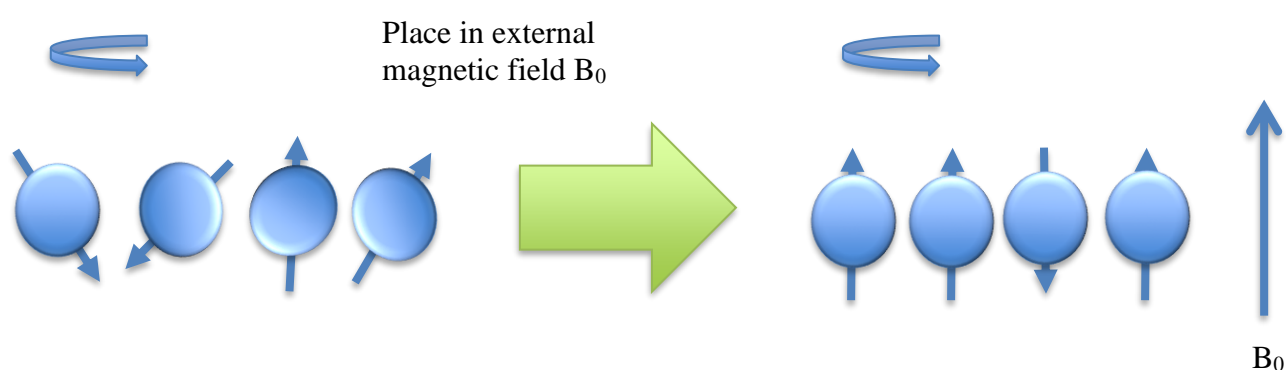


Figure 2.26. Illustration of the random pattern of protons spinning inside a human body. After an external magnetic field is applied, most of the protons align in the same direction as the main magnetic field ( $B_0$ ). (Cavalca Cardoso, 2019).

After the precession process, a radiofrequency (RF) pulse is applied in order to resonate the protons (D'Anjou, 2018). The resulting absorption of energy excites the protons and instantaneously changes their plane of orientation (transverse magnetization) flipping this by 90 degrees to the transverse axis (figure 2.27) (D'Anjou, 2018). As soon as the RF pulse is turned off, the  $H^+$  ions return to the previous position (longitudinal axis parallel to the main magnetic field) in a process called relaxation, and two events are observed simultaneously in an attempt

to reach equilibrium: T1 and T2 relaxation during the returning of the protons in order to form images (D'Anjou, 2018). At the same time, the longitudinal vectorial component of magnetization increases and the transverse decreases (figures 2.28 and 2.29 respectively) (Sharma, 2009). T1 or longitudinal relaxation time refers to the time it takes for the protons to return to 63% of its original longitudinal value, whereas T2 or transverse relaxation is the time it takes for the protons to return to 37% of its original transverse value (Sharma, 2009). Tissue contrast is achieved because of the differences for T1 and T2 time for each tissue, and their properties contribute to the image contrast (Sharma, 2009).

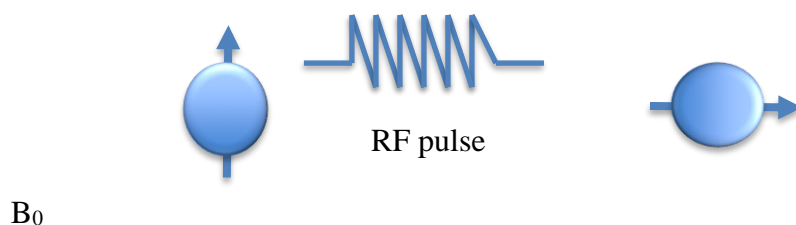


Figure 2.27. A RF pulse is applied making the protons flip to the transverse plane. (Cavalca Cardoso, 2019).

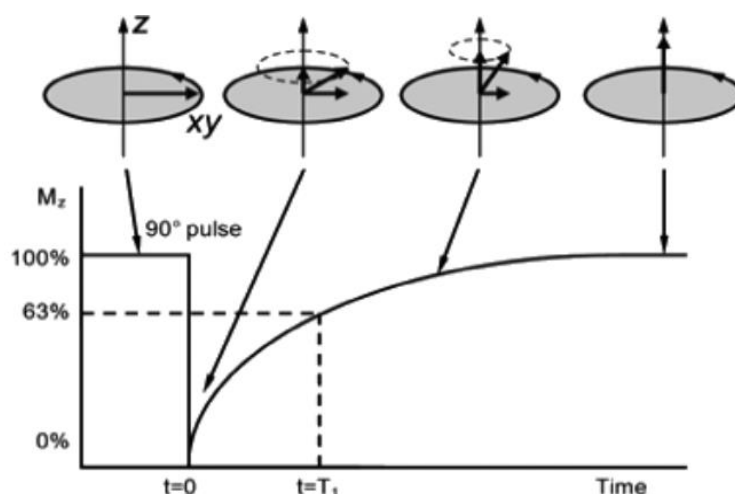


Figure 2.28. T1 Relaxation time. Retrieved from Sharma, 2009. Reprinted with permission.

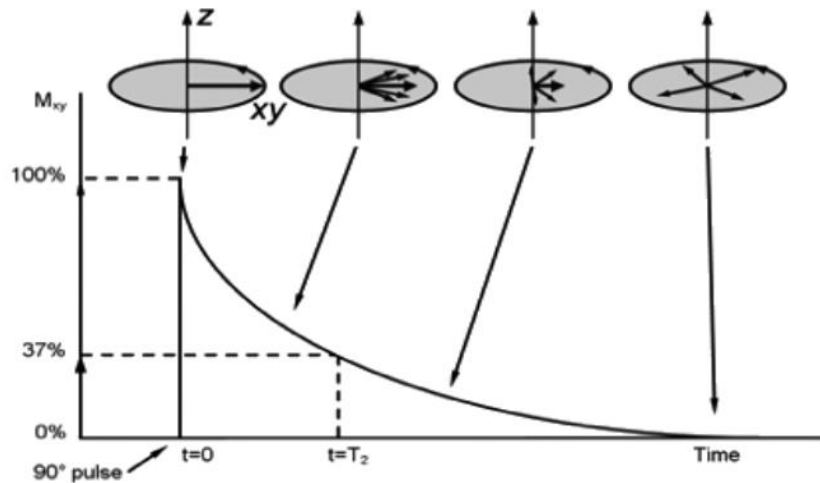


Figure 2.29. T2 Relaxation time. Retrieved from Sharma, 2009. Reprinted with permission.

Once the tissue has been submitted to the magnetic field and the RF pulse, it will generate signals (echoes) that are perceived by receiving coils and processed by a computer (D'Anjou, 2018). Also, in order to solve the issue of difference among T1 and T2 relaxation times, the use of variable *sequences* (spin echo and gradient recalled) control the time and duration of the originated and received pulses (D'Anjou, 2018). Simplifying, the consequence of adding an extra pulse allows slow protons to catch up to faster protons and generate an echo together, and this period of time is called time of echo (TE), and the time it takes to run this sequence is known as time to repetition (TR) (D'Anjou, 2018). Moreover, adjusting both TE and TR is used for optimizing T1 and T2 images; this is essential for tissue differentiation: short TR and short TE results in T1 weighting and long TE and long TR results in T2 weighting (D'Anjou, 2018).

Contrast media given intravenously, such as gadolinium, can be used, and it affects the protons surrounding the contrast reducing their T1 and T2 relaxation time, preferentially to lower T1 relaxation and result in better resolution (D'Anjou, 2018). Image quality can be affected by artifacts due to interference in the magnetic field caused mainly by metallic objects (D'Anjou, 2018).

The use of MRI to assess the prostate gland is more common in men than dogs, but [Jia et al., 2005](#) used MRI to assess the prostate volume in beagles and obtained a good correlation between the *in vivo* MRI volume and the *ex vivo* actual volume.

Prostatic volume and changes in response to therapies for BPH is an important key to help select correct treatments and to calculate the degree of involution of the prostate with different medical treatments of BPH. In a study, [Rahmouni et al al., 1992](#) compared the prostatic *in situ* volume determination of 48 men using MRI and TRUS with the ‘wet weight’ of the excised prostates of these men who underwent prostatectomy due to diagnosis of an adenocarcinoma. The results of this study showed that T2 weighted MRI allowed differentiation of the high signal peripheral zone from the low signal periurethral transition zone where BPH arises ([Rahmouni et al al., 1992](#)). This study proved that MRI is a precise and accurate technique to measure prostatic volume and superior to TRUS for this purpose ([Rahmouni et al al., 1992](#)).

A review of the use of MRI for determining prostatic volume in BPH in men conducted by [Garvey et al., 2014](#) emphasized that MRI is more reliable than TRUS and it confirmed that T2 MRI images better differentiates the transitional from the peripheral zone. [Emad-Eldin, Halim, Metwally, & Abdel-aziz, 2014](#) showed that, although other diseases of the prostate, including prostatitis and BPH, can display the same low signal for T2W as PCa, if T2 weighted imaging (T2WI) is combined with diffusion weighted imaging (DWI) this may allow differentiation of PCa from other prostatic diseases. An MRI image of the normal human prostate gland and a patient with BPH are illustrated below (figure 2.30).

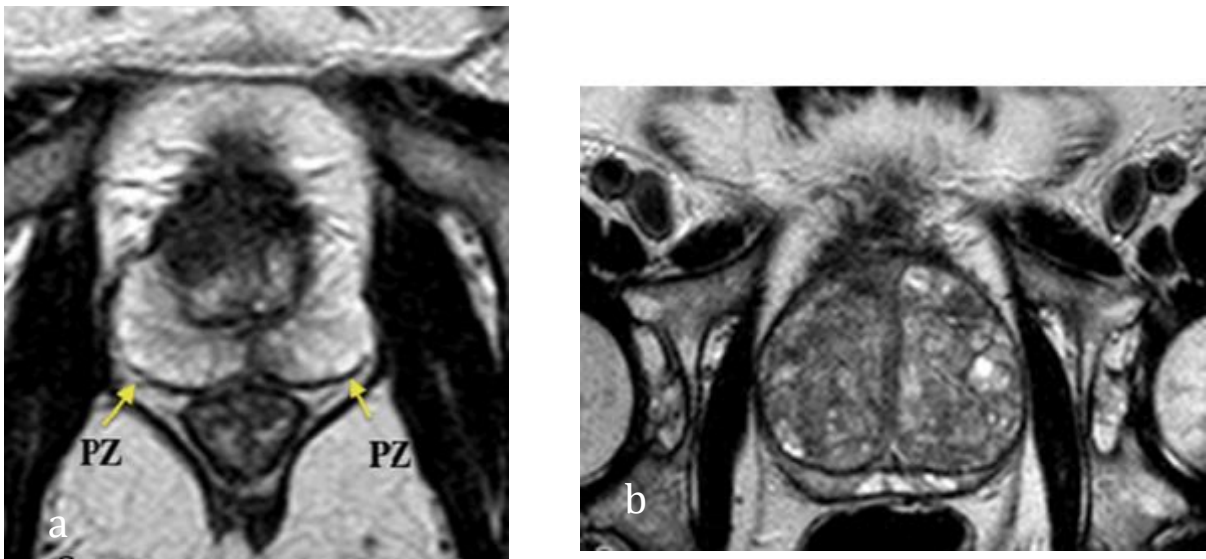


Figure 2.30. MRI T2 weighted imaged of a human patient. (a) Normal prostate gland with hyper-intense peripheral zone; (b) BPH gland with an enlarged and heterogeneous central zone compressing the peripheral zone. Retrieved from Emad-Eldin et al., 2014. Reprinted with permission.

### 2.9.5 Positron Emission Tomography

The PET technology aims to detect the distribution and radioactivity of a radiotracer inside the body (Lawrence, Rohren, & Provenzale, 2010). A radiotracer is a sterile substance produced and labelled with a radionuclide in a cyclotron; this is then administered, generally by intravenous injection, to a patient prior to performing a PET scan (Lawrence et al., 2010). The most widely used radiopharmaceutical is  $^{18}\text{F}$ -FDG (fluorodeoxyglucose) (Lawrence et al., 2010).

It is necessary to understand how nuclear medicine works in order to understand the physics behind a PET scan. An atom is composed of a nucleus with a cloud of electrons surrounding it (Saha, 2016). Within the nucleus, there are protons and neutrons, and their sum is called the mass number (Saha, 2016). The total number of protons is also known as atomic number, and when the number of electrons is the same as protons, the atom is stable or uncharged (Saha, 2016). The electrons orbiting the nucleus are negatively charged while

protons are positively charged, and neutrons have no charge (neutral) (Saha, 2016). A nuclide is an atom with a particular mass number and atomic number; and nuclides that have the same atomic number but different mass numbers are called isotopes (Saha, 2016). If an isotope is unstable, it undergoes radioactive decay by emitting radiation, a process where the isotope returns to the ground state to achieve stability and, therefore, radionuclides (radioactive nuclide) are radioactive isotopes (Bushberg et al., 2002). An important parameter associated with the decay process is the physical half-life ( $T_{1/2}$ ), described as the time it takes for the radioactivity to be reduced by half (Bushberg et al., 2002). The half-life of an isotope is an important parameter used for monitoring radioactivity within the organ or body system after administration of an isotope (Bushberg et al., 2002). More stable nuclides will decay slowly and have a longer  $T_{1/2}$  while less stable nuclides decay very quickly and have shorter  $T_{1/2}$  (Bushberg et al., 2002). When a radiotracer like  $^{18}\text{F}$ -FDG is injected, it will be absorbed by various tissues just as normal glucose would be uptaken for cellular metabolism (Lawrence et al., 2010). Because cancerous cells, particularly very aggressive malignant tumour cells, are characterized by a high metabolic rate when  $^{18}\text{F}$ -FDG is administered the cancer cells will uptake the tracer in increased amounts compared to normal tissues (Lawrence et al., 2010). Once inside the tumour cells,  $^{18}\text{F}$ -FDG is trapped, the radionuclide will decay and this decay is what is detected with a PET scan (Basu et al., 2014).

Among the types of radionuclide decay, PET relies on beta-plus (positron) emitting radionuclides (Basu, Kwee, Surti, Akin, & Yoo, 2011). With beta-positron emitters, the element that is unstable and rich in protons achieves stability by losing one proton (Basu et al., 2011). When this occurs, the proton is converted into a neutron; this leads to an increase in the number of neutrons by one in the nuclei and a neutrino and positron also result, as illustrated in figure 2.31 (Basu et al., 2011; Basu et al., 2014). The neutrino does not interact with the nearby material; however, the positron travels a short distance and is subject to interactions with an orbiting anti-particle (an electron), resulting in a process called annihilation (Basu et al., 2014).

Importantly, this equation represents an isobaric decay in which the originating daughter element (on the right of the equation) has the same mass number of the original parent element (on the left of the equation) but a different atomic number (Bushberg et al., 2002).

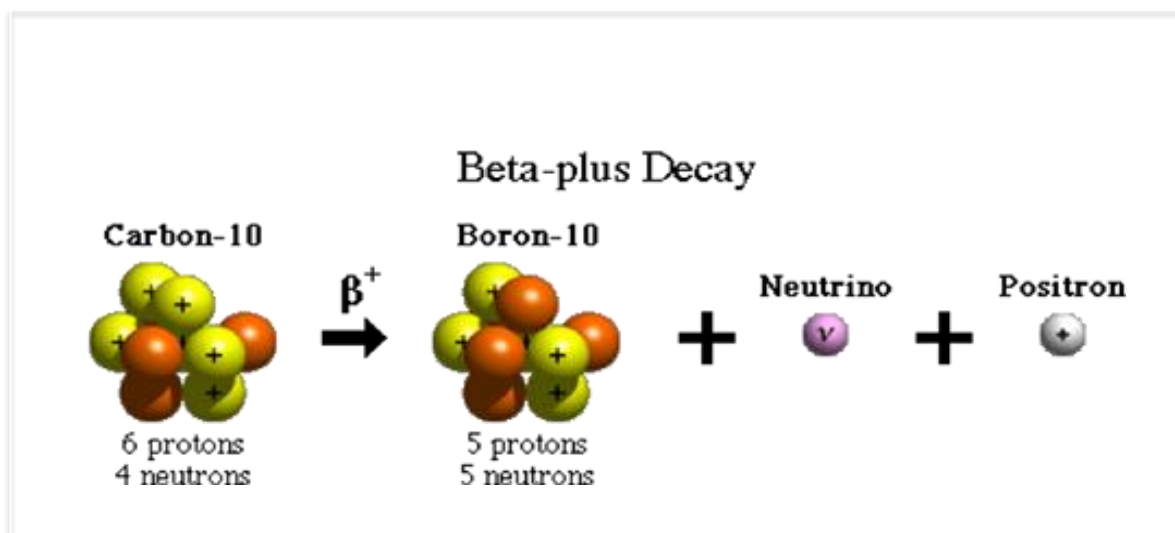


Figure 2.31. Beta plus decay. Parent element (carbon-10) originates a daughter element (boron-10), a positron and a neutrino. Jefferson Lab, US Dept. of Energy. Retrieved from NASA Physics Online Course on January 3, 2017. <http://nasaphysics.cet.edu/radioactive-decay.html> Reprinted under public domain

When annihilation occurs, this results in the conversion of the mass from the positron and the electron into electromagnetic energy, which is released as two photons that travel in opposed directions ( $180^\circ$  degrees) as shown in the figure 2.32 below (Cherry & Dahlbom, 2006). Each of the photons has an energy equivalent to 511 keV, (Cherry & Dahlbom, 2006) and the energy / radiation resulting from the annihilation is detected by PET scanners when both photons collide with a scintillator detector at the same time (Das, 2015). This information is stored and an algorithm is used to retrieve the radioactivity pattern, so that a distribution “map” of the radionuclide activity in the body is gathered (Lawrence et al., 2010).

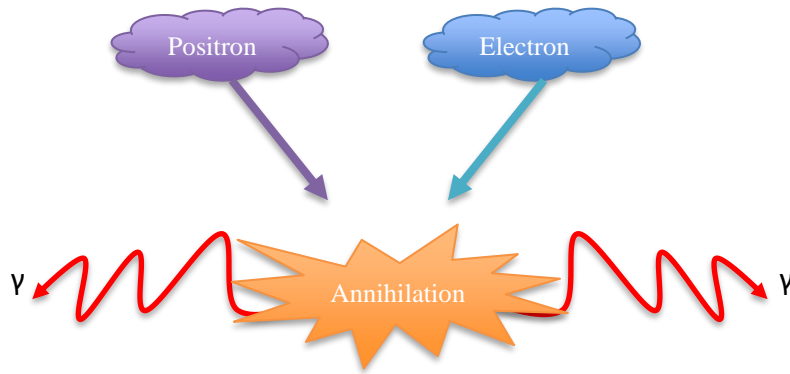


Figure 2.32. Annihilation process showing a positron reacting with an electron and originating two photons in opposite directions (180°). (Cavalca Cardoso, 2019).

$^{18}\text{F}$ -FDG is the most used radiopharmaceutical in routine PET imaging and has a  $T_{1/2}$  of 118 minutes, which allows it to be produced at a cyclotron facility and delivered to a hospital ready for use (Lawrence et al., 2010). The radiotracer F18 is an isotope of fluorine with nine protons and nine neutrons (Cherry & Dahlbom, 2006). F18 is also a glucose analogue which is important because cancer cells use glucose as a source of energy during glycolysis and uptake it at an increased rate compared to normal tissues (Basu et al., 2014).

$^{18}\text{F}$ -FDG enters the cell through several glucose membrane transporters, which are overexpressed on the surface of malignant cancer cells or on activated inflammatory cells (Bouchelouche & Oehr, 2008). After uptake, it is phosphorylated, but unlike regular glucose it cannot be used in glycolysis but remains metabolically trapped inside the cells where the radiotracer will undergo decay (Bouchelouche & Oehr, 2008). It is essential that prior to injection of  $^{18}\text{F}$ -FDG a patient must fast for a minimum of six hours and not be active (Das, 2015). This ensures that only FDG, not competing glucose from intake of food, is used as a source of energy (Das, 2015). This also limits uptake of FDG into tissue, such as muscle, due to increased demand associated with activity (Basu et al., 2014).

Because PET CT combines 3D cross-sectional imaging along with functional imaging it has several advantages over other imaging modalities like CT and MRI, which only detect



changes in structure but not function (Basu et al., 2011). This means PET CT is able to detect a disorder earlier in its course before there is any structural or anatomic change and that increases the ability to show the extent of the disease in a patient (Lawrence et al., 2010). PET CT can also help with monitoring response to treatment to allow a quantitative measurement of the effectiveness of different treatments (Lawrence et al., 2010). FDG PET CT has largely been used for detecting other types of cancers (breast and brain tumours) (Das, 2015); it has not been widely used for detection and staging of prostate cancer (Bouchelouche & Oehr, 2008). This is in part because it has a low uptake by PCa cells and is also rapidly excreted in the urine (Li et al., 2008). Liu et al., 2006 described a sensitivity of only 4% for the primary detection of PCa with the use of F18-FDG PET CT in men. Not only do reports suggest that PET-CT has a low sensitivity and specificity for detecting PCa, but using  $^{18}\text{F}$ -FDG it also cannot reliably differentiate between normal tissue, BPH or PCa (Castellucci et al., 2015).

$^{11}\text{C}$ -choline is a different radioactive isotope for PET-CT that has recently been used for detecting PCa in men (Fuccio, Rubello, Castellucci, Cristina, & Fanti, 2011). Studies suggest there is a correlation between  $^{11}\text{C}$ -choline uptake and PSA serum levels, suggesting this radiotracer could be useful in those patients with PCa showing fast growing PSA kinetics (velocity and doubling time) (Fuccio et al., 2011) and possibly leading to better results for PCa detection (Bouchelouche & Oehr 2008). Choline participates in a series of natural reactions in the body, being mainly integrated into a major membrane phospholipid, called phosphatidylcholine (Chotipanich et al., 2016). Malignant cells use more choline for phosphorylation and biosynthesis of cell membranes, due to their rapid duplication rate (Li et al., 2008). The 20-minute half-life of  $^{11}\text{C}$ -choline, however, is much shorter than  $^{18}\text{F}$ -FDG, which is a negative characteristic making the substance unavailable, most of the time, unless the cyclotron facility that produces the isotope is close to the PET-CT facility (Bouchelouche & Oehr 2008).

Scher et al., 2007 conducted a study with 58 patients with clinical suspicion of PCa using  $^{11}\text{C}$ -choline PET CT for detection of prostate cancer. In this study, 37 patients were diagnosed with PCa. The sensitivity and specificity for detection of PCa reported were 86.5% (32/37) and 61.9% (13/21), respectively. Although there are good results towards the detection and differentiation of PCa from normal tissue (Bouchelouche & Oehr 2008), data presented by Yoshida, Nakagomi, Goto, Futatsubashi, & Torizuka, 2005 demonstrated no differences in the ability to differentiate BPH from PCa in men with this radiotracer. This discrepancy is due to an overlap in the uptake of this isotope by BPH and PCa cells (Castellucci et al., 2015). No work has been done in dogs with any radiotracer to determine if PET CT is useful for detecting either PCa or BPH or if it is able to help with differentiation of these two disorders.

Figure 2.33 and figure 2.34 compare both radiotracers –  $^{18}\text{F}$ -FDG and  $^{11}\text{C}$ -choline – for the detection of prostate cancer in different human patients and in different studies. It is possible to see that the PET exam using  $^{11}\text{C}$ -choline provides a higher uptake by the prostate gland compared to with  $^{18}\text{F}$ -FDG (Li et al., 2008).

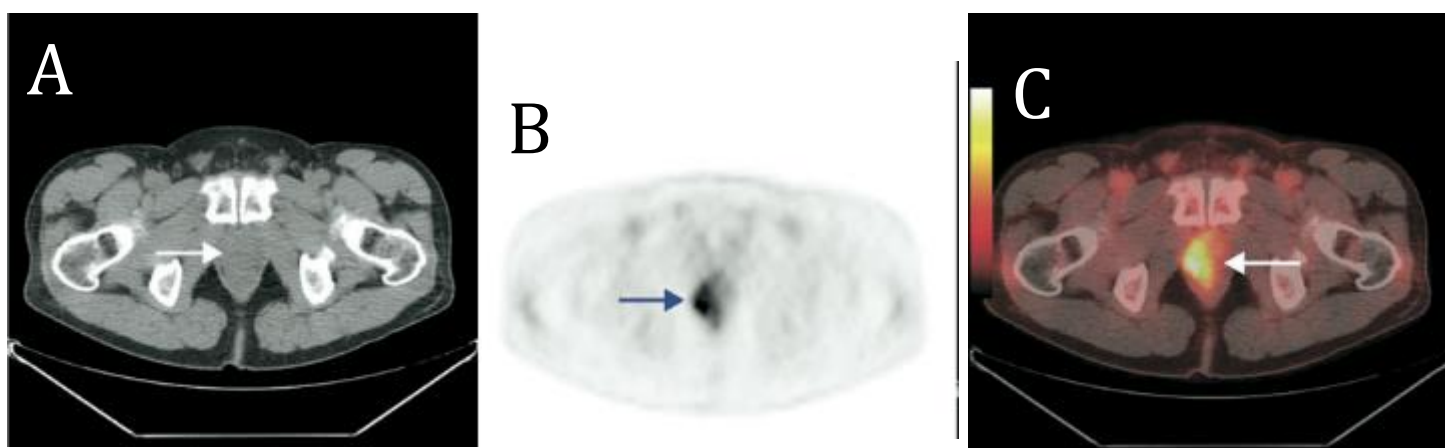


Figure 2.33. (A) Transaxial CT, (B) PET, (C) PET-CT fusion of the prostate of a man with prostate cancer using  $^{18}\text{F}$ -FDG. Retrieved from Bouchelouche & Oehr, 2008. Reprinted with permission.

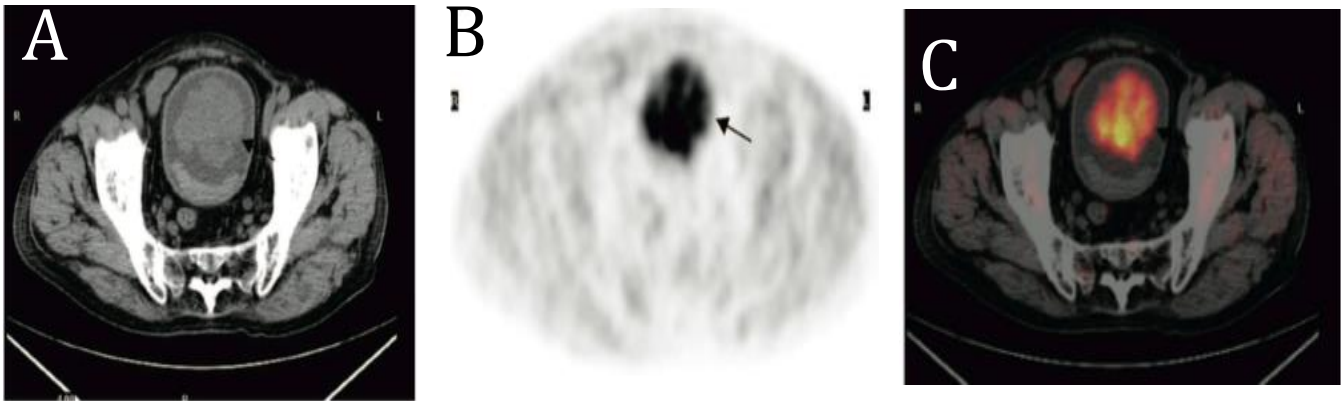


Figure 2.34. Transaxial (A) CT, (B) PET, (C) PET-CT fusion of the prostate of a man with prostate cancer using  $^{11}\text{C}$ -choline. Retrieved from Li et al., 2008. Reprinted with permission.

#### 2.9.6 PC-CT Phase Contrast Computed Tomography Synchrotron

The Canadian Light Synchrotron (CLS), located in Saskatoon, Saskatchewan is a third generation synchrotron facility, capable of generating different types of powerful energy from the electromagnetic spectrum ([Canadian Light Source Inc. 2012](#)). Synchrotrons are classified into four generations, a term used to categorize the facilities according to the level of technology applied ([Willmott, 2011](#)). The CLS is a third generation synchrotron ([Canadian Light Source Inc. 2012](#)). This means it has a storage ring and also insertion devices installed within the ring, which increases the intensity of the light produced ([Willmott, 2011](#)).

Synchrotron accelerates electrons to approximately the speed of light by using electromagnetic fields and radio frequency waves, resulting in a brilliant light ([Canadian Light Source Inc. 2012](#)). The brilliance is produced when magnets change the pathway of the electrons, and this can be increased with the use of insertion devices ([Canadian Light Source Inc. 2012](#)). Different types of energy from the electromagnetic spectrum can be selected – ultraviolet, infrared or X-rays – which are split off and focused for use in the appropriate beamline at a synchrotron ([Canadian Light Source Inc. 2012](#)). At the CLS, the Biomedical Imaging and Therapy (BMIT) uses X-rays to image biological tissues or samples, such as the

prostate, and provides advanced imaging for biological tissue in extraordinary detail (Canadian Light Source Inc. 2012). BMIT has two hutches where different experiments can be conducted: the first one uses a bending magnet (BM) that is capable of changing the direction of the light, and the other uses a powerful superconducting wiggler (ID insertion device) that moves the electrons constantly backward and forward (Canadian Light Source Inc. 2012).

The main components that are part of a third generation synchrotron facility and that provide the resultant beam are shown in figure 2.35, and they are the electron gun, the linear accelerator (linac), the booster ring, the storage ring, and the radiofrequency supply (RF) (Willmott, 2011). The electron gun is the source of electrons that are accelerated by a linear accelerator (linac) (Willmott, 2011). The booster ring provides more acceleration for the electrons that are kept within the storage ring, where magnets keep them on track (Willmott, 2011). The radiofrequency supply within the storage ring provides the electrons with additional energy whenever they pass through it to help compensate for any loss in energy (Willmott, 2011). These components are arranged in a circle, and the beamlines come out tangentially composed of an optics hutch, experimental hutch and workstations (Willmott, 2011). The first section of a beamline, known as the ‘front end’ has different functions and filtering the low energy rays is one of them (Willmott, 20011). Finally, in the optics hutch, the beam is focused, or a monochromator is used before it can enter the experimental hutch (Willmott, 2011).

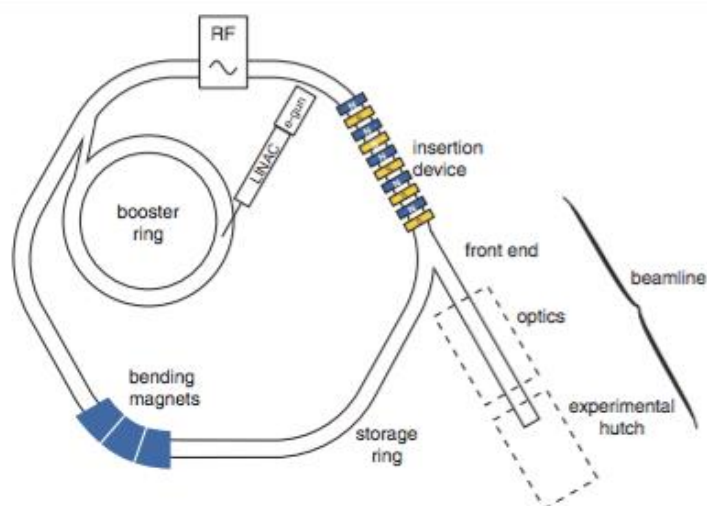


Figure 2.35. An illustration of a synchrotron facility and its components: electron gun (source

of electrons), linear accelerator (linac accelerates the electrons), an evacuated booster ring (more acceleration for the electrons). The electrons are injected into the storage ring, kept in a path passing through bending magnets and insertion device, generating radiation. The beamlines are tangentially and use the light from insertion devices (wigglers or undulators) and from the bending magnets. The radio frequency (RF) supply recharge the energy lost by the electrons. Retrieved from Willmott, 2011. Reprinted with permission.

Because conventional X-ray and CT are not capable of providing intra organ details differentiating variable tissue densities within the organ, which is important in the diagnosis of diseases such as BPH or PCa (Melli et al., 2015), these imaging modalities have some significant limitations for investigating prostatic diseases. In order to help resolve this problem, the use of phase contrast computed tomography (PC-CT), where there is a change in the phase of X-rays as they pass through different tissues in an organ or sample has been developed (Melli et al., 2015). This technique can improve the differentiation amongst soft tissue structures, providing higher tissue contrast and spatial resolution for imaging organs such as the prostate gland (Melli et al., 2015).

In a synchrotron facility, phase contrast can be achieved with a setup known as propagation based imaging (PBI), which means that the detector or camera is moved away from the object/sample resulting in a larger distance between the two (Langer, Cloetens, Guigay, Peyrin, 2008). When the distance is long enough, it allows Fresnel diffraction fringes to be formed as the X-ray beam passes through the sample and moves towards the detector, as shown in figure 2.36 (Kitchen et al., 2005). The importance of the fringes is that they result in “edge enhancement” at any the tissue boundary where there is a density variation and a consequent refraction intensity change in the formed image improving spatial resolution in the image obtained (Kitchen et al., 2005).

Unlike conventional CT, which relies only on the absorption of X-rays, PC-CT uses the phase shift (figure 2.37) as the main property to form the image (Langer et al., 2008). Some of the phase reaching the detector is lost and, consequently, the object information is also lost (Langer et al., 2008). A relationship between the phase shift of the object and the contrast

captured by the detector can be measured and used as a solution to retrieve the phase lost for each angle with the use of a reconstruction algorithm (Langer et al., 2008).

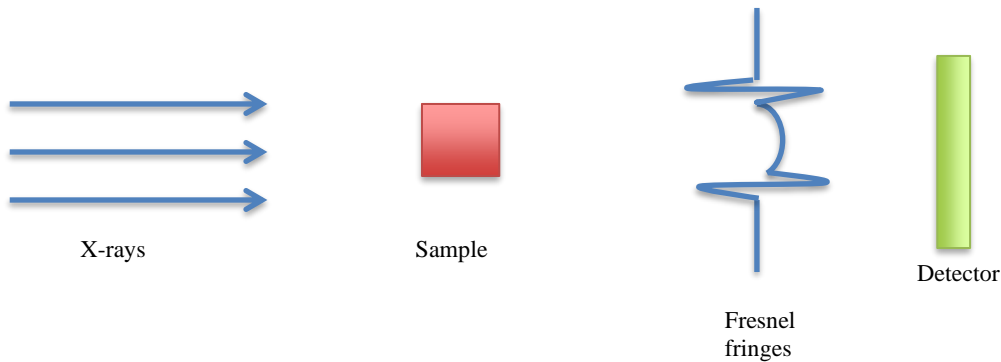


Figure 2.36. The scanning setup for a PBI PC-CT imaging, showing Fresnel fringes forming as the beam propagates towards the detector. (Cavalca Cardoso, 2019).

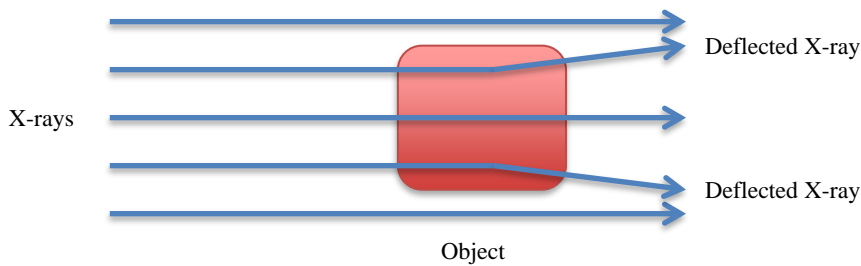


Figure 2.37. Illustration of PC-CT. X-rays penetrating an object are attenuated and deflected due to refraction at boundaries where there is a change in tissue densities. (Cavalca Cardoso, 2019).

Previous studies using PC-CT for imaging other tissues have been conducted. In order to improve the lung imaging in humans, Kitchen et al., 2005 developed a rabbit and mouse model study comparing conventional radiographs and phase contrast imaging of the animals' lung. The results showed an increase in lungs visibility with PC-CT compared to projection conventional radiographs (Kitchen et al., 2005). Another study used cadaver piglets to evaluate internal organs with PC-CT (Zamir et. al, 2016). They showed that the main body organs were better visualized with the PC-CT technique presenting better soft tissue contrast and resolution compared to absorption contrast images (raw free spatial propagation without the phase

contrast) (Zamir et al., 2016). Grandl et al., 2016 imaged *ex vivo* breast tissue from patients with mammary carcinoma with PC-CT and compared this to images from conventional modalities, such as mammography and ultrasound, to assess the effects of chemotherapy treatment. The results showed that PC-CT was the best technique to visualize the excised breast tissue architecture and the alterations in the tissue resulting from chemotherapy treatment, which correlated with the histopathological findings (Grandl et al., 2016).

At the University of Saskatchewan, the prostate research team used excised prostates of a dog and imaged them at the BMIT-BM at the CLS (Wolkowski et al., 2015). The images generated had better contrast than a conventional CT and showed increased “spatial resolution in the micrometer range”, suggesting that this technique can be useful to for imaging the prostate gland (Wolkowski et al., 2015). Taking this into consideration, this present work sought to investigate the use of PC-CT for *in vivo* imaging of the prostate gland of dogs with induced BPH.

## CHAPTER 3: OBJECTIVES

### Thesis Objectives:

To determine if dogs can be used as a model for induced BPH and to see if PC-CT imaging at the CLS may allow for early diagnosis.

#### *Objective 1:*

To reproduce a previously reported protocol for inducing BPH in the intact dog model (in mixed-breed Huskies) as described by DeKlerk et al 1979 who used intramuscular injections of a combination of the hormones DHT and estradiol in Beagle dogs. Consequently, we evaluated histological samples from the prostate glands to determine whether BPH was induced or not (Chapter 4).

#### *Objective 2a:*

To perform *in-situ* PC-CT imaging of the prostate glands of six live dogs (three control dogs and three dogs treated with hormones to induce BPH) at the BMIT-CLS (Chapter 5).

#### *Objective 2b:*

To compare the images from PC-CT imaging of the prostate gland of these six live dogs with conventional imaging modalities (MRI, PET CT, CT and US), to verify whether PC-CT is a superior technique to visualize the gland *in situ* (Chapter 5).



## CHAPTER 4: INDUCTION OF BENIGN PROSTATIC HYPERPLASIA IN INTACT DOGS WITH 17 $\beta$ -ESTRADIOL AND 5 $\alpha$ -DIHYDROTESTOSTERONE HORMONES

Natalia Cavalca Cardoso, Murray Pettitt, Jaswant Singh, Ahmad Al-Dissi, Elisabeth Snead

### 4.1 Abstract

Benign prostatic hyperplasia (BPH) refers to hypertrophy and hyperplasia of the prostate gland that can lead to lower urinary tract symptoms. Other than men, the dog is the only species that develops BPH spontaneously making the dog an excellent animal model for studying this disease in men. This placebo-controlled study tests the induction of BPH in intact mixed-breed huskie dogs (age unknown; ~ 1-5 y.o.) using a combination of 25 mg 5 $\alpha$ -dihydrotestosterone (DHT) and 0.25 mg 17 $\beta$ -estradiol in triolein 3 times per week for 35 weeks. Parameters used to assess the success of the model included digital rectal exam (DRE), semen analysis (motility, progressive motility and concentration of sperm), hormone levels (estradiol, testosterone, DHT and canine prostate-specific arginine esterase CPSE), volume of *in vivo* and *ex vivo* prostates, and physical measurements of the excised gland (height, width, length). The following morphometric parameters of the prostates were assessed to distinguish between the placebo and the BPH group (n=3 dogs per group): area of the prostate, area of acini, number of intra-papillary projections and thickness of septa. Histological diagnosis of BPH was based on a scoring system (0-3) for the three parameters: cystic formation, glandular hyperplasia, stroma hyperplasia.

The results of DRE score showed that prostates of all control and BPH induction group dogs were enlarged in size at the end of the study. Motility, progressive motility and concentration of sperm values were reduced in all dogs from both groups, except dog #5 (control group); however semen analysis values were not statistical significant among the two groups. Plasma levels of DHT and testosterone differed for week and the treatment\*week interaction ( $p < 0.05$ ). Estradiol values differed for week ( $p < 0.05$ ). Exogenous DHT reduced

testosterone and estradiol values via negative feedback, inducing chemical castration in treated dogs but continued maintenance of prostate growth. Based on the manufacture's recommendations of the CPSE hormone test, one of three dogs of the control group (33%) spontaneously developed BPH and one of three dogs of the induction group (33%) was classified as having BPH after receiving the hormone injections. Although there were no statistical differences ( $p>0.05$ ), values were numerically higher in the treatment group compared to controls for height, width, length and volume of the prostate glands. The morphometric endpoints did not differ ( $p>0.05$ ) between the groups. The histopathological scores classified all dogs with BPH, either naturally occurring or induced. Further research is necessary to investigate the induction protocol in the dog as well as investigation of the concentration of the drugs and the length of time they are administered in different breeds.

Keywords: Benign prostatic hyperplasia, BPH, Prostate Gland, Dog, Dihydrotestosterone, Estradiol, CPSE

## 4.2 Introduction

BPH is a common disease affecting men and dogs that is characterized as the enlargement of the prostate gland (Brooks et al., 1973; J. Smith, 2008; Johnston et al., 2000). Both species spontaneously develop this condition and the dog is considered an acceptable animal model for studying BPH (DeKlerk et al., 1979). In men, BPH typically results in symptoms of urinary retention due to urethral compression (Pearson & Williams, 2014), whereas in the dog clinical signs are mostly associated with constipation and/or tenesmus (difficulty in defecation) resulting from compression of the colon from prostatomegaly (Levy et al., 2014; Williams, 2013). Diagnosis of BPH in both species relies on the investigation by the physician/veterinarian of the patient's history, performance of a physical examination, including a digital rectal exam (DRE), and findings from complementary examinations (laboratory, medical imaging) (Nickel et al., 2010; Nizanski et al., 2014; Pearson & Williams,

2014; Vuichoud & Loughlin, 2015). Treatment of BPH in men typically involves medical therapies (use of 5-alpha reductase inhibitors) that reverse and prevent prostatic hypertrophy and hyperplasia by blocking the intracellular conversion of testosterone to dihydrotestosterone (DHT) (Nickel et al., 2010). Dogs on the other hand are typically treated by castration to reduce androgen-induced hypertrophy and hyperplasia of the prostate gland (Nizanski et al., 2014). Castration typically leads to involution of the gland within 12 weeks (Nizanski et al., 2014).

While the pathophysiology of BPH in dogs and men remains incompletely understood (Brooks et al., 1973; Johnston et al., 2000; J. Smith, 2008) dogs have been used as a model to help elucidate aspects of the underlying pathophysiology (Walsh & Wilson, 1976). Two different studies where BPH was induced in dogs in the 1970's reveal interesting but in some cases conflicting results. Walsh & Wilson (1976) produced BPH in the castrated dog with androstenediol alone or in combination with estradiol following 12 months of hormonal induction. Walsh & Wilson (1976), however, failed to induce BPH with a combination of DHT and estradiol. However, in a study by DeKlerk et al., (1979) BPH was induced using a combination of DHT and estradiol therapy. Also, DeKlerk et al., (1979) included castrated and intact animals and were able to induce BPH after only four months of hormonal therapy. They induced BPH in the intact group using androstenediol alone or in combination with estradiol and with DHT alone or in combination with estradiol. Androstenediol and estradiol was the most effective hormonal combination for inducing BPH; however we did not receive the approval from Health Canada to use androstenediol in our research. So we decided to use DHT because DHT with estradiol was the next most effective protocol (DeKlerk et al., 1979). DeKlerk et al., (1979) showed that BPH could be induced in both castrated and intact dogs with the administration of different combinations of reproductive hormones.

The goal of this study was to induce BPH in intact dogs using a protocol similar to that described by DeKlerk et al., (1979) using the administration of estradiol and DHT. Moreover,

we performed conventional imaging (radiography, US, CT and MRI) along the course of the study. The CT images were used to calculate *in vivo* prostate volume changes over time. Images collected with all modalities were used for comparison purposes with synchrotron-based phase contrast computed tomography (PC-CT) -generated images as reported in chapter 5.

### 4.3 Materials and Methods

#### 4.3.1 Animals

Six healthy male dogs (n=6, mixed-breed huskies, age unknown but approximately 1-5 years of age, body weight range= 19.5 – 29.5kg) were randomly assigned using a random number generator to either a treatment (BPH induction) (dogs#3, 4 and 6, n=3) or control (dogs# 1, 2 and 5, n=3) group (table 4.1). All dogs had an initial physical examination by a licensed veterinarian (ES). The dogs were initially kept in quarantine for 40 days to allow them to acclimatize to their new surroundings and they were all vaccinated for rabies (Merial INC. Athens, GA, USA) and for distemper, parvovirus, infectious canine hepatitis and canine parainfluenza using Vanguard®Plus (Zoetis INC. Kalamazoo, MI, USA). For the duration of the study all dogs were housed in individual kennels that did not restrict their movement and provided access to an indoor and outdoor area. Water was provided *ad libitum*; they were fed twice a day a commercial dry dog kibble (Hills® ScienceDiet® Adult Advanced Fitness) and walked once a day.

Table 4.1. Random assignment of dogs to a control or BPH induction group.

Control group	Treatment for BPH induction group
Dogs# 1, 2 and 5	Dogs# 3, 4 and 6

All procedures described in this study were carried out in full accordance with the guidelines for animal experimentation of the Canadian Council on Animal Care and approved by the University of Saskatchewan Animal Care Animal Research Ethics Board.

#### 4.3.2 Physical Exams and Samples Collected

At the start of the study, all dogs underwent a complete physical examination, a digital rectal exam (DRE), and blood samples were collected for a complete blood count (CBC), a serum biochemistry profile, and creatine kinase. CBC and serum biochemistry were used to confirm the dogs were healthy at baseline, and creatine kinase was initially measured at week 2 in order to monitor for potential muscle necrosis associated with the frequent intramuscular injections. Leftover serum and plasma were saved for future hormone analysis and stored at -20°C until required. Urine was collected by catheterization and submitted for a complete urinalysis. The dogs also had baseline-imaging examinations performed including a lateral abdominal radiograph, ultrasound and CT of their prostate glands. Throughout the duration of the study, a DRE was repeated weekly as part of a physical examination and the prostate gland evaluated according to the following scoring system: 0 to 3, where 0= no signs of enlargement; 1= gland slightly enlarged; 2= prostate enlarged with or without cysts and asymmetry between lobes appreciated but animal not displaying any signs of the hyperplasia; and 3= prostate prominently enlarged, asymmetry between lobes appreciated, presence of cysts, hyperplasia leading to clinical signs such as urethral discharge, tenesmus and/or constipation. Blood, urine and semen were also collected once a month (total length of the study was 35 weeks or 243 days with first injection performed on week 0 or day 1). Semen was collected by ejaculation, urine by catheterization and blood by routine venipuncture. Serum creatine kinase was also measured at the end of the second week following initiation of intramuscular injections of the hormones in order to monitor for any evidence of muscle injury. All routine laboratory analyses were performed by Prairie Diagnostic Centre Inc. (PDS) at the Western College of Veterinary

Medicine (WCV), University of Saskatchewan. Hormone analyses were performed through the Endocrine laboratory in the Department of Veterinary Biomedical Sciences at the University of Saskatchewan. Further details on the hormonal analysis is provided later.

For the semen collection, ejaculate samples were collected following manual stimulation using a teaser female once a month. The sperm-rich fraction was then subjected to semen analysis to assess sperm motility and concentration. Left over samples were centrifuged at 500xG for 10 minutes and the seminal plasma component stored at -80° C for future analysis if required. Semen analysis was performed by trained personnel (MP) in the Male Reproduction laboratory in the Department of Animal Poultry Science at the University of Saskatchewan. The findings from all the urine, CBC, serum biochemistry, semen and DRE results for all the dogs at all time points are included in the appendix section.

Figure 4.1 illustrates a flow diagram outlining the study design, including baseline examinations, first injection, each time point for collection of samples, and imaging examinations.

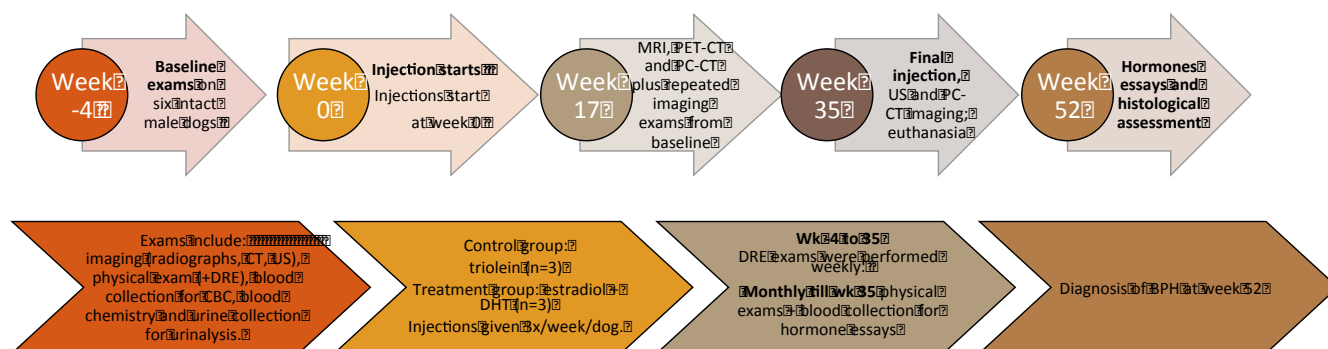


Figure 4.1. Flow diagram outlining the study design (wk=week).

#### 4.3.3 Preparation of the Injection Solutions

Reconstitution of the hormones 17 $\beta$ -Estradiol (Sigma Catalog # E-8875; 1,3,5[10]-Estratriene-3,17 $\beta$ -diol, Oakville, ON, Canada) and Androstanolone (Toronto Research Chemicals Catalog A637540; 5  $\alpha$  , 17 $\beta$ -17-Hydroxyandrostan-3-one or 5  $\alpha$  -

Dihydrotestosterone, Toronto, ON, Canada) was performed using aseptic technique using benzyl alcohol (PCAA Professional Compounding Centers of America Catalog # 55-1391-100ml, London, ON, Canada) added to the carrier triolein (TCI Tokyo Chemical Industry America Catalog # G0089, Portland, OR, USA) in a biosafety hood, based on the protocol in DeKlerk et al., (1979) with some modifications. To prepare the treatment for BPH induction solution, 37.5 mg of 17  $\beta$  -Estradiol powder was mixed with 30 mL benzyl alcohol (Malhi et al., 2006), the solution was stirred for 20-30 minutes or until the estradiol had been completely dissolved. This was followed by the addition of 3750 mg 5  $\alpha$  -Dihydrotestosterone powder, which was again stirred until completely dissolved. The addition of the triolein carrier was then done to make up the final volume of 150 mL. The solution was then left in an open top flask in a fume hood for 2 weeks to evaporate the alcohol. After this time the volume of the solution was remeasured and additional Triolein was added in order to achieve a final volume of 150 mL. The control solution consisted of 30 mL of benzyl alcohol and 120 mL of triolein and was processed in the same manner as the treatment for BPH induction solution. The final solutions were then passed through a 0.22  $\mu$ m sterile filter (Millex® GS, Merck Millipore Ltd., Tullagreen, Co. Cork, Ireland) into sterile bottles in a sterile biological safety cabinet to allow for safe injection. The volume administered to both the treatment for BPH induction and control dogs was 1.0 mL IM per animal per injection.

#### 4.3.4 Hormone Injections

The control group (n=3) received 1 ml of the carrier triolein as an intramuscular injection and the treatment for BPH induction group (n=3) received the reproductive hormones at the following doses, 25 mg/mL of 5 $\alpha$ -DHT and 0.25mg/mL of 17  $\beta$ -estradiol, made up to a volume of 1mL with the triolein carrier. All intramuscular injections were administered in the left and right side of the epaxial muscles of the lumbar region (see figure 4.2). Injections were performed every Monday, Wednesday and Friday, alternating sites so that each site was only

used for injection once every two weeks, with the exception for the BPH induction dogs that were not injected on days 148, 150 (week 21) and 206 (week 29) due to delays in the evaporation process of the alcohol during injection preparation. The control group followed the same pattern of injections for the same days/week so both groups were treated the same.

Injections were administered for a period of eight months (35 weeks). Use of all controlled drugs, including use of dihydrotestosterone, were approved by the Office of Controlled Substances, Health Canada.

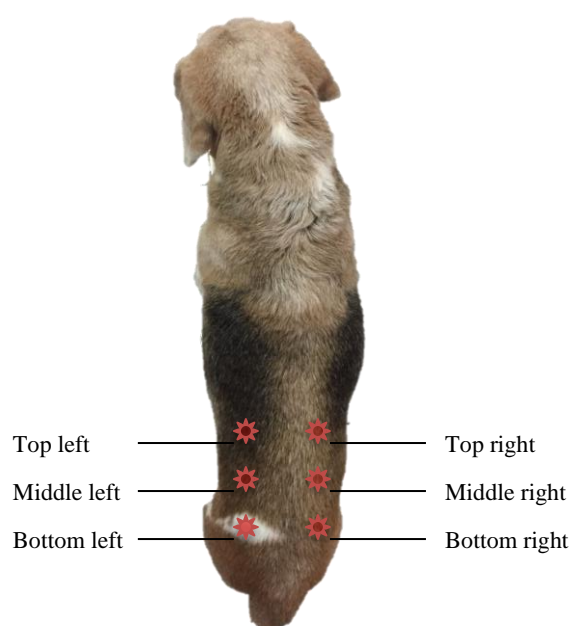


Figure 4.2. Dorsal view of a dog showing the site for injections in the epaxial muscle of the lumbar region.

#### 4.3.5 Hormone Analysis

Blood samples were collected on the same days as the physical examinations (once a month). Samples were collected into clot and EDTA containing tubes, centrifuged at 1500xG for 10 min within 20 min of collection, and the resulting serum and plasma collected and stored at -20°C for further hormone analysis. The hormones measured included canine prostate specific arginine esterase (CPSE) and DHT using ELISA kits, and testosterone and estradiol using radioimmunoassay ELISAs. CPSE is a protein produced by the prostate in healthy dogs



and has been shown to be elevated with BPH in dogs (Pinheiro et al, 2017). Hence, this was used as a marker for BPH induction in this protocol (CPSE Odelis®). DHT and estradiol were measured to document absorption in the BPH induction group and to show differences between the levels in the treatment and control groups. With DHT and estradiol administration, negative feedback on testosterone secretion was anticipated so testosterone, a precursor to both DHT (Madersbacher et al., 2019) and estradiol (Ajayi & Abraham, 2018), was also measured to investigate if there were differences between the treatment and control groups.

CPSE was analysed using a ELISA kit (Odelis® CPSE, Virbac, France) previously validated for use in dogs, which gives a clinical threshold of 61ng/mL (range 54ng/mL – 67ng/mL) for the diagnosis BPH (Pinheiro et al., 2017). This assay has a reported sensitivity of 97.1%; specificity of 92.7% for detection of BPH with this proposed cut off. For this protocol an intra-assay CV of 2.20% and 12.82% and inter-assay CV of 9.64% were obtained. Concentrations of DHT were determined by a canine specific kit (US Biological Life Sciences, Dihydrotestosterone Bioassay™ ELISA kit, Salem, Massachusetts, USA) used according to the manufacturer's instructions. Assay sensitivity was 1pg/mL and calculated CV values were 45.4% and 44.1% for intra-assay and 41.5% for inter-assay; although these CV values are high, control animals were always below 1000 pg/mL and the treatment animals were never below 1750 pg/mL as observed in the results. A radioimmunoassay (RIA) kit (ImmunoChem™ Double Antibody Testosterone <sup>125</sup>I RIA kit, ICN Biomedicals, Inc., Costa Mesa, CA, USA) was used to measure the serum testosterone concentrations. The intra-assay CV was 13.5% for low and 14.5% for high control serum samples. The estradiol radioimmunoassay performed was a non-commercial test. The protocol was adapted from Joseph, Currie and Rawlings (1992) with the only modifications being to use 250µL serum instead of 500µL, and 4 mL of ether instead of 5 mL. The assay sensitivity was 1pg/mL and the intra CVs were 51.3% for low and 27.8% for high reference serum. For estradiol, if the CV of the duplicates was >20% the most appropriate of the two raw values was selected for analysis and the other value ignored.

#### 4.3.6 *In vivo* Imaging

All the six dogs underwent identical imaging throughout the study. Baseline imaging performed at week -4 included ultrasound, CT and radiography of the prostate gland. Ultrasound, CT, PC-CT, radiography, MRI and PET-CT were performed at week 18 and PC-CT and ultrasound were performed again at week 35. Dogs were fasted for 12h prior to collection of blood or urine and prior to all imaging exams. The same protocol was used for sedation for all dogs to permit US, CT and radiographs and consisted of hydromorphone (Hydromorphone Hydrochloride Injection USP, Sandoz, Canada, 10 mg/mL, 0.05mg/kg IM), dexmedetomidine (Dexdomitor, Pfizer Canada Animal Health Inc, Kirkland, Quebec, Canada, 0.5mg/mL, 0.002mg/kg IM) and ketamine (Vetalar, Bioniche Animal Health Canada Inc., Belleville, Ontario, Canada, 100mg/mL, 2mg/kg IM). For anesthesia, required for MRI, PC-CT and PET-CT imaging, the following protocol was utilized for all dogs: IV fluids (Normosol-R electrolyte injection solution, 1000mL, maintenance fluid rate 4mL/kg/hr), premedication with hydromorphone (Hydromorphone Hydrochloride Injection USP, Sandoz, Canada, 10 mg/mL, 0.1mg/kg) and acepromazine (Atravet, Boehringer Ingelheim, Burlington, Ontario, Canada, 10mg/mL, 0.05mg/kg) IM; induction with propofol (Propofol Injectable Emulsion, Fresenius Kabi Ltda, Richmond Hill, Ontario, Canada, 10mg/mL, 5mg/kg) IV and maintenance with isoflurane (Isoflurane, USP 99.9%, Halocarbon Products Corporation, New Jersey, USA, inhalant) and oxygen.

After the final *in vivo* live imaging using PC-CT, the dogs were maintained in the positioning device and humanly euthanized with Pentobarbital Sodium (Euthanyl Forte, Bimeda-MTC Animal Health Inc, Cambridge, Ontario, Canada) at a dose of 1mL/5kg body weight injected into a catheter in the cephalic vein. Immediately following euthanasia, heparin sodium (Fresenius Kabi Ltda, 50000 USP units/5mL, Ontario, Canada, 5ml/dog) was intravenously injected in each dog through the catheter in the cephalic vein to limit coagulation. Dogs were then reimaged as cadavers without removal from the positioner device.

Following repeat PC-CT imaging, a cut down was made to expose the external iliac vein and the cadavers were perfused either with 10% formalin (dogs #2 and #5) or 4% paraformaldehyde (dogs #1, #3, #4 and #6) IV using a volume of 3L/dog.

#### 4.3.7 Prostate Volume Measurements

The estimated volume measurement for each dog's prostate glands were calculated at three different time points using the imaging studies: at baseline (week -4) before the hormone injections were initiated, at week 17 and at the end of the study (week 35). For both the week -4 and 17 measurements, the prostate volume was calculated using the *in vivo* CT images. Using the free hand tool in HOROS® software (<https://horosproject.org/>), a line was drawn around each CT prostate image transverse slice, thus delimitating the surface of the gland. Once this step was done, the 3D volume rendering was obtained. After euthanasia at week 35, each prostate gland was harvested and fixed in 10% formalin for 24 h and then the true volume of each excised prostate was measured by water displacement.

#### 4.3.8 Histological Preparation

Following euthanasia and injection of either 10% formalin IV or 4% paraformaldehyde using a volume of 3L/dog into the external iliac vein, the prostate gland along with the urinary bladder and a portion of the pelvic urethra was removed on mass from each dog and fixed in 10% formalin for 24h. After 48 hours, excess adipose tissue was dissected away from around each prostate gland and an electronic digital calliper (Star Asia USA, LLC d.b.a Titan, Seattle, Washington, USA) was used to record the height, length and width of the individual glands. Consecutively, each gland was weighed using a laboratory scale (TR-403 series balances, Denver Instrument Company Ltd., Arvada, CO, USA) and the volume was estimated by water displacement. Although the bladder was still attached to the prostatic urethra, it was carefully held out of the scale to not be included in the volume determination. Photographs of each prostate and the attached bladder can be seen in the appendix section.

Subsequently, the prostate glands were then placed in a container with 10% phosphate buffered saline (PBS) for four weeks and afterwards embedded in clear gelatin (Knox® gelatin, Associated Brands LP) inside a cylindrical container (h= 9.8 cm x r=2.4 cm).

Once the gelatin had set, the prostate gland within the gelatin mould was removed from the cylindrical container (figure 4.3) and placed in a custom purpose-built metal slicing holder (RMD Engineering Inc, Saskatoon, SK, Canada). Additional gelatin was added into the holder to surround the prostate gland and fix the sample in place. Yellow dividers were placed between the holder fins at a distance of three mm from each other to facilitate accurate slicing of the prostate gland into three mm thick transverse slices. Using a 15 cm long microtome blade (Fisher Scientific, Ottawa, Ontario, Canada), three mm thick transverse tissue slices of the prostate for histology were prepared from the excised gland (see figure 4.3 and appendix for more details of the protocol).

After slicing, the individual segments of the prostate were carefully removed and tissue ink (red and blue, washable finger paint, HandyArt Inc., Milton, WI, USA) was applied on the dorsal and right side of the prostate for orientation purposes. Each slice was placed on a blank piece of white paper in numbered order starting from the most cranial to the most caudal slice. A small notch was made with a scalpel blade on the right side of each prostate slice again for orientation purposes. Excess gelatine was delicately removed, ink reapplied to the dorsal and right margins of the prostate gland and then each slice was placed caudal face up individually in into a histology cassette and labeled with the dog number and the slice number. All pictures from the slicing process illustrated in figure 4.3 were taken with a digital camera obtained using the macro setting (Canon Power Shot A620, Canon Inc., China).

The individual cassettes containing the prostate slices for each dog (total of 9-12 slices/dog) were placed in 10% formalin and submitted to the Royal University Hospital, Pathology and Laboratory Medicine. Routine histological processing included dehydration, clearing (ethanol and xylene) and embedding in paraffin. From the tissue blocks, histological sections were cut at 5  $\mu$ m, mounted on a poly-L-lysine coated glass slide and stained with H-E (hematoxylin-eosin).

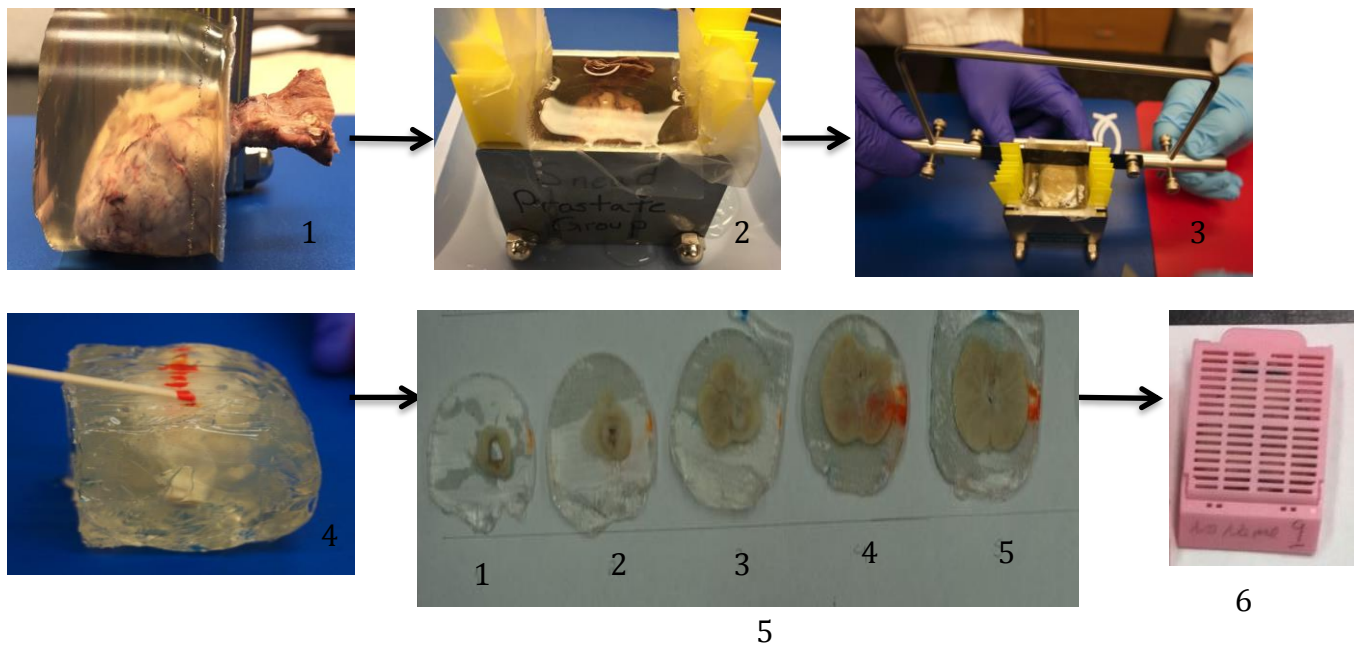


Figure 4.3. Preparation steps for excised prostates. 1) Excised prostate is embedded in gelatin initially in a cylinder container (removed here) and 2) the prostate encased in gelatin is placed inside the custom-made slicing holder with additional gelatin added. 3) Slicing of the prostate gland was done where the yellow dividers were originally placed (3mm distance between each divider). 4) The individual slices were removed and inked on the cranial (orange ink) and right side (blue ink but not shown) for orientation purposes, and then 5) the separated slices of the prostate encased in gelatin are placed on a sheet of paper with numbers assigned to each slice (arranged in a cranial to caudal direction) with the caudal surface visible. Extra gelatin was carefully removed and the cranial and right sides of each slice were then re-inked and then each individual single slice was placed inside a labelled and numbered cassette with the caudal surface facing up for histological processing (4).

#### 4.3.9 Morphometric Analysis

Each section of prostate was scanned by an Olympus (Olympus BX61VS virtual microscopy system, software VS-ASW 2.9) and converted into a virtual microscopy (VM)

digital file (camera Allied VC-50) for morphometric analysis using OlyVIA (Olympus OlyVIA 2.9) software. An average of 11 slides per dog were analyzed (number of slides/dog range 9-12). In each slide, the surface area of the entire section was first measured and recorded. Acinar size was assessed by measuring the surface area of 15 randomly selected acini within each section in all slides. Within each of the 15 selected acini, the number of papillary projections was also counted. Stromal hyperplasia was assessed by measuring the thickness of interlobular septa at 3 random locations within each section. Means were calculated from all recorded values (in each category) to generate a final mean/dog. Figure 4.4 shows how the scanned slides are visualized. All morphometric parameters were assessed and counted by the first author (NC) after being trained by a board certified pathologist (ANA).

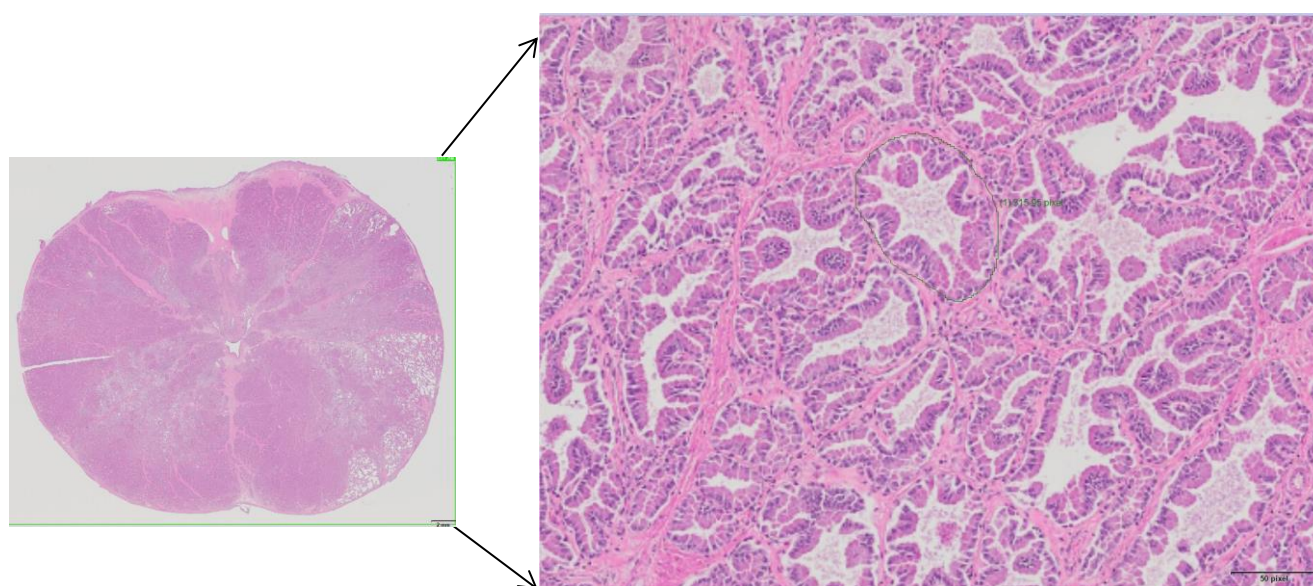


Figure 4.4. Scanned slides for morphometric analysis. Low power magnification (4x) was used for the calculation of the surface area of the gland, which was drawn around each slide, and the measurement of thickness of the interlobular septa (left). The surface area of acini along with the count of the intrapapillary projections were measured using high power magnification 20x (right).

#### 4.3.10 Histological Scoring



Two sections of the prostate from each dog were examined and 3 parameters: cystic formation, glandular hyperplasia, and stromal hyperplasia were subjectively scored from 0-3 with 0= indicating the absence of change, 1= indicating the presence of mild change observed in < 20% of the section (at least one portion of the prostate), 2= indicating the presence of moderate change covering 20-50% of the section (more than one portion of the gland) and 3= indicating the presence of severe change in more than 50% of the section (multiple parts of the prostate). For each parameter, an average score was calculated from the scores obtained from the two sections. The average scores of each of the three parameters were added and a BPH score was calculated. Figure 4.5 shows the acini (A) or glandular component of the gland and also the stroma (S).

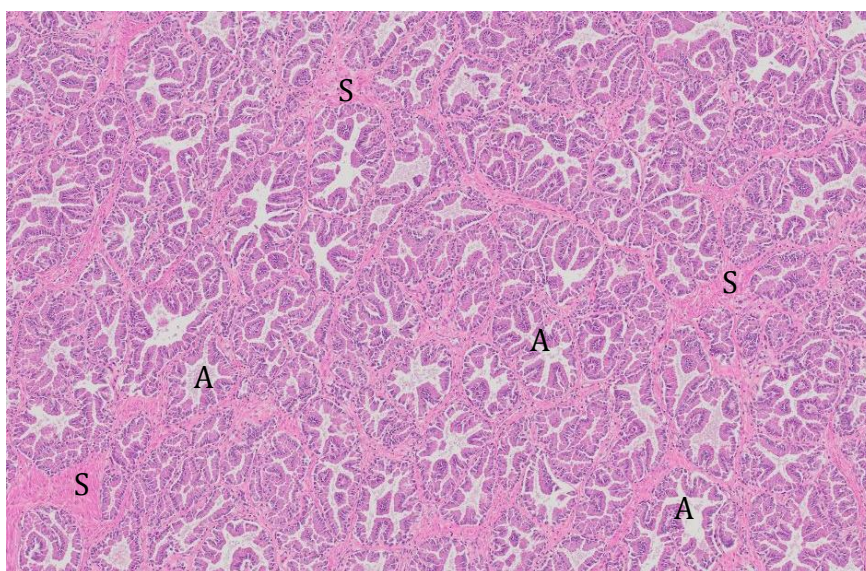


Figure 4.5. A histological slide displaying the acini (A) and the supporting stroma (S) of the prostate gland.

#### 4.3.11 Statistical Analysis

All variables analyzed in this study were tested for normality and the appropriate test used (parametric if data is normally distributed or nonparametric if data is not normally distributed).

For the prostate volume, the *in vivo* data were statistically analyzed in two different scenarios. The first scenario compared the BPH induction and control group prostate volumes from week 17 to each other using an unpaired t-test; the second scenario compared the volume within the same group between the different time points (between week -4 vs week 17) using a non-parametric test, Mann-Whitney U (GraphPad Prism®6 2018 software CA, USA <https://www.graphpad.com/scientific-software/prism/>). For the *ex vivo* volume data, a parametric unpaired t-test (GraphPad Prism®6 2018 software CA, USA) was used to compare the prostate volume determined by water displacement for the treatment for BPH induction versus control groups at week 35. For the physical measurements of the prostate gland (height, length and width) the two groups were analyzed with a parametric unpaired t-test (GraphPad Prism®6 2018 software CA, USA).

For morphometric analysis data, a non-parametric Mann-Whitney U was performed for number of intrapapillary projections (GraphPad Prism®6 2018 software CA, USA); however area of acini, surface area of prostate/slice and thickness of septa were analyzed with a parametric unpaired t-test (GraphPad Prism®6 2018 software CA, USA).

The hormonal data from the CPSE, testosterone, DHT and estradiol assays were evaluated using a generalized linear mixed model (known as proc glimmix in SAS) for repeated measures analysis performed by a Statistical Analysis System software (SAS 9.4; SAS Institute Inc., Cary, NC, USA). The use of this model was necessary because the data was not normally distributed. A code was written by a statistician specialized in SAS (Dr Peiqiang Yu) and adapted to fit the present hormone data, and the best covariance structure model found for all four hormones was compound symmetry. The model consisted of the explanatory variables treatment, week and the treatment\*week interaction and repeated factor dog number. Data are presented as means of the duplicates.

For all the parameters evaluated, a P value  $\leq 0.05$  were accepted as statistically significant and data are presented as mean  $\pm$  standard error of mean (SEM).



## 4.4 Results

### 4.4.1 Physical examination

The baseline (-4weeks) mean  $\pm$  SEM weight of the dogs was 25.8kg  $\pm$  1.52kg (range 19kg to 29.5kg), median 26.8kg and the final (week 35) mean  $\pm$  SEM was 27.98  $\pm$  2.05kg (range 19.5kg to 33kg), median 28.95kg. There were no differences ( $P>0.05$ ) between the control and BPH induction groups for all time points.

All six dogs were clinically normal at all time points when examined, with the exceptions of dog #3 and dog #6, both from the BPH induction group. Three weeks after initiating injections, dog #3 developed a small lump at one of the injection sites; further lumps also arose at different injection sites, during the study. A licensed veterinarian (ES) examined the dog and also performed an ultrasound exam of the lumps, concluding that no subdermal abnormalities were associated and the injections were continued because the dog was otherwise in great health. Dog #6 presented signs of swelling and redness of both testicles during week 11 following initiation of the injections. A licensed veterinarian (ES) examined the dog and diagnosed the dog with superficial scrotal pyoderma and possible orchitis. For the superficial scrotal pyoderma chlorhexidine (Stanhexidine, chlorhexidine gluconate solution, 4%, Omega Laboratories limited, Montreal, Canada) was prescribed to clean the scrotum and an e-collar placed to prevent the dog licking the region. On week 19, after no improvement of the clinical signs, dog #6 received oral antibiotics (Enrofloxacin 68mg, 4mg/kg) resulting in total resolution of the swelling and redness after one week.

Based on DRE score evaluation (0-3), and subjective results, by the end of the study all control dogs (dog #1, #2 and #5) had a slightly enlarged prostate with a DRE score of 1, with the only difference that dog#1 had an easily palpable prostate throughout the study (see table 4.2). For the BPH induction group one had a slightly enlarged prostate (dog#6) with a score of 1 and two had moderate enlargement of the prostate (dog #3 and #4) with a score of 2; and for one of these dogs (#4) a cyst was palpable from week 27 onwards. In the control group, dog 1

changed from score 0 to 1 at week 26, dog 2 at week 27 and dog 5 at week 25. In the BPH induction group, dog 3 changed from score 0 to 1 at week 5, dog 4 at week 6 and BPH induction dog 6 at week 5. Also, in the BPH induction group dog 3 changed from score 1 to 2 at week 28, and dog 4 from score 1 to 2 at week 26.

Table 4.2. DRE score for baseline (week -4) and for last evaluation (week 35). Control dogs: 1, 2 and 5 and treatment dogs: 3, 4, and 6.

	Control Dogs			Treatment for BPH Induction Dogs		
	Dog# 1	Dog# 2	Dog# 5	Dog# 3	Dog# 4	Dog# 6
Week -4	0	0	0	0	0	0
Week 35	1	1	1	2	2	1

#### 4.4.2 Creatine kinase (CK) analysis

The values obtained after 14 days of injection for five of the dogs were all within the reference range (51-418 U/L). For one control dog (dog#5) the CK was slightly elevated at 532 U/L, but this was not considered clinically significant and not elevated enough to suggest any myonecrosis. There was no statistical difference between the control and BPH induction group ( $P>0.05$ ).

#### 4.4.3 Routine diagnostic laboratory data: CBC, serum biochemistry analysis, urinalysis (UA) and semen analysis

Minor abnormalities were seen but the findings of the CBC, serum biochemistry profile and urinalysis confirmed that all the dogs were healthy and there was no statistical difference between the control and BPH induction group ( $P>0.05$ ). One control dog (#5) did have moderate pyuria and hematuria and mild proteinuria on the initial UA associated with very highly concentrated urine. The semen analysis results of all the dogs for baseline and end of the study are displayed in table 4.3 (see appendix for all reported values). It is possible to observe that by the end of the study the sperm concentration decreased

for all six dogs, especially for the dogs in the BPH induction group, which had zero concentration or in the case of dog 4 from the BPH induction group had so few sperm that the concentration could not be estimated by the haemocytometer. Motility and progressive motility decreased in all dogs except dog#5 (control group) over time. The overall volume of seminal plasma collected increased for all dogs over the course of the study. Table 4.4 displays the statistical analysis for the semen parameters between control and BPH induction (treatment group). The volume of semen collected from BPH induction group at the end of study in week 32 ( $7.23 \pm 1.03$  mL) was greater ( $p=0.0088$ ) than at the beginning of study in week -4 ( $1.7 \pm 0.63$  mL)

Table 4.3. Semen analysis of all six dogs displaying volume, motility, progressive motility and concentration of sperm. Baseline data for all dogs are from week -4, except dogs #5 and #6, collected at week 0 and week 4 respectively. End of collection date for all dogs was week 32.  $P>0.05$  for all parameters: control baseline vs end, treat baseline vs end and control end vs treat end, except volume treatment baseline vs end was  $P<0.05$ .

		Volume (mL)		Motility (%)		Progressive motility (%)		Concentration of sperm ( $\times 10^6$ /mL)	
		Baseline	End	Baseline	End	Baseline	End	Baseline	End
Control Group	Dog#1	1	7.5	100	55	76	50	68.4	62.5
	Dog#2	0.2	4.6	98	55	80	50	965	37.5
	Dog#5	4.3	5.5	60	70	50	65	48.75	42.5
Treatment for BPH Induction Group	Dog#3	0.5	5.2	98	0	66	0	287.4	0
	Dog#4	2	6.6	100	50	82	45	94.9	0*
	Dog#6	2.6	8	96	0	73	0	125.7	0

\*0= ND: non-determinable due to a very low concentration that could not be determined with a haemocytometer.

Table 4.4 Statistical analysis of the semen. P value, mean and SEM for control and BPH induction (treatment) groups are shown below for both baseline and end time points. (treatment= treat).

Semen parameters	P value											
	Control baseline vs Control end	Control baseline vs Treat. baseline	Control end vs Treat. end	Treat. baseline vs Treat. end	Control baseline		Control end		Treatment baseline		Treatment end	
	Mean	SEM	Mean	SEM	Mean	SEM	Mean	SEM	Mean	SEM	Mean	SEM
Volume (mL)	0.1202	0.9288	0.3646	0.0088	1.83	1.26	5.87	0.86	1.7	0.63	6.6	0.81
Motility (%)	0.2816	0.4103	0.2000	0.2500	86	13.01	60	5	98	1.16	16.67	16.67
Progressive motility (%)	0.4748	0.6583	0.1000	0.2500	68.67	9.41	55	5	73.67	4.63	15	15
Sperm concentration ( $\times 10^6$ /mL)	0.2500	0.7000	0.1000	0.2500	360.72	302.20	47.5	7.64	169.33	59.70	0	0

Figure 4.6 shows the sperm concentration for all dogs in both the control and BPH induction (treatment) groups. Based on this information and the fact that dogs' spermatogenic cycle lasts 62 days (Amann R. P, 1986), and the epididymal transit time is approximately 12 days (Robaire, B., Hinton, B. T., Orgebin-Crist, M.C. 2006) summing to a total of 74 days, the termination of spermatogenesis was calculated for each dog of the treatment group. This is another indication that the hormonal treatment was having a biological effect and was individually performed for each dog by subtracting 74 days from the number of days it took for a sperm concentration of 0 to be first observed. Dog #3 stopped production of sperm at week 12, dog #6 at week 24 and dog #4 at week 32 (sperm count was too low to be determined by a haemocytometer). Thus, for dog#3 the inhibition of normal testicular function occurred by 10 days, for dog#4 by 150 days and for dog#6 by 94 days following the first hormone injection.

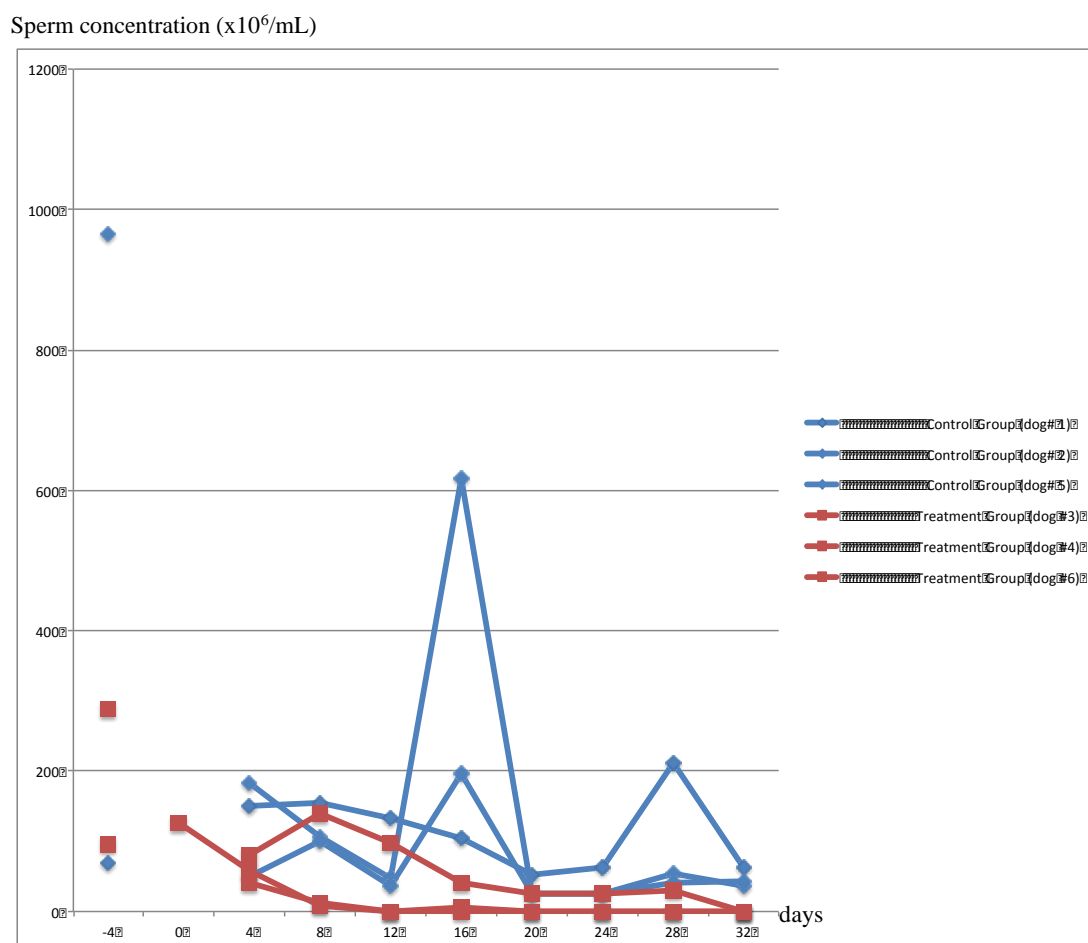


Figure 4.6. Sperm concentration over time for control dogs# 1, 2 and 5 (blue) and treatment (BPH induction) dogs# 3, 4 and 6 (red).

#### 4.4.4 CPSE, DHT, testosterone and estradiol

The results of the CPSE, DHT, estradiol and testosterone analyses are shown below. For all the upcoming analysis, ‘h’ (hormone group) corresponds to BPH induction group and ‘c’ corresponds to control group. Table 4.6 shows the statistical analysis for treatment (P=0.6615) and week (P=0.0029). Figure 4.7 shows the mean and SEM for the CPSE concentration for the control and BPH induction groups and the interaction between treatment\*week (P=0.1785). Values were higher in week 16 and 20 than in week -4 (week P=0.0029). For the CPSE ELISA, the manufacturer indicates that a diagnosis of BPH in a dog can be inferred when the CPSE level is > 61ng/mL. According to this, only dog 1 from the control group and dog 4 from the treatment for BPH induction group had CPSE values > 61ng/mL (table 4.5) and had thus developed BPH. CPSE mean value was higher than 61 ng/mL on weeks 4, 12, 16, 20, 24, 28 and 32 for the control group and then on weeks 8, 12, 20 for the BPH induction group.

Table 4.5. CPSE mean concentration (ng/mL) detected by ELISA in two groups of dogs (control and treatment) over time. SEM= standard error of mean. P =0.6615 for treatment, P=0.0029 for week. Within row, means without a common superscript are significantly different.

Treatment (ng/mL)		sem (ng/mL)	p value	n
Control	Hormone	33.4211	0.6615	3
70.0729	50.9663			

Week (ng/mL)									sem (ng/mL)	pvalue	n
-4	4	8	12	16	20	24	28	32	34.5319	0.0029	6
35.1410 <sup>b</sup>	62.2821 <sup>ab</sup>	57.0220 <sup>ab</sup>	78.4718 <sup>a</sup>	73.7873 <sup>a</sup>	94.5021 <sup>a</sup>	47.2982 <sup>ab</sup>	55.0217 <sup>ab</sup>	19.9891 <sup>ab</sup>			

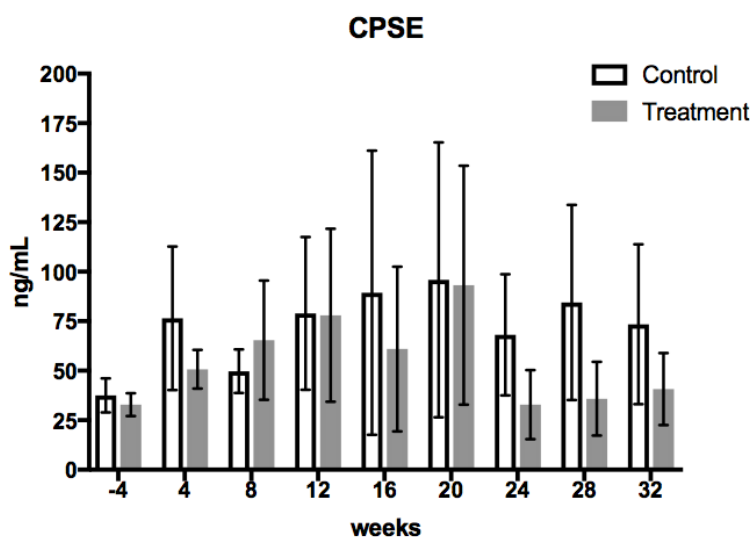


Figure 4.7. Treatment\*week interaction for mean CPSE concentrations for the control and treatment groups and SEM (black bars) over time (P=0.1785).

Although table 4.6 shows significant effects of treatment (p=0.0058) and week (p=0.0273) for DHT, it is the significant treatment\*week interaction (p=0.0388) graphed in figure 4.8 that is to be considered. Serum levels of DHT in the control group were lower than those for BPH induction group for all the weeks (week\*treatment p=0.0388). Figure 4.8 shows mean DHT concentrations for the control and treatment groups and SEM over time.

Table 4.6 DHT mean concentration (ng/mL) detected by ELISA in two groups of dogs (control and treatment) over time. SEM= standard error of mean. P =0.0058 for treatment, P=0.0273 for week. Within row and column, means without a common superscript are significantly different.

Treatment (pg/mL)		sem	p value	n
Control	Hormone	(pg/mL)		
586.95 <sup>a</sup>	2909.66 <sup>b</sup>	614.26	0.0058	3

Week (pg/mL)									sem	p	n
-4	4	8	12	16	20	24	28	32	(pg/mL)	value	
1438.25 <sup>a</sup>	1385.06 <sup>a</sup>	1481.42 <sup>a</sup>	1357.82 <sup>a</sup>	1423.03 <sup>a</sup>	1283.11 <sup>a</sup>	1136.43 <sup>a</sup>	1154.54 <sup>a</sup>	1158.09 <sup>a</sup>	239.03	0.0273	6

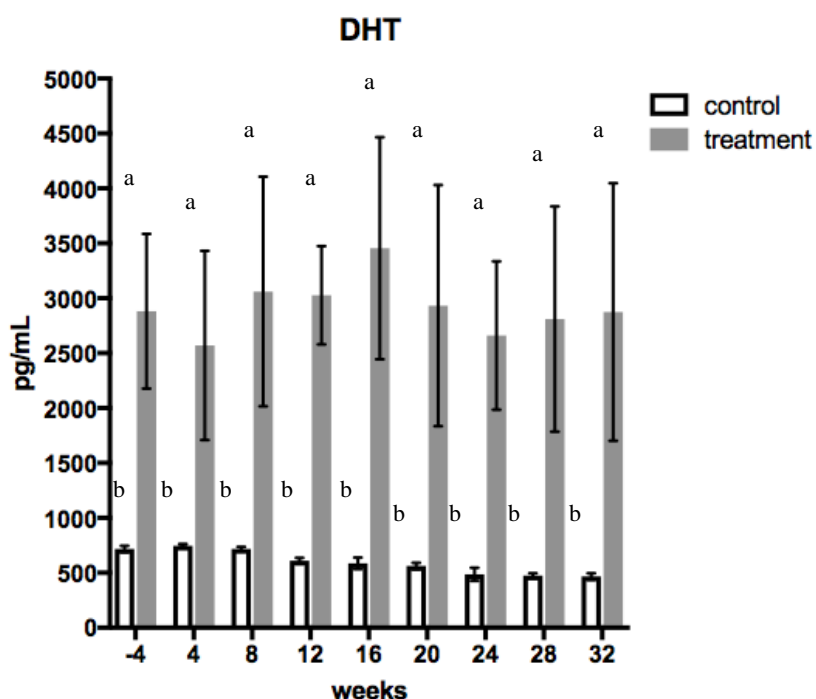


Figure 4.8. Treatment\*week interaction for mean DHT concentrations for the control and treatment groups and SEM (black bars) over time (P=0.0388). Means without a common superscript are significantly different

Table 4.7 shows the statistical analysis of estradiol. Figure 4.9 shows the mean and SEM concentrations for estradiol for the control and BPH induction groups over time. Three extreme values from individual dogs at different time points were not compatible with *in vivo* concentrations of estradiol and had to be removed from the analysis (dog#4 and dog#6 week 12 and dog#6 for week 28). These were probably incorrect measurements from the RIA test. The plasma level of estradiol (averaged between treatment groups) was higher on week 12 compared to week 20 and 24 (week p=0.020). Treatment and interaction of treatment\*week were not statistically significant between groups (P=0.1423).

Table 4.7. Estradiol mean concentration (pg/mL) detected by RIA in two groups (control and treatment) over time. SEM= standard error of mean. P=0.1227 for treatment, P=0.0020 for week. Within row, means without a common superscript are significantly different.

Treatment (pg/mL)		sem	p value	n
Control	Hormone	(pg/mL)		
9.4862	5.7221	1.7033	0.1227	3

Week (pg/mL)								sem	pvalue	n	
-4	4	8	12	16	20	24	28	(pg/mL)			
10.4614 <sup>ab</sup>	8.4193 <sup>ab,c</sup>	11.3480 <sup>ab</sup>	15.1457 <sup>a</sup>	6.5694 <sup>ab,c</sup>	4.2995 <sup>c</sup>	4.8811 <sup>bc</sup>	5.0970 <sup>ab,c</sup>	6.0125 <sup>ab,c</sup>	4.4490	0.0020	6

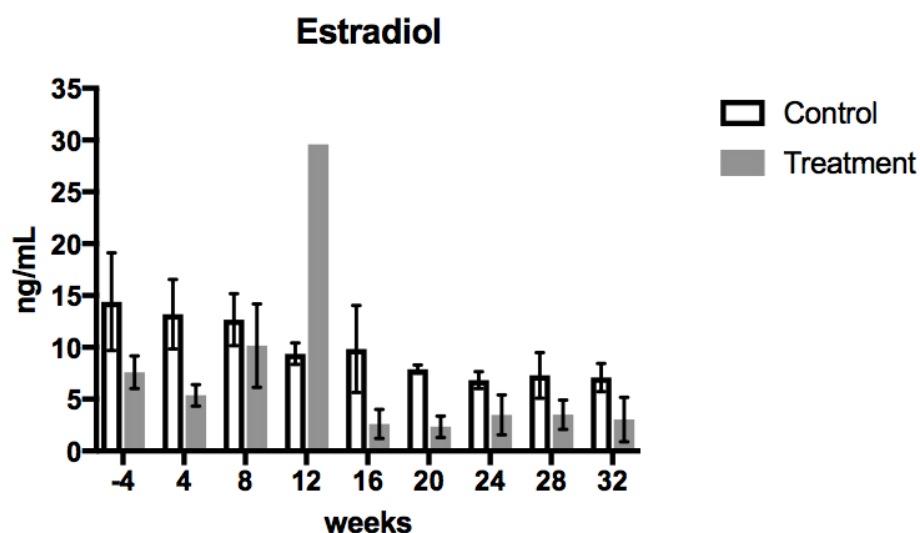


Figure 4.9. Treatment\*week interaction for mean estradiol concentrations for the control and treatment groups and SEM (black bars) over time (P=0.1423).

Table 4.8 shows that the effect of the treatment is not significantly different (P=0.1173) between the control and BPH induction groups, but the effect of week (P<0.0001) is different. The testosterone concentration at week 32 was lower than all previous weeks (week -4, 4, 8, 12, 16, 20), and also the results for week 24 and 28 were lower than week -4 and 12. Figure 4.10 shows mean testosterone and SEM concentrations for the control and BPH induction groups over time and the interaction treatment\*week was statistically significant (P=0.0013). Testosterone concentration in the BPH induction group was lower at week 24 and 28 when compared to week 12, and at week 32 was lower than week 20, 16, 12, 8, 4 and -4; also, BPH group at week 32 is lower than the control group at all weeks.

Table 4.8. Testosterone mean concentration (ng/mL) detected by RIA in two groups (control and treatment) over time. SEM= standard error of mean. P=0.1173 for treatment, P<0.0001 for week. Within row and column, means without a common superscript are significantly different.

Treatment (ng/mL)		sem	p value	n
Control	Hormone	(ng/mL)		
1.9777	0.6361	0.7966	0.1173	3

Week (ng/mL)									sem	p value	n
-4	4	8	12	16	20	24	28	32	(ng/mL)	<.0001	6
3.2177 <sup>a</sup>	1.4138 <sup>ab</sup>	1.5432 <sup>ab</sup>	2.7693 <sup>a</sup>	1.4221 <sup>ab</sup>	0.9918 <sup>ab</sup>	0.6992 <sup>bc</sup>	0.7023 <sup>bc</sup>	0.2087 <sup>c</sup>	1.2646	<.0001	6

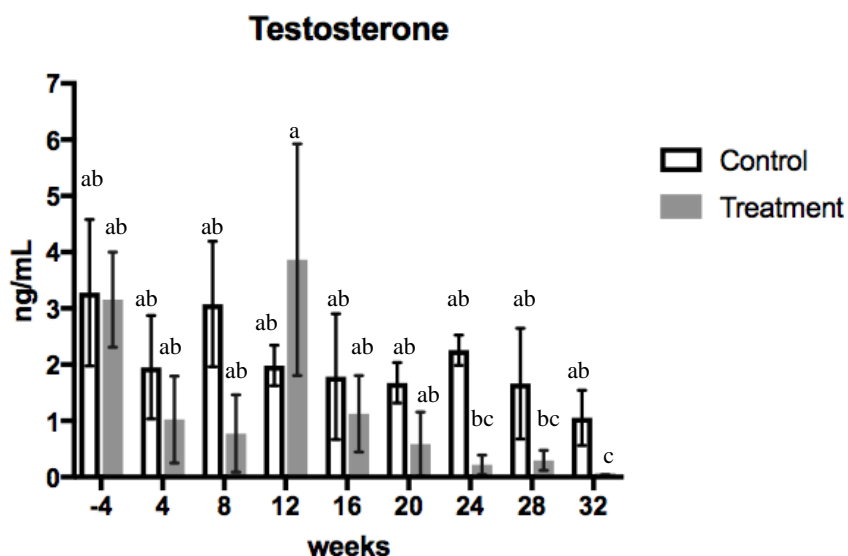




Figure 4.10. Treatment\*week interaction for mean testosterone concentrations for the control and treatment groups and SEM (black bars) over time (P=0.0013). Means without a common superscript are significantly different.

#### 4.4.5 Physical Measurements and Volume of the Prostate Glands

Volume measurements calculated using the *in vivo* dimensions from the computed tomography (CT) imaging studies for the control and BPH induction groups are plotted in figure 4.11 and the final measured *ex vivo* volume for the control and treatment groups measured by water displacement are shown in figure 4.12. For the *in vivo* volume investigation, two different statistical comparisons were performed: the first was a within group comparison at week -4 (control mean =  $15.70 \pm 2.23 \text{ cm}^3$  and BPH induction group mean =  $18.33 \pm 1.79 \text{ cm}^3$ ) and week 17 (control mean =  $18.43 \pm 4.28 \text{ cm}^3$  and BPH induction group mean =  $29.17 \pm 6.26 \text{ cm}^3$ ) for the control and BPH induction groups, and the second was between groups (control versus BPH induction) groups at week -4 and at week 17. There were no significant differences within either the control (P=0.6250) or BPH induction (P=0.2170) between week -4 and week 17 (figure 4.10). Also, there were no statistically significant differences between the control versus BPH induction groups at week -4 (P=0.4139) and week 17 (P=0.4164) (figure 4.11).

Based on *ex vivo* prostate volume measurements (figure 4.12; measured with water displacement) there was a strong tendency (P=0.0538) for the BPH induction group to have a larger prostate size at week 35 than the control group (control mean= $16.67 \pm 3.53 \text{ cm}^3$  and BPH induction group mean= $27.33 \pm 1.76 \text{ cm}^3$ ). Height, width and length of the excised prostates were also measured and compared between groups; although values were numerically larger in BPH induction group than the control group, the differences did not reach significance (height: control mean= $2.68 \pm 0.12 \text{ cm}$ , BPH induction group mean= $3.08 \pm 0.20 \text{ cm}$ , P=0.1649; length: control mean= $2.63 \pm 0.35 \text{ cm}$ , BPH induction group mean= $3.50 \pm 0.27 \text{ cm}$ , P=0.1185; and width: control mean= $3.20 \pm 0.15 \text{ cm}$ , BPH induction group mean= $3.56 \pm 0.26 \text{ cm}$ , P>0.9999) (figure

4.13). Moreover, the weight of the excised testis and epididymis were lower in the BPH group when compared to the control group (more details in the appendix).

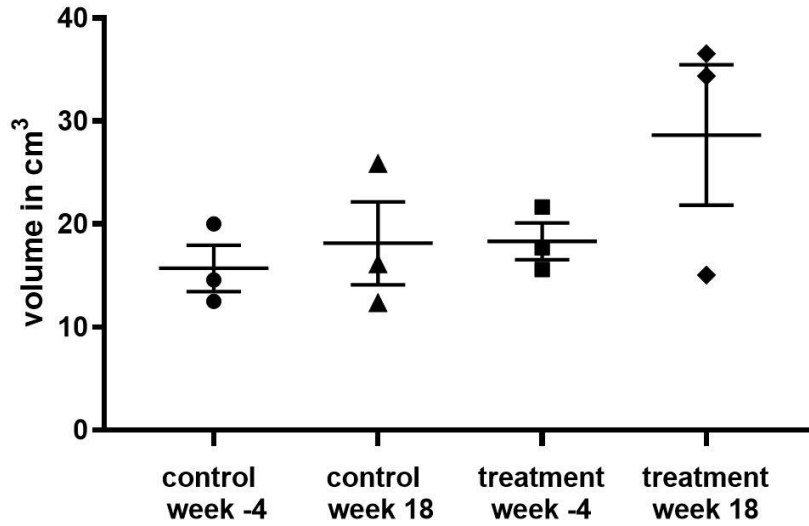


Figure 4.11 Prostatic volume calculated based on *in vivo* CT images for the control and treatment groups at week -4 (baseline) and week 17 (mean  $\pm$  SEM and volume for each dog). Volume is not statistically different between the dogs in the control (week -4 vs week 17, control (P=0.6250) and treatment groups (week -4 and week 17, P=0.2170) or between the control and treatment groups during week -4 (P=0.4139) or week 17 (P=0.4164).

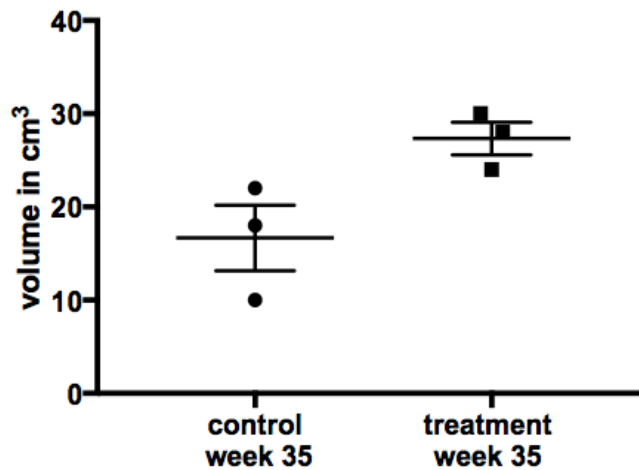


Figure 4. 12. Mean  $\pm$  SEM prostatic volume of *ex vivo* control and treatment groups at week 35 and individual volumes for each dog. Volume is not statistically different between the control and treatment groups (P=0.0538).

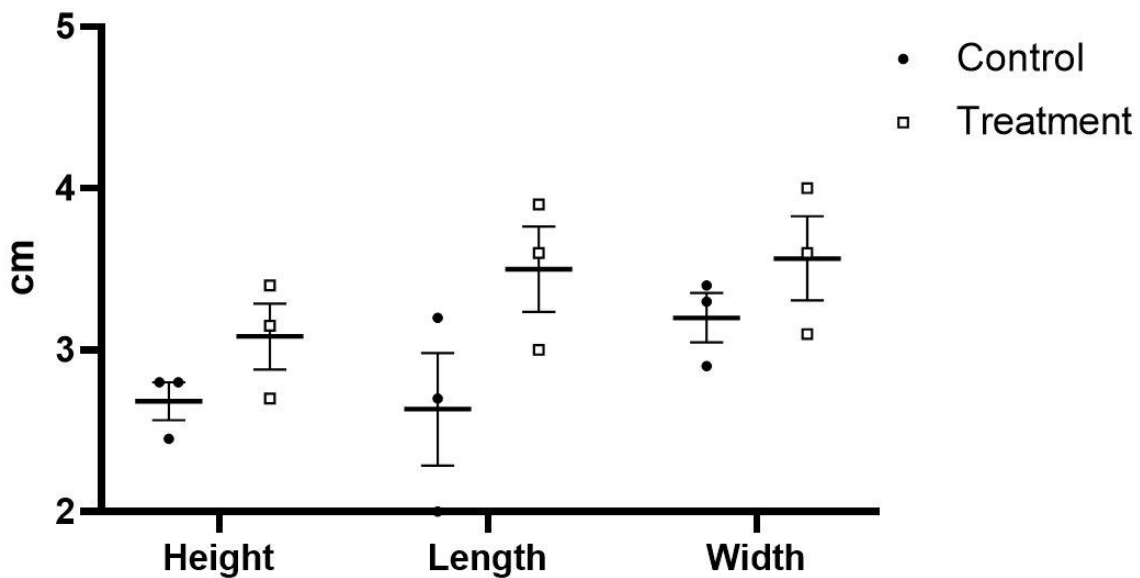


Figure 4.13. Mean  $\pm$  SEM prostate gland measurements (*ex vivo*) for the control and treatment groups at week 35. The mean  $\pm$  SEM height, length and width (cm) are plotted; there were no significant statistical differences between any of the measurements between the 2 groups observed (height  $P=0.1649$ , length  $P=0.1185$  and width  $P>0.9999$ )

#### 4.4.6 Morphometric analysis

The morphometric analyses of the surface area of acini, number of intra-papillary projections, thickness of the septa and area of the prostate gland did not differ significantly between the control and treatment for BPH induction groups (surface area of acini  $P=0.3607$ , number of intra-papillary projections  $P=0.4000$ , thickness of the septa  $P=0.4613$  and area of the prostate gland  $P=0.1585$ ). Table 4.9 displays the mean and SEM values for each structure.

Table 4.9 Mean  $\pm$  SEM and p values for morphometric analyses of each virtual slide of the prostate. OlyVIA software was used to assess the parameters. Area of acini was calculated using 15 random acinis/ slide and the same acinis had their intrapapillary projections counted. Surface area of prostate was drawn and calculated for each slide. Thickness of interlobular septa was calculated at three random locations.

Parameters	Control mean $\pm$ SEM	Treatment mean $\pm$ SEM	P value
Area Of Acini $\mu\text{m}$	43997.22 $\pm$ 3339.49	54468.10 $\pm$ 9589.85	0.3607
Intrapapillary Projections	3.72 $\pm$ 0.51	5 $\pm$ 0.97	0.4000
Area Of Prostate $\mu\text{m}^2$	471638988.8 $\pm$ 579670173.3	634343493.2 $\pm$ 73991041.8	0.1585
Thickness Of Septa $\mu\text{m}$	365.53 $\pm$ 7.63	386.21 $\pm$ 24.25	0.4613

#### 4.4.7 Histological analysis of the prostate slices

The BPH score on the analysis of the slides performed by a certified veterinary pathologist (AA) is shown in table 4.10. Histological assessment of control and treated dogs revealed the presence of hyperplastic features in both groups. Marked variation in lobular size was present. Multifocally, merging of adjacent lobules and loss of lobular pattern was also seen. Within prostatic lobules, many dilated and branching acini were present and were lined by variably thick epithelium. Many of these acini contained multiple long finger-like papillary epithelial projections towards the lumen. Increased thickness of interlobular septa was present multifocally. The histopathologic evaluation revealed that all six dogs showed evidence of glandular and stroma hyperplasia, and surprisingly all control dogs (#1, 2 and 5) and only one treatment dog (#4) also had evidence of intraparenchymal cystic formation.

Table 4.10. Histopathological diagnosis scoring system (0-3) used for all six dogs (control: 1, 2 and 5, and treatment: 3, 4 and 6) based on three categories: cystic formation, glandular hyperplasia, and connective tissue hyperplasia. The average score of the two slides are displayed below.

	Dog #	Cystic formation	Glandular hyperplasia	Stroma hyperplasia	Total (0-9)
Control Group	1	3	3	3	9
	2	2	2	1	5
	5	3	3	1	7
Treatment for BPH Induction Group	3	0	1	1.5	2.5
	4	3	2.5	3	8.5
	6	0	2.5	1.5	4

#### 4.5 Discussion

The combination of all the exams and results in the investigation of the induction of BPH lead to a conclusion that all the dogs from both control and treatment groups developed BPH, either with the injection of hormones or naturally. We achieved our objectives of inducing BPH in three dogs of the BPH induction group and this was confirmed by the evaluation of parameters such as DRE, semen analysis, prostate volume and 3D measurements,

hormone concentrations (CPSE, DHT, estradiol, testosterone) and histological analyses. First, the DRE analysis demonstrated enlargement of the size of the canine prostate glands for all six dogs when compared to the baseline score; however, the BPH induction group had a change in score from 0 to 1 earlier than the control and this is an indirect evidence that the hormone injections were effective in enlarging the prostate. As a subjective examination, DRE should be used only as a crude guide by the veterinarian during a routine physical examination for the detection of BPH but certainly it could be the basis on which to request other diagnostic tests such as medical imaging or biopsy of the gland (Das et al., 2017). Although the p value was not significant (probably due to the low n), semen analysis demonstrated a decrease in the motility, progressive motility and sperm count by the end of the study for all the dogs, except #5 (control dog), who had an increase in semen progressive motility. The mean volume of the ejaculate of all dogs also increased when compared with baseline but could have been a result of the dogs becoming more accustomed to manual collection or the personnel becoming more experienced and there was significant difference between volume collected at baseline and end of the study for BPH induction group.

Moreover, the sperm count for all the BPH induction group dogs by the end of the study was zero and also the weight of testis and epididymis of BPH induction group were lower than control, indicating the effect of injectable hormones used in that group on testicular function and negative feedback suppressing LH/FSH hormone secretion by the pituitary gland. Krakowski et al (2015) compared semen quality in normal dogs and dogs with naturally occurring BPH and they found there were no statistical differences in the semen analysis between the two group of dogs; nor did we. However, in the end of the study sperm concentrations in the BPH induction group decreased compared to the control group and the volume increased for the induction group, which is numerically different than Krakowski et al (2015). Despite the differences, it is possible to point out that we induced BPH with hormone injections and, therefore, this contrasts from the Krakowski et al (2015) study, in which they

used dogs with spontaneously developed BPH. Also, in both studies the n was small (n=5) which could have negatively impacted the power of the statistical analysis. Administration of testosterone in men can negatively impact fertility and spermatogenesis due to the negative feedback suppression that occurs with the hypothalamic-pituitary-gonadal axis (Crosnoe et al., 2013). Rajalakshmi et al., (1989) injected different doses of DHT in rhesus monkeys (*Macaca mulatta*) and observed that it impacted negatively in structural and morphological changes of the spermatozoa.

This present study intended to induce BPH based on a slightly modified protocol previously reported on dogs in the literature by DeKlerk et al., (1979), using a combination of the hormones DHT and estradiol. The hormone concentrations used in our protocol were identical to those used by DeKlerk et al (25 mg/mL of 5 $\alpha$ -DHT and 0.25mg/mL of 17  $\beta$ -estradiol), however, the preparation of the injectable solution was different from the sonication method proposed by DeKlerk et al., (1979). In our initial attempts at preparing the solutions using the sonication method, the hormones did not dissolve in triolein and ended up forming a precipitate, which could not therefore be used for the injections. This led to a modification in the preparation method as described previously in the material and methods, where the hormones were initially dissolved in benzyl alcohol. Another difference is that the DeKlerk et al. (1979) study used beagles with body weight range of 7 to 18.6kg (11.3 $\pm$ 2.2kg), whereas Walsh and Wilson's study (1976) used mixed breed dogs with average body weight per group I to V equal to 18, 14, 14, 15 and 22 kg (16.6 $\pm$ 3.44kg). Also, both studies used 1mL of triolein solution containing 25mg/mL of androgen and 0.25mg/mL of estrogen. This aspect may be relevant since the dose of the hormones used in our study was not adjusted for dogs weighing more than an average beagle. The time for inducing BPH in our study was 8 months, which is exactly in the middle of the time periods from the 2 studies. DeKlerk et al., (1979) used DHT and estradiol was four months, however, in the Walsh and Wilson's (1976) study BPH induction time using androstanediol and estradiol was longer at 12 months. Other research

using different animal models to induce BPH with injectable hormones include Jeyaraj et al., (2000) who induced BPH in rhesus monkeys (*Macaca mulatta*, body weight range 8-10kg) with the administration of DHT and estradiol with different dose (2.5mg/mL of DHT and 0.5mg/mL of estradiol diluted in olive oil) for a period of 24 months of injection. These observations suggest that a longer period of time and or a possible adjustment of the dose/body weight of hormones used for induction might have been warranted in our study to induce BPH in this population of dogs.

Two weeks after the initiation of the injections, CK was evaluated in all the dogs. For the CK results, only one dog had a mild elevation (control dog#5= 532 U/L) and this could result from restraint or be normal for this dog. From a clinical standpoint, elevations in CK would need to be > 4000 IU/L to cause concern (<http://eclinpath.com/chemistry/muscle/creatin-kinase/>). One treatment dog (#3 from treatment group) did on a few occasions show some mild swellings at the hormone injection sites but this was short lived and there was no evidence that this involved more than the superficial skin layer. Based on these findings, there is no evidence to support any significant complications associated with injection of the carrier or the hormones at the sight of injection in the dogs used in this study.

Although there were no statistical differences for the reported *ex vivo* prostate volumes measured by water displacement in the control and treatment groups (larger volume for treatment dog prostates than control), the p value was very close to being accepted as significant (p=0.058) and it is very likely that our study was underpowered due to the small n. The volume calculated for the *in vivo* prostates using the HOROS® software did not show any statistical differences for any of the time points for the BPH induction versus the control groups. The disparities in the volume values obtained for the *in vivo* and *ex vivo* measurements might be because the free hand tool used to draw the area from each CT slice, rendering the region of interest (ROI) volume, is not overly precise because it has to be manually drawn

making it subject to error. Also, the fixation process of the prostates might have interfered in the volume measured at the end of the study, probably in a similar way that brains fixed in formalin experience volume changes (Frýdl, Koch, & Závodská, 1989). It is known that increase in the size of the prostate gland is a consequence of the hypertrophy and hyperplasia seen with BPH, however, it is also true that the volume of the prostate gland should not be used by itself to predict disease severity, because clinical signs may be absent in dogs with histologically confirmed BPH (Zambelli, Cunto & Gentilini, 2012).

CPSE has been studied as a biomarker for detecting BPH with a cut-off value of > 61 ng/ml used to confirm BPH in dogs according to one study by Pinheiro et al., (2017). They reported that CPSE is a reliable test for detecting BPH and showed that it has a moderate correlation with prostatic volume with this cut off used (sensitivity 96.6% and specificity 90.3%). However, by contrast, Holst et al., (2017) reported that some dogs with BPH with large prostate glands have low CPSE concentrations and some dogs with small prostate glands have high concentrations of CPSE. The dogs used in that study had their prostates evaluated and measured by ultrasound and were separated in two groups based on whether they had clinical signs or not from prostatic diseases. The majority of dogs had a concentration of CPSE >61ng/mL and displayed no clinical signs of BPH; these investigators recommended that a higher cut-off value for dogs with an enlarged prostate was appropriate. In our study, only two dogs – one control and one in the BPH induction group dogs met the threshold of > 61 ng/ml for the diagnosis of BPH. Based on our findings CPSE might be a valid test to help diagnosis BPH; however early stage of BPH might not be detectable using this test and this is in agreement with Holst et al., (2017). Alternatively CPSE may not be a definitive marker for BPH or may lack specificity or not correlate at all with severity of BPH.

The analysis of the hormone DHT administered to the BPH induction group does show a significant effect compared to the control dogs (P=0.058). Towards the end of the study, the difference between the DHT concentration values for the control and induction groups was



more evident (as seen in figure 8). The absorption of the exogenous administration of DHT to the BPH induction group is proven by the drastic distinction of hormone concentration values between the two groups. The effects of exogenous administration of DHT also impacted endogenously produced testosterone as evidenced by the lower concentrations in the BPH induction group from negative feedback on the pituitary from the DHT. At the cellular level testosterone is naturally converted into the active metabolites DHT and estradiol under the action of  $5\alpha$ -reductase (prostate gland and other tissues) and aromatase (majority in adipose tissue), respectively. Overall, testosterone level in the BPH induction group was statistically lower than in the control group (except for week 12 which may possibly be from a measurement error). Towards the end of the study the testosterone concentrations in the BPH induction group dogs were much lower than what was detected in them in the first few weeks of the study; this is due to the negative feedback on pituitary by exogenous DHT leading to decreased FSH/LH secretion and therefore decreased endogenous testosterone secretion by the testes (Page et al., 2011). This drop in endogenous testosterone was also seen by Jeyaraj et al., (2000) with the administration of DHT and estradiol to induce BPH in rhesus monkeys. In men, secretion of testosterone can be influenced by the circadian rhythm (Loeb et al., 2009), so the time of day when sampling is performed can affect the serum concentrations measured. Fukuda et al., (1990) studied whether serum testosterone secretion also is affected by circadian rhythms in male dogs. Although previous works suggested that lighting is an important modulator in controlling serum testosterone, the circadian rhythm influence in testosterone production is believed to be intrinsic through some other mechanism other than by the lighting (Fukuda et al., 1990).

As estradiol was the second hormone administered to induce BPH (injected in combination with DHT), we also expected estradiol levels to be higher in the BPH induction group compared to the control group similarly to what was reported by Jeyaraj et al., (2000) in their research. In our study, at weeks 8 and 12 the mean serum estradiol concentration was

indeed much higher in the BPH induction group compared to the controls but only at these two time points was the case. After week 12, the mean concentration of the estradiol in the BPH induction group also significantly decreased. As mentioned previously, three extreme high values of estradiol were removed from the analysis (treatment dog#4 and dog#6 week 12 and dog#6 for week 28) because they were not compatible with *in vivo* concentrations of estradiol provided in the literature. Hence, only one value for estradiol was left to be reported in the BPH induction group for week 12. However, there was no statistical difference between control and BPH induction groups for treatment and treatment\*week interaction. Overall the values detected in the treatment group were lower than the control group (except week 8 and 12, which treatment values were higher). It would have been noteworthy to send the hormone preparations to a chemical laboratory to test for its purity prior to the injections. [Page et al., 2011](#) study with exogenous administration of transdermal gel 0.7% DHT daily in healthy men for 28 days reported that serum estradiol decreases as well as testosterone (via negative feedback hypothalamic-pituitary-gonadal axis) so this may account for the lower the estradiol levels in the BPH induction group but this should have been balanced by increased detection of estradiol that was administered exogenously in the treatment group.

Among the parameters assessed in the morphometric analysis, a study in Beagles reported that intrapapillary projections area a pathological feature seen with spontaneous BPH ([Zhao et al., 2013](#)). Also, [Das et al., 2017](#) reported cystic acini and hyperplasia of acinar epithelium as histological features of BPH in dogs. In rhesus monkeys that received DHT and estradiol for the induction of BPH, stromal hyperplasia was observed [Jeyaraj et al., \(2000\)](#). In our study, none of the parameters assessed – surface area of acini, number of intrapapillary projections, area of the prostate and thickness of the septa – were significantly different between the control and BPH induction groups. In other words, the morphometric analysis of the histological slides of the prostate glands did not provide enough evidence to confirm BPH was induced in the treatment group relative to the controls over the 35 week trial. This result

could be a consequence of the low n interfering in the statistical power or more likely due to the decision to not neuter the control dogs.

The evaluation of the histological slides by a veterinary pathologist and the grading score for cystic formation, glandular hyperplasia and stroma hyperplasia provides the highest score (9/9) for dog#1 (control group) and #4 (BPH induction), revealing an agreement with the CPSE results that diagnosed BPH for these two dogs. The other dogs had scores ranging from a minimum of 3/9 to 7/9 indicating the presence of some histological features of BPH in all the dogs, probably in different stage of the detection.

Research studies vary at what is the youngest age dogs can develop BPH. Some suggest BPH can be seen in dogs as young as age 2-3 y.o ([DeKlerk et al., 1979](#)) and report a prevalence of 16% ([J, Li et al., 2018](#)). Others suggest the disease can be present in 50% of dogs by 4 yrs of age ([J, Li et al., 2018](#)), but these dogs are asymptomatic for BPH at this early stage and clinical signs are only observed if the prostate is enlarged enough to cause the symptoms ([Sun, Baez-Diaz & Sanchez-Margallo, 2017](#); [Zambelli, Cunto & Gentilini, 2012](#)). However, it is important to stress that in the dog population the size of the prostate can differ without the presence of the clinical signs associated with BPH and the breed can influence detection of prostatomegaly ([Holst et al., 2017](#)).

This study intended to induce BPH with the administration of DHT and estradiol as previously reported in the literature. The small n per group (n=3) was a limiting factor for the performance of statistical analysis for some parameters. Moreover, control dogs also developed BPH spontaneously due to the fact that it is a highly prevalent disease in the (older) dog population and the age of the subjects were unknown. A solution for this would have been the castration of the control group, which would have made the distinction with the BPH induction group more evident. Many studies have been conducted in the past with the administration of various androgens and estradiol to observe the effects on the prostate in dogs and monkeys, and results were similar: DHT and estradiol do produce hyperplasia in the dog (and monkey). The

further analysis of serum hormone levels and impact in the semen and fertility has been investigated as well and our testosterone and DHT levels are in agreement with the literature. Unfortunately, estradiol did not agree with published data so far; CPSE cut-off value for BPH diagnosis was just seen in 1 dog in each group (33% control and 33% treatment group) and it was expected to observe in all three subjects of the BPH induction group. The failure to document an increased CPSE in the other two BPH induction group dogs may have to do with the duration of the protocol, the dose of the hormones used, and/or variation in the severity of the BPH in the individual dogs; perhaps with a longer induction period we would have seen elevations in the CPSE in all the BPH induction group dogs. Reduction in the semen parameters (motility, progressive motility, sperm concentration) in the BPH induction group versus control group is in contrast with reported literature using spontaneous BPH. Although volume and physical measurements of the prostate glands between the two groups was not statistically different (again possibly due to small n), the graphs show a trend of higher values in the BPH induction group. There are also differences between the manifestation of spontaneous BPH versus induced BPH reported in the literature and this may have also played a role in our findings.

Therefore, we can concluded that BPH was induced in the treatment group with the administration of DHT and estradiol, confirming [DeKlerk et al., \(1979\)](#) study, and also BPH naturally occurred in the control group, as proved by the histological analysis, volume and physical measurement of the prostate, DRE, and semen evaluation. The magnitude of the effect for the BPH induction group, however, was not expected to be as large as reported.

## CHAPTER 5: LIVE IMAGING OF IN SITU DOGS' PROSTATES WITH PC-CT TECHNIQUE AT THE CANADIAN LIGHT SOURCE SYNCHROTRON AND ITS COMPARISON WITH CONVENTIONAL IMAGING MODALITIES

Natalia C. Cardoso, Jaswant Singh, Murray Pettitt, Elisabeth Snead

### 5.1 Abstract

The prostate gland can be the site of different disorders such as benign prostatic hyperplasia (BPH) and prostate cancer (PCa) and establishing the correct diagnosis is essential for directing the appropriate treatment and determining the prognosis of the patient. Conventional imaging techniques are used to help establish diagnosis for patients with prostatic disease but unfortunately, at this time, none of these allow non-invasive differentiation between BPH and early PCa. Based on previous research that revealed that phase contrast computed tomography (PC-CT) imaging of excised canine prostate glands can provide better resolution of the internal gland than conventional CT, we decided to investigate the use of the PC-CT technique to image the prostate gland of live dogs with induced BPH at the Canadian Light Source Synchrotron (CLS) as a potential new diagnostic tool for the early detection of prostatic diseases.

A protocol was established involving two steps. First, a placebo controlled pilot study was conducted in which BPH was induced using a combination of the hormones estradiol and dihydrotestosterone (n=3 per group; chapter 4) for a period of 35 weeks. Second, *in situ* prostate glands of live dogs were imaged at week 17 with computed tomography (CT), magnetic resonance imaging (MRI), and positron CT (PET CT) and at week 35 imaged with US and PC-CT at the CLS. Lateral radiographs were taken to assess prostatomegaly. One axial slice of each imaging modality (except radiographs) were compared with each other to evaluate the best imaging modality to resolve features of the prostate. The prostate was not seen in all the radiographs (four out of six) and it did not show any evidences of prostatomegaly. The results revealed that the best modality to see parameters such as urethra and verumontanum

(visualized in all dogs), and cysts (seen in four dogs) is MRI T2. Cysts were also seen in CT (three dogs) and US (five dogs). Parenchyma was better visualized with MRI T2 (four dogs), MRI T1 (two dogs), US (four dogs) and CT (three dogs). PC-CT and PET-CT allowed the visualization of lobes and median septum as well as the urethra with tracer (all dogs for PC-CT and two dogs for PET-CT). PC-CT was inferior in quality when compared to US, CT and MRI and displayed lower levels of contrast and resolution thus PC-CT is not an appropriate imaging modality for *in situ* evaluation of the prostate gland at this time.

This study describes the first attempt at PC-CT imaging of the prostate gland *in situ* in live dogs using the CLS. Regrettably at this time, image quality expectation was not comparable to PC-CT of excised canine prostate glands previously obtained by our group. The PC-CT images of the canine prostate glands obtained reveal that the level of detail required for clinical diagnostic purposes is not yet possible with this technique for *in situ* imaging. However, just as with the development of any new imaging technique (e.g., mammography, MRI) the path to developing the appropriate technique begins with an initial attempt and requires further work to refine and improve the diagnostic resolution.

Keywords: prostate gland, dog, CLS, synchrotron, PC-CT, *in vivo* imaging

## 5.2 Introduction

The two most common diseases of the prostate – the major accessory sexual gland in both man and dog – are benign prostatic hyperplasia (BPH) and prostate cancer (PCa) (C. H. Lee et al., 2011). BPH is the most common prostatic disorder affecting men and intact dogs (Vuichoud & Loughlin, 2015; Geddes, 2011). BPH is a benign disorder characterized by the enlargement of the prostate gland (Tanguay et al., 2009), resulting in lower urinary tract symptoms (LUTS) in men while in dogs typically either constipation and tenesmus and less commonly LUTS are seen (Pearson & Williams, 2014). On the other hand, carcinoma of the prostate is a malignant disease, and is the most common non-skin cancer affecting Canadian men (Bostwick, 2004; Fradet et al., 2009). According to the Canadian Cancer Society

[www.cancer.ca](http://www.cancer.ca), PCa is the third leading cause of death among cancers in men in Canada. Because BPH and PCa require very different treatment and the prognosis is also radically different establishing a definitive diagnosis is an important decisive step in the management of the patient (Alcaraz, Hammerer, Tubaro, Schröder, Castro, 2009).

Discomfort associated with prostatic disease typically leads a human patient to seek medical care (Vuichoud & Loughlin, 2015). Factors such as the history, the symptoms and what is found on physical examination play an important role in the physician's decision to potentially investigate further, using imaging modalities such as ultrasound or CT, or prostatic biopsy to help determine the underlying cause of the prostatic disease (Tanguay et al., 2009, Wei et al., 2009, Nickel et al., 2010). Currently, definitive diagnosis requires biopsy and histological analysis of the prostate – the gold standard diagnostic method for distinguishing PCa from BPH (Singh & Emberton, 2013). Biopsy of the prostate gland, can be a painful procedure for the patient (Ukimura et al., 2011) and there can be issues related to both false negative and false positive results depending on the area of the prostate sampled, the degree of secondary inflammation. In addition there is also a risk of bleeding and sepsis with biopsy of the prostate, especially when biopsy is performed transrectally as is common in men (Ukimura et al., 2011).

Imaging techniques such as transrectal ultrasound (TRUS), magnetic resonance imaging (MRI) and computed tomography (CT) have been used to indirectly assess the prostate gland (Ghose et al., 2012). Determination of the prostatic size/volume with ultrasound and MRI can be helpful to help establish the diagnosis of BPH and to monitor for the response to medical treatments for BPH (Rahmouni et al., 1992, Jia et al., 2005). Positron Emission Tomography – Computed Tomography (PET-CT) is another imaging modality that has been used to aid the diagnosis of both BPH and PCa, with some data suggesting that in some cases it is possible to differentiate between these two diseases with this imaging modality (Bouchelouche & Oehr 2008). However, the use of PET-CT for the differentiation between both diseases remains a

challenge for physicians because BPH and PCa cannot always be definitively distinguished especially with patient with early disease (Yoshida et al., 2005, Li et al 2008, Castellucci et al., 2015).

In order to improve the resolution, and therefore the sensitivity and specificity of imaging for the prostate gland, propagation-based imaging (PBI) or in-line phase contrast computed tomography (PC-CT) has been studied at the Canadian Light Source synchrotron facility as a possible alternative diagnostic imaging modality (Melli et al., 2015). The physics underlying PC-CT technique is based on two principles both of which are determined by the properties of the sample: 1) the refraction of X-rays and change of their direction (Fresnel fringes), and 2) change in the phase (phase shift) of the x-rays. The refracted phase shifted X rays result in improved soft tissue imaging when captured by a detector. Prior imaging of excised canine prostate glands by our group using PC-CT resulted in improved resolution compared to conventional CT, allowing the internal details of the gland to be visualized with a resolution that approached findings seen with low power (4-10X) microscopic histological imaging (Wolkowski et al., 2015). Based on this promising result this study was undertaken to see if similar image resolution could be achieved with *in-situ* imaging of the prostate in a live dog.

This study was divided into two parts: 1) induction of BPH in intact male dogs (chapter 4), and 2) *in situ* imaging of live dog prostates with different modalities including US, MRI, CT, PET-CT and PC-CT. This paper describes the live imaging features of the canine prostate using different imaging modalities and is the first successful experiment documenting phase-contrast computed tomography imaging done on six live dogs under general anesthesia at the BMIT beamline at the CLS (part 2).

### 5.3 Material and Methods



### 5.3.1 Animals and Experimental Model

The subjects of the study were six intact male dogs (mixed breed huskies, unknown age but approximately 1-5 y.o, body weight range 19.5-29.5 kg) randomly assigned to a treatment (n=3) or control (n=3) group. Dogs from both groups were given intramuscular (IM) injections three times per week (every Monday, Wednesday and Friday) for a period of eight months (35 weeks). The treatment group (dogs #3, 4 and 6) was given a combination of hormones (25 mg 5 $\alpha$ -dihydrotestosterone and 0.25 mg 17 $\beta$ -estradiol) in 1 mL triolein per IM injection and the control group (dogs# 1, 2 and 5) was given the carrier triolein as described in chapter 3. All experiments described in this study were approved by the University Animal Care Committee (UACC), University Committee on Animal Care and Supply (UCACS), and Animal Research Ethics Board (AREB) of University of Saskatchewan. The six dogs were housed individually in kennels with access to an indoor and outside area, with water *ad libitum* and food (Hills® Science Diet® Adult Dogs) provided twice a day. Their movement was not restricted and they were exercised once a day.

### 5.3.2 Imaging

The dogs (control group dogs#1, 2 and 5 and treatment group dogs# 3, 4 and 6) were imaged at baseline prior to initiation of hormonal induction of BPH (week -4; ultrasound, radiographs, CT) and following four months of induction (week 17; ultrasound, radiographs, CT, MRI, PET-CT, PC-CT) in order to compare the findings between the different imaging modalities. In reality, the week 17 imaging was actually performed over a three-week period due to the logistics of collecting all of the different images (week 17 $\pm$ 1 week), which were not all available in the same facility. General anesthesia was necessary for PET-CT and PC-CT. Hormonal induction was also continued past the 17 week period due to unforeseen challenges encountered when acquiring the live animal PC-CT images. The PC-CT imaging of the live dogs at week 17 indicated that the canine holding device, which has been purposely constructed

for this project and had been tested prior to this using cadavers, was unable to maintain the live dogs perfectly still in a vertical position without motion artefact for imaging. This movement resulted in an inability to appropriately reconstruct the images acquired using PC-CT. This necessitated that we continue the hormone induction protocol to allow time to modify the design of the canine holder and repeat the synchrotron PC-CT imaging. The dogs were subsequently imaged again with ultrasound and PC-CT during week 35±1 (reported as week 35) following initiation of hormonal injections. The week 35 images for PC-CT and US were then compared with MRI, CT and PET CT from week 17. Immediately after completing the *in vivo* PC-CT live animal imaging at week 35 and while still in the positioning device, all six dogs were humanely euthanized using Pentobarbital Sodium (Euthanyl Forte, Bimeda-MTC Animal Health Inc, Cambridge, Ontario, Canada) at a dose of 1mL/5kg body weight, IV. All dogs were then immediately re-imaged with PC-CT as cadavers, so both live and cadaver images could be compared.

#### 5.3.2.1 Sedation and General Anesthesia

For the ultrasound, radiography, and CT imaging of the prostate, all the dogs were sedated with hydromorphone (Hydromorphone Hydrochloride Injection USP, Sandoz, Canada, 10 mg/mL, 0.05mg/kg IM), dexmedetomidine (Dexdomitor, Pfizer Canada Animal Health Inc, Kirkland, Quebec, Canada, 0.5mg/mL, 0.002mg/kg IM) and ketamine (Vetalar, Bioniche Animal Health Canada Inc., Belleville, Ontario, Canada, 100mg/mL, 2mg/kg IM). For PET-CT, MRI and PC-CT imaging modalities dogs were maintained under general anesthesia according to the following protocol: premedication with hydromorphone (10 mg/mL, 0.1mg/kg) and acepromazine (Atravet, Boehringer Ingelheim, Burlington, Ontario, Canada, 10mg/mL, 0.05mg/kg) IM; induction with propofol (Propofol Injectable Emulsion, Fresenius Kabi Ltda, Richmond Hill, Ontario, Canada, 10mg/mL, 5mg/kg) IV and maintenance with isoflurane (Isoflurane, USP 99.9%, Halocarbon Products Corporation, New Jersey, USA) inhalant and

oxygen. In addition, all dogs received intravenous (IV) fluids (NORMOSOL®-R Hospira, St. Laurent, QC, CA) through the cephalic vein while under general anesthesia at a maintenance rate of 4ml/kg/h.

### 5.3.2.2 Radiographs

Abdominal radiographs were taken twice during the experiment, with a lateral projection radiograph taken at week -4 and again at week 17 at the WCVM Veterinary Medical Center (VMC) with a Philips X-ray machine - Class I - type B IEC 60601-1 Optimus 50. Figure 5.1 shows a schematic diagram of a lateral view of the caudal abdomen highlighting the relative position of the prostate gland and bladder, and alongside it, there is an actual lateral radiographic projection of the caudal abdomen.

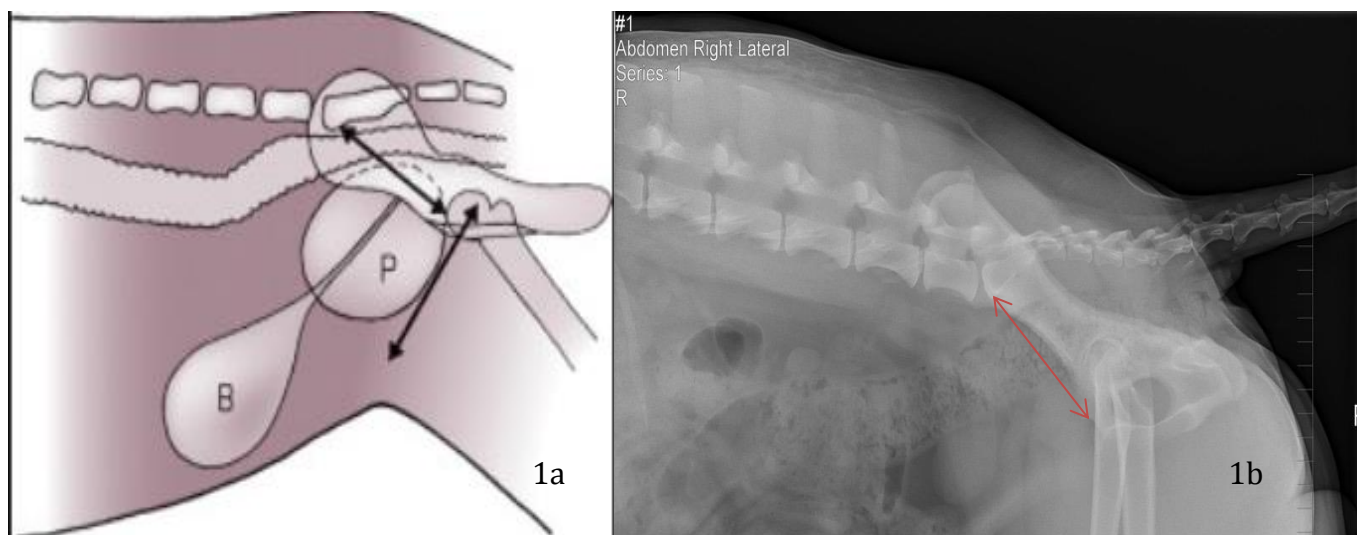


Figure 5.1. Illustration of the lateral view of the caudal abdomen of a dog (1a) with the position of a hyperplastic prostate shown in relation to other surrounding structures (P is prostate and B is bladder); in comparison 1b shows a lateral radiographic projection of the caudal abdomen of a dog (1b) where the red arrow shows the distance between the sacral promontory and the pubis

(DSPP) which is used to evaluate for prostatic enlargement. (1a. Measurement of prostatic size, Dennis, R., Kirberger, R. M., Barr, F., Wrigley, R. H. (2010). Urogenital tract. *Handbook of small animal radiology and ultrasound: Techniques and differential diagnoses*, retrieved from <https://ars.els-cdn.com/content/image/3-s2.0-B9780702028946000111-gr18.jpg> on Aug 30 2018, reprinted with permission).

### 5.3.2.3 Ultrasonography

Ultrasound images were collected at the Western College of Veterinary Medicine (WCVM) Veterinary Medical College (VMC). Due to replacement of the ultrasound unit during the period of the study, different machines were used to collect the baseline and the final images. Baseline images were taken with a Canon Toshiba Viamo ultrasound machine (Toshiba Medical Systems, ON, Canada) at week -4 and at week 35 images imaged were collected using a Canon Toshiba ultrasound machine - Aplio 300 (Toshiba Medical Systems, ON, Canada).

Dogs were placed in dorsal recumbency for this procedure and ultrasound gel was applied to the skin and a 4-11Mhz ultrasound convex-array probe (PVT-712BT Toshiba Medical Systems, ON, Canada) was used to collect both transverse and sagittal projection images of the prostate gland. Measurements at the widest points of both planes were taken with the caliper tool using Gray scale B-mode images (width, height, length).

### 5.3.2.4 CT

Data from baseline (week -4) and week 17 was collected using a CT Scanner (Toshiba Aquilion TSX-101A 16 slice multi-detector; America Medical Systems, CA, US) at the WCVM VMC.

Dogs were positioned in ventral recumbency on the gantry and had their entire body imaged at a 1mm slice thickness prior to and immediately post-administration of an intravenous injection of an iodinated contrast medium (Omnipaque<sup>TM</sup>, Iohexol injection, GE Healthcare Canada Inc., Mississauga, Ontario, Canada).

### 5.3.2.5 MRI

The prostate gland of each dog was imaged using a MRI 3T scanner (Skyra, Syngo VE11C software, Siemens – Erlangen, Germany) at the Royal University Hospital (RUH), University of Saskatchewan at week 17. Both T1 and T2 weighted images were acquired of the prostate gland in the axial plane. Specifications for T1 MRI exams were spin-echo (SE) and fast spin-echo (FSE) for T1 with an acquisition time of 4 min 44s, repetition time of 5.08 ms, echo time of 1.77 ms and slice thickness of 3.5 mm. Specifications for T2 MRI exams were turbo spin-echo (TSE) for T2 with acquisition time 2 min 18s, repetition time of 6500 ms, echo of time 93 ms and slice thickness of 3.5 mm weighted (W) images. Gadovist® (Gadobutrol, Bayer Inc. Mississauga, ON, Canada, dose – 1mL/10kg animal weight) was used to obtain axial post-contrast FSE T1 W images with fat suppression on all the dogs to assess the uptake of the contrast agent by the prostatic gland tissue.

### 5.3.2.6 PET-CT

The PET-CT scanner used in this study was a Discovery 710 (General Electric, Milwaukee, USA) located at the RUH and images were obtained at week 17. Prior to imaging, the dogs had their blood glucose concentration measured, which were all within the accepted normal range (3.1-6.3 mmol/L). Dogs were anesthetized and positioned in ventral recumbency and received a 4.5 MBq/kg dose of the radiopharmaceutical F18–FDG administered IV prior to imaging. The radiopharmaceutical was supplied from two different sources based on availability with three dogs receiving F18–FDG from the Centre for Probe Development and Commercialization (CPDC), Hamilton, ON, Canada, and the other three dogs receiving F18–FDG produced by the Saskatchewan Centre for Cyclotron Sciences (SCCS), Saskatoon, SK, Canada. Sixty minutes after administration of <sup>18</sup>F–FDG, a PET (ultra-low dose for attenuation correction) scan was performed. Following this, iodinated contrast (Iopamidol, Isovue Multipack, Bracco Imaging Canada, Montreal, QC, Canada) was administered IV and 60s later,

a full CT scan was completed. After recovery from anesthesia, each dog was maintained in isolation until their background radiation readings, measured using a dosimeter (ESM FH40G-L, Thermo Eberline, Thermo-Fisher Scientific, Germany), were less than  $5\mu\text{Sv/h}$  at the surface. At this time they were returned to their regular kennels.

### 5.3.2.7 PC-CT

The phase contrast images were acquired at the Canadian Light Source synchrotron facility at week 35 using the BMIT-ID beam line. The detector used was DALSA Shad-o-box 3K HS (Teledyne, Canada) camera with a resolution of  $49.5\ \mu\text{m}/\text{pixel}$ , and the energy level used was 120 keV.

Figure 5.2 illustrates the set up for the live animal imaging of the dogs. One of the main differences between CT and PC-CT is that with CT the subject is stationary, lying down on a table in the horizontal position and the source of x-rays and the detector rotates around the patient, whereas with PC-CT the x-ray source and detector are stationary and the subject, positioned inside a holder device (here after referred to as the Conine), has to rotate  $180^\circ$  perpendicular to the x-ray beam. Also, the distance between the patient and the detector for a conventional CT is much shorter at around 50 cm; this compares to a distance of 2.8m for PC-CT.

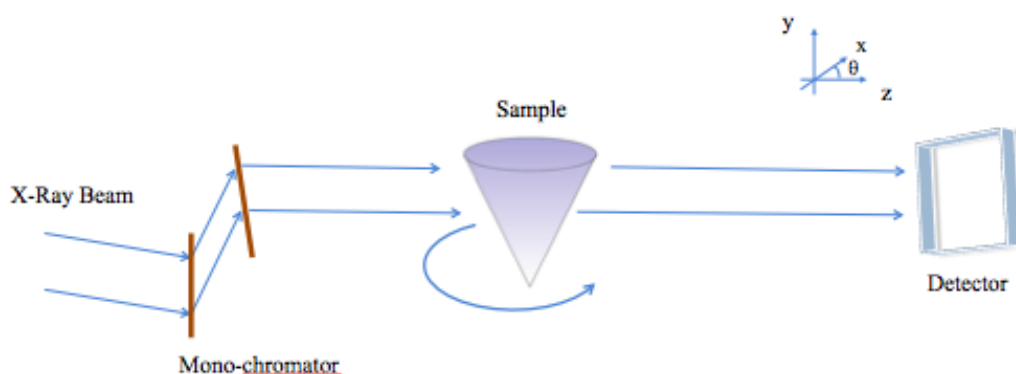


Figure 5.2. A schematic set up for live dog PC-CT imaging at the BMIT-ID at the CLS. The Sample here represents the dog held in a vertical position using the Conine holding device.

As previously alluded to it was necessary to perform the live dog PC-CT imaging twice (at weeks 17 and 35) due to technical problems encountered during the first imaging attempted at week 17 where the canine holder used initially could not maintain the dogs perfectly still in a vertical position. The degree of vertical motion encountered was not evident to the naked eye but on the order of 49.5  $\mu\text{m}$  (equivalent to the resolution of the camera). However, this was sufficient to result in an inability to reconstruct any images from the data. Therefore, it was decided to continue with the hormone injections and redesign and develop a new holder in the intervening additional 18 weeks, and re-image all the dogs at week 35. The resulting holder (Conine) made of polypropylene was conical in design with a tapering shape; this along with creative use of air cushions around the patient reduced the amount of vertical motion (slumping) eliminating the motion artifact problem that was encountered with the initial design. Also, in the intervening time between the initial and final imaging attempts, other adaptations were installed within the BMIT hutch alongside the new holder. This included an anesthesia ventilator (Mallard Medical Inc., model number 2400, serial number 240832, CA, USA) which was used to control the respiration rate in the dogs, further reducing any motion artifact from breathing. In addition, a respiration triggered device was also developed to enable the ventilator to trigger image acquisition by the CLS computers between each breath, again further reducing imaging artifact from the breathing motion. And finally a remote anesthesia monitor (B3MVet Next© device, Bionet America Inc, Tustin, CA) was also connected to a computer outside of the hutch allowing all the vital information of the patient to be tracked and monitored in real-time during imaging. The use of the ventilator required an extra oxygen tank (7000L) to be placed within the hutch, in addition to the small 700L O<sub>2</sub> cylinder that was mounted to the positioning device. Both cylinders had an oxygen regulator (Easy Dial Reg™ oxygen regulator, Precision Medical Inc, Northampton, PA, USA) to display the amount of gas remaining in the tank so this could be monitored throughout the procedure. Figure 5.3a

illustrates the Conine with a dog inside it, the rotating stage and the ventilator; figure 5.3b shows the remote anesthesia monitor, the small oxygen tank and also the Conine with the dog.

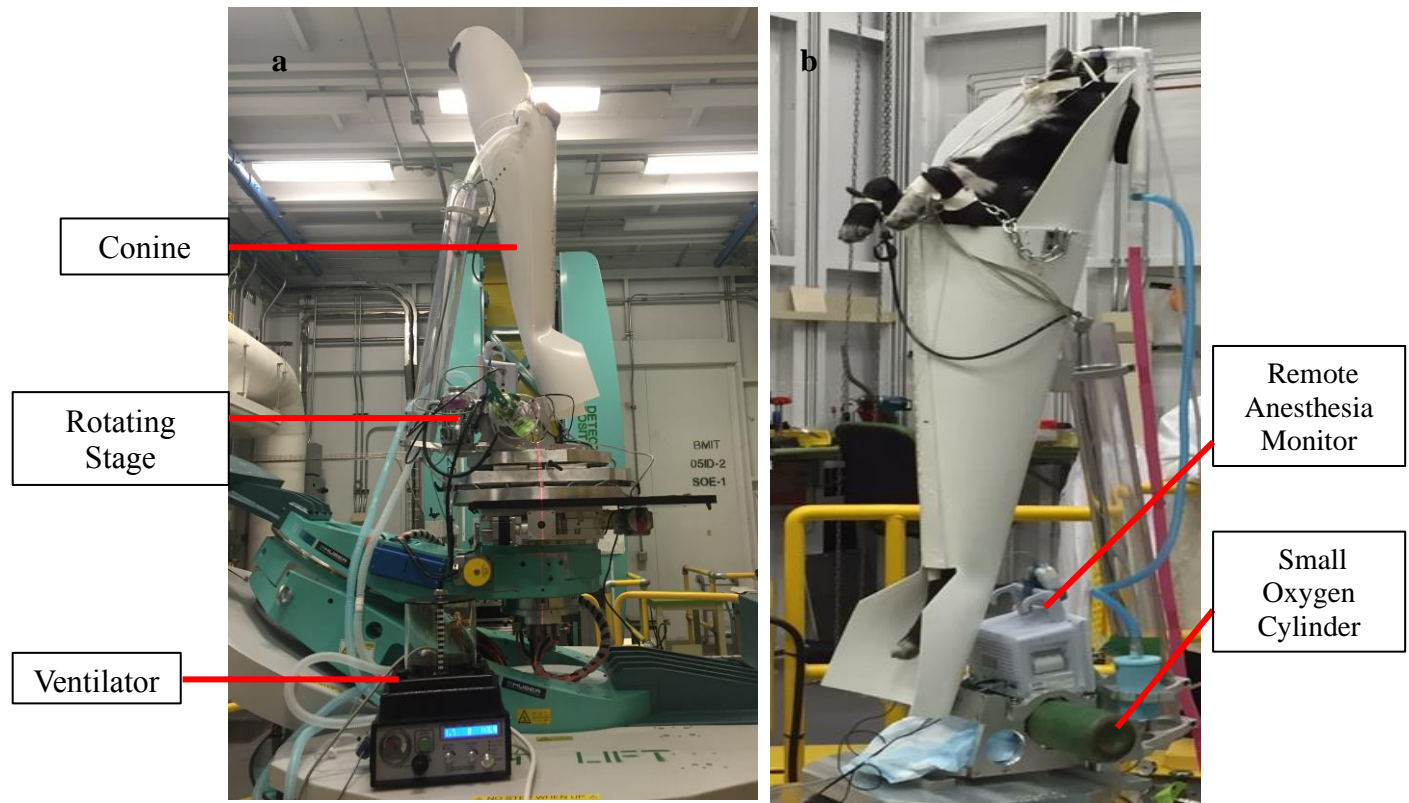


Figure 5.3. A live dog being imaged at the CLS BMIT ID Beam Line inside the Conine holder (white) located on top of the rotating stage (metallic) and the ventilator that was used can be seen within the hutch (a). The small oxygen cylinder, the remote anesthesia monitor and the dog inside the conine are also displayed (b).

In order to facilitate the localization of the prostate and to keep the urinary bladder small, each dog had an 8 F Foley urinary catheter inserted prior to being placed into the Conine holder. Iodinated contrast (diatrizoic acid, H919 98%, 3mL, AK Scientific, Inc. CA, USA) was used to inflate the catheter balloon within the bladder. Once the balloon with the contrast was visualized at the neck of the bladder using the CLS computer, this allowed the region of the prostate, which is immediately caudally to that position to be located. The stage was moved up 3 cm, allowing the prostate to be placed in front of the detector and perpendicular to the X-ray beam. The stage with the Conine plus dog mounted upon it was then rotated through 180° during imaging, using a total of 2000 projections, an average radiation dose of 22Gy (measured by an ion chamber inside the hutch) and exposure time of 50ms. Only one slice (3mm height)



was acquired per dog in order to avoid excess radiation exposure. Furthermore, the time required with the dogs under anesthesia to position them within the Conine, move them into the hutch and attach all the monitoring devices, and then acquire the images meant it was only feasible to acquire images for reconstruction of a single slice of the prostate gland for each dog. The total time for imaging the dog was around 5 hr per dog and it included anesthesia induction and maintenance, positioning of the dog in the hutch and imaging *per se*, which was an average of 2.5h (range of 2-3h) This attempt at PC-CT imaging represents the first time live dogs, weighing on average 28kg, have been imaged at the CLS. Prior to this, the largest live animal imaged was a rabbit (average weight 3-3.5 kg).

Three types of images are collected during the PC-CT imaging: tomographs (or set of projection images collected as the sample is rotated over 180 degrees), which contain the raw data, and dark and flat images that are collected twice both before and after the tomographs (projection images) that are used to correct for any detector pixel sensitivity variations and non-uniform X-ray irradiation that will occur with decreasing energy of the beam overtime in between the beamline fills. Dark images are images taken without the beam and just include the filter; flat images are images taken of the absolute X-ray (without any object on the beam pathway).

The PC-CT reconstruction was done in two steps and involving two separate software programs: ImageJ (Rasband 1996-2016) and XTract (CSIRO, Australia). The raw synchrotron image data was first processed in Image J, and prepared for CT reconstruction with Xtract software package in which the sinograms was done and the final CT slices were calculated. The processing in ImageJ consisted of cropping a region of interest (ROI) from the raw projection image data, dark and flat images, as illustrated in figure 5.4. In order to remove the part of the images produced by the non-irradiated regions of the x-ray image detector, the raw projection images were cropped using the rectangular selection tool in Image J and the same selection was then used to crop the dark and the flat images. ImageJ was also used to remove a vertical center

line - an x-ray detector artefact appearing at the place where the two detector sensors meet (figure 5.5). The image was zoomed to its maximum and the center line was selected along with the two adjacent lines, each of them one pixel wide, and a median value of 1 was inserted for the pixels of the center line. The flat images and the projection images had to be taken with different filters in the x-ray beam due to the large attenuation of the sample. The flat images were taken with additional polymethyl methacrylate (PMMA) filters inserted in the x-ray beam to prevent detector saturation. Thus before applying the standard image normalization procedure, the flat images had to be multiplied by an additional correction factor accounting for the attenuation of the X-ray beam by the PMMA material inserted into the beam before taking the flat images. The image multiplication was done in the ImageJ software, and the correction factor was calculated for each data set using the web based X-ray attenuation and transmission calculator ([https://web-docs.gsi.de/~stoe\\_exp/web\\_programs/x\\_ray\\_absorption/index.php](https://web-docs.gsi.de/~stoe_exp/web_programs/x_ray_absorption/index.php), see figure 5.6). The thickness of the PMMA filters, with which the flat images and the projection images were taken, was given to us by the BMIT scientist. Entering the X-ray beam energy and the thickness of the PMMA filter in the web based calculator (see figure 5.6) we obtained the transmission values for the two cases. The needed correction factor for the flat images multiplication is then given by the ratio of the attenuation values ( $\text{Transmission}_{\text{tomographs}}/\text{Transmission}_{\text{flats}}$ ).

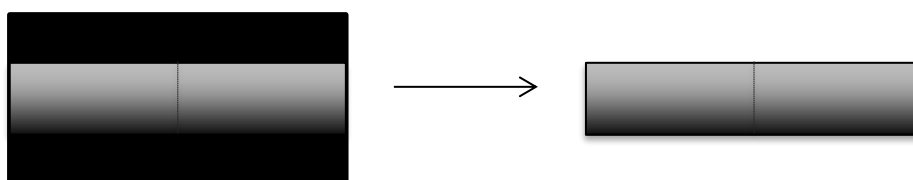


Figure 5.4. Schematic representation of one raw tomographic projection (on the left), and the ROI is grey in color located in the center of it. By trimming and removing the extra top and bottom black strip, we obtain the final grey strip that contains the data (on the right).

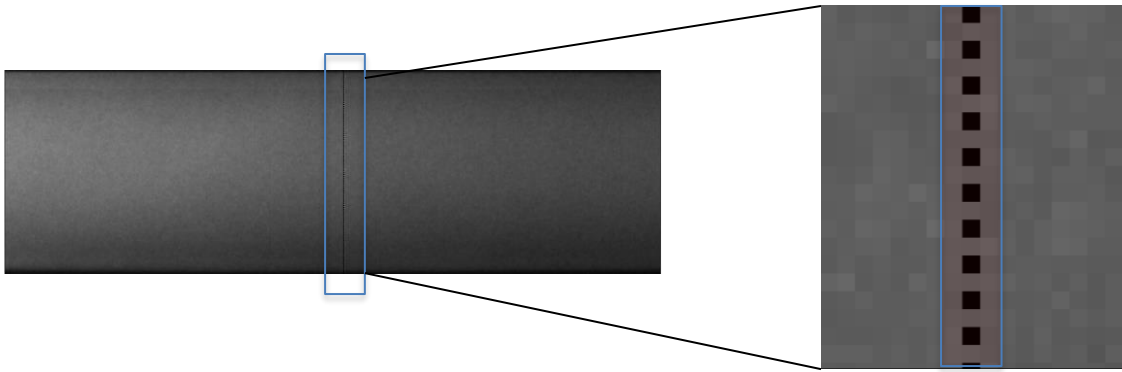


Figure 5.5. A raw tomographic projection showing the vertical center line (on the left) and the selection of the two adjacent pixels with the center line to calculate the median (on the right).

Target Material:	<input type="text" value="PMMA"/>	<b>RESULTS:</b>
X-Ray Energy [keV]:	<input type="text" value="120"/>	Attenuation [%]: 93.1933
Target length [mm]:	<input type="text" value="160"/>	Transmission [%]: <input type="text" value="6.8067"/>
Pressure (only gases) [atm]:	<input type="text" value="1"/>	
	<input type="button" value="Calculate!"/>	

Figure 5.6. X-Ray attenuation and absorption calculator. The target material in this case is PMMA and the calculation is based on tomographic and flats values for transmission. The X-ray energy level (in this case 120 keV) and the target length (variable, according to the information provided by the scientists from the CLS) are entered for flats and tomographs one at a time. The website then calculates the transmission value obtained for the tomograph transmission/flat transmission ratio.

The projection flat and the dark images pre-conditioned in ImageJ as described above were then used to generate sonograms in the pre-processing step of the Xtract software. It is also in this step that phase extraction and ring artefact removal are performed. Rings are artefacts that can appear for different reasons, including from the misalignment of the detector, with the end result of causing visual pollution. After obtaining sinograms, reconstruction processing is performed such that images are aligned and a filter is applied, resulting in the final

image with artefacts removed. For more details, refer to the Xtract User Information (in the appendix section).

The conventional MRI, CT and PET-CT image findings per dog were compared side by side within the same week (week 17) and with the US and PC-CT images from week 35. Analysis and comparisons between each imaging modality in the live dogs was performed by assessing the ability to identify macro structures such as the prostate capsule, visualization of internal septa, the urethra, the lobular structure, medium septa, parenchymal texture and the verumontanum (also known as seminal colliculus, it is visualized as a bulging area on the prostatic urethra, which is the mark for the prostatic and ejaculatory ducts). For each image an assignment of either a ‘yes’ for the presence of the macro structure in the modality or a ‘no’ for the absence was recorded. They were also graded for the times the structure could be seen in each of the six dogs versus just in one individual dog.

#### 5.4 Results

In chapter 4, the analysis of semen, DRE, hormones, volume and 3D measurement of the gland, morphometric analysis and histological diagnosis revealed that all dogs developed BPH, either spontaneously or induced with hormones.

Figures 5.7 and 5.8 show the side-by side lateral projection radiographic images from each dog (control group dogs#1, 2 and 5 in figure 5.7 and treatment group dogs# 3, 4 and 6 in figure 5.8) taken at baseline (week -4) and at week 17. A board-certified radiologist marked each radiograph with a “P” when the region of the prostate gland was clearly visualized.

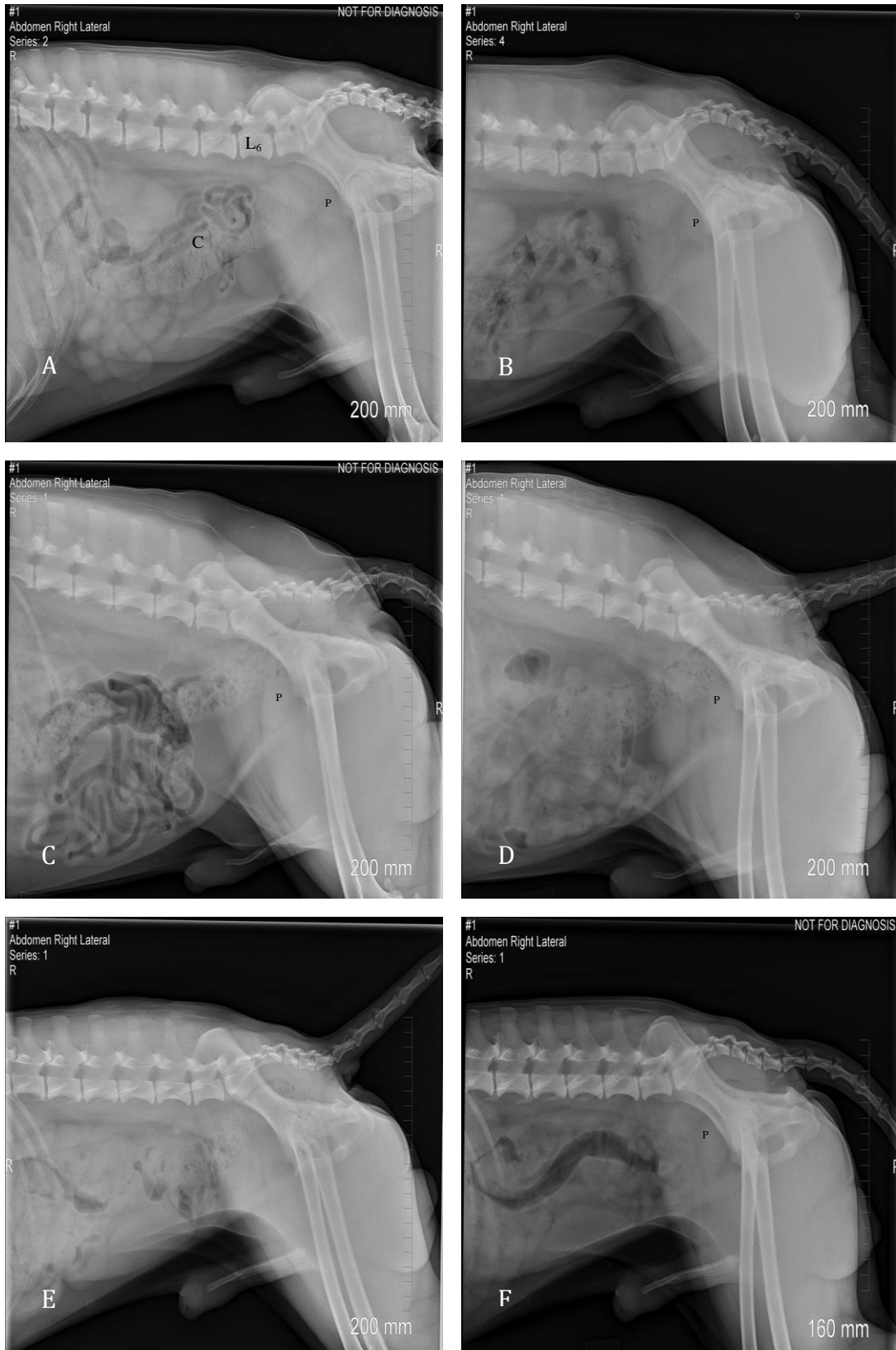


Figure 5.7. Side by side lateral radiographic projections from control dogs #1(A and B), #2 (C and D), #5 (E and F), obtained at week - 4 (left) and week 17 (right). L6 is the sixth lumbar vertebrae, C is for colon, P is the prostate.

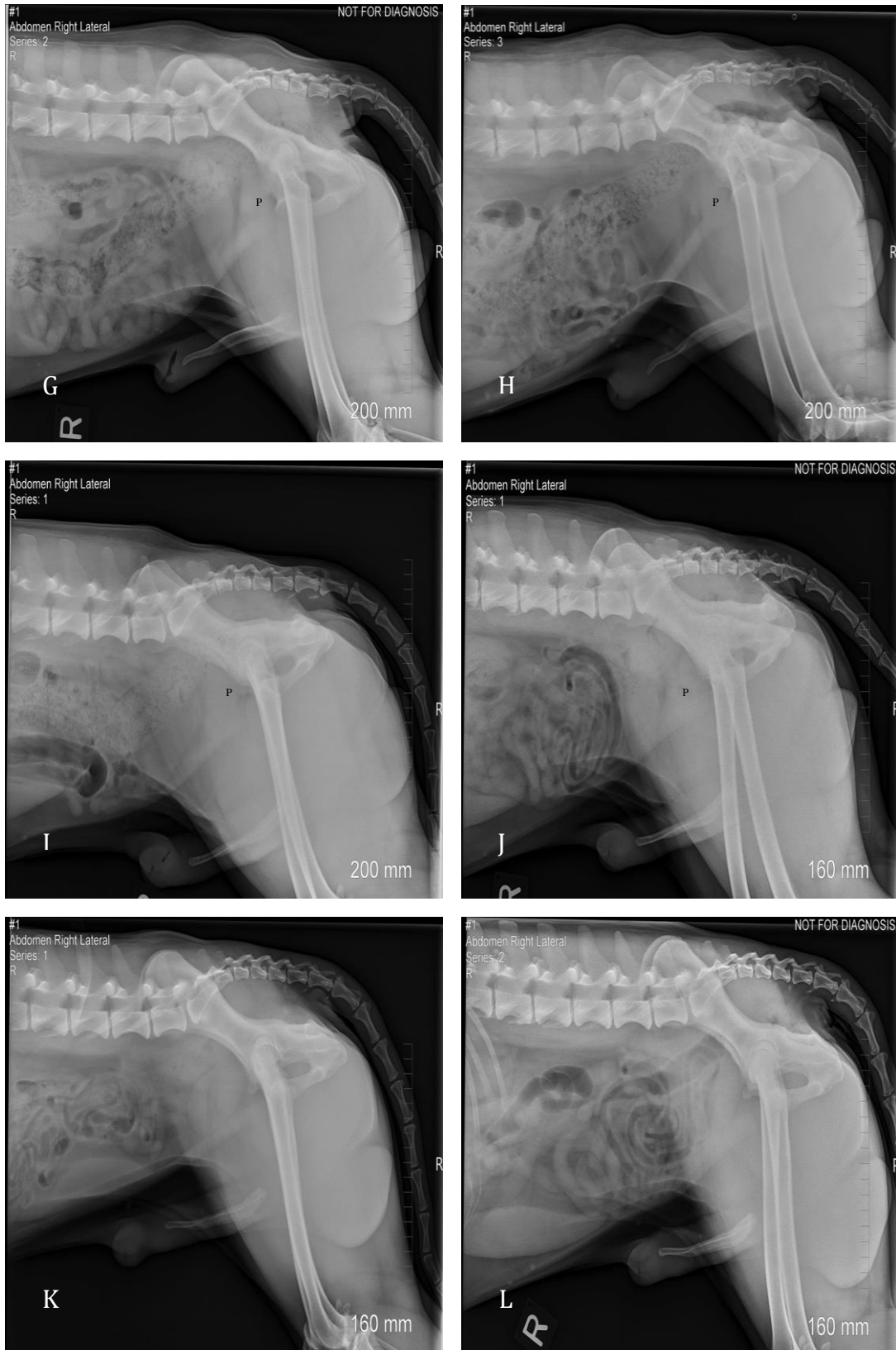


Figure 5.8. Side by side lateral radiographic projections from treatment dogs #3(G and H), #4(I and J), #6 (K and L), obtained at week - 4 (left) and week 17 (right). L6 is the sixth lumbar vertebrae, C is for colon, P is the prostate.

The identification of the gland was possible in 4 out of 6 dogs at Week -4 and 5 out of 6 dogs at Week 17. The prostatic diameter was less than 70% of the DSSP, therefore, none of the glands, regardless of experimental group, was classified as hyperplastic solely based on this measurement. In three out of twelve of the images, the margins of the prostate were not distinguishable from the surrounding radio-opacities indicating that radiography is not the best imaging modality to assess the prostate. No internal architecture within the glands is appreciable.

Representative side-by-side CT, PET-CT, MR-T1 (figure 5.9) and MRI-T2 , US and PC-CT (figure 5.10) images of control dogs #1, 2 and 5 and treatment dogs #3, 4 and 6 collected at week 17 for each dog are shown below, along with the ultrasound and PC-CT images obtained at week 35. The only imaging modality that was repeated again at week 35 was US; the other modalities (CT, PET-CT, MRI) previously collected at week 17 were not repeated at week 35 due to cost. However, for the purposes of this thesis, this interval difference does not interfere in the objective of illustrating and comparing the images. One axial image at the largest diameter of gland of each modality (i.e. largest cross section from the middle of gland) was selected for comparison purposes. It is impossible to perfectly match images to exactly the anatomical slice of the prostate, however, they are all relatively close to each other. See appendix for a different arrangement of the *in vivo* imaging comparison.

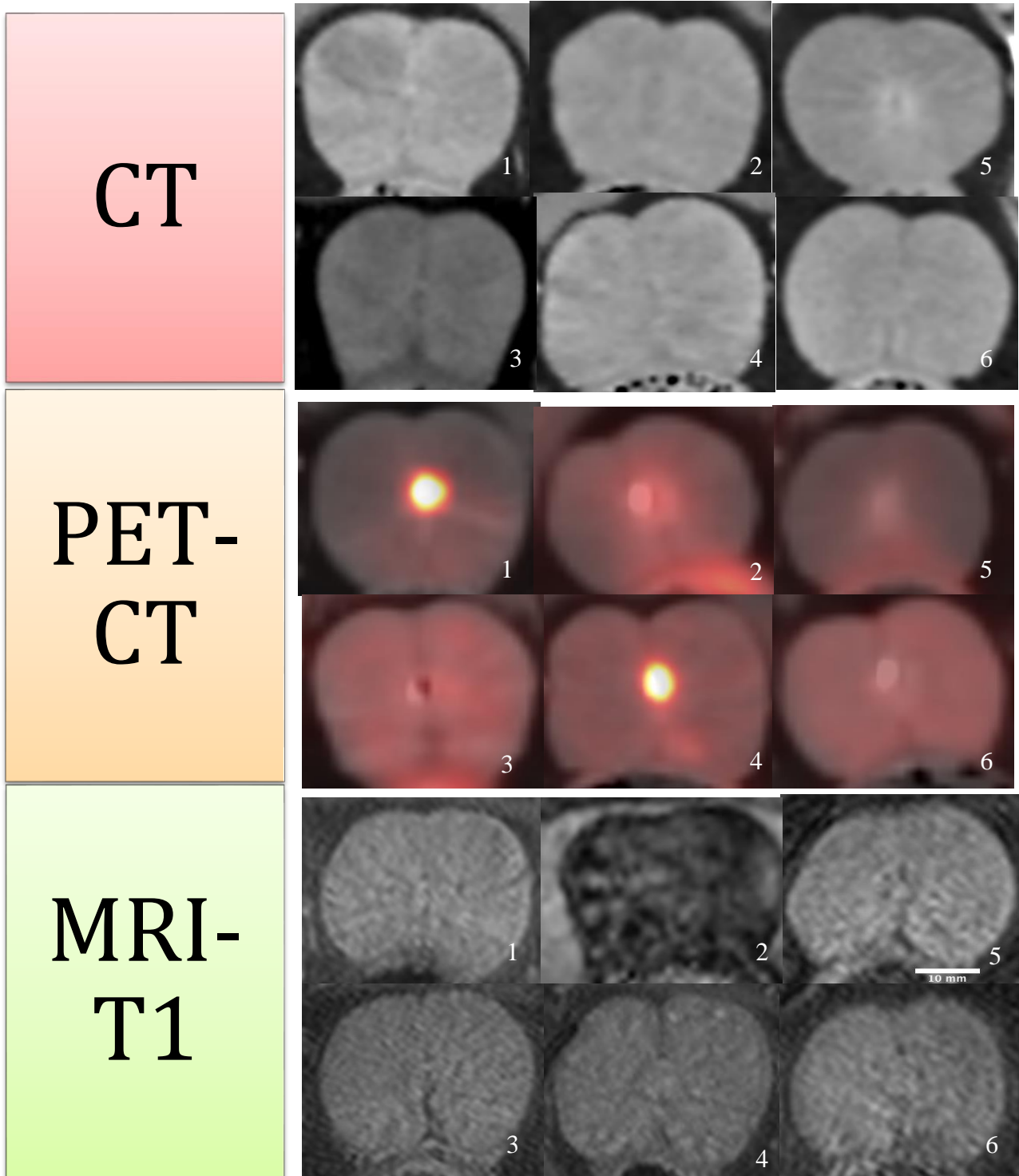


Figure 5.9. *In situ axial* images of the prostate of control (top row) and treatment dogs (bottom row) taken with the imaging modalities: CT, PET-CT and MRI-T1 all collected at week 17



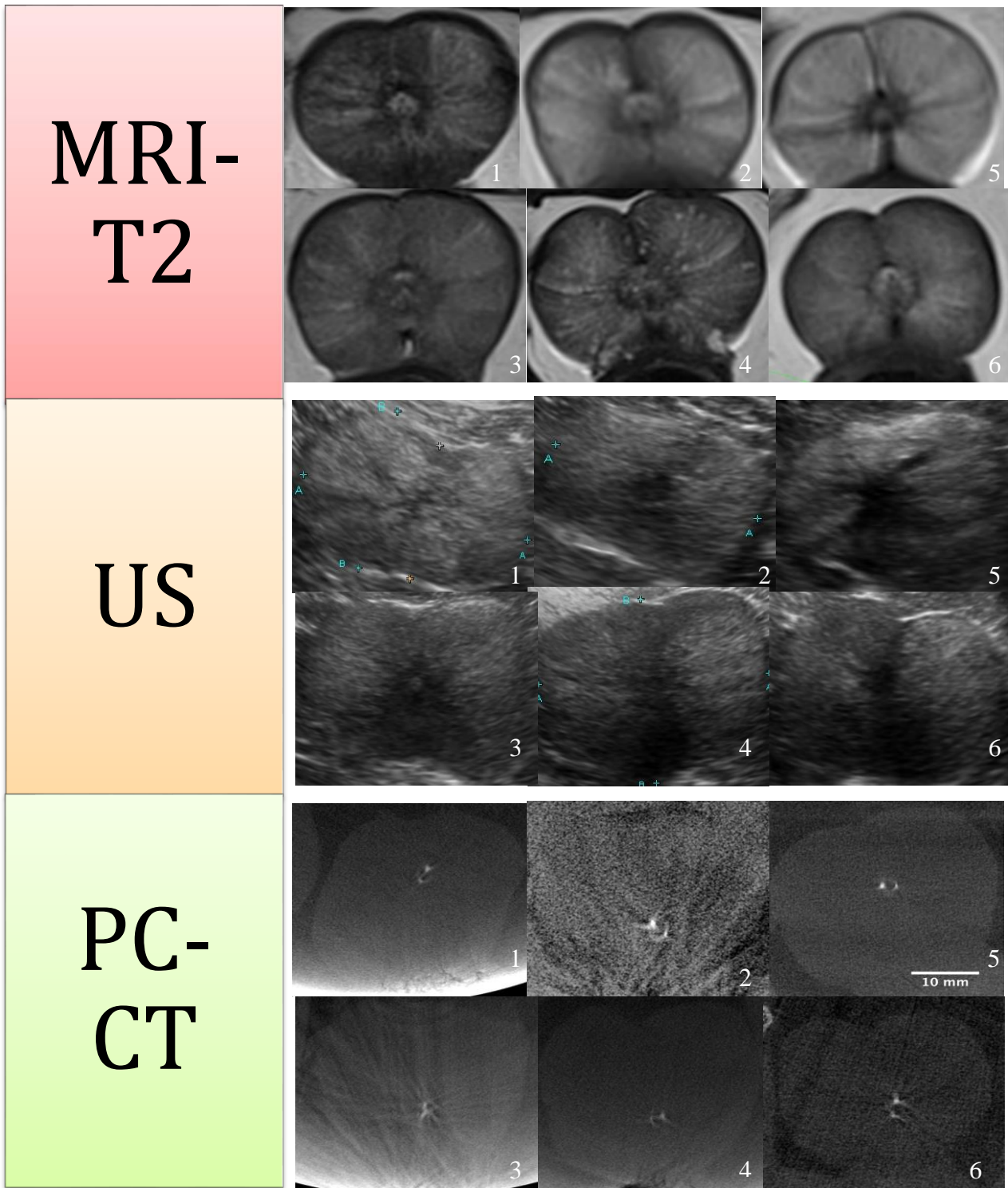


Figure 5.10. *In situ axial* images of the prostate of control (top row) and treatment dogs (bottom row) taken with the imaging modalities: MRI-T2 (collected at week 17), US and PC-CT (collected at week 35).

Figures 5.11 and 5.12 display *in situ* images of the canine prostate glands in control dogs#1, 2 and 5 and treatment dogs#3, 4 and 6 using the PC-CT technique in imaged pre- and post euthanasia dogs, respectively.

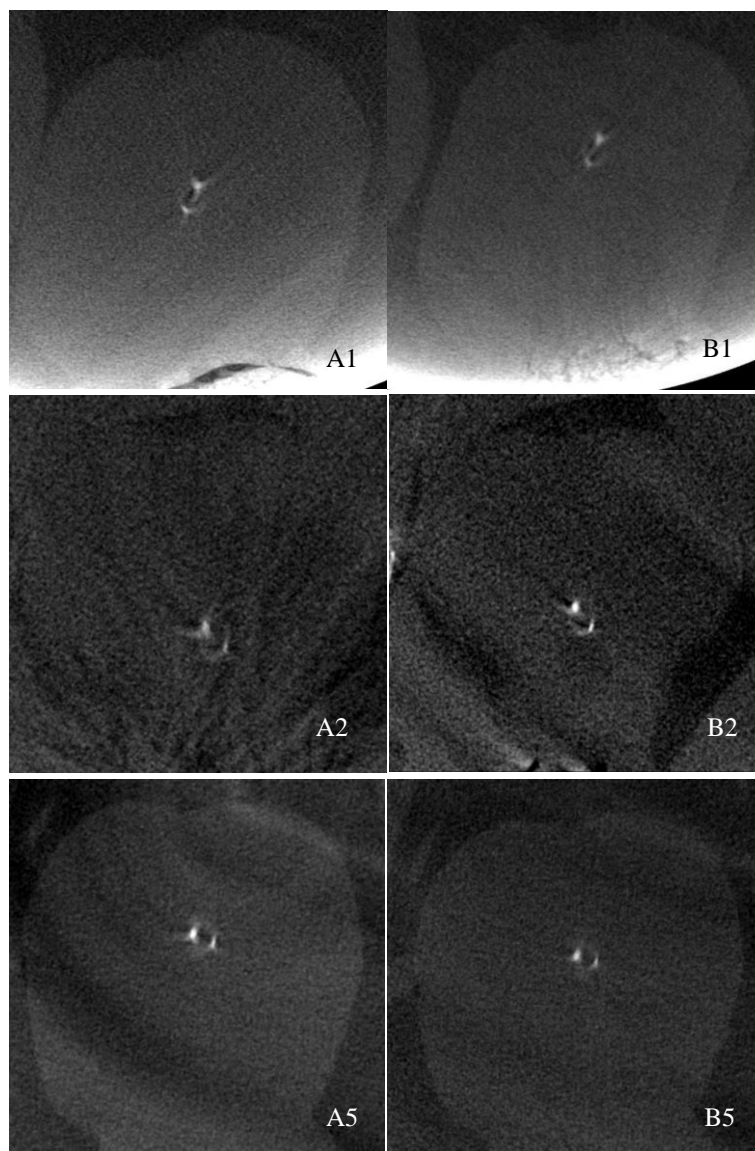


Figure 5.11. Side by side PC-CT images of the prostate gland of the control dogs imaged pre (A1, A2, A5) and post (B1, B2 and B5) euthanasia.

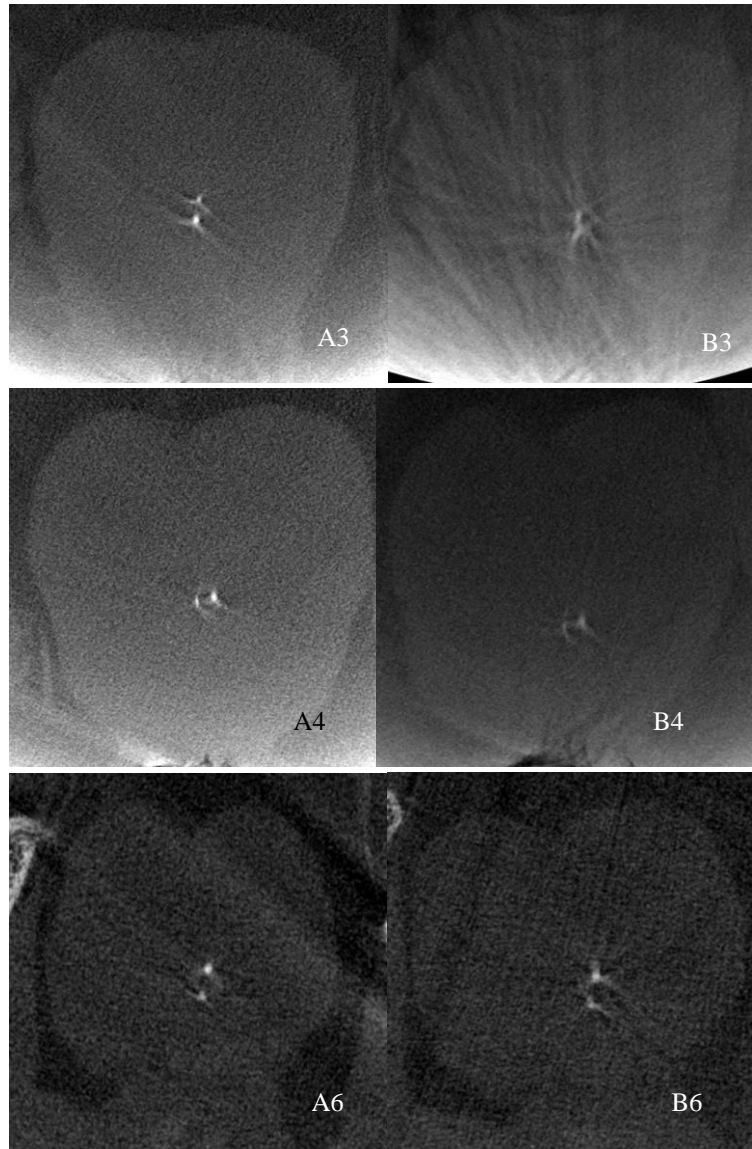


Figure 5.12. Side by side PC-CT images of the prostate gland of the treatment dogs imaged pre (A3, A4 and A6) and post (B3, B4 and B6) euthanasia.

The conventional MRI, CT and PET-CT were compared side-by-side within the same week (week 17) and with the US and PC-CT images from week 35. Table 5.1 provides the results from image analysis done to compare the different imaging modalities with respect to their ability to identify the previously listed macrostructures. The best modality to visualize the gland was T2 W MRI, which was able to distinguish the capsule from the parenchyma, allow visualization of the urethra and verumontanum and also connective tissue septa infiltrating into the gland. Ultrasonography was the next best imaging modality to distinguish the soft tissue details with the prostate. It was possible to see the urethra in CT images of dogs 1 and 5

(control) and 3 and 4 (treatment), in the US images of dogs 1 and 2 (control) and all three treatment dogs and in MRI T1 images of dogs 1 and 5 (control) and 3 and 4 (treatment). The median septum could be visualized in all images and consequently the two lobes of the prostate. PET CT and PC-CT are just able to display the urethra filled with the radiotracer F18-FDG (excreted via urine) and iodinate contrast (filling up the urinary catheter balloon), respectively. It is possible to observe that none of the modalities provide great or substantial information about the internal architecture of the prostate gland to the level of detail (resolution) that would likely allow for the differentiation of prostatic diseases such as BPH versus early PCa. A PC-CT image of the dogs' prostates pre and post euthanasia were also displayed in figures 5.15 and 5.16, confirming that there are no major differences in these images, apart from artefacts caused by bone and feces in the rectum.

In regards to the evaluation of the images for features of BPH, heterogeneity of the parenchyma was visualized in CT (dog 1 from the control and dogs 3 and 4 from the treatment group), US (all control dogs and dog 4 from the treatment group), MRI T2 (dogs 1 and 2 from the control and dogs 3 and 4 from treatment group) and MRI T1 (dog 1 from the control and dog 4 from the treatment group). Intraparenchymal cysts were generally visualized in CT (dogs 1 from the control and 3 and 4 from the treatment group), MRI-T2 (dog 1 from the control and all dogs from the treatment group) and US (dogs 1 and 5 from control and all dogs from the treatment group) images.

CT data was used to calculate the volume of *in vivo* images (week-4 and week 17) and there was no difference in the mean volume of the prostate gland between the control and treatment groups as detailed in chapter 3 (week 17: control mean=18.4cm<sup>3</sup>, treatment mean=29.2cm<sup>3</sup>, P=0.4164)

Table 5.1. *In vivo* imaging modality comparison of the macrostructure features of the prostate glands in the control and treatment dogs. Visualization of the main macro structures of the prostate was evaluated in all the images acquired *in vivo*. The images were assigned a ‘yes’ for the presence of the structure seen in that modality and ‘no’ for the absence. Images were also graded for how many times the structure could be seen in each of the six total dogs (numbers in brackets).

	CT	US	PET CT	MRI T1	MRI T2	PC CT
Urethra	Yes (3/6)	Yes (3/6)	Yes (6/6) (radiolabel)	Yes (1/6)	Yes (6/6)	Yes (6/6) (contrast)
Capsule	No	No	No	No	Yes (6/6)	No
Lobe	Yes (6/6)	Yes (5/6)	Yes (6/6)	Yes (4/6)	Yes (6/6)	Yes (5/6)
Parenchyma homogeneity	No	No	Yes (6/6)	No	No	Yes (6/6)
Verumontanum	Yes (3/6)	Yes (1/6)	No	No	Yes (6/6)	No
Median septum	Yes (6/6)	Yes (6/6)	Yes (6/6)	Yes (6/6)	Yes (6/6)	Yes (6/6)

## 5.5 Discussion and Conclusion

The first objective of this study was to image the prostate gland of live dogs with the PC-CT technique and be able to reconstruct them; the second objective was to acquire high-resolution PC-CT images when compared to the other conventional modalities and be able to compare the images of dogs with BPH to control normal dogs in order to characterize the findings of BPH using PC-CT. We were able to fulfil the first objective by acquiring for the first time images of the prostate gland of live dogs using PC-CT at the Canadian Light Source Synchrotron. However, the second objective was not achieved and the resolution of the *in situ* glands was not as great as expected. In addition to this, all current conventional imaging techniques (ultrasound, CT, radiographs, MRI and PET-CT) that are used to help in the diagnosis of prostatic diseases have their limitations in regards to the visualization of the internal structures of the prostate gland.

The most commonly used imaging modality for the diagnosis of prostatic disease in dogs and people is ultrasound (Ruel et al., 1998). This modality does not use X-rays, but ultrasound waves. Ultrasound, however, is a modality that is highly dependent on the

experience of the operator performing the examination, resulting in interpersonal and intrapersonal variation, which means that different ultrasonographers may collect different measurements of the gland (Leroy et al., 2013). Apart from this drawback, it is considered a simple, fast and relatively easy examination to perform, and it gives relevant information regarding the size, the consistency of the parenchyma (homogenous or heterogenous) and presence or absence of intraparenchymal cysts (J. Smith, 2008; Williams, 2013; Levy et al., 2014), which may aid in the diagnosis of BPH. It may also allow evaluation of regional lymph nodes (e.g., the sublumbar) and the urinary system. According to Lattimer and Essman (2007) a normal prostate gland imaged with ultrasound displays distinct margins and a homogenous echogenicity similar to the adjacent fat. When BPH occurs, the margins of the gland are still smooth, the gland becomes slightly hyperechoic, cysts can be visualized and the enlargement that is generally symmetrical becomes irregular if cysts are present (Lattimer & Essman, 2007). Also, ultrasound is a good technique that provides real time visualization of the urethra, allowing for assessment of any compression of the urethra from prostatomegaly (Lattimer & Essman, 2007). In dogs, ultrasound of the prostate is largely done through the abdominal wall while in people this typically involves insertion of the ultrasound probe transrectally. Transrectal or abdominal ultrasound can also be used to guide the collection of a biopsy sample from the prostate used to aid in the differentiation of BPH from early PCa (Ukimura et al., 2011). In agreement to previous studies, our ultrasound images provided information on the echogenicity of the parenchyma (heterogenic for dogs 1, 2 and 5 from control group and 4 from treatment group) and this was arguably the best modality for highlighting cysts within the parenchyma (cysts seen in all dogs except dog2 from control group).

Radiographs, computed tomography and PET-CT all use X-rays to produce images. They all have a major drawback for imaging soft tissues because x-rays are best for imaging very dense tissues like bones and do not provide good resolution of difference in the internal structure of soft tissues. Indeed as our study verified plain radiography cannot be relied on to

distinctly define of the margins of the prostate gland unless the gland is clearly hyperplastic (Johnston et al., 2000). Also, the size of the prostate gland assessed by plain radiographs tends to be overestimated because of other organs (colon) and structures (abdominal wall, soft tissue) silhouetting over the gland in the same region (Atalan et al., 1999). However, radiography can be very useful in cases of PCa to help identify for possible skeletal metastasis that can occur mainly to bones of the spine and/or pelvis (Dennis et al., 2010). Lateral plain radiography in the dogs in this study was able to delineate the prostate gland only to a limited extent. The presence of feces in the colon and distension of the urinary bladder with urine can both interfere with the ability of clearly identifying the borders of prostate gland. Performing an enema and urinary catheterization to empty the urinary bladder along with possibly the injection of a small volume of iodinated contrast medium into the prostatic urethra may have helped better delineate the radiographic boundaries of the prostate gland in dogs and could have been done in this study to try to increase the information obtained from this imaging modality. However as is apparent, plain radiography is highly inferior to other modalities with respect to its ability to highlight any of the internal architectural features of the prostatic parenchyma.

CT has been investigated in research studies as a potential technique to assess the prostate. Lee, K. J. et al., (2011) found that characteristics such as the homogeneity of the parenchyma of the gland using both pre- and post- injection of iodinated contrast, presence or absence of intraparenchymal cysts and detection of mineralisation of the parenchyma may be appreciated alongside prostatic measurement when assessing the prostate. Pasikowska et al., (2015) and Kuhnt et al., (2017) also confirms that CT technique performed in dogs with BPH is able to identify prostatomegaly, integrity of the capsule, heterogeneity of the parenchyma and presence of cysts in the canine prostate gland. Among CT, US and radiographs, CT is the modality of choice when it comes to investigation of the prostate gland's size and shape (Lee K.J. et al., 2011) because US can underestimate the size of the prostate, especially in the initial stages of BPH (Lévy et al., 2014). In our study, we are able to see the heterogeneity in the



parenchyma of all the dogs, but most pronounced in dogs 1, 3 and 4 and less in dogs 2, 5 and 6. Overall, CT is a modality that demands more time to be performed and is more expensive than ultrasound. In some of our CT images we were able to see heterogeneity of the parenchyma and cysts in dogs 1 (control group), 3 and 4 (treatment group), but the capsule was not clearly discernable.

PET-CT combines 3D cross-sectional CT imaging with functional imaging following the administration of F18-FDG, a radiotracer that is a glucose analogue that is taken up by highly metabolically active cells, including at sites of cancer and/or inflammation (Basu et al., 2014). PET-CT has the potential advantage therefore of being able to help identify diseases in the early stages before there is any disruption or change in the structure or anatomy of the gland. It may also be superior for determining the extent of disease through the detection of any spread of cancer or inflammation to local or distant organs. PET CT also provides a means of monitoring the evolution of the disease in response to prescribed therapy allowing quantitative measurement of the effectiveness of such therapies (i.e., assessment of response to chemotherapy or radiation for PCa or assessment of involution of the gland in response to anti-androgen therapy for BPH) (Lawrence et al., 2010). The CT part of the combined PET-CT image is able to help in the diagnosis, differentiation and anatomical identification of the region where the uptake is higher as a consequence of a population of malignant or inflammatory cells (Lawrence et al., 2010). Unfortunately, there is not a consensus about the best radiotracer to use to help differentiate BPH from early PCa (Bouchelouche & Oehr 2007; Castellucci et al., 2015). F18-FDG has not been able to provide satisfactory results for the detection of PCa in past studies. This has led to the use of new radiotracers, such as C11-choline, which have shown improved capability for restaging the extent of PCa in cases of patients with increasing PSA (Fuccio et al., 2011) and in high risk patients, due to the low sensitivity and high specificity of the PET-CT exam (Castellucci et al., 2015). In our images, as expected there was no uptake of F18-FDG in the prostate gland in the dogs from either the control or the treatment



group, but the tracer was present in the urethra and the bladder as F18-FDG is excreted via the urine.

MRI is a modality that does not rely on ionizing radiation for diagnostic imaging. Instead it relies on magnetisation of hydrogen atoms within the patient's body in response to changes in a surrounding magnetic field. Two types of sequences– MRI T1-weighted and T2-weighted images– are used to image soft tissues including the prostate gland. Studies involving the prostate have shown that T1 demonstrates a more homogenous internal signal for the gland (Jia et al., 2005), and in people this MRI sequence has been useful for helping to discern post-biopsy haemorrhage from PCa (Pedler et al., 2015). On the other hand, T2 -weighted imaging has been shown to be superior to T1 weighted imaging for isolation and delineation of the prostate from surrounding tissues (Jia et al., 2005). While MRI does not result in any risk to the patient from exposure to radiation, it is an expensive technique that requires significantly more time to acquire images compared to CT, US or plain radiography (Jia et al., 2005). T2 W MRI images have been demonstrated to be able to differentiate the zones of the prostate in humans with BPH (Garvey et al 2014) and to be superior to US for more accurately calculating the volume of the prostate gland in patients with BPH. Unfortunately, however, T2 imaging has not been shown to be able to reliably differentiate PCa from BPH (Emad-Eldin et al., 2014; Garvey et al., 2014). In our study MRI T2 was subjectively and objectively the superior technique as it was able to distinguish the capsule from the parenchyma (dogs 1 from control group and 3, 4 and 6 from treatment group), cysts (dogs 1 from control group and 3, 4 and 6 from treatment group) allow visualization of the urethra and verumontanum (all dogs), small cysts within the parenchyma and also allow identification of connective tissue septa infiltrating into the gland (all dogs).

Finally, PC-CT imaging has been investigated for imaging a variety of tissues at various synchrotrons around the world. Two different studies, one using mice and rabbit cadavers and the other using piglet cadavers, also have shown that soft tissue can be better visualized with

synchrotron imaging resulting in images that are of higher quality than plain radiographs (Kitchen et al 2005; Zamir et al., 2015). In our study, PC-CT imaging was performed uniquely and successfully for the first time in live dogs by the Prostate Research Group at the University of Saskatchewan. The achievement of the acquisition of the image of live dogs required previous research and a collaborative effort between CLS scientists and members of the Prostate Research team. Different holders were tested and initial design issues had to be overcome in order to achieve the vertical stability of the dog required to allow reconstruction of the final images. The final version of the holder device used in this study (the Conine) did in the end allow us to maintain the dog in a stationary vertical position without appreciable vertical motion and it proved to be safe for live animal imaging. However, although the acquisition and reconstruction of *in vivo* canine prostate PC-CT images was possible, the quality of the reconstructed images obtained at this time is inferior when compared to more conventional CT, MRI or US images. *In vivo* PC-CT images in our study were similar to those acquired from PET-CT scanning. Previous *ex-vivo* imaging of the canine prostate gland housed in gelatin and imaged using PC-CT performed by our group has shown that with good penetration the internal structures of the gland can be seen in greater detail than with any form of conventional imaging available. Indeed the images acquired of *ex-vivo* prostates are similar to that seen with low power histological microscopic imaging (4-10X magnification), proving that higher resolution can be achieved by the PC-CT technique. Our findings show that unfortunately, there are still some technical challenges that need to be overcome in order to obtain the required image quality and resolution with *in vivo* imaging as seen with *ex vivo* imaging. Those include thickness of the sample, when considering the diameter of the dog's pelvic region in comparison with just the excised prostate for the X-rays to pass through; distance of the sample from the detector, which if increased could potentially improve phase contrast but is not possible within the current BMIT hutch where the distance has already been maximized, and

finally increased energy level, keeping in mind that this comes at price of increased radiation exposure and there is a finite limit here to maintain this within safe and acceptable limits.

In conclusion, we acquired for the first time images of the *in situ* prostate glands of live dogs using the PC-CT technique at the CLS. It was extremely important to immobilize the dogs in the restraint device to prevent any movement in a vertical direction during the PC-CT scan, and this was only possible with trial and error failures that ultimately lead to the development of the final version of the Conine holding device. Also, adaptations such as the use of remote anesthesia control, respiratory trigger device and two oxygen tanks inside the hutch were essential for the completion of this experiment. Moreover, in chapter 3, where the induction of BPH in male dogs is described, we were not able to make the difference between the two groups (control and treatment) distinct enough and this interfered in the ability to differentiate the images portrayed in this chapter (4)., The contrasts in the images are not as pronounced as we hoped and the quality of the prostate images taken *in vivo* was less than those obtained previously by our group using *ex vivo* samples. Consequently, we failed to achieve the high resolution and internal details of the prostate gland we had seen with *ex-vivo* imaging, resulting in images of inferior quality compared to those from other conventional modalities, with the possible exception of PET-CT studies. This indicates that there is still more investigation and research required in order to hopefully one day achieve a similar level of resolution as was obtained with imaging of the excised prostate glands. Those improvements might be able to unveil the correct combination of such parameters such as the as energy level, the distance from subject to detector, type of detector that provides the best results, etc. that will ultimately allow such a revolutionary imaging technique for the *in vivo* diagnosis of prostatic diseases, including BPH and prostate cancer, without the need for an invasive diagnostic biopsy.

The need for an innovative imaging technique that could potentially improve the early identification and differentiation of prostatic diseases is extremely important, potentially

avoiding the need for a patient to undergo an invasive biopsy in order to obtain a definitive diagnosis. The collection of the tissue involves risks of sepsis and it may or may not procure a representative sample of the area of cancer, which most of the time cannot be visualized with TRUS. Previous research using synchrotron imaging has yielded good visualization of soft tissues with *ex vivo* or very small animal imaging. Indeed, excised canine prostates imaged with PC-CT resulted in very high resolution images superior to other conventional imaging modalities in terms of the level of internal structural detail that could be resolved. However our research also proved that imaging the prostate of dogs *in vivo* with PC-CT is feasible but that much more research is still necessary before diagnostic quality images in live animals using the synchrotron are possible.

## CHAPTER 6: GENERAL DISCUSSION AND FUTURE PERSPECTIVE

Benign prostatic hyperplasia (BPH) is a common condition in ageing men and it is the most common disorder of the prostate gland (Vuichoud & Loughlin, 2015). BPH is characterized by the enlargement of the gland (Tanguay et al., 2009). Men over 50 years of age should be aware of BPH and seek for medical services if any symptom is present or even just for regular check up. Apart from the urinary symptoms, BPH is not a cause of death, but prostate cancer is and it is one of the most common forms of cancer diagnosed in Canadian men (Canadian Cancer Society). The sooner it is diagnosed, the better for improving and increasing the life expectancy. Other than men, dogs can also develop BPH and, despite the particularities of how BPH affects the prostate of each species, they are an acceptable model to study BPH (Walsh & Wilson, 1976; DeKlerk et al., 1979).

A variety of imaging methods to evaluate the prostate volume and parenchyma features are available. MRI and PET-CT demonstrated to be efficient in diagnosing prostate cancer and BPH but most of the times they are not possible to differentiate between these two diseases (Yoshida et al., 2005, Li et al 2008, Castellucci et al., 2015). This inaccuracy leads to more invasive methods such as biopsy – the gold standard procedure – to precisely diagnosis prostatic diseases (Singh & Emberton, 2013). Considering the above facts, two studies were conducted as part of this thesis. First study objective was to induce BPH in dogs with a hormonal protocol described by DeKlerk et al., (1979) (chapter 4) and the second study objective was to image live dogs, control and with induced BPH, using a non-conventional imaging modality (PC-CT) and compare it with different imaging modalities currently used in the clinic routine (ultrasound, CT, MRI, PET-CT and radiographs) (chapter4). The rationale comes from the outstanding results (higher resolution and contrast) obtained previously with the images of excised prostate glands of dogs using the PC-CT modality by our Prostate Research Group and published in Wolkowski et al., 2015.

The first study of this thesis (induction of BPH, chapter 4) describes the use of a combination of the hormones 5-alpha dihydrotestosterone and 17-beta estradiol as published in the literature. An initial issue was the preparation of the drugs using the exact sonication methodology for mixture of the substances as [DeKlerk et al., \(1979\)](#) specified, which was not possible. When using the sonication for trying to mix the hormone powders and triolein oil, the result was a heterogeneous substance. This lead us to search in the literature and seek for another trusted method of mixing the hormones with triolein ([Malhi et al., 2006](#)), which is then used as described in chapter 4. Furthermore, the combined evaluation of the hormones testosterone, dihydrotestosterone, estradiol and the protein CPSE values, with results of the DRE, volume and morphometric analysis, and histological assessment, lead to the conclusion that all six dogs (three control and three treatment) developed BPH either naturally or induced. In order to improve our outcome and avoid the control dogs to spontaneously develop BPH, one possible solution could have been the administration of a drug to treat BPH such as flutamide ([Nizański et al., 2014](#)) or finasteride ([J. Smith, 2008](#)) to the controls to have a negative control rather than an actual control group. This would have contributed to make the comparison by imaging and histology more apparent. Another alternative for the spontaneously developed BPH could have been neutering the dogs from the control group and this would have led to the prostatic involution in 12 weeks ([Nizanski et al., 2014](#)). This way, we would have seen stark contrasts in the two groups in terms of not only the size of the prostate but also features of the prostate in our imaging and ultimately also on histology.

The second study (chapter 5), which involved the *in situ* imaging of live control and BPH induction dogs (treatment group), encountered some obstacles. The induction time set to be four months, as described by [DeKlerk et al., \(1979\)](#) ended up being extended to eight months. This happened due to the troubleshooting in the collection of the PC-CT imaging (vertical motion of dogs and breathing motion) and our inability to reconstruct the images. This delay in recollecting the PC-CT images was inevitable and limited us in imaging comparison

since the other modalities (MRI, CT, and PET-CT) had already been collected on the first imaging date (four months after the hormone induction started). So because of the difference in the date the images were collected, our image comparison is not entirely precise. Additionally, the resulted PC-CT images did not display the level of resolution we intended. Some limitations of the study include the size of the dogs and the distance between the sample and detector. The size of the dogs could have been an obstacle for the penetration of the beam and for future studies choosing smaller dogs (slim breeds such as Greyhounds) could perhaps improve the quality of the images. In order to obtain a better effect of the phase contrast physics, future studies could employ a larger distance between the sample and the detector, this would have to be performed in another Synchrotron that possesses this distance. Lastly, the primary objective of chapter 5 was to use PC-CT to image dogs with BPH and compare the images to control normal dogs in order to characterize the findings of BPH using PC-CT and this was not possible because our control group dogs also had BPH and so effectively we have six dogs with features of BPH and one control and one treatment dog perhaps with slightly more pronounced features based on the CPSE.

## APPENDIX

Table A.1. Complete Blood Count and Serum Biochemistry profile data for all six dogs (control #1, #2 and #5, and treatment #3, #4, and #6) at week -4.

Parameters	Control			Treatment			Reference	P-value
	Mean	SEM	n	Mean	SEM	n		
WBC( $\times 10^9/L$ )	11.7	2.022	3	11.37	1.317	3	4-9	>0.9999
Neutrophils( $\times 10^9/L$ )	8.706	1.876	3	7.395	0.4197	3	3.000	0.5327
Lymphocytes( $\times 10^9/L$ )	1.804	0.3675	3	2.568	0.6411	3	1.200	0.36
Monocytes( $\times 10^9/L$ )	0.6033	0.08329	3	0.548	0.146	3	0.080	0.7
Eosinophils( $\times 10^9/L$ )	0.6253	0.2372	3	0.8557	0.2045	3	0.000	0.5029
RBC( $\times 10^{12}/L$ )	7.623	0.4772	3	7.46	0.08145	3	5.80	0.7528
Hemoglobin(g/L)	175.7	10.35	3	178.3	5.812	3	133	0.8333
Hematocrit(L/L)	0.5187	0.02643	3	0.5243	0.01602	3	0.390	0.8635
Total Protein(g/L)	63.33	2.028	3	62	0.5774	3	55	0.5614
Albumin(g/L)	38	1	3	38.33	0.3333	3	32	>.9999
Globulin(g/L)	25.33	1.333	3	23.67	0.6667	3	20	0.3
Total Bilirubin( $\mu\text{mol}/L$ )	1.66	0.3	3	1.667	0.5175	3	1.0	2.6
ALP(U/L)	44.33	9.939	3	44	11.36	3	9	0.9834
ALT(U/L)	45	5.292	3	48.67	6.642	3	19	0.6882
Amylase(U/L)	914	209.8	3	582.3	244.2	3	343	0.3612
Lipase(U/L)	45	4.726	3	39.33	14.9	3	25	0.7354
GGT(U/L)	1.333	0.6667	3	1.333	0.6667	3	0	>0.9999
Cholesterol(mmol/L)	5.19	0.09238	3	4.91	0.9271	3	2.70	0.7788
Glucose(mmol/L)	5.667	0.3528	3	5.567	0.2816	3	3.1	0.8214
Urea(mmol/L)	5.333	0.1202	3	4.56	0.7638	3	3.5	0.3418
Creatinine( $\mu\text{mol}/L$ )	90.67	6.009	3	80	9.504	3	41	0.3965
Sodium(mmol/L)	149.7	0.8819	3	148.3	0.3333	3	140	0.4
Potassium(mmol/L)	4.5	0	3	4.367	0.08819	3	3.8	0.4
Chloride(mmol/L)	111	1.155	3	111	0.5774	3	105	>0.9999
Calcium(mmol/L)	2.663	0.01202	3	2.65	0.0493	3	1.91	0.858
Phosphorus(mmol/L)	1.387	0.1135	3	1.197	0.1081	3	0.63	0.292
Bicarbonate(mmol/L)	21	1.528	3	20.67	0.6667	3	15	>0.9999
Magnesium(mmol/L)	0.8433	0.03283	3	0.83	0.02	3	0.70	0.6
CK(U/L)	202.7	23.31	3	209.7	33.23	3	51	0.8715

Table A.2. Urinalysis findings of all six dogs (control #1, #2 and #5, and treatment #3, #4, and #6) in week -4.

Parameters	Control			Treatment		
	Dog#1	Dog#2	Dog#5	Dog#3	Dog#4	Dog#6
Colour	dark yellow	dark yellow	dark yellow	dark yellow	dark yellow	dark yellow
Urine specific gravity	slightly cloudy	slightly cloudy	moderately cloudy	moderate cloudy	moderately cloudy	slightly cloudy
pH	1.052	1.050	1.075	1.056	1.043	1.052
Glucose	8	6	6	6	6	7
Ketone	normal	normal	normal	normal	normal	normal
Bilirubin	negative	negative	negative	negative	negative	negative
Blood	2+	1+	2+	1+	2+	2+
Protein	negative	4+	4+	negative	negative	negative
Crystals	negative	negative	1+	negative	negative	1+
epithelial cells	moderate	struvite	scant	struvite	scant	struvite
RBC	struvite	scant	scant	struvite	scant	scant
WBC	struvite	scant	scant	struvite	scant	scant
casts	struvite	scant	scant	struvite	scant	scant
fat	struvite	scant	scant	struvite	scant	scant
other	struvite	scant	scant	struvite	scant	scant



Table A.3. Semen analysis (volume, motility, progressive motility and sperm concentration) for all dogs during the study. n/d=non determinable

Week		Control Group			Treatment Group		
		#1	#2	#5	#3	#4	#6
-4	Volume (mL)	1	0.2		0.5	2	
	Motility (%)	100	98		98	100	
	Progressive Motility (%)	76	80		66	82	
	Sperm Concentration (x10 <sup>6</sup> /mL)	68.4	965		287.4	94.9	
0	Volume (mL)						2.6
	Motility (%)						96
	Progressive Motility (%)						73
	Sperm Concentration (x10 <sup>6</sup> /mL)						125.7
4	Volume (mL)	5	1.75	4.3	2.8	11	2
	Motility (%)	90	90	60	90	95	75
	Progressive Motility (%)	85	80	50	85	90	70
	Sperm Concentration (x10 <sup>6</sup> /mL)	150	182.5	48.75	40	81.25	58.5
8	Volume (mL)	2.8	1.1	5.5	0.5	2	4.2
	Motility (%)	75	85	20	0	15	0
	Progressive Motility (%)	75	85	20	0	15	0
	Sperm Concentration (x10 <sup>6</sup> /mL)	155	107.5	100	12.5	140	8.75
12	Volume (mL)	8.6	7	11.6	1	7.9	8.8
	Motility (%)	45	80	80	n/d	95	n/d
	Progressive Motility (%)	40	75	75	n/d	90	n/d
	Sperm Concentration (x10 <sup>6</sup> /mL)	132.5	47.5	37.5	n/d	97.5	n/d
16	Volume (mL)	11.6	1.4	2.1	0.3	7.5	1.6
	Motility (%)	35	80	90	n/d	90	40
	Progressive Motility (%)	30	75	85	n/d	85	40
	Sperm Concentration (x10 <sup>6</sup> /mL)	105	617.5	197.5	n/d	40	5
20	Volume (mL)	10.7	5.4	8.3	2.7	4.4	11.4
	Motility (%)	75	75	95	n/d	80	10
	Progressive Motility (%)	70	70	90	n/d	75	10
	Sperm Concentration (x10 <sup>6</sup> /mL)	52.5	25	25	n/d	25	0.05
24	Volume (mL)	8.2	5.4	8.3	2.7	4.4	7
	Motility (%)	40	75	95	n/d	80	n/d
	Progressive Motility (%)	35	70	90	n/d	75	n/d
	Sperm Concentration (x10 <sup>6</sup> /mL)	62.5	25	25	n/d	25	n/d
28	Volume (mL)	3.2	6	6.3	5	8.5	8.2
	Motility (%)	60	80	20	n/d	50	n/d
	Progressive Motility (%)	55	75	10	n/d	45	n/d
	Sperm Concentration (x10 <sup>6</sup> /mL)	212.5	55	40	n/d	30	n/d
32	Volume (mL)	7.5	4.6	5.5	5.2	6.6	8
	Motility (%)	55	55	70	n/d	50	n/d
	Progressive Motility (%)	50	50	65	n/d	45	n/d
	Sperm Concentration (x10 <sup>6</sup> /mL)	62.5	37.5	42.5	n/d	n/d	n/d

Table A.4. Testis and epididymis weight (g) for both control and BPH induction groups

	Dog#	Testis + Epididymis (Weight)		Testis alone (Weight)		Epididymis alone (Weight)	
Control group	1	1) 18.1g	2) 18.7g	1) 13.6g	2) 13.7g	1) 4.5g	2) 5.0g
	2	1) 14.8g	2) 15.9g	1) 10.7g	2) 11.5g	1) 3.9g	2) 4.2g
	5	1) 13.3g	2) 14.2g	1) 10.6g	2) 11.6g	1) 2.8g	2) 2.6g
BPH induction group	3	1) 9.9g	2) 9.6g	1) 5.6g	2) 5.3g	1) 4.3g	2) 4.2g
	4	1) 5.9g	2) 7.3g	1) 3.2g	2) 4.1g	1) 2.7g	2) 3.2g
	6	1) 7.1g	2) 6.4g	1) 4.7g	2) 4.6g	1) 2.4g	2) 2.3g

Table A.5. DRE score (0-3) for all the six dogs during the study.

WEEK	CONTROL 1	CONTROL 2	TREATMENT	TREATMENT 4	CONTROL 5	TREATMENT 6
0	0	0	0	0	0	0
1	0	0	0	0	0	0
2	0	0	0	0	0	0
3	0	0	0	0	0	0
4	0	0	0	0	0	0
5	0	0	1	0	0	1
6	0	0	1	1	0	1
7	0	0	1	1	0	1
8	0	0	1	1	0	1
9	0	0	1	1	0	1
10	0	0	1	1	0	1
11	0	0	1	1	0	1
12	0	0	1	1	0	1
13	0	0	1	1	0	1
14	0	0	1	1	0	1
15	0	0	1	1	0	1
16	0	0	1	1	0	1
17	0	0	1	1	0	1
18	0	0	1	1	0	1
19	0	0	1	1	0	1
20	0	0	1	1	0	1
21	0	0	1	1	0	1
22	0	0	1	1	0	1
23	0	0	1	1	0	1
24	0	0	1	1	0	1
25	0	0	1	1	1	1
26	1	0	1	2	1	1
27	1	1	1	2	1	1
28	1	1	2	2	1	1
29	1	1	2	2	1	1
30	1	1	2	2	1	1
31	1	1	2	2	1	1
32	1	1	2	2	1	1
33	1	1	2	2	1	1
34	1	1	2	2	1	1
35	1	1	2	2	1	1

## Canine Prostate Slicing Manual for Histology

- 1) Place prostate in cylinder container (figure 7.1) and fill it with gelatin in the previous day. After gelatin is solidified, remove the set gelatin and prostate carefully from the container (figure 7.2).



Figure A.1. Cylinder container



Figure A.2. Prostate inside gelatin.

- 2) In the prostate slicer, place the yellow dividers in each indicating position that is 3mm between one divider and the next, and also is the place to be sliced. Place parafilm surrounding the internal part of the slicer to avoid that gelatin leaks (figure A.3).

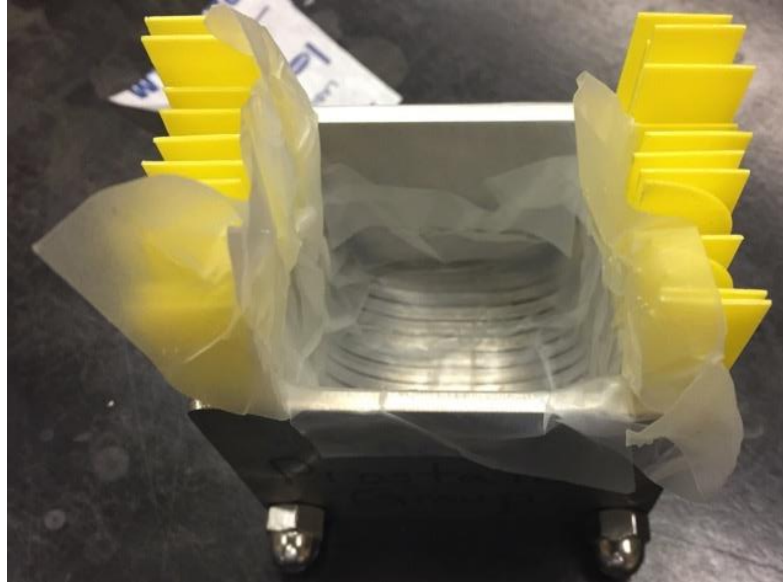


Figure A.3. Yellow dividers and parafilm placed in the slicer.

- 3) Place the set prostate and gelatin in the slicer with the ventral side down and fill it with gelatin until the prostate is completely covered (figure A.4).

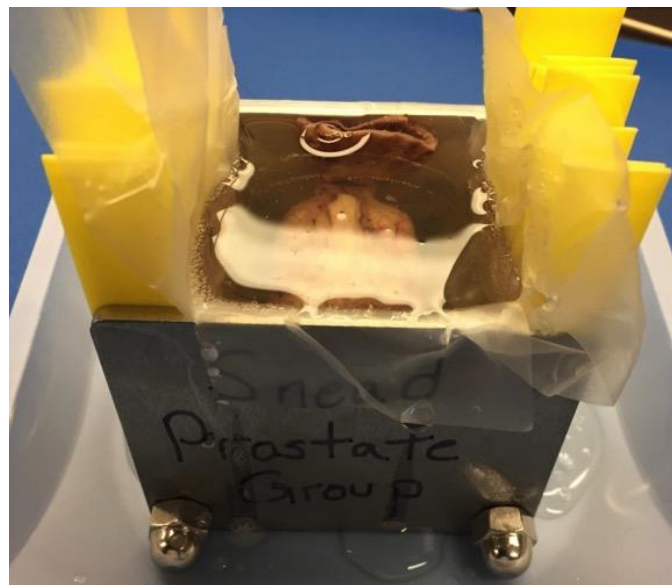


Figure A.4. Prostate in the slicer filled with gelatin

- 4) Slice prostates where the yellow dividers are placed using a 13cm microtome blade attached to the holder device designed for this purpose (figures A.5 and A.6).



Figure A.5. Microtome blade attached to the holder device.

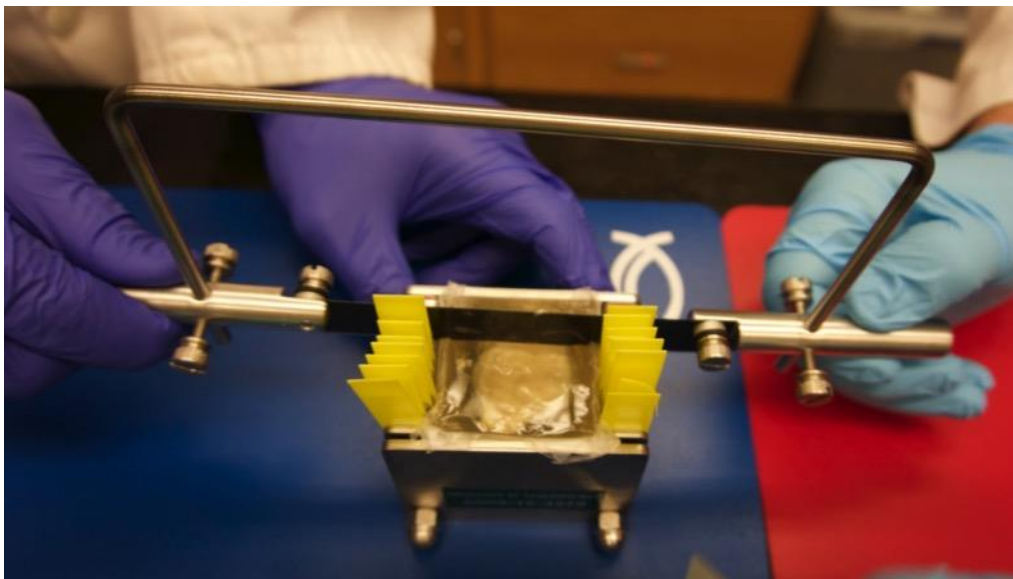


Figure A.6. Slicing prostate in the specified spacing (yellow dividers).

- 1) Once finished slicing, remove entire prostate and gelatin as a block and peel off parafilm. Ink gelatin block for orientation purposes (red color on right side, blue on dorsal) (figure A.7).

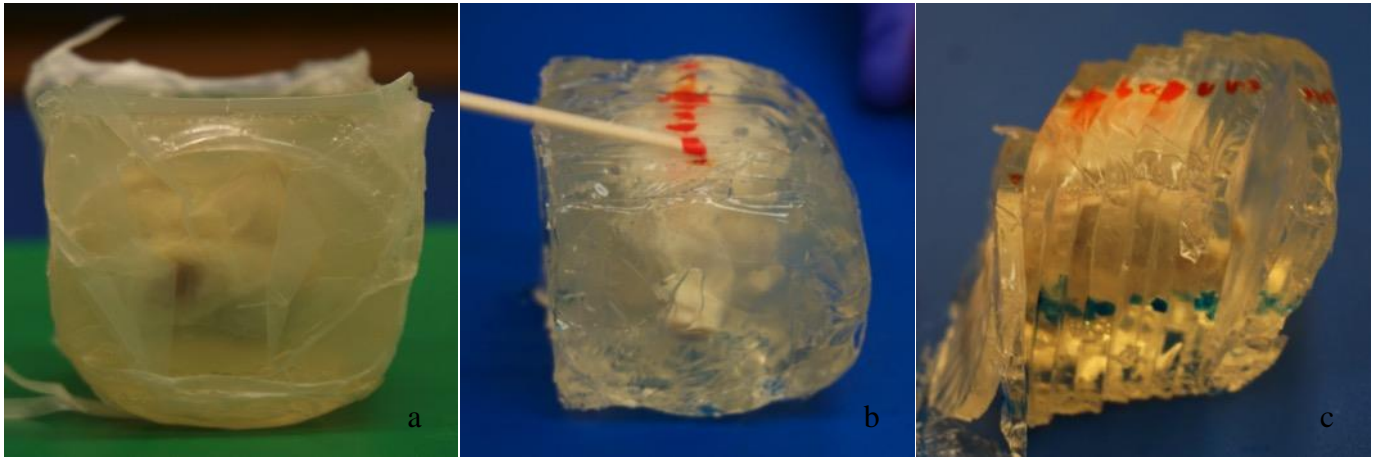


Figure A.7. Series of three images showing (a) the prostate, gelatin and parafilm removed as a block from the slicer, (b) inking the right part with red ink, (c) ink applied for orientation purposes: red on right and blue on dorsal.

- 2) Keep gelatin and place slices on paper following the sequence: starting at slice # 1 (most cranial) until last slice (most caudal). The slices must be with the caudal side facing up, dorsal at top and right side facing right (figure A.8). Cut a small incision along the right side for orientation (notch: 2-3mm deep) (figure A.9).

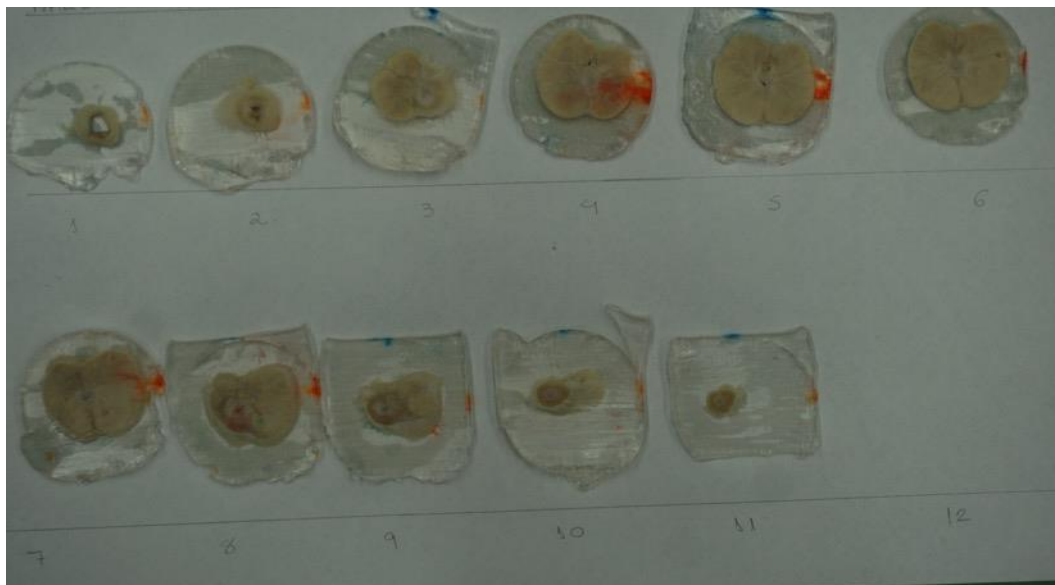


Figure A.8. Slices of prostate and gelatin inked and numbered.



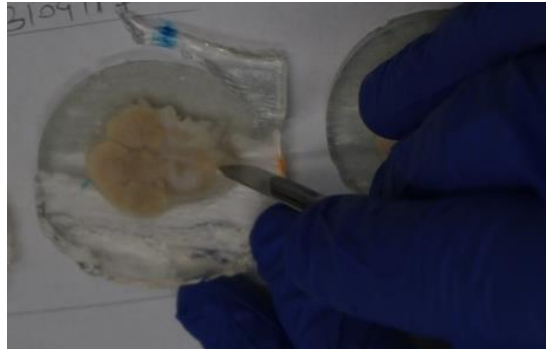


Figure A.9. Applying notch on the right side of the prostate

- 3) Trim gelatin close to tissue. Pat slice dry before re-ink. Re-Ink the right side red and dorsal side with blue on the caudal face of the slice (non-cutting face). Make sure bottom of slice (cranial side) does not get any ink. (figure A.10)

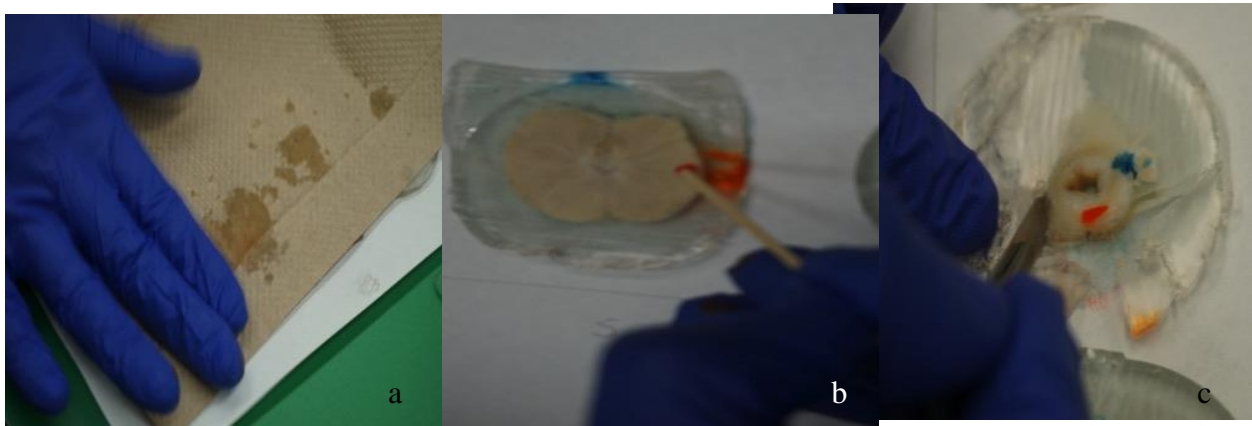


Figure A.10. a) pat drying gently with paper towel; b) re-inking the prostate tissue; c) trimming excess of gelatine

- 4) Measure the thickness of slices with electronic digital calliper (Star Asia USA, LLC d.b.a Titan, Seattle, Washington, USA) (figure A.11). Also, measure and record the distance of reference point from caudal side of slice1 (same as cranial side of slice2).

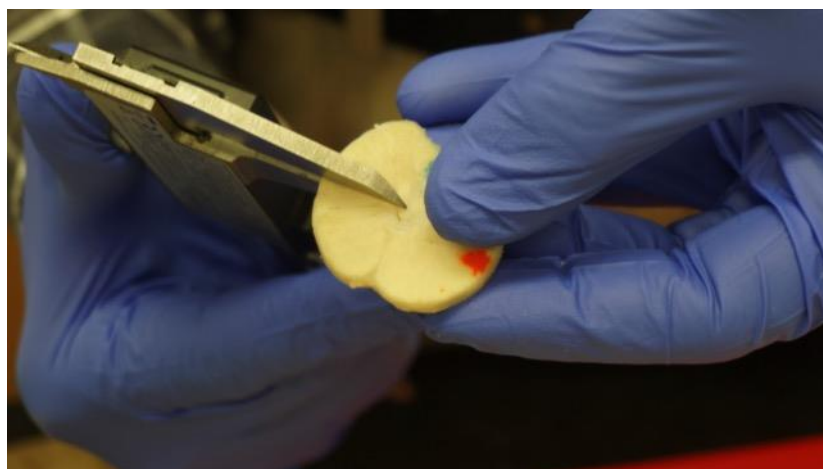


Figure A.11. Measuring thickness of prostate slice (dorsal, left, ventral and right side resulting in a mean value) with electronic digital caliper

- 5) Place the sliced prostate in labeled cassettes (write name and number of dog with pencil): caudal side up the ink side facing up (i.e non cutting side) (figure A.12)



Figure A.12. Cassette labeled with dog name and number of slice

### Excised prostate glands



Figure A.13 Excised prostate glands attached to urinary bladder in control dogs (#1, 2 and 5). Ventral (a) and dorsal (b) views.



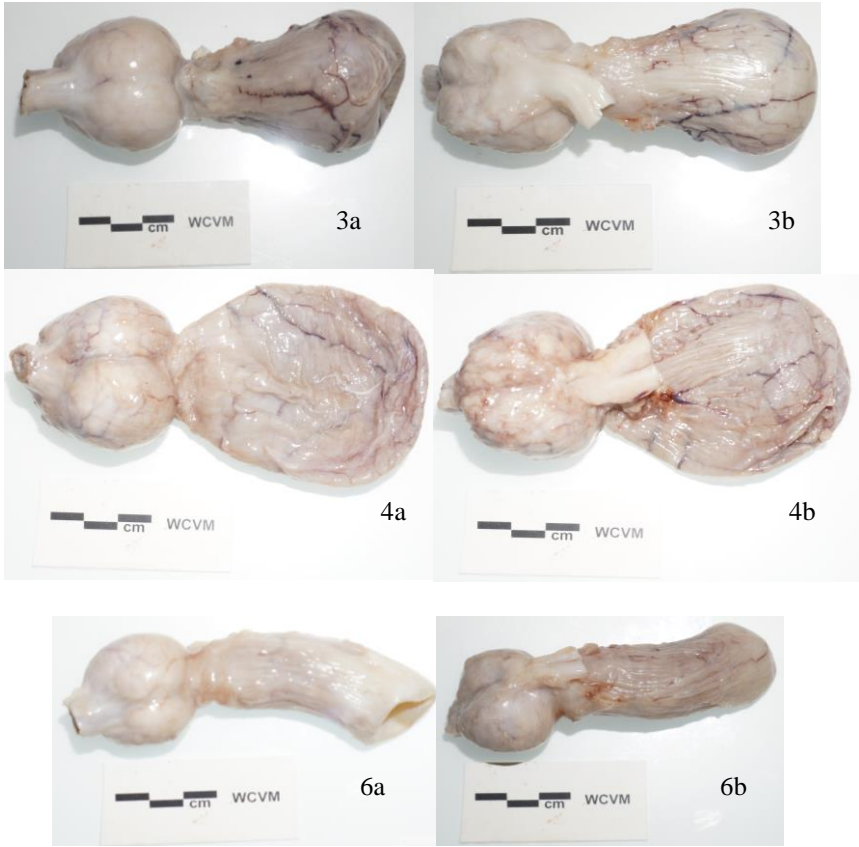


Figure A.14. Excised prostate glands attached to urinary bladder in BPH induction dogs (#3, 4 and 6). Ventral (a) and dorsal (b) views.

***In vivo* Imaging Comparison**

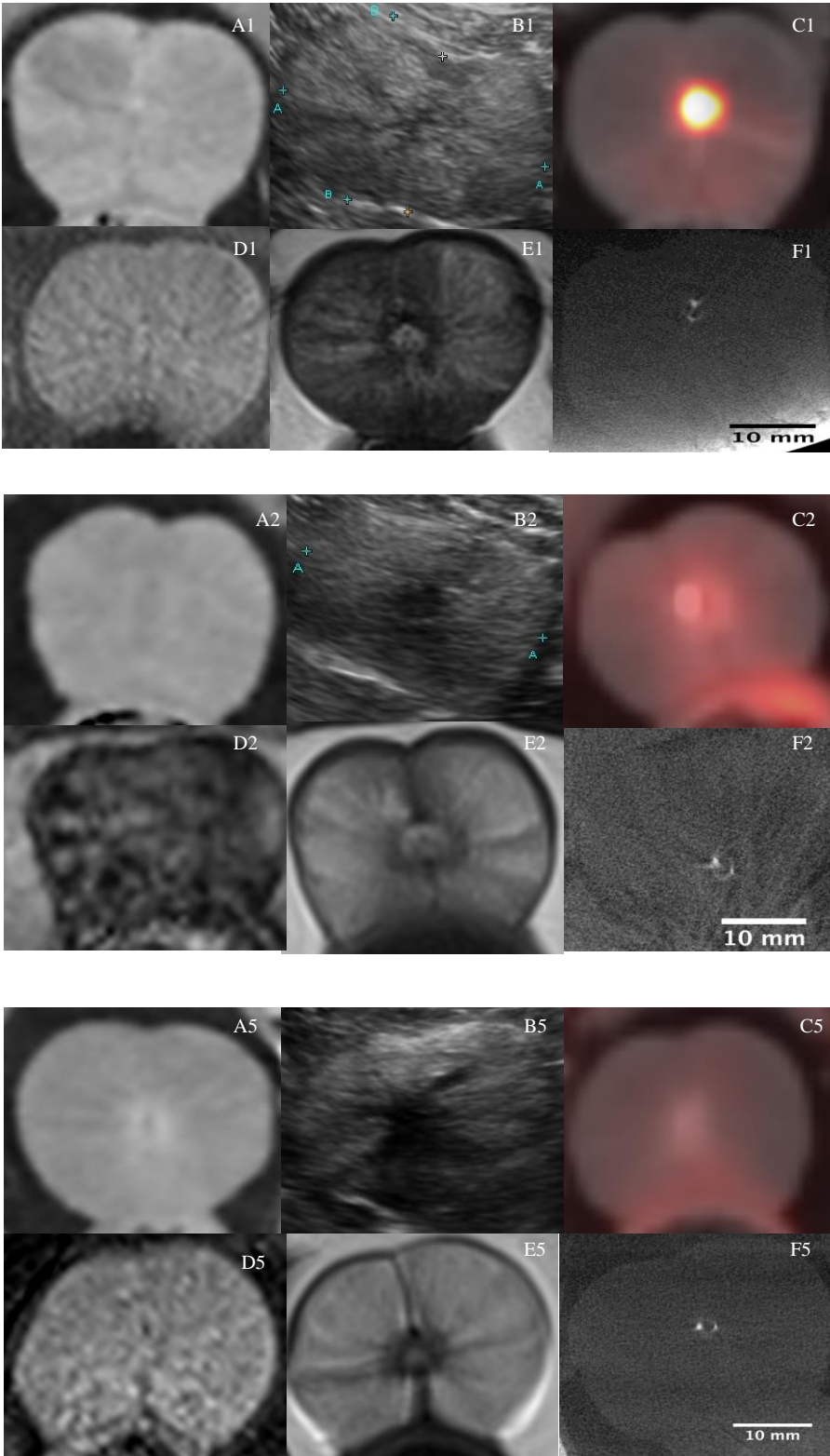


Figure A.15 *In situ* axial images of the prostate of control dogs #1, 2 and 5 taken with different imaging modalities: A) CT, B) US, C) PET-CT, D) MRI-T1, E) MRI-T2, F) PC-CT.

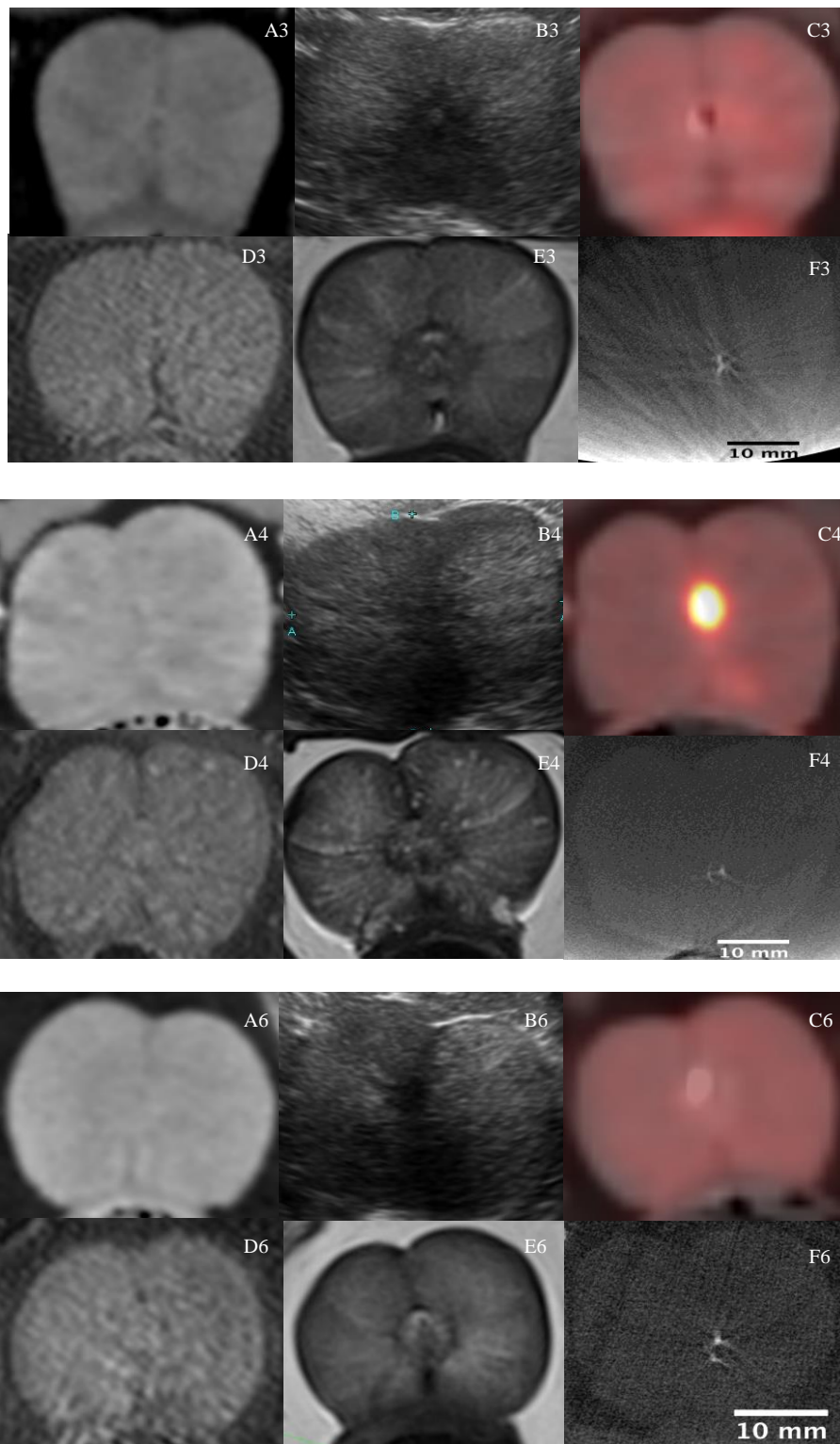


Figure A.16 *In situ* axial images of the prostate of treatment dogs #3, 4 and 6 taken with different imaging modalities: A) CT, B) US, C) PET-CT, D) MRI-T1, E) MRI-T2, F) PC-CT.

## **X-TRACT USER MANUAL**

How to reconstruct In-Line Propagation Based Phase Contrast – Computed Tomographic  
images

V.1.0

Jay Keith  
26<sup>th</sup> May 2016

---

This is a brief tutorial on how to use X-TRACT to reconstruct data collected at the Canadian Light Source, Biomedical Imaging and Therapy beamline. Phase-Contrast CT imaging has many benefits over conventional CT imaging. X-TRACT is designed to use these benefits to create a reconstruction with more contrast and improve overall image quality.

I have one important note before you start regarding phase extraction and X-TRACT:

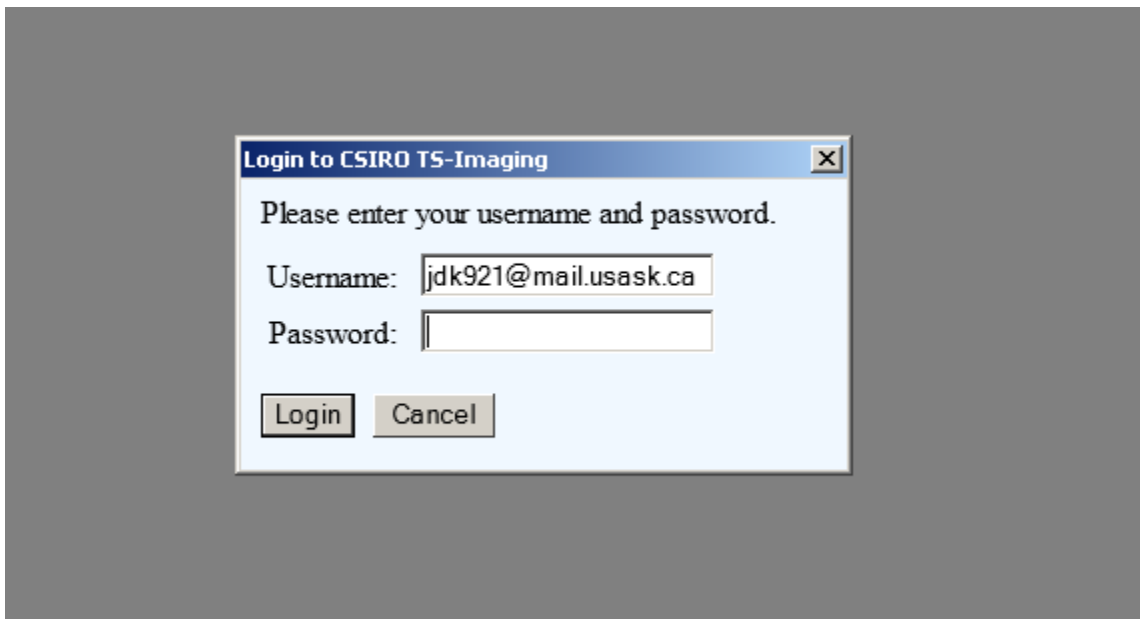
**If you do not plan on using Phase Extraction in the preprocessing part of the reconstruction, use a different program all-together. Phase extraction is the only benefit of X-TRACT, there are easier and better programs to use if you only want to do simple reconstructions. I suggest NRecon.**

In order to use X-TRACT, a license must be acquired from CSIRO, the company that created and licenses' the software. [This link](#) will allow you to create an account through CSIRO, although I have not had the best luck with them fully completing the registration process. You can contact Darren Thompson directly, an IT Advisor at CSIRO to activate your account. Darren's info is shown below:

Darren Thompson  
IT Advisor | Scientific Computing  
Information Management and  
Technology CSIRO  
+61 3 9518 5940  
[Darren.thompson@csiro.au](mailto:Darren.thompson@csiro.au)

Let him know that you are a researcher, and want to use X-TRACT from research purposes when contacting him. If the program is not downloaded you will need to [log onto](#) the CSIRO website, and enter your email and password you previously created.

When X-TRACT is started the program will prompt you to enter your username and password:



Either enter your new username and password, or you can use mine until December 27<sup>th</sup>, 2017. My username and password are:

Username: [jdk921@mail.usask.ca](mailto:jdk921@mail.usask.ca)  
Password: Aa25802580

After a valid username and password are entered, X-TRACT will allow you to use it.

---

There are two main parts to CT reconstruction using X-TRACT.

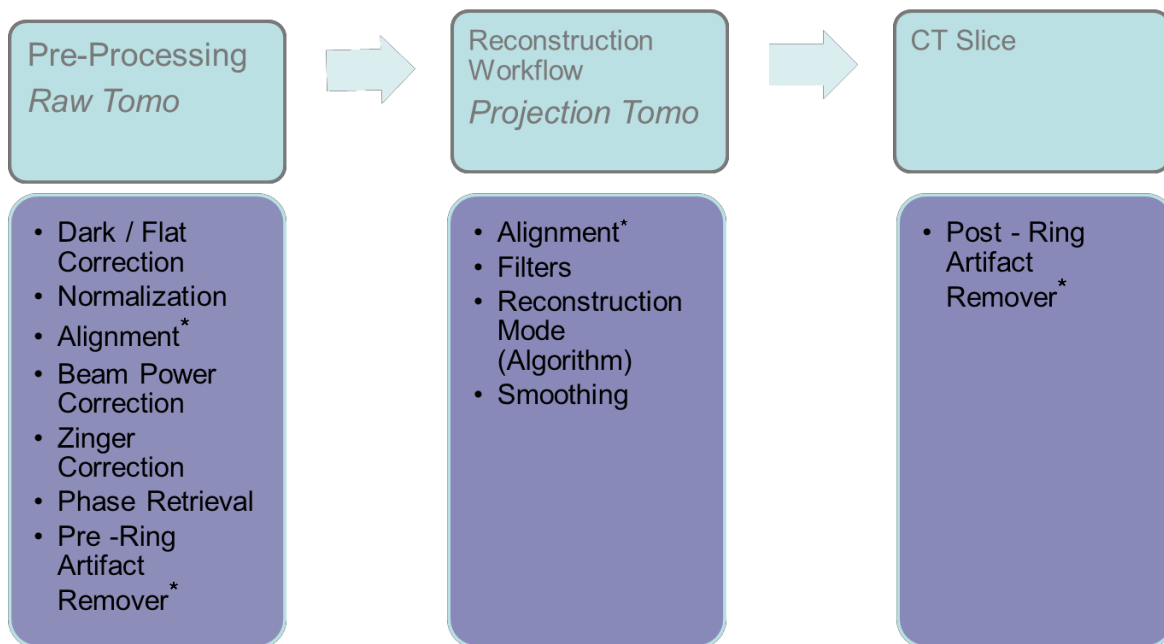
\*Preprocessing data (PRE)

\*Ct Reconstruction (REC)

A third step of post-Ring artefact remover can be performed in MATLAB. This step will not be discussed in this manual (at least not yet).

Both PRE and REC have multiple variable inputs that need to be finely tuned in order to get the best possible reconstruction. Unfortunately, a bit of trial and error is needed with X-TRACT. I will give you hints and tips, but ultimately you may need to run several trials on each data set before a reconstruction of sufficient quality is generated. By trials I mean comparing between different inputs of the same variable to see which one produces the “best” image. E.g. changing the phase extraction parameter delta/beta from 500 to 1000 and comparing which is better.

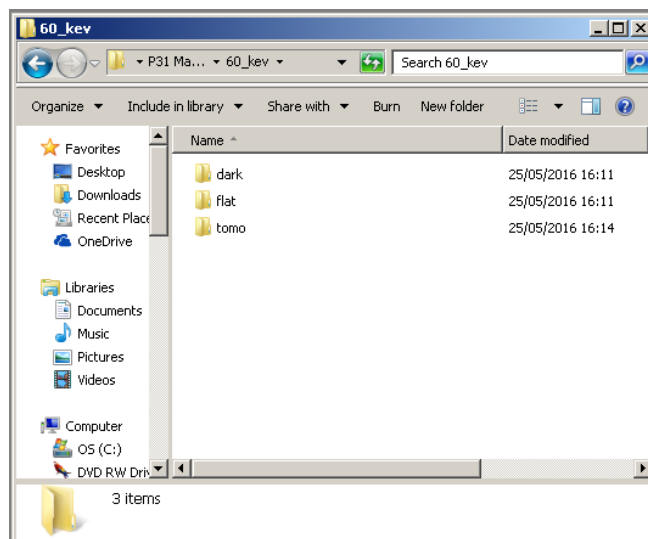
I will go into further detail on PRE and REC later, I just want to give you a generalized view of the workflow of X-TRACT, from raw data all the way through to final CT reconstruction.



\*- Found in both PRE and REC stages

You will begin with “raw” tomographs, which are the projection images generated by some detector at the CLS. These images should be saved as .TIF. In general, X-TRACT does not care what the file name of the images are, as long as they are number appropriately (e.g. Image\_0001 is appropriate, SampleX\_0001 is acceptable, but SampleX\_1 is not appropriate. Number padding is needed for all data sets).

The arrangement of your raw data is important. Put all the flat projection images into a folder, all the dark images into a folder and all the tomo’s into a folder. An example is shown below:



You are now ready to begin PRE

## Preprocessing

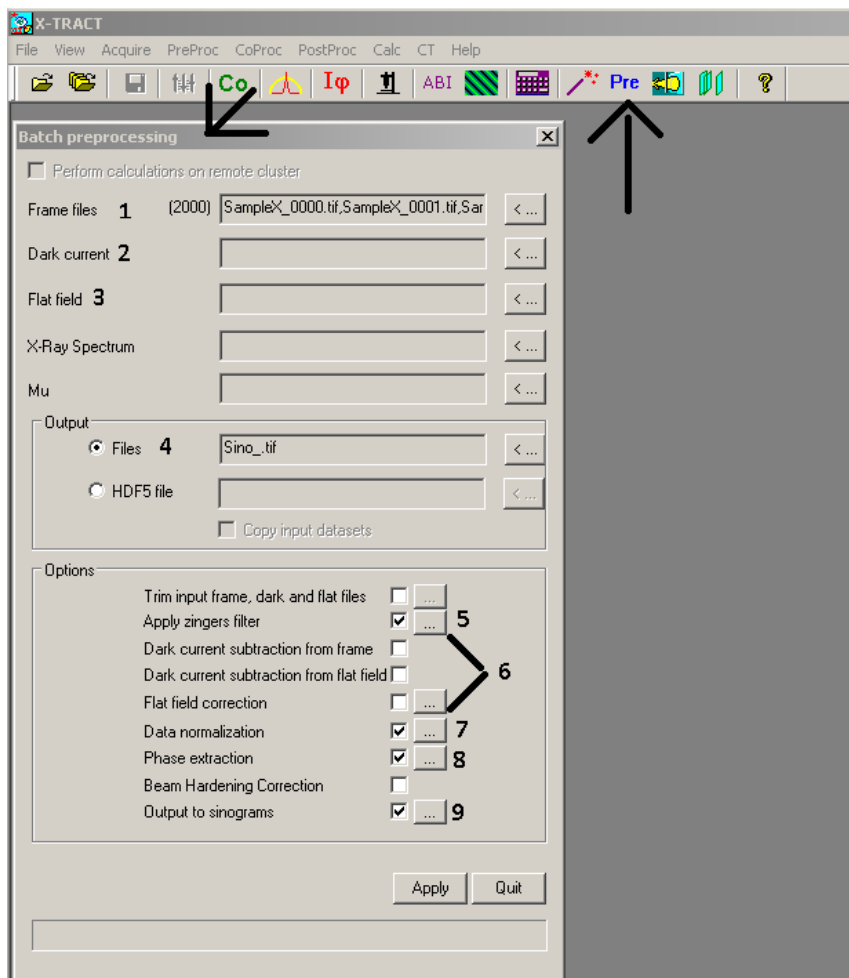
I have copied and pasted X-TRACT's help manual info on PRE in PRE Background (found below). It contains valuable information about why each step in the process is performed. PRE Background should be collapsed by default. (click the  $\diamond$  beside PRE Background to open/close the text). **The objective of the PRE is to process the raw tomo's into sinograms.** Sinograms are used in the REC part of X-TRACT. An example of a sinogram is found at the bottom of the PRE Background tab.

**I have summarized the steps in PRE Summary, found after PRE Background.**

## PRE Background

### PRE summary

To open the Preprocessing tab, click the blue "Pre" button found in the top bar in X-TRACT. Once clicked, a window called Batch Preprocessing should open:






**There are 9 important variables in this window**, labelled conveniently above. Things that are not labelled should not be used in this workflow, and therefore are not explained.


**\*\*\*\*\*Important Note\*\*\*\*\***

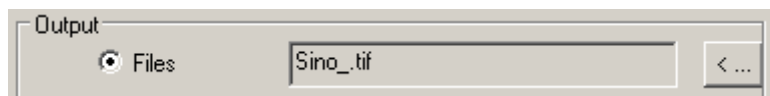
This manual assumes that you have **not** done anything to the raw tomo's, including using the ImageJ plugin for CT processing. If you have already used the Micro-CT processing ImageJ plugin and generated SampleX\_.tifs, in step #1 use the corrected SampleX tomo's instead.


1. **Frame Files:** This is where the raw tomo's go (or corrected SampleX\_.tifs). Click the 1<sup>st</sup>  button to the right of the Frame Files. This displays a new window titled "Select Projection Files". Navigate into where you tomo files are, then **make sure to select every tomo** before clicking open. (Click on a single .tif and press Ctrl + A to select all the tomo's in the folder). Once all the tomo's are selected, press the open button.

The number beside the "Sample X\_0001.tif" in the above figure shows how many files are open, double check to make sure this number is appropriate.

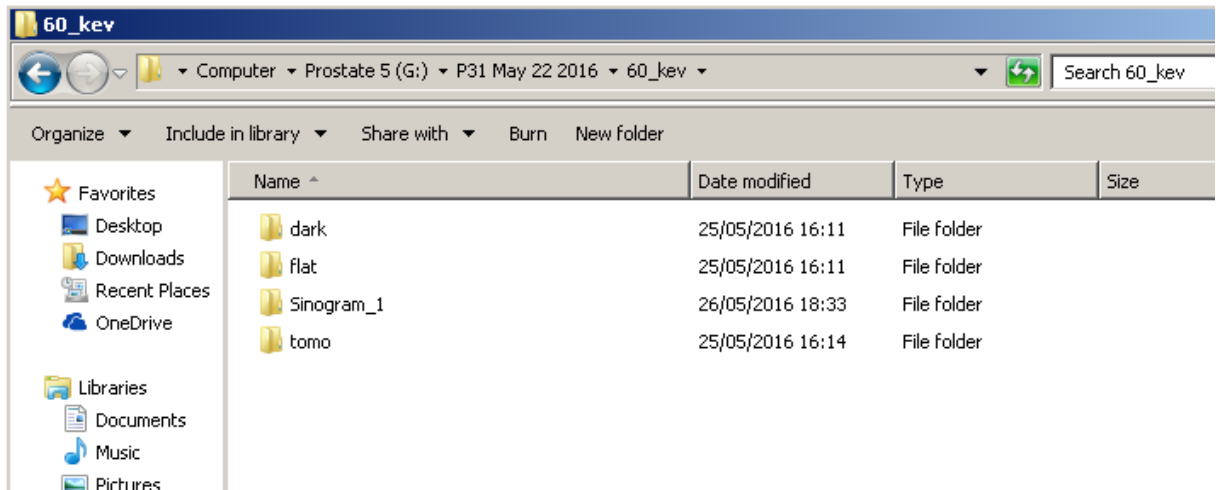
**\*\*Steps 2 and 3 should only be done if using raw tomo's\*\***

2. **Dark Current:** Just a fancy way of saying dark field. Click the 2<sup>nd</sup>  to the right of dark current. Do the same thing as above for frame files, just selecting all the darks instead. Again, make sure all the darks are selected before pressing open.
3. **Flat field:** This is where the flats go. Same as #1 and #2, just select all the flats.
4. **This is the output section.** Make sure Files is selected:




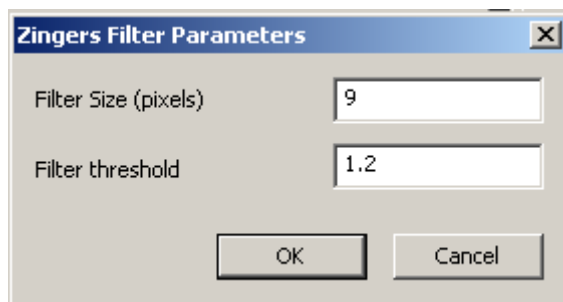
and use the  to select a folder where the sinograms will be saved. Create a new folder, and I usually name this folder Sino\_1. See below:





Make sure to name the files “Sino\_.tif” and that the save as type is .tiff.

5. **Apply Zingers Filter:** Zingers are isolated pixels or small clusters of pixels in which the signal is much higher than that in the surrounding part of the image, Zingers are typically caused by high-energy photons (or cosmic rays) hitting the detector. Clicking  opens a dialogue box called Zingers Filter Parameters:



**Filter size** is the number of pixels used to assess the local intensity of a pixel, and **the filter threshold** is the multiple of the local intensity needed for a pixel to be classified as a zinger. If a zinger is found it is replaced by an interpolation of the surrounding pixels. The values seen above are usually adequate.


**\*\*\*\*\*Boxes in Step 6 should only be checked if using raw tomo’s\*\*\*\*\***


6. **Dark current subtraction from frame, dark current subtraction from flat and flat field correction:** These three parameters revolve around the flat-dark image correction formula:

$$C = I_0 - D / F - D$$

Where  $C$  is the corrected tomo,  $I_0$  is the raw tomo (Image original),  $D$  is the dark field, and  $F$  is the flat field.

Checking the first box (**Dark current subtraction from frame**) allows for the numerator in the above equation, and checking the second box (**Dark current subtraction from flat field**) allows for the denominator in the above equation. The third box (**Flat field correction**) allows the above equation to be performed on the input frame files (i.e. the raw tomo's).

The flat field correction  opens a window called flat field options. Only flat field method should be selected, **not thresholded median filter**. Make sure Average all flats are selected and press okay.


7. **Data Normalization:** This step applies a  $-\text{Log}$  to the input files, which is an essential step in the preprocessing workflow. It is required for absorption images to be processed correctly, and should always be selected. Clicking the  opens a window called image normalization parameters. The Region normalisation box should **not** be selected, as it is only for specific data sets that this variable will work correctly. You can read about it more in the PRE Background if you wish.

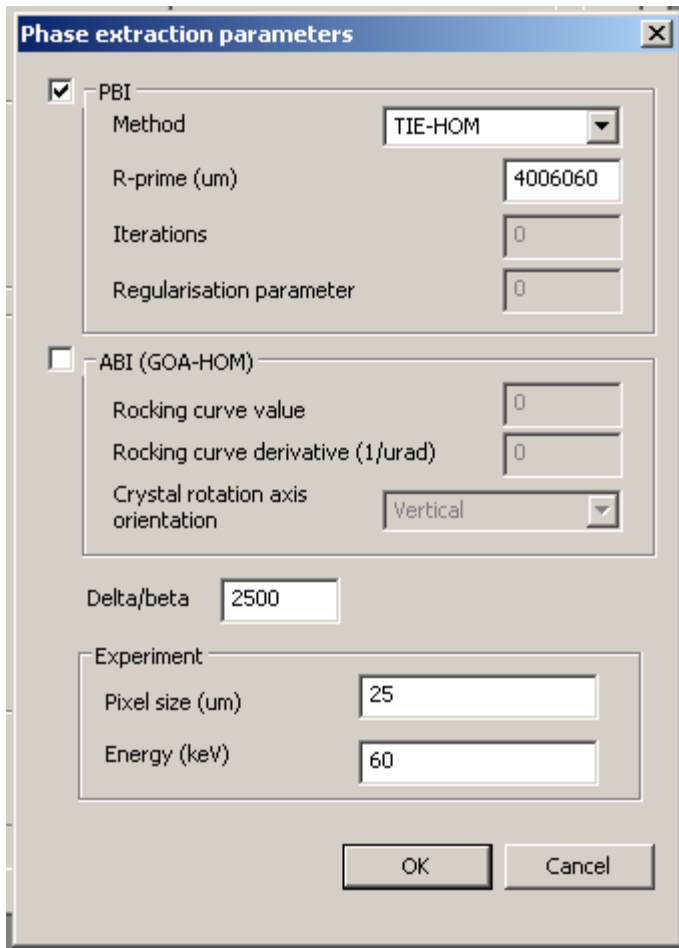
**The -logarithm box should always be selected.** If the data is noisy (which, with dogs it usually is) a  $3 \times 3$  filter can be applied. This smooths some of the noise out of the dataset, but as a rule of thumb, any object smaller than  $3 \times$  the pixel size is lost. (e.g. if the pixel size is 25 microns, no object smaller than 75 microns can be seen in the reconstruction).

8. **Phase extraction:**

**If you do not use this parameter, use a different program all-together to do the reconstructions. Phase extraction is the only benefit of X-TRACT, there are easier and better programs to use if you only want to do simple reconstructions.**

check the phase extraction box in order to include phase-retrieval in the list of preprocessing operations to be applied to input images. Unfortunately, Phase extraction is not very easy to use, and can seem quite daunting at first. It sometimes requires trial and error to get right. **Yet this is the main reason why we use X-TRACT, so you will eventually need to figure it out.**

Clicking the  button opens a new window called Phase extraction parameters, shown below:



PBI stands for propagation based imaging, which is how the PC-CT imaging is done at BMIT. ABI stands for Analyser based imaging, which is more like DEI or grating based imaging, neither of which I have ever used before so if you need to switch to them good luck! There are two different phase retrieval algorithms that X-TRACT can use, TIE-HOM and Born Iterative. TIE-HOM stands for Transport-Of-Intensity - homogenous, more information can be found at the end if wanted under *TIE-HOM*.

- a) TIE-HOM is the easiest to use of the two algorithms, and I do not have a lot of experience with the Born Iterative algorithm, but I will try to provide at least a little information on the latter.

The R-prime is the effective propagation distance in microns of the x-ray beam. It is equal to:

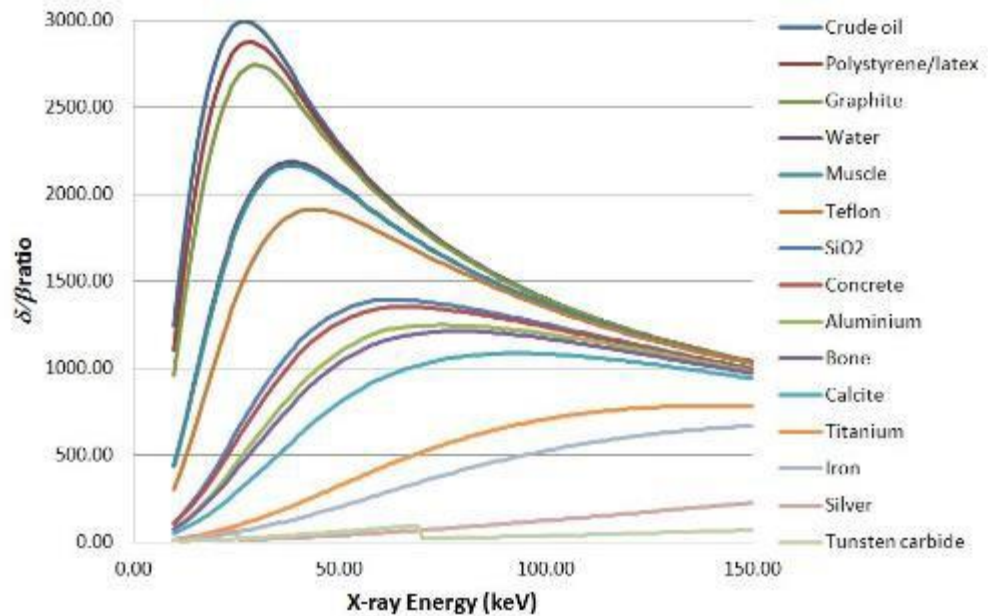
$$R' = R_1 R_2 / R_1 + R_2$$

Where  $R_1$  is equal to the source to sample distance, and  $R_2$  is equal to sample to detector distance. **Therefore, for the BMIT-ID line,  $R'$  is equal to 4006060 microns**

( $R_1 = 55\text{m}$ ,  $R_2 = \sim 5\text{m}$ )

If you are only using the TIE-HOM algorithm, then you can skip the part b).

- b) If you are using the born iterative algorithm, first of all good luck. Information can be found after the TIE-HOM section found at the end. **The number of iterations is typically between 1-4.** I once put 25 into this section and it crashed the program so please stick with those values. **Regularization parameter has a typical value between 6-10,** depending on the noise of the tomo's. For noisy tomo's (which are typical for us) use a value of 10, for less noisy images use 6.
- c) The delta/beta ratio. Lord help us, this is a tricky number to guess sometimes. Luckily, there is this handy graph to make our lives easier.




This graphs the relationship between the monochromatic x-ray energy of the beam and the appropriate delta/beta ratio for different materials. Most important to us is water, muscle, and bone, shown in the graph as purple, blue, and a slightly different shade of purple, respectively. Notice that water and muscle are very similar, while bone is somewhere between aluminium and calcite. Different delta/beta ratios will emphasise different signals in the final reconstruction. If the reconstruction looks overly-smooth, try reducing the delta/beta ratio, and if lots of edge-enhancement is still apparent, try increasing it.

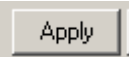
- d) Finally, in the experiment box, insert the pixel size of the detector (or the apparent pixel size) and the energy of the beam used to collect the data.

*TIE-Hom*  
*Born Iterative*

## 9. Output to sinograms:

This box needs to be checked in order to generate the sinograms needed for REC. Pressing  the button opens a new window called sinogram parameters. Here you can enable ring artefact remover by clicking the box. There is also an input for filter size (in pixels). It should be an odd number. The higher the number, the more rings will be smoothed out. 1 is no ring removed, 17 is quite a large amount of smoothing, and beyond that is not usually recommended. If there is a large amount of rings in the reconstructions, I would suggest using a low filter size (e.g. 3) and doing post-processing ring remover with MATLAB.

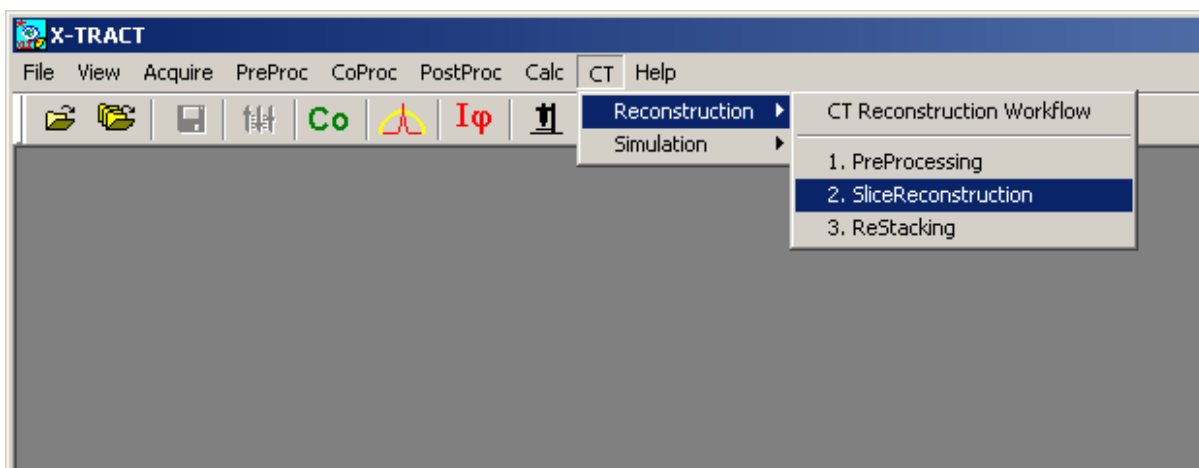
You are now ready to press the Apply button at the bottom of the batch processing window. This will generate a sinogram for each pixel height of your tomographs. I.e. if your input tomograph dimensions are 4000x250 pixels, 250 sinograms will be generated and saved in the file you selected back in step 4.

10. Press  at the bottom of the batch preprocessing. The status bar at the bottom of the window will show the progress of the program, though it doesn't always work perfectly.

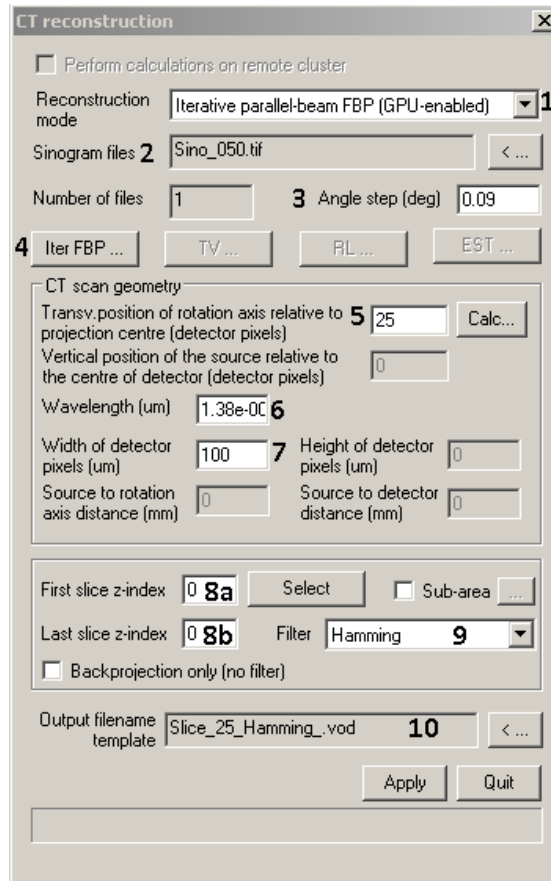
This process may take between 10 minutes and one hour, depending on size of data and capabilities of the computer processor. One complete, move onto the REC processing stage of X-TRACT.

## REC Processing

The REC processing converts sinograms made in the PRE stage into reconstructed CT slices. To access the REC workflow window, Click the *CT* drop-down menu near the top left of X-TRACT, Click *Reconstruction* from the list, then select *2. SliceReconstruction*.



Clicking this will open the CT reconstruction workflow window.



1. **Reconstruction Mode** - There are 10 different reconstruction modes to choose from.

- FBP parallel-beam (GPU-enabled)
- Cylindrical FBP parallel-beam
- TJD-FDK cone-beam (GPU-enabled)
- YL-FDK fast cone-beam (high RAM)
- Cylindrical FDK fast cone-beam (high RAM)
- Iterative parallel-beam FBP (GPU-enabled)
- Iterative parallel-beam TV (GPU-enabled)
- Iterative parallel-beam RL (GPU-enabled)
- Gridrec
- EST

**FBP (Filtered Backprojection) Parallel-beam (GPU-enabled)** is the “bread and butter” of CT reconstructions, and should be most commonly selected.

**Cylindrical FBP** is not useful

**TJD-FDK cone-beam** is not useful

**YL-FDK fast cone-beam** is not useful

**Cylindrical FDK fast cone beam** is not useful

**All three Iterative parallel-beam** are a different type of reconstruction mode, and can be used if desired.

**Gridic and EST** are not useful.

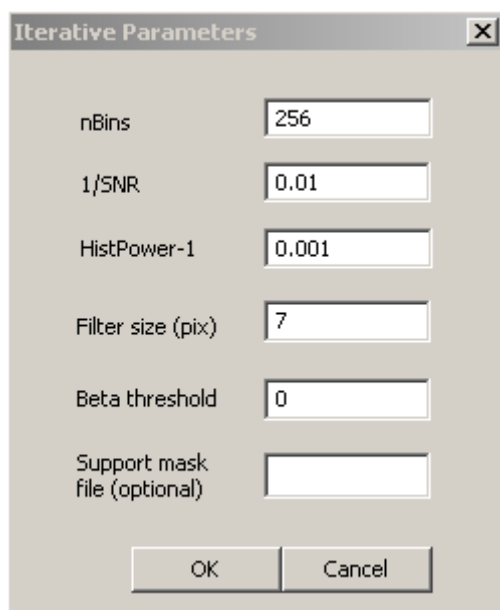
**Iterative parallel-beam FBP** is the easiest of the three different Iterative approaches for reconstructions. Either this or **FBP Parallel-beam** should be selected from this list.

Choosing either will not change the workflow dramatically, **except for STEP 4**. Selecting **Iterative parallel-beam FBP** as the reconstruction mode will enable step 4. **FBP Parallel- beam** does not require step 4, and the “Iter FBP” box will be unselectable if this mode is selected.

The difference between these two reconstruction modes:

<b>FBP Parallel-beam (GPU-enabled)</b>	<b>Iterative parallel-beam FBP (GPU-</b>
A straightforward implementation of the filtered back-projection algorithm for tomographic reconstruction of parallel-beam data. This is quite slow, but has been very well tested, and so can be used to check the results of other algorithms if desired.	An iterative version of the FBP parallel-beam algorithm that involves multiple cycles of CT reconstruction and re-projection, enforcing certain constraints, (such as positivity and a finite number of distinct levels (“bins”) in the reconstructed data, at each iteration.

2. **Sinogram files:** The series of sinogram files to be used for the *CT reconstruction* is selected using the "< ..." button next to the *Sinogram files* text box. All sinograms in the series must be selected. These were just created in the PRE stage of the manual.
3. **Angle step:** this is the angular increment between orientations, also in degrees. If the Angle step is incorrect the resultant reconstruction will be distorted. Simply calculated by taking the total number of projections captured and dividing by 180°.
4. **Iter FBP:** This button is only enabled if the **Iterative parallel beam** reconstruction algorithm is selected. This algorithm is used when there is a known and limited number of different material in the object being reconstructed. Clicking the button opens the following window:



**nBins** - The number of non-empty bins (distinct “grey” levels) in a histogram of the reconstructed slice (this number should be equal or larger than the a priori known number of different materials in the samples). Recommended values are 256 or 512, but any positive integer is acceptable in principle.

**1/SNR** - This is the average noise-to-signal ratio in the experimental CT projections (e.g. 0.05 for 5% noise).

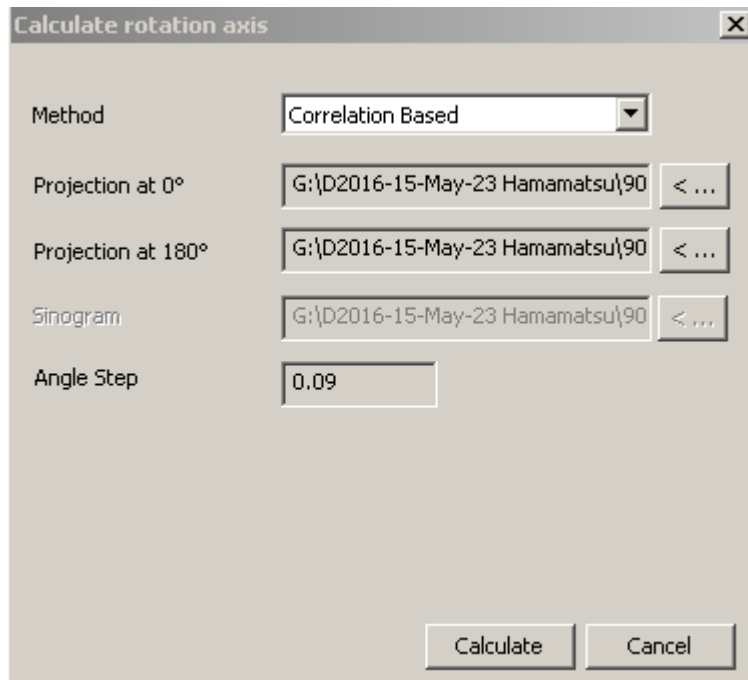
**HistPower-1** - This is a real value, typically from the interval (0, 1], that corresponds to the power (minus 1) to which the histogram values are raised at each iteration in order to “promote the peaks”.

**Filter size (pix)** The manual doesn’t discuss this value. I assume it is a smoothing filter, but do not know for sure. Would suggest a value of 7.

**Beta threshold** no idea what this mean, would recommend leaving at 0 or trying increments of 200.

**Support mask file** leave empty

5. **Transverse position of rotation axis relative to projection centre (detector pixels)** - this value is critical for the reconstruction. If this value is incorrect point features will appear as semi-circles or circles (depending on whether the scan was 180 or 360 degrees). The "**Calc ...**" button can be used to open the **Calculate rotation axis** dialog to calculate this value.



There are three methods to choose from: Correlation based, Error Based, and Sinogram based. Correlation based and Error based both require a projection at 0° and 180°. Therefore, click the "< ..." button next to projection at 0° and select the first projection image (Flat-Dark corrected with ImageJ works best). Click the "<..." button next to projection at 180° and select the last projection image.



Sinogram based requires a sinogram, use the middle one of the data created. Once you have entered in the correct images, press the calculate button.

This will produce a new value in the box beside the Calc button. It may or may not be accurate, depending on if there was a large amount of slumping with the dog. The more slumping, the more inaccurate the value will be. There is no real way around this (besides preventing slumping in the first place).

6. **Wavelength (um)** - The x-ray wavelength in microns. Easily calculated by dividing 1.24 by the photon energy in eV. (i.e.  $1.24/60\ 000\ \text{eV} = 2.06\text{e-}5$ )

7. **Width of detector pixels (um)** – how big are the pixels?

8. a/b - **First slice z-index** and **Last slice z-index** allow the user to calculate a limited range of slices. This is particularly helpful when doing preliminary calculations to optimize conditions. Slices are numbered from 0 at the top of the reconstructed volume (or sample) increasing downwards. Basically First slice should be 0 and last slice should be 1- total number of sinograms selected in step 2.

9. **Filter:** Select one the available standard filters for CT reconstruction. Linear-Ramp or Shepp-Logan are both usually suitable for most CT data). Leave Backproject only (no filter) unchecked always.

10. **Output basename:** the browse button activates a file dialog box used to define the destination directory and the filename prefix for the series of slice files.

PRESS APPLY this button is used to start the tomographic reconstruction process.

I would recommend only selecting one sinogram to reconstruct during the REC stage, because it will allow you to see if the values you selected in 1-10 are accurate. There is a troubleshooter in the X-tract help which goes through what values to change if the reconstructions come out poor.

## REFERENCES

- Acher, P., & Dooldeniya, M. (2013). Prostate biopsy: Will transperineal replace transrectal? *BJU International*, 112(5), 533-534. <https://doi-org.cyber.usask.ca/10.1111/bju.12299>
- Aichinger, H., Dierker, J., Joite-Barfuß, S., Säbel, M. (2012). *Radiation Exposure and Image Quality in X-Ray Diagnostic Radiology Physical Principles and Clinical Applications* (2nd ed.). Berlin, HDB: Springer. DOI 10.1007/978-3-642-11241-6
- Ajayi, A. & Abraham, K. (2018). Understanding the role of estrogen in the development of benign prostatic hyperplasia. *African Journal of Urology*, 24(2), 93-97. <https://doi.org/10.1016/j.afju.2018.01.005>
- Alcaraz, A., Hammerer, P., Tubaro, A., Schröder, F., & Castro, R. (2009). Is there evidence of a relationship between benign prostatic hyperplasia and prostate cancer? Findings of a literature review. *European Urology*, 55(4), 864-875. <https://doi.org/10.1016/j.eururo.2008.11.011>
- Amann, RP (1986) Reproductive physiology and endocrinology of the dog. In Morrow DA (ed) *Current therapy in theriogenology 2*. Philadelphia, PA: WB Saunders
- Atalan, G., Holt, P. E., Barr, F. J. & Brown, P. J. (1999). Ultrasonographic estimation of prostatic size in canine cadavers. *Research in Veterinary Science*, 67(1), 7-15. <https://doi.org/10.1053/rvsc.1998.0267>
- Attwood, D. T. (1999). *Soft X-rays and extreme ultraviolet radiation: Principles and applications*. Cambridge, NY: Cambridge University Press

- Bacha, W. J., & Bacha, L. M. (2012). Male reproductive system. *Color atlas of veterinary histology* (3rd ed., pp 225-242). Chichester, WS: Wiley-Blackwell. <https://ebookcentral.proquest.com/lib/usask/detail.action?docID=818227>
- Basu, S., Kwee, T., Surti, S., Akin, E., Yoo, D., & Alavi, A. (2011). Fundamentals of PET and PET/CT imaging. *Annals of the New York Academy of Sciences*, 12281(1), 1-18 <https://doi.org/10.1111/j.1749-6632.2011.06077.x>
- Basu, S., Hess, S., Braad, P. N., Olsen, B. B., Inglev, S., & Højlund-Carlsen, P. F. (2014). The basic principles of FDG-PET/CT imaging. *PET Clinics*, 9(4), 355-370. <https://doi.org/10.1016/j.cpet.2014.07.006>
- Bostwick, D., Cooner, W., Denis, L., Jones, G., Scardino, P., & Murphy, G. (1992). The association of benign prostatic hyperplasia and cancer of the prostate. *Cancer*, 70(S1), 291-301 <http://link.galegroup.com/apps/doc/A12348738/GRGM?u=usaskmain&sid=GRGM&xid=f3747c25>.
- Bouchelouche, K., & Oehr, P. (2008). Positron emission tomography and positron emission tomography/computerized tomography of urological amlignancies: An update review. *The Journal of Urology*, 179(1), 34-45. <https://doi.org/10.1016/j.juro.2007.08.176>
- Brett, T. (2011). Prostate specific antigen. *Australian Family Physician*, 40(7), 497-500. <https://doi.org/10.1016/j.juro.2007.01.072>
- Briganti, A., Capitanio, U., Suardi, N., Gallina, A., Salonia, A., Bianchi, M., ... Montorsi, F. (2009). Benign Prostatic Hyperplasia and Its Aetiologies. *European Urology, Supplements*, 8(13), 865–871. <https://doi.org/10.1016/j.eursup.2009.11.002>
- Brooks, J. R., Busch, R. D., Patanelli, D. J., & Steelman, S. L. (1973). A study of the effects of a new anti-androgen on the hyperplastic dog prostate. *Proceedings of the Society for Experimental Biology and Medicine*. 143(3), 647-55.
- Brown, A. K. (2013). How to interpret plain radiographs in clinical practice. *Best Practice & Research Clinical Rheumatology*, 27(2), 249-269. <https://doi.org/10.1016/j.berh.2013.03.004>
- Bushberg, J. T., Seibert, J. A., Leidholdt Jr, E. M., Boone, J. M. (2002) *The essential physics of medical imaging* (2nd ed.), Philadelphia, PA: Lippincott Williams & Wilkins.
- Canadian Cancer Society <https://www.cancer.ca/en/cancer-information/cancer-type/prostate/statistics/?region=on> Access on April 3, 2017.
- Canadian Light Source Inc. 2012 [https://www.lightsource.ca/about\\_the\\_cls](https://www.lightsource.ca/about_the_cls) Access on November 5, 2016.
- Castellucci, P., Ceci, F., Graziani, T., Juarez, A. R., Nieto, L. F. A., & Fanti, S.

- (2015). PET/CT in prostate cancer. *Medecine Nucleaire*, 39(1), 54-58.  
<https://doi.org/10.1016/j.mednuc.2015.01.001>
- Cherry S.R., Dahlbom M. (2006) PET: Physics, Instrumentation, and Scanners. In: Phelps M.E. (eds) PET. New York, NY: Springer [https://doi-org.cyber.usask.ca/10.1007/0-387-34946-4\\_1](https://doi-org.cyber.usask.ca/10.1007/0-387-34946-4_1)
- Chotipanich, C., Kunawudhi, A., Promteangtrong, C., Tungsuppawattanakit, P., Sricharunrat, T., & Wongsa, P. (2016). Diagnosis of hepatocellular carcinoma using C-11 choline PET/CT: Comparison with F-18 FDG, contrast-enhanced MRI and MDCT. *Asian Pacific Journal of Cancer Prevention*, 17(7), 3569-3573 [http://journal.waocp.org/article\\_32556.html](http://journal.waocp.org/article_32556.html)
- Cooney, J. C., Cartee, R. E., Gray, B. W., & Rumph, P. F. (1992). Ultrasonography of the canine prostate with histologic correlation. *Theriogenology*, 38(5), 877-895. [https://doi.org/10.1016/0093-691X\(92\)90163-L](https://doi.org/10.1016/0093-691X(92)90163-L)
- Cormack, D. (2001). *Essential histology* (2nd ed.). Philadelphia, PA: Lippincott Williams & Wilkins
- Corrada, Y., Arias, D., Rodríguez, R., Spaini, E., Fava, F., & Gobello, C. (2004). Effect of tamoxifen citrate on reproductive parameters of male dogs. *Theriogenology*, 61(7-8), 1327-41  
<https://doi.org/10.1016/j.theriogenology.2003.07.020>
- Costello, L. C., & Franklin, R. B. (2009). Prostatic fluid electrolyte composition for the screening of prostate cancer: A potential solution to a major problem. *Prostate Cancer and Prostatic Diseases*, 12(1), 17-24.  
<https://doi.org/10.1038/pcan.2008.19>
- Currie, S., Hoggard, N., Craven, I. J., Hadjivassiliou, M., & Wilkinson, I. D. (2013). Understanding MRI: Basic MR physics for physicians. *Postgraduate Medical Journal*, 89(1050), 209–223. <https://doi.org/10.1136/postgradmedj-2012-131342>
- D'Anjou, M.-A. (2018). Principles of Computed Tomography and Magnetic Resonance Imaging. In D. Thrall (Ed.) *Textbook of veterinary diagnostic radiology* (7th ed.) (pp 71-95). St. Louis, MO: Elsevier Saunders  
<https://doi.org/10.1016/B978-0-323-48247-9.00017-6>
- Das, B. K. (2015). Positron emission tomography: An overview. In B. K, Das (ed) *Positron Emission Tomography: A Guide for Clinicians* (pp 1-6). New Delhi, India: Springer [https://doi-org.cyber.usask.ca/10.1007/978-81-322-2098-5\\_1](https://doi-org.cyber.usask.ca/10.1007/978-81-322-2098-5_1)
- Davis, M., Sofer, M., Kim, S. S., & Soloway, M. S. (2002). The procedure of transrectal ultrasound guided biopsy of the prostate: A survey of patient preparation and biopsy technique. *The Journal of Urology*, 167(2), 566-570  
[https://doi.org/10.1016/S0022-5347\(01\)69087-6](https://doi.org/10.1016/S0022-5347(01)69087-6)
- DeKlerk, D. P., Coffey, D. S., Ewing, L. L., McDermott, I. R., Reiner, W. G., Robinson, C. H., . . . Zirkin, B. R. (1979). Comparison of spontaneous and

- experimentally induced canine prostatic hyperplasia. *Journal of Clinical Investigation*, 64(3), 842-849. <https://doi.org/10.1172/JCI109532>
- Dennis, R., Kirberger, R. M., Barr, F., Wrigley, R. H. (2010). Urogenital tract. *Handbook of small animal radiology and ultrasound: Techniques and differential diagnoses* (2<sup>nd</sup> ed., pp. 297-330) Churchill Livingstone/Elsevier. <https://doi.org/10.1016/B978-0-7020-2894-6.00011-1>
- Drost, W. T (2018). Physics of ultrasound imaging. In D. Thrall (Ed.) *Textbook of veterinary diagnostic radiology* (7th ed.) (pp 58-70). St. Louis, MO: Elsevier Saunders. <https://doi.org/10.1016/B978-0-323-48247-9.00016-4>
- eClinPath.com – Cornell University College of Veterinary Medicine <http://eclinpath.com/chemistry/muscle/creatine-kinase/> accessed July 4th, 2018
- Emad-Edin, S., Halim, M., Metwally, L. I. A., & Abdel-aziz, R. M. (2014). Diffusion-weighted MR imaging and ADC measurement in normal prostate , benign prostatic hyperplasia and prostate carcinoma. *The Egyptian Journal of Radiology and Nuclear Medicine*, 45(2), 535–542. <https://doi.org/10.1016/j.ejrm.2014.02.017>
- Epstein, J. I., Cubilla, A. L., & Humphrey, P. A. (2011). *Tumors of the prostate gland, seminal vesicles, penis, and scrotum*. Washington, DC: American Registry of Pathology in collaboration with the Armed Forces Institute of Pathology
- Foster, R. A. (2015). Chapter 5 Male Genital System. In M. G. Maxie. *Jubb, Kennedy & Palmer's Pathology of Domestic Animals*. (6<sup>th</sup> ed, Vol 3) (pp. 465-510) St Louis, MO: Elsevier. <https://doi.org/10.1016/B978-0-7020-5319-1.00016-5>
- Fradet, Y., Klotz, L., Trachtenberg, J., & Zlotta, A. (2009). The burden of prostate cancer in Canada. *Canadian Urological Association Journal = Journal De L'Association Des Urologues Du Canada*, 3(3 Suppl 2), S92-S100. <https://www.ncbi.nlm.nih.gov/cyber.usask.ca/pmc/articles/PMC2698782/>
- Frýdl, V., Koch, R., & Závodská, H. (1989). The effect of formalin fixation on several properties of the brain. *Zentralblatt Fur Allgemeine Pathologie U. Pathologische Anatomie*, 135(7), 649-655
- Fuccio, C., Rubello, D., Castellucci, P., Cristina, M., & Fanti, S. (2011). Choline PET / CT for prostate cancer: Main clinical applications. *European Journal of Radiology*, 80(2), 50–56. <https://doi.org/10.1016/j.ejrad.2010.07.023>
- Fukuda, S. (1990). Circadian rhythm of serum testosterone levels in male beagle dogs – Effects of lighting time zone. *Exp. Anim.* 39(1), 65-68. [https://doi.org/10.1538/expanim1978.39.1\\_65](https://doi.org/10.1538/expanim1978.39.1_65)

- Fulton, R. M. (2013). Focused – Basic ultrasound principles and artifacts. In G. Lisciandro (Ed.), *Focused ultrasound techniques for the small animal practitioner* (pp. 1-16) Oxford: John Wiley & Sons.
- Garvey, B., Turkbey, B., Truong, H., Bernardo, M., Periaswamy, S., & Choyke, P. L. (2014). Clinical value of prostate segmentation and volume determination on MRI in benign prostatic hyperplasia. *Diagnostic And Interventional Radiology*, 20(3), 229–233. <https://doi.org/10.5152/dir.2014.13322>
- Ghose, S., Oliver, A., Martí, R., Lladó, X., Vilanova, J. C., Freixenet, J., . . . Meriaudeau, F. (2012). A survey of prostate segmentation methodologies in ultrasound, magnetic resonance and computed tomography images. *Computer Methods and Programs in Biomedicine*, 108(1), 262-287. <https://doi.org/10.1016/j.cmpb.2012.04.006>
- Geavlete, P., Muțescu, R., Mirciulescu, V., Geavlete, B. Verumontanum (2016). In P. Geavlete (Ed). *Endoscopic Diagnosis and treatment in urethral pathology*, chapter 12, pp.199-214. Elsevier-Academic Press <https://doi.org/10.1016/B978-0-12-802406-5.00012-4>
- Geddes, C. B. (2011). Benign Prostatic Hyperplasia in Dogs. *Veterinary Nursing Journal* 26(11), 388-389. <https://doi-org.cyber.usask.ca/10.1111/j.2045-0648.2011.00116.x>
- Ghose, S., Oliver, A., Martí, R., Lladó, X., Vilanova, J. C., Freixenet, J., . . . Meriaudeau, F. (2012). A survey of prostate segmentation methodologies in ultrasound, magnetic resonance and computed tomography images. *Computer Methods and Programs in Biomedicine*, 108(1), 262-287. <https://doi.org/10.1016/j.cmpb.2012.04.006>
- Ginther, O. (1995). *Ultrasonic imaging and animal reproduction*. Cross Plains, WI: Equiservices Publishing
- Grandl, S., Sztrókay-Gaul, A., Mittone, A., Gasilov, S., Brun, E., Bravin, A., ... Coan, P. (2016). Detection of post-therapeutic effects in breast carcinoma using hard X-ray index of refraction computed tomography – A feasibility study. *Journal Plos One*, 11(6), 1–13. <https://doi.org/10.1371/journal.pone.0158306>
- Haidekker, M. A. (2013). Computed tomography. In *Medical Imaging Technology*. SpringerBriefs in Physics (pp-37-53). New York, N.Y: Springer. DOI: [https://doi-org.cyber.usask.ca/10.1007/978-1-4614-7073-1\\_3](https://doi-org.cyber.usask.ca/10.1007/978-1-4614-7073-1_3)
- Haaga, J. R. & Jordan, D. W. (2016) Imaging Principles in Computed Tomography. In J. R. Haaga, and D. T. Boll. (Eds). *CT and MRI of the whole body* (6<sup>th</sup> ed.) (pp 3-30). Philadelphia, PA: Elsevier. <https://www-clinicalkey-com.cyber.usask.ca/#!/content/book/3-s2.0-B9780323113281000012>
- Harvard Health Publishing, 2009. PSA: Prostate-specific antigen, persisting ambiguities. *Harvard Men's Watch*. Retrieved from:

[https://www.health.harvard.edu/newsletter\\_article/PSA-Prostate-Specific-Antigen-Persisting-Scientific-Ambiguities](https://www.health.harvard.edu/newsletter_article/PSA-Prostate-Specific-Antigen-Persisting-Scientific-Ambiguities) online access December 2, 2016

- Hoffmann, P. (2010). Physical fundamentals of X-ray physics. *X-Ray Spectrometry*, 39(1), 70. <https://doi-org.cyber.usask.ca/10.1002/xrs.1239>
- Holst, B.S., Holmroos, E., Friling, L., Hanås, S., Langborg, L.-M., Franko, M. A., & Hansson, K. (2017). The association between the serum concentration of canine prostate specific esterase (CPSE) and the size of the canine prostate. *Theriogenology*, 93, 33–39  
<https://doi.org/10.1016/j.theriogenology.2017.01.032>
- Horos Project 2015. DICOM image viewing and measuring. [Horos]. <http://www.horosproject.org/>
- Informed Health Online (Internet). Cologne, Germany: Institute for Quality and Efficiency in Health Care (IQWiG). “How does the prostate work?” (February 15, 2011, updated August 23, 2016). Retrieved from <https://www.ncbi.nlm.nih.gov/books/NBK279291/> online access November 8, 2016
- Jeyaraj, D. A., Udayakumar, T. S., Rajalakshmi, M., Pal, P. C., & Sharma, R. S. (2000). Effects of long-term administration of androgens and estrogen on rhesus monkey prostate: Possible induction of benign prostatic hyperplasia. *Journal of Andrology*, 21(6), 833-41. <https://doi-org.cyber.usask.ca/10.1002/j.1939-4640.2000.tb03413.x>
- Jia, G., Baudendistel, K. T., von Tengg-Kobligk, H., Heverhagen, J. T., Polzer, H., Henry, H., ... & Knopp, M. V. (2005). Assessing prostate volume by magnetic resonance imaging: A comparison of different measurement approaches for organ volume analysis. *Investigative radiology*, 40(4), 243-248. DOI: 10.1016/S0022-5347(05)00195-3
- Johnston, S. D., Kamolpatana, K., Root-Kustritz, M. V., & Johnston, G. R. (2000). Prostatic disorders in the dog. *Animal Reproduction Science*, 60, 405-415  
[https://doi.org/10.1016/S0378-4320\(00\)00101-9](https://doi.org/10.1016/S0378-4320(00)00101-9)
- Juniewicz, P., Lemp, B., Batzold, F., & Reel, J. (1989). Transrectal ultrasonography as a method to monitor canine prostatic size in situ: Measurements following endocrine manipulation and ejaculation. *Prostate*, 14(3), 265-277
- Junqueira, L., & Carneiro, José. (2005). *Basic histology text & atlas* (11th ed.). New York, NY: McGraw-Hill.
- Kalender, W. (2011). *Computed tomography : Fundamentals, system technology, image quality, applications* (3rd ed.). John-Willey & Sons
- Kashefi, C., Partin, A. W., Parsons, J Kellogg. (2010). Serum markers and screening. In S. Li-Ming (Ed.) *Prostate cancer* (Early diagnosis and treatment of cancer series) (pp. 1-7). Gainesville, FL: Elsevier.



- Kealy, J. K., McAllister, H., Graham, J. P. (2011). *Diagnostic radiology and ultrasonography of the dog and cat* (4th ed.). St. Louis, MO: Elsevier Saunders. <https://doi.org/10.1016/C2009-0-46814-4>
- Kitchen, M., Lewis, R., Yagi, N., Uesugi, K., Paganin, D., Hooper, S., . . . Pavlov, K. (2005). Phase contrast X-ray imaging of mice and rabbit lungs: A comparative study. *The British Journal of Radiology*, 78(935), 1018-27 <https://doi.org/10.1259/bjr/13024611>
- Kuhnt, N. S. M., Harder, L. K., Nolte, I., & Wefstaedt, P. (2017). Computed tomography: a beneficial diagnostic tool for the evaluation of the canine prostate? *BMC Veterinary Research*, 13(123), 1–11. <https://doi.org/10.1186/s12917-017-1016-5>
- Kustritz, M. V. R. (2006). Collection of tissue and culture samples from the canine reproductive tract. *Theriogenology*, 66(3 SPEC. ISS.), 567-574. <https://doi.org/10.1016/j.theriogenology.2006.05.003>
- Kyprianou, Tu, & Jacobs. (1996). Apoptotic versus proliferative activities in human benign prostatic hyperplasia. *Human Pathology*, 27(7), 668-675. [https://doi.org/10.1016/S0046-8177\(96\)90396-2](https://doi.org/10.1016/S0046-8177(96)90396-2)
- Lakrimi, M., Thomas, A. M., Hutton, G., Kruip, M., Slade, R., Davis, P., . . . Marshall, C. A. (2011). The principles and evolution of magnetic resonance imaging. *Journal of Physics: Conference Series*, 286(1), 1–11. <https://doi.org/10.1088/1742-6596/286/1/012016>
- Langer, M., Cloetens, P., Guigay, J-P., Peyrin, F. (2008). Quantitative comparison of direct phase retrieval algorithms in in-line phase tomography. *Medical Physics* 35(9), 4556-4566. DOI: 10.1118/1.2975224
- Lattimer, J. C & Essman, S. C. (2018). Prostate gland. In D. Thrall (Ed.) *Textbook of veterinary diagnostic radiology* (7th ed.) (pp 871-879). St. Louis, MO: Elsevier Saunders. <https://doi.org/10.1016/B978-0-323-48247-9.00056-5>
- Lawrence, J., Rohren, E., & Provenzale, J. (2010). PET/CT today and tomorrow in veterinary cancer diagnosis and monitoring: Fundamentals, early results and future perspectives. *Veterinary and Comparative Oncology*, 8(3), 163-187 <https://doi.org/10.1111/j.1476-5829.2010.00218.x>
- Lee, C., & Kuo, H. (2017). Pathophysiology of benign prostate enlargement and lower urinary tract symptoms: Current concepts. *Ci Ji Yi Xue Za Zhi = Tzu-chi Medical Journal*, 29(2), 79-83. DOI: 10.4103/tcmj.tcmj\_20\_17
- Lee, C. H., Akin-Olugbade, O., & Kirschenbaum, A. (2011). Overview of prostate anatomy, histology, and pathology. *Endocrinology and Metabolism Clinics of North America*, 40(3), 565-575. <https://www-clinicalkey-com.cyber.usask.ca/#!/content/playContent/1-s2.0-S0889852911000612?returnurl=null&referrer=null>



- Lee, K. J., Shimizu, J., Kishimoto, M., Kadohira, M., Iwasaki, T., Miyake, Y. I., & Yamada, K. (2011). Computed tomography of the prostate gland in apparently healthy entire dogs. *Journal of Small Animal Practice*, 52(3), 146-151. <https://doi-org.cyber.usask.ca/10.1111/j.1748-5827.2011.01041.x>
- Lee, K. L., & Peehl, D. M. (2004). Molecular and cellular pathogenesis of benign prostatic hyperplasia. *The Journal of Urology*, 172(5), 1784-1791. <https://doi.org/10.1097/01.ju.0000133655.71782.14>
- Leroy, C., Conchou, F., Layssol-Lamour, C., Deviers, A., Sautet, J., Concordet, D., Mogenicato, G. (2013). Normal canine prostate gland: Repeatability, reproducibility, observer-dependent variability of ultrasonographic measurements of the prostate in healthy intact beagles. *Journal of Veterinary Medicine Series C: Anatomia Histologia Embryologia*, 42(5), 355-361. <https://doi-org.cyber.usask.ca/10.1111/ahc.12022>
- Lévy, X., Nizański, W., von Heimendahl, A., & Mimouni, P. (2014). Diagnosis of common prostatic conditions in dogs: An update. *Reproduction in Domestic Animals*, 49(SUPPL.2), 50-57. <https://doi.org/10.1111/rda.12296>
- Li, J., Tian, Y., Guo, S., Gu, H., Yuan, Q., & Xie, X. (2018). Testosterone-induced benign prostatic hyperplasia rat and dog as facile models to assess drugs targeting lower urinary tract symptoms. *PLoS ONE*, 13(1), 1-13. DOI [10.1371/journal.pone.0191469](https://doi.org/10.1371/journal.pone.0191469)
- Li, X., Liu, Q., Wang, M., Jin, X., Liu, Q., Yao, S., . . . Li, Jun. (2008). C-11 choline PET/CT imaging for differentiating malignant from benign prostate lesions. *Clinical Nuclear Medicine*, 33(10), 671-676. DOI: 10.1097/RLU.0b013e318184b3a0
- Liu, I., Lai, Y., Espiritu, J., Segall, G., Srinivas, S., Nino-Murcia, M., & Terris, M. (2006). Evaluation of fluorodeoxyglucose positron emission tomography Imaging in metastatic transitional cell carcinoma with and without prior chemotherapy. *Urologia Internationalis*, 77(1), 69-75. <https://doi.org/10.1159/000092937>
- Loeb, S., Kettermann, A., Carter, H. B., Ferrucci, L., Metter, E. J., & Walsh, P. C. (2009). Prostate volume changes over time: Results from the Baltimore longitudinal study of aging. *The Journal of Urology*, 182(4), 1458-1462. DOI 10.1016/j.juro.2009.06.047
- Madersbacher, S., Sampson, N., & Culig, Z. (2019). Pathophysiology of Benign Prostatic Hyperplasia and Benign Prostatic Enlargement: A Mini-Review. *Gerontology*, 1-7. DOI:10.1159/000496289
- Malhi, P. S., Adams, G. P., Pierson, R. A. & Singh, J. (2006). Bovine model of reproductive aging: Response to ovarian synchronization and superstimulation. *Theriogenology*, 66, 1257-1266. DOI: 10.1016/j.theriogenology.2006.02.051

- McConnell, J. D. (1991). The pathophysiology of benign prostatic hyperplasia. *Journal of Andrology*, 12(6), 356-363. <https://doi-org.cyber.usask.ca/10.1002/j.1939-4640.1991.tb00272.x>
- McVary, Roehrborn, Avins, Barry, Bruskewitz, Donnell, Foster, Gonzalez, Kaplan, Penson, Ulchaker, and Wei (2011). Update on AUA guideline on the management of benign prostatic hyperplasia. *The Journal of Urology*, 185(5), 1793-1803. <https://doi.org/10.1016/j.juro.2011.01.074>
- Melli, A., Wahid K. A., Babyn P., Montgomery, J., Snead E., El-Gayed, A. . . . Wesolowski, M. (2016). A compressed sensing based reconstruction algorithm for synchrotron source propagation-based X-ray phase contrast computed tomography. *Nuclear Instruments and Methods in Physics Research*, A, 806(1), 307-317 <https://doi.org/10.1016/j.nima.2015.10.013>
- Mescher, A. L. (2016). Accessory Glands. In *Junqueira's basic histology: Text and atlas*. New York: McGraw Hill. <https://doi.org/10.1016/B978-0-12-374144-8.00001-1>
- Montgomery JE, Barboza T, Pettitt M, Singh J, Snead E, Babyn P, Belev G, Wei Z, Chibbar R, Visvanathan K, Boire S, Chapman D, El-Gayed A, Buhr M, Adams G. (2013) Comparison of synchrotron phase contrast computed tomography with 3T magnetic resonance imaging, computed tomography, diagnostic ultrasound and histopathology of normal and diseased *ex vivo* canine and human prostates. Taking x-ray phase contrast imaging into mainstream applications, The Royal Society, London, UK, February 12
- National Cancer Institute (NCI), August 26 2008. *Exam, Digital Rectal*. (Illustration) (Retrieved from <https://visualsonline.cancer.gov/details.cfm?imageid=7136> on November 5, 2016)
- Nickel, J. (2006). The economics of medical therapy for lower urinary tract symptoms associated with benign prostatic hyperplasia. *Current Prostate Reports*, 4(3), 132-137 <https://doi-org.cyber.usask.ca/10.1007/s11934-996-0007-z>
- Nickel, J. Curtis, Mendez-Probst, Carlos E., Whelan, Thomas F., Paterson, Ryan F., & Razvi, Hassan. (2010). 2010 Update: Guidelines for the management of benign prostatic hyperplasia (CUA Guideline)(Report). *Canadian Urological Association Journal (CUAJ)*, 4(5), 310. DOI:10.5489/cuaj.10124
- Nizański, W., Levy, X., Ochota, M., & Pasikowska, J. (2014). Pharmacological treatment for common prostatic conditions in dogs – benign prostatic hyperplasia and prostatitis: An Update. *Reproduction in Domestic Animals*, 49 (SUPPL.2), 8-15. <https://doi.org/10.1111/rda.12297>
- Page, S. T., Lin, D. W, Mostaghel, E. A., Marck, B. T., Wright, J. L., Wu, J., . . . Matsumoto, A. M. (2011). Dihydrotestosterone administration does not increase intraprostatic androgen concentrations or alter prostate androgen action in

- healthy men: A randomized-controlled trial. *The Journal of Clinical Endocrinology and Metabolism*, 96(2), 430-7. <https://doi-org.cyber.usask.ca/10.1210/jc.2010-1865>
- Panchbhai, A. (2015). Wilhelm Conrad Röntgen and the discovery of X-rays: Revisited after centennial. *Journal of Indian Academy of Oral Medicine and Radiology*, 27(1), 90-95. <https://doi.org/10.4103/0972-1363.167119>
- Partin, A. W., Oesterling, J. E., Epstein, J. I., Horton, R. & Walsh, P. C. (1991). Influence of Age and Endocrine Factors on the Volume of Benign Prostatic Hyperplasia. *The Journal of Urology*, 145(2), 405-409. [https://doi.org/10.1016/S0022-5347\(17\)38353-2](https://doi.org/10.1016/S0022-5347(17)38353-2)
- Pasikowska, J., Hebel, M., & Nowak, M. (2015). Computed tomography of the prostate gland in healthy intact dogs and dogs with benign prostatic hyperplasia. *Reproduction in Domestic Animals*, 50(5), 776–783. <https://doi.org/10.1111/rda.12587>
- Pearson, R., & Williams, P. M. (2014). Common questions about the diagnosis and management of benign prostatic hyperplasia. *American family physician*, 90(11), 769-774. <https://www.clinicalkey.com/#!/content/journal/1-s2.0-S0002838X14603841>
- Pedler, K., Kitzing, Y., Varol, C., & Arianayagam, M. (2015). The current status of MRI in prostate cancer. *Australian Family Physician*, 44(4), 225-230. <http://cyber.usask.ca/login?url=https://search.proquest.com/docview/1673949516?accountid=14739>
- Pinheiro, D., Machado, J., Viegas, C., Baptista, C., Bastos, E., Magalhaes, J., . . . Martins-Bessa, A. (2017). Evaluation of biomarker canine-prostate specific arginine esterase (CPSE) for the diagnosis of benign prostatic hyperplasia. *BMC Veterinary Research*, 13(1), 1-7. <https://doi-org.cyber.usask.ca/10.1186/s12917-017-0996-5>
- Rahmouni, A. M., Yang, A. K., Tempany, C., Ricci, C., Frenkel, Epstein, J., ... Zerhouni, E., (1992). Accuracy of in-vivo assessment of prostatic volume by MRI and transrectal ultrasonography. *Journal of Computer Assisted Tomography*, 16(6), 935-940.
- Rajalakshmi, M., Sukanya, V., Ramakrishnan, P., & Kaur, J. (1990). Effect of dihydrotestosterone on ultrastructural changes in rhesus monkey spermatozoa. *Andrologia*, 22(2), 144-51. <https://doi-org.cyber.usask.ca/10.1111/j.1439-0272.1990.tb01955.x>
- Rasband, W.S., ImageJ, U. S. National Institutes of Health, Bethesda, Maryland, USA, <https://imagej.nih.gov/ij/>, 1997-2016
- Risbridger, G. P., & Taylor, R. A. (2006). Physiology of the male accessory sex structures: The prostate gland, seminal vesicles, and bulbourethral glands. In Knobil, E., Neill, Jimmy D, ScienceDirect, & Elsevier. *Knobil and Neill's*

- Physiology of Reproduction* (3rd ed.). (pp. 1149-1172). Chapter 23. Melbourne, VIC:Elsevier. <https://doi.org/10.1016/B978-012515400-0/50028-2>
- Robaire, B., Hinton, B. T., Orgebin-Crist, M.C. (2006). The epididymis. In Knobil, E., Neill, Jimmy D, ScienceDirect, & Elsevier. *Knobil and Neill's Physiology of Reproduction* (3rd ed.). (pp. 1071-1148). Melbourne, VIC:Elsevier
- Ruel, Y., Barthez, P., Mailles, A., & Begon, D. (1998). Ultrasonographic evaluation of the prostate in healthy intact dogs. *Veterinary Radiology & Ultrasound*, 39(3), 212-216. <https://doi-org.cyber.usask.ca/10.1111/j.1740-8261.1998.tb00342.x>
- Saha, G. P. (2016). Radioactive decay and interaction of radiation with matter. In *Basics Of Pet Imaging: Physics, Chemistry, And Regulations* (3rd ed.) Switzerland: Springer. <https://doi-org.cyber.usask.ca/10.1007/978-3-319-16423-6>
- SAS Institute Inc (2011a). SAS/STAT Product Documentation. SAS Institute Inc., Cary, NC. URL <http://support.sas.com/documentation/onlinedoc/stat/>.
- Saunders, J. & Ohlerth, S. (2011). CT physics and instrumentation: Mechanical design. In T. Schwarz, T. and J. Saunders (Eds.). *Veterinary computed tomography*. John Wiley & Sons DOI:10.1002/9781118785676
- Scher, B., Seitz, M., Albinger, W., Tiling, R., Scherr, M., Becker, H., . . . Dresel, S. (2007). Value of 11 C-choline PET and PET/CT in patients with suspected prostate cancer. *European Journal of Nuclear Medicine and Molecular Imaging*, 34(1), 45-53. <https://doi.org/10.1007/s00259-006-0190-7>
- Setchell, B. P., & Breed, W. G. (2006). Anatomy, Vasculature, and Innervation of the Male Reproductive Tract. In Knobil, E., Neill, Jimmy D, ScienceDirect, & Elsevier. *Knobil and Neill's Physiology of Reproduction* (3rd ed.). (pp. 771-825). Melbourne, VIC:Elsevier
- Shah R. & Ming Z. (2012). Prostate needle biopsy sampling techniques: Impact on pathological diagnosis. *Prostate biopsy interpretation: An illustrated guide*. (pp. 11- 14). Berlin: Springer-Verlag. DOI: 10.1007/978-3-642-21369-4\_2
- Sharma, H. (2009). MRI physics—basic principles. *Acta Neuropsychiatrica*, 21(4), 200-201. DOI: 10.1111/j.1601-5215.2009.0404.x
- Singh, P. B., Moore, C. M., & Emberton, M. (2013). Prostate biopsy. In A. Tewari (Eds), *Prostate cancer: A comprehensive perspective* (pp. 511-524). Springer-Verlag London <https://doi-org.cyber.usask.ca/10.1007/978-1-4471-2864-9>
- Smith, J. (2008). Canine prostatic disease: A review of anatomy, pathology, diagnosis, and treatment. *Theriogenology*, 70(3), 375-383. <https://doi.org/10.1016/j.theriogenology.2008.04.039>
- Smith, S. W. The Scientist and Engineer's guide to digital signal processing – “Chapter 25 Special Imaging Techniques - CT” 1998. <http://www.dspguide.com/ch25/5.htm>. Online access December 12th, 2016

- Soares, J., Avelar, G., & França, L. (2009). The seminiferous epithelium cycle and its duration in different breeds of dog (*Canis familiaris*). *Journal of Anatomy*, 215(4), 462-471.
- Solano-Gallego, L. (2010). Reproductive System. In R. Raskin, & D. J. Meyer. *Canine and feline cytology: A color atlas and interpretation guide* (2nd ed.) (pp. 274-308) St. Louis, Mo: Saunders Elsevier.
- Sun, F., Báez-Díaz, C., & Sánchez-Margallo, F. (2017). Canine prostate models in preclinical studies of minimally invasive interventions: Part II, benign prostatic hyperplasia models. *Translational Andrology and Urology*, 6(3), 547-555. doi: [10.21037/tau.2017.03.62](https://doi.org/10.21037/tau.2017.03.62)
- Tanguay, S., Awde, M., Brock, G., Casey, R., Kozak, J., Lee, J., . . . Saad, F. (2009). Diagnosis and management of benign prostatic hyperplasia in primary care. *Canadian Urological Association Journal = Journal De L'Association Des Urologues Du Canada*, 3(3 Suppl 2), S92-S100. <https://doi.org/10.1175/MWR-D-13-00349.1>
- Thrall, D. E., Widmer, W. R., (2018). Radiation protection and physics of diagnostic radiology. In D. Thrall (Ed.) *Textbook of veterinary diagnostic radiology* (7th ed.) (pp 2-22). St. Louis, MO: Elsevier Saunders. <https://doi.org/10.1016/B978-0-323-48247-9.00002-4>
- Troisi, A., Orlandi, R., Bargellini, P., Menchetti, L., Borges, P., Zelli, R., & Polisca, A. (2015). Contrast-enhanced ultrasonographic characteristics of the diseased canine prostate gland. *Theriogenology*, 84(8), 1423–1430. <https://doi.org/10.1016/j.theriogenology.2015.07.029>
- Ukimura, O., Hung, A. J., & Gill, I. S. (2011). Innovations in prostate biopsy strategies for active surveillance and focal therapy. *Current Opinion In Urology*, 21(2), 115-120 <https://doi.org/10.1097/MOU.0b013e3283435118>
- Ultrasound for Regional Anesthesia (USRA). Online access: Dec13, 2016. <http://www.usra.ca/regional-anesthesia/introduction/basic.php#ultrasoundimage>
- Vuichoud, C. R., & Loughlin, K. (2015). Benign prostatic hyperplasia: Epidemiology, economics and evaluation. *The Canadian Journal of Urology*, 22, 1-6 [https://www.canjurol.com/html/free-articles/JUV22I5S1F\\_06\\_DrLoughlin.pdf](https://www.canjurol.com/html/free-articles/JUV22I5S1F_06_DrLoughlin.pdf)
- Wadhera, P. (2013). An introduction to acinar pressures in BPH and prostate cancer. *Nature Reviews Urology*, 10(6), 358-366. <https://doi-org.cyber.usask.ca/10.1038/nrurol.2013.86>
- Walsh, P., & Wilson, J. (1976). The induction of prostatic hypertrophy in the dog with androstanediol. *The Journal of Clinical Investigation*, 57(4), 1093-7 DOI: 10.1172/JCI108353

- Washington State University. Online access: Nov 27, 2016.  
<https://www.vetmed.wsu.edu/outreach/Pet-Health-Topics/categories/cat-and-dog-anatomy/urogenital-system-of-the-dog>
- Wei, J., Miner, M., Steers, W., Rosen, R., Seftel, A., Pasta, D., . . . Roehrborn, G. (2011). Benign prostatic hyperplasia evaluation and management by urologists and primary care physicians: Practice patterns from the observational bph registry. *The Journal of Urology*, 186(3), 971-976. DOI:10.1016/j.juro.2011.04.081
- Williams, J. (2013). Disease facts: Benign prostatic hyperplasia (BPH) in dogs. *Companion Animal*, 18(9), 428-429. DOI: 10.12968/coan.2013.18.9.428
- Willmott, P. (2011). Synchrotron Physics In *An introduction to synchrotron radiation: Techniques and applications*. (pp 39-86) Chichester, WS: John Willey & Sons <https://doi-org.cyber.usask.ca/10.1002/9781119970958.ch3>
- Wilson, J. D. (1980). The pathogenesis of benign prostatic hyperplasia. *The American Journal of Medicine*, 68(5), 745-756. [https://doi.org/10.1016/0002-9343\(80\)90267-3](https://doi.org/10.1016/0002-9343(80)90267-3)
- Wolkowski, B., Snead, E., Wesolowski, M., Singh, J., Pettitt, M., Chibbar, R., . . . Montgomery, J. (2015). Assessment of freeware programs for the reconstruction of tomography datasets obtained with a monochromatic synchrotron-based X-ray source. *Journal of Synchrotron Radiation*, 22(4), 1130-1138. <https://doi-org.cyber.usask.ca/10.1107/S1600577515008437>
- Yayla, S., Öztürk, S., Aksoy, Ö., Kiliç, E., & Yildiz, S. (2012). Normal ultrasonographic Anatomy of the Prostate in Kars Shepherd Dogs. *Kafkas Universitesi Veteriner Fakultesi Dergisi*, 18(1), 27–30. Article Code: KVFD-2011-4528
- Yoshida, S., Nakagomi, K., Goto, S., Futatsubashi, M., & Torizuka, T. (2005). 11 C-choline positron emission tomography in prostate cancer: Primary staging and recurrent site staging. *Urologia Internationalis*, 74(3), 214-220. DOI:[10.1159/000083551](https://doi.org/10.1159/000083551)
- Young, B., Woodford, P., & O'Dowd, G. (2014). Male Reproductive System. In *Wheater's functional histology: A text and colour atlas* (6th ed) (pp 337-350). Philadelphia, PA: Churchill Livingstone (Elsevier).
- Zaer, N. F., Amini, B. & Elsayes, K. M. Chapter 1: Overview of Diagnostic Modalities and Contrast Agents. In Elsayes, K. M., & Oldham, S. A. A. (2014). *Introduction to diagnostic radiology*. New York, NY: McGraw-Hill Medical.  
<http://accessmedicine.mhmedical.com.cyber.usask.ca/content.aspx?bookid=1562&sectionid=95874457>



- Zambelli, D., Cunto, M., & Gentilini, F. (2012). Validation of a model to develop a symptom index for benign prostatic hyperplasia in dogs. *Reproduction in Domestic Animals*, 47(S6), 229-231. <https://doi.org/10.1111/rda.12084>
- Zamir, A., Arthurs, O., Hagen, C., Diemoz, P., Brochard, T., Bravin, A., . . . Olivo, A. (2016). X-ray phase contrast tomography; Proof of principle for post-mortem imaging. *The British Journal of Radiology*, 89(11), 1-6. DOI: 10.1259/bjr.20150565
- Zhao, X.-F, Yang, Y., Wang, W., Qiu, Z., Zhang, P., & Wang, B. (2013). Effects of competitive and noncompetitive 5 alpha-reductase inhibitors on serum and intra-prostatic androgens in beagle dogs. *Chinese Medical Journal*, 126(4), 711-715. DOI: 10.3760/cma.j.issn.0366-6999.20122496